City Research Online

City, University of London Institutional Repository

This is the accepted version of the paper.

This version of the publication may differ from the final published version.

Permanent repository link: https://openaccess.city.ac.uk/id/eprint/28530/

Link to published version:

AN EXPERIMENTAL AND COMPUTATIONAL STUDY OF LAMINAR COMBINED NATURAL AND FORCED CONVECTION IN VERTICAL DUCTS

John Sydney Lewis

A thesis submitted to The City University for the degree of

Doctor of Philosophy

JUNE 1992

School of Mechanical and Manufacturing Engineering,

Faculty of Engineering, Science and Mathematics,

Middlesex University.

In memory of my parents

Ivor and Prudence Hannah Lewis

CONTENTS

LIST OF FIGURES

ACKNOWLEDGEMENTS

DECLARATION

I grant powers of discretion to The University Librarian to allow this thesis to be copied in whole or in part without further reference to me. This permission covers only single copies made for study purposes, subject to normal conditions of acknowledgement.

J.S.Lewis   June 1992

ABSTRACT

Buoyancy forces can exert significant influences on convective heat transfer for internal flows. This study considers some aspects of combined natural and forced convection for laminar flows in vertical ducts. Both computational and experimental approaches are employed.

A common framework is developed for the parabolic equations governing hydrodynamically and thermally developing duct flows exhibiting planar or axisymmetric two–dimensionality. A variable–property, quasi–incompressible fluid is assumed. Although primarily developed for the purpose of studying combined convection heat transfer in vertical ducts, the theoretical development is also applicable to the corresponding natural convection problem and to pure forced flows with or without heat transfer. The analysis caters for numerous possible combinations of duct geometry (circular, concentric annular and parallel plates), thermal boundary conditions (uniform wall temperature or uniform heat flux) and inlet flow profile (uniform, partially developed or fully–developed). A marching procedure for obtaining numerical solutions of the fully–implicit, finite–difference versions of the governing equations is described.

Local heat transfer results are reported from an accompanying experimental investigation of water flowing upward in a uniformly heated vertical tube almost 160 diameters long. The data presented cover a range of inlet Reynolds number from 75 to 1180 and values of the buoyancy parameter Gr_q/Re from 71 to 2070 (based on inlet bulk properties). The experimental local Nusselt numbers shown exhibit an increase with Gr_q/Re which is more marked at longer axial distances. In many tests, the variation of the local Nusselt number is characterised by a minimum value at some intermediate axial position followed by a rise in the downstream portion of the tube. Examples are included of transient records obtained of wall temperature fluctuations which have also been observed in previous studies using similar apparatus. The fluctuations, which are generally

believed to indicate departure from steady laminar flow, increase in magnitude with both flow rate and heat flux, and appear to be responsible for a marked improvement in the local heat transfer.

Numerical predictions of local Nusselt number and wall temperature are compared with the experimental results for selected conditions. The predictions are restricted to regions where the flow remains unidirectional. The agreement seen is generally good, except in regions where either strong wall temperature fluctuations or upstream axial wall conduction is evident in the measured data, thus precluding a strict comparison with the numerical model which assumes steady laminar flow and uniform heating. The prediction of the Nusselt number minima is particularly pleasing.

The experimental data collected in this study are also compared with published correlations for estimating the convection regime and the Nusselt number.

NOMENCLATURE

$a_0 \cdots a_n$	coefficients in nth–degree ψ versus T polynomial
$a_{\psi 1} \cdots a_{\psi n}$	coefficients in nth–degree ψ versus $(T - T_0)$ polynomial
$A_{\psi 1} \cdots A_{\psi n}$	dimensionless coefficients in nth–degree ψ^* versus θ polynomial
A	constant in equn.(7.2)
A	square coefficient matrix
A_c	flow cross–sectional area
$A_m^{(\ )}$	coefficient in finite–difference equation, subscript denotes transverse grid location where equation evaluated, superscript number in brackets identifies the equation and associated variable
$\tilde{A}_m^{(\ )}$	modified coefficient $A_m^{(\ )}$ accomodating boundary conditions
A_w	tube wall cross–sectional area for axial conduction
b	radial width of duct or problem domain, $(r_2 - r_1)$
B	exponent in equn.(7.2)
B	column matrix of right–hand side constants
Bi	Biot number, $h\delta_w/k_w$
$B_m^{(\ )}$	right–hand side constant in finite–difference equation, subscript denotes transverse grid location where equation evaluated, superscript number in brackets identifies the equation
$\tilde{B}_m^{(\ )}$	modified constant $B_m^{(\ )}$ accomodating boundary conditions
Br	Brinkmann number, $\mu u_m^2/k\Delta T_r$
c	specific heat capacity, for fluid if no subscript used
c_m	mean specific heat capacity for range T_0 to T, $\int_{T_0}^{T} c \, dT/(T - T_0)$
c^*	specific heat capacity ratio, c/c_0
c_m^*	mean specific heat capacity ratio, c_m/c_0
c_1, c_2	constants in μ versus T power law, equn.(3.40)
C_1, C_2	dimensionless constants in μ^* versus θ power law, equn.(3.80), $C_1 = \Delta T_r/(T_0 + c_1)$, $C_2 = c_2$
d	tube diameter

d_h	duct hydraulic diameter, $4A_c/P_w$, for a circular tube $d_h = d = 2b$, for a concentric annulus $d_h = 2b$, for parallel plates $d_h = 4b$ for symmetric problems and $d_h = 2b$ for asymmetric problems
e	specific internal energy
E	dimensionless energy function, defined by equns.(3.117)–(3.120)
F	general dependent variable
F(Y)	function of Y, $r* + (1 - r*)Y$
Fo	modified Fourier number, $(k/\rho c)_w/\omega\delta_w^2$
g	acceleration due to gravity
G	dimensionless gravitational parameter, gb^3/ν_o^2
Gr	Grashof number based on wall–to–bulk temperature difference, $g\beta\rho^2 d_h^3(T_w - T_b)/\mu^2$
Gr_q	Grashof number based on heat flux, $g\beta\rho^2 d_h^4 q_w/k\mu^2$
Gr_T	Grashof number based on wall–to–inlet temperature difference, $g\beta\rho^2 d_h^3(T_w - T_o)/\mu^2$
h	convective heat transfer coefficient, $q_w/(T_w - T_b)$
i	general index
I	instantaneous electric current in heated test section
$\tilde{I}$	rms electric current in heated test section
k	thermal conductivity, for fluid if no subscript used
k*	thermal conductivity ratio, k/k_o
K	axial wall conduction parameter, $k_w\delta_w/k\,b$
L	length of heated test section
L_{hy}^*	dimensionless hydrodynamic entrance length, $(L_{hy}/d_h)/Re$
L_{th}^*	dimensionless thermal entrance length, $(L_{th}/d_h)/RePr$
m	finite–difference grid location in transverse direction
M	number of transverse divisions in finite–difference grid
n	finite–difference grid location in axial (marching) direction
Nu	Nusselt number, hd_h/k
p	static pressure

$\hat{p}$	pressure contribution due to fluid motion, $p + \rho_0 gz$
P	dimensionless pressure, $(\hat{p} - \hat{p}_0)/\rho_0 u_m^2$
P_w	wetted perimeter of duct
Pe	Peclet number, $RePr$
Pr	Prandtl number of fluid, $c\mu/k$
q_g	heat generation rate in tube wall per unit heat transfer area
q_r	reference heat flux, $[\,|q_{w_1}|, |q_{w_2}|\,]$
q_w	wall–to–fluid heat flux, q_{w_1} for a duct wall at $y = 0$, q_{w_2} for a duct wall at $y = b$
$\dot{Q}_{corr}$	corrected rate of heat transfer to fluid, $\dot{Q}_g - \dot{Q}_{loss}$
$\dot{Q}_g$	rate of electrical power input to test section, $\tilde{I}\tilde{V}$
$\dot{Q}_{loss}$	rate of heat loss from test section, estimated from equn.(5.3)
$\dot{Q}_{meas}$	measured rate of energy rise of fluid, $\rho_0 \dot{V} c_{b_m}(\Delta T_b)_{meas}$
r	radial coordinate
r_1	radius of inner transverse boundary at $y = 0$
r_2	radius of outer transverse boundary at $y = b$
r^*	radius ratio, r_1/r_2
r_{max}	radius at which maximum axial velocity occurs
r_q	heat flux ratio, q_w/q_r, r_{q_1} for a duct wall at $y = 0$, r_{q_2} for a duct wall at $y = b$
r_T	ratio of wall temperature differences, $(T_{w_1} - T_0)/(T_{w_2} - T_0)$ with $T_{w_2} \geq T_{w_1}$, $(T_{w_2} - T_0)/(T_{w_1} - T_0)$ with $T_{w_1} \geq T_{w_2}$
R	dimensionless radial coordinate, r/b
R_e	electrical resistance of heated test section
R_{max}	dimensionless radius at which maximum axial velocity occurs
Ra	Rayleigh number, $g\beta\rho^2 c d_h^4 (dT_b/dx)/16\mu k$
Re	Reynolds number, $\rho u_m d_h/\mu$
Re_b	Reynolds number based on radial width b, $\rho u_m b/\mu$
S	buoyancy term multiplier, $S = +1$ for upward flow, $S = -1$ for downward flow, $S = 0$ for pure forced convection

t	time
T	temperature
$\bar{T}$	time–averaged temperature
T_{amb}	ambient air temperature
T_b	fluid bulk temperature
T_f	fluid film temperature, $(T_b + T_w)/2$
$\mathcal{T}_i(\xi)$	Chebyshev polynomial of degree i in ξ, defined in Appendix B
T_w	duct wall temperature, T_{w_1} for a duct wall at $y = 0$, T_{w_2} for a duct wall at $y = b$
ΔT_b	bulk temperature rise
ΔT_r	reference temperature difference, $[\lvert T_{w_1} - T_o \rvert, \lvert T_{w_2} - T_o \rvert]$ for UWT conditions, $[\lvert q_{w_1}b/k_o \rvert, \lvert q_{w_2}b/k_o \rvert]$ for UHF conditions, $\lvert q_w b/k \rvert$ for mixed UHF/UWT conditions
u	axial velocity
u_m	mean axial velocity
U	dimensionless axial velocity, u/u_m
v	transverse velocity
V	dimensionless transverse velocity, v/u_m
$\dot{V}$	volume flow rate
$\tilde{V}$	rms voltage applied to heated test section
W	dimensionless stream function, defined by equns.(3.108)–(3.110)
x	axial coordinate
x_a	adiabatic entry length, x_{a_1} for a duct wall at $y = 0$, x_{a_2} for a duct wall at $y = b$
x^+	axial coordinate for hydrodynamic development region, $(x/d_h)/Re$
x^*	axial coordinate for thermal development region, $(x/d_h)/RePr$
X	dimensionless axial coordinate, x/b
ΔX	finite–difference grid spacing in axial (marching) direction
y	transverse coordinate
Y	dimensionless transverse coordinate, y/b

ΔY	finite–difference grid spacing in transverse direction
z	vertically upward coordinate
Z	column matrix of unknown dependent variable values

Greek symbols

α	temperature coefficient of electrical resistivity
β	thermal expansion coefficient of fluid, $(-1/\rho)(\partial\rho/\partial T)$
$\gamma(x)$	dimensionless function of x alone
δ_w	tube wall thickness
ϵ	electrical resistivity of tube wall material
ζ	ratio of absolute temperature to ice–point temperature
θ	dimensionless temperature, $(T - T_o)/\Delta T_r$
$\boldsymbol{\theta}$	column matrix of unknown dimensionless temperature values
$\hat{\theta}$	dimensionless temperature in Appendix C, $(T - \bar{T})/(\bar{T} - T_b)$
κ	flow index, $\kappa = 0$ for two–dimensional flow, $\kappa = 1$ for axisymmetric flow
μ	dynamic viscosity of fluid
μ^*	dynamic viscosity ratio, μ/μ_o
ν	kinematic viscosity of fluid, μ/ρ
ξ	normalised temperature, defined in Appendix B
π	3.14159...
ρ	density, for fluid if no subscript
ρ^*	density ratio, ρ/ρ_o
σ	standard deviation, $\left[\frac{1}{n-1}\sum_1^n (x_i - \bar{x})^2\right]^{\frac{1}{2}}$
τ	dimensionless time, ωt
ϕ	azimuthal coordinate
Φ	viscous dissipation function, defined by equn.(3.8)
ψ	any fluid property
ψ^*	any fluid property ratio, ψ/ψ_o
ω	angular frequency of alternating current

Subscripts

b	fluid bulk value or value evaluated at fluid bulk temperature; also used with Reynolds number based on radial width b
cl	centreline value
cr	critical value
e	duct exit value
fd	fully–developed value
F	pure forced convection
i	refers to inner surface of tube wall
j	test section wall thermocouple position number, $j = 0, 1, \cdots, 13$
lm	logarithmic mean
m	mean values; also used for grid location in Y direction
max	maximum value
meas	measured value
min	minimum value
n	grid location in X direction
N	pure natural convection
o	duct inlet value, also refers to outer surface of tube wall
p	at constant pressure
v	at constant volume
x	local value
w	refers to a property of duct wall material or value at wall
ρ	pertains to fluid density
ψ	pertains to any fluid property
1	refers to inner transverse boundary at $y = 0$ (wall or centreline)
2	refers to outer transverse boundary at $y = b$ (wall)
∞	freestream value

<u>**Superscript**</u>

•   denotes value of dependent variable at previous step or iteration

<u>**Special symbols**</u>

O order of

TE   truncation error of finite—difference approximation

UHF   uniform heat flux thermal boundary condition

UWT   uniform wall temperature thermal boundary condition

[ ]   largest of enclosed quantities

PART 1

CONTEXT AND PREVIOUS WORK

CHAPTER 1

GENERAL INTRODUCTION

1.1 Classification of Convective Duct Flows

The convective mode known as combined natural and forced convection, or sometimes mixed convection, occurs in situations where buoyancy forces and an externally generated pressure force act simultaneously and both have a significant effect in determining the resulting flow field and hence the characteristics of the associated transport processes. Buoyancy forces are generated when density differences, caused by temperature, pressure or concentration differences, interact with a body force field, such as that due to gravity or rotation. Although combined natural and forced convection can occur in both external and internal flows, only duct flows are considered here and the superimposed natural convection effects are assumed to be thermally–induced under the action of a gravitational body force (i.e. so–called thermogravitational flows).

Combined convection duct flows may be either laminar, transitional or turbulent and can be further classified according to the duct cross–section shape, the kind of thermal boundary conditions imposed at the duct walls and the direction of flow in relation to the buoyancy force. For horizontal ducts the gravitational body force is perpendicular to the tube axis. In the case of a laminar flow in a horizontal circular tube this leads to the development of a parallel pair of contra–rotating vortices in the tube cross–section. Vertical duct flows can be divided into two essentially different types. Upward heated flows and downward cooled flows both give rise to buoyancy forces which act in the same direction as the forced flow and accordingly are termed buoyancy–aided (or assisted) flows. In contradistinction, upward cooled flows and downward heated flows are known as buoyancy–opposed flows.

1.2 Aims and Approaches

Both experimental and computational approaches were adopted in the study of laminar combined natural and forced convection heat transfer in vertical ducts reported on in this thesis.

Heat transfer measurements have been made for upflow of water in a uniformly heated vertical tube to provide data for verification of the numerical predictions. A wide range of Reynolds number and the buoyancy parameter Gr_q/Re were covered by the experiments which encompassed a variety of combined convection phenomena, including flow reversals and wall temperature fluctuations.

The aim of the computational approach, which builds on the work of several previous investigators, was to develop a unified method for the treatment of duct geometries exhibiting plane or axisymmetric two—dimensionality; namely circular tubes, concentric annuli and parallel plate ducts. The procedure developed is based on finite—difference approximations of the parabolised conservation equations for a quasi—incompressible, variable—property Newtonian fluid.

The new numerical procedure has been applied to make predictions for:

i)   laminar flow, forced convection with constant properties;

ii)   local Nusselt numbers and wall temperature variations for laminar combined convection conditions with variable properties to compare with the experimentally determined values;

Information is also presented about other numerical studies conducted by the author using another numerical procedure. These include a study of combined convection between vertical parallel plates and a thermosyphon loop study.

CHAPTER 2

SURVEY OF RELEVANT LITERATURE

2.1 Scope of Survey

The purpose of this chapter is to describe the contributions made by previous research to the literature on combined natural and forced laminar convection of Newtonian fluids in vertical ducts. Consideration is given to experimental investigations as well as theoretical studies; the latter including both analytical and numerical treatments. Only studies dealing with buoyancy—aided or buoyancy—opposed flow under steady—state thermal boundary conditions are included. Transient combined convection and combined convection with simultaneous mass transfer, thermal radiation or internal energy generation are excluded from consideration. Although the literature on the limiting case of pure natural convection in vertical ducts has facilitated the author's understanding and has also been extensively drawn upon by combined convection researchers this topic is not addressed. The literature examined spans a period of approximately 50 years up to the end of 1991 and the majority of papers are written in English.

Published reviews covering the subject area defined above were provided by Chato (1969), Petukhov et al (1982), Aung (1987) and Jackson et al (1989). In addition, a section of the Heat Exchanger Design Handbook contributed by Churchill (1983) is a useful source of relevant information. The material considered here is categorised in a manner similar to that utilised by Aung (1987), in that separate sections are devoted to studies of fully—developed flow, developing flow and instability and transition. Further subdivisions are made in each section to deal with the three main duct geometries considered by previous workers; namely circular tubes, concentric annuli and parallel plate ducts. Only passing mention is made of studies of combined convection in ducts with other cross—sections.

In order to avoid frequent repetition it is noted here that, unless otherwise stated, certain simplifications can be assumed to have been made in the theoretical studies mentioned below. These include the assumption of steady laminar two–dimensional (plane or axisymmetric) conditions, the use of the boundary layer approximations, the treatment of all fluid properties as constant, other than the inclusion of a linear density variation in the buoyancy force term (Boussinesq approximation), and the neglect of viscous dissipation. The thermal boundary conditions imposed at duct walls, usually either uniform heat flux (UHF) or uniform wall temperature (UWT), and the hydrodynamic entrance conditions assumed are stated for each study. Finally, it should be noted that in the literature, results for combined convection have generally been expressed in terms of dimensionless parameters, including Reynolds number, Prandtl number and either a Grashof number or a Rayleigh number. Several different definitions of the last two nondimensional groups have been adopted by workers in this field, mainly as a result of the different thermal boundary conditions and duct geometries investigated. To avoid confusion in discussing previous work, Grashof number and Rayleigh number are only denoted by symbols when the definitions given in the Nomenclature apply directly, or differ by a constant factor only. Numerical values have been converted accordingly. Furthermore, as noted by Petukhov et al (1982), the Rayleigh number defined as $Ra = g\beta\rho^2 c d_h^4 (dT_b/dx)/16\mu k$, is unambiguously interconnected with the parameter Gr_q/Re. For example, in the case of a circular tube heated at UHF, $Ra = (Gr_q/Re)/4$. Where Grashof number or Rayleigh number are referred to by name only in this chapter, the original works should be consulted for the exact definitions.

2.2 Fully–Developed Combined Convection in Vertical Ducts

Several workers have made theoretical investigations of the characteristics of hydrodynamically and thermally fully–developed laminar combined convection in vertical ducts. These limiting conditions are assumed to be approached asymptotically at axial distances far downstream of the duct entrance. The basic

assumptions of fully–developed flow and heat transfer and their implications are briefly examined below prior to reviewing the contributions in this area which cover both UHF and UWT boundary conditions. The simplified forms of the momentum and energy equations which apply to fully–developed conditions allow solutions to be obtained by exact analytical means. In published analyses for fully–developed combined convection it is commonly assumed that fluid properties are constant, except for density in the body force term of the momentum equation, which is treated as a linear function of temperature. Indeed, this assumption is a requirement for the establishment of strictly fully–developed conditions.

The fundamental postulate for a fully–developed flow is that the axial velocity profile is independent of axial distance. It follows from the continuity equation that the transverse velocity is zero everywhere and the flow streamlines are parallel to the duct walls. When $\partial u/\partial x$ and v are put to zero in the governing equations, the inertia terms are eliminated from the momentum equation and the convection terms of the energy equation reduce to $u(\partial T/\partial x)$. Using these simplified forms, it can be shown (e.g. Cheng et al, 1990) that the axial temperature gradient must be constant for any transverse position, including the ducts walls. This characteristic of thermally fully–developed flows implies that the normal temperature gradients at the walls, and hence the Nusselt numbers, also become constant under fully–developed conditions. It is noted that such invariance of the temperature profile is realised with fully–developed flows for both UHF boundary conditions, where $\partial T/\partial x$ is constant, and for UWT boundary conditions, where $\partial T/\partial x = 0$. Furthermore, it may also be demonstrated (e.g. Cheng et al, 1990) that a constant axial pressure gradient exists in fully–developed combined convection for the UWT boundary condition. This remains true for a duct with two walls (e.g. parallel plates) if one wall is at UWT and the other is insulated or subject to UHF, although $\partial P/\partial X$ is not constant for exclusively UHF boundary conditions. However, in the analysis of fully–developed combined convection for the latter condition, a constant pseudo–pressure gradient parameter is sometimes

employed for convenience.

Tao (1960a) pointed out that the energy equation is independent of the velocity field for fully–developed combined convection in a vertical duct with UWT boundary conditions. However, situations where the axial wall temperature gradient is constant, as encountered with UHF heating or cooling, present a more complicated problem because the energy and momentum equations remain coupled. In most analyses for UHF conditions these equations are combined to give a 4th–order differential equation. This equation is then solved in terms of elementary functions for flows between parallel plates or Bessel and associated functions for circular and annular duct flows. Tao (1960a), however, preferred a complex function method. In this approach, the momentum and energy equations are combined to give a Helmholtz wave equation (a 2nd–order equation) expressed in terms of a complex function with real and imaginary parts related to the velocity and temperature fields respectively. Tao (1960a) claimed that this alternative method is more direct and powerful than solving the usual 4th–order differential equation.

Sections 2.2.1–2.2.3 below are concerned with the literature on fully–developed laminar combined convection in vertical ducts for the circular, concentric annular and parallel plate geometries respectively.

It is noted in passing that other duct cross–section shapes have been treated, including rectangular (Tao, 1960a), circular sector (Lu, 1960; Tao, 1960b), triangular and rhombic (Aggarwala and Iqbal, 1969; Iqbal et al 1969) and rod bundle subchannels (Iannello et al, 1988). Del Giudice et al (1978) and Efthimiadis and Todreas (1985) presented methods for handling ducts with arbitrary cross–sections. These works, which employed a variety of mathematical techniques, are not further discussed in this survey.

2.2.1 Circular Tubes

Several analyses of fully–developed combined natural and forced laminar convection in a vertical circular tube with either UHF heating or cooling of the tube wall (equivalent to dT_w/dx = constant for fully–developed conditions) were published in the period 1950 − 1960, including works by Ostroumov (1952), Hallman (1956), Hanratty et al (1958), Brown (1960), Morton (1960) and Tao (1960). The UWT boundary condition is not of special interest in the context of fully–developed combined convection because buoyancy effects subside as the fluid temperature approaches that of the wall and the axial velocity profile and local Nusselt number assume the same shape and value respectively as found for pure forced convection.

Hallman's (1956) analysis for UHF cooling or heating also includes the effect of internal energy generation in the fluid. The velocity and temperature distribution solutions given for the zero heat source case are appropriate for buoyancy–aided flows only and are reported to be equivalent to those derived by Ostroumov (1952). The corresponding fully–developed Nusselt number versus Gr_q/Re predictions, which are well represented by $Nu_{fd} = 0.95\,(Gr_q/Re)^{0.28}$ for $400 \leq Gr_q/Re \leq 40\,000$, were subsequently compared with experimental data for water flowing upward in a uniformly heated tube (Hallman, 1961). Good agreement was achieved when all fluid properties were evaluated at the local film temperature, thus establishing the concept of "locally fully–developed" heat transfer. Experimental Nusselt numbers for downward heated flow (Hallman, 1961) were underestimated by the fully–developed analysis which took no account of either the wall temperature asymmetry or the unsteady flow observed in practice. Hanratty et al (1958), Brown (1960) and Morton (1960) used broadly similar methods to Hallman (1956) in their analytical treatments for UHF boundary conditions but presented solutions for buoyancy–opposed flow in addition to the buoyancy–aided case.

Velocity and temperature profiles predicted in the above studies for the buoyancy–aided case exhibit certain noteworthy peculiarities associated with the reversed flows which occur at high Rayleigh number to compensate for the accelerated wall flow. Flow reversal first appears at the tube centreline but for a sufficiently strong buoyancy effect the position of the maximum reverse flow velocity moves radially outward. In fact the solutions admit the possibility of a central core of positive velocity with a surrounding annular reverse flow. This is clearly shown in the velocity profiles presented by Hallman (1956), Brown (1960) and Morton (1960). Furthermore, the predictions of Hallman (1956), Hanratty et al (1958) and Brown (1960) show that the temperature distributions are also non–monotonic under reversed flow conditions.

Tao (1960b) used a previously developed complex function method (Tao, 1960a) to derive the variations of Nusselt number and pressure drop with Rayleigh number for fully–developed buoyancy–aided flow in a vertical circular tube with a constant axial wall temperature gradient.

2.2.2 Concentric Annuli

Although it is theoretically possible to specify any combination of UHF and UWT boundary conditions for the two walls of an annular duct it would appear from a search of the literature that only the former kind have been considered in analyses made for fully–developed combined convection in vertical annuli.

Sherwin (1968) analysed the case where the inner surface is uniformly heated and the outer surface is thermally insulated. Both upward and downward flows were considered. For the aiding flow case it was found that the effect of increasing the buoyancy parameter Gr_q/Re is to increase the velocity near to the heated surface, resulting in an improvement in the fully–developed Nusselt number. Above a certain value of Gr_q/Re it was predicted that a compensatory reversed flow would occur near to the insulated wall. Conversely, for opposed flow, Sherwin (1968)

predicted that Nusselt number decreases with increase in Gr_q/Re, due to the reduction in velocity adjacent to the heated wall, where a flow reversal occurs for a sufficiently strong buoyancy effect. The critical value of Gr_q/Re at the onset of flow reversal was found to be greater for aiding flow than opposed flow and decreased with the annulus radius ratio r* in both cases; this dependence being more marked in the latter case. The flow reversal criteria predicted theoretically by Sherwin (1968) were confirmed experimentally for downflow (Sherwin and Wallis, 1968) and upflow (Sherwin and Wallis, 1972) of water in an internally heated annulus (r* = 1/3) using flow visualization of injected dye streams. Except at the lowest Reynolds numbers, the experimental Nusselt numbers measured by Sherwin and Wallis (1968, 1972) fall higher than predicted by the fully—developed theory (Sherwin, 1968) and show a strong dependence of Nu on Re, suggesting that full development was not achieved. Furthermore, for downflow with heating, Sherwin and Wallis (1968) observed that the reversed flow regime eventually became unstable for high values of Gr_q/Re. The experimental Nusselt numbers determined under these unsteady conditions are generally much higher than the theoretical values and exhibit a contrary variation with Gr_q/Re.

Maitra and Subba Raju (1975) employed the same thermal boundary conditions as Sherwin (1968) in their analysis of buoyancy—aided flow which extended the available Nusselt number solutions to higher Rayleigh numbers and additional values of the annulus radius ratio r*. The same authors made local heat transfer measurements for water flowing upward in a concentric annulus (r* = 0.38) with uniform heating of the inner wall. Experimental Nusselt numbers for downstream positions, judged by Maitra and Subba Raju (1975) to exhibit fully—developed characteristics, are on average 45% higher than the theoretical values but show the same $Ra^{\frac{1}{4}}$ dependence. These deviations were attributed to flow unsteadiness resulting from instability of the distorted velocity profile.

Rokerya and Iqbal (1971) included the effect of viscous dissipation in their analysis for upward flows subject to constant heat input per unit length. Two cases were considered: (i) uniform heating at either the inner or the outer wall alone with the other wall adiabatic and (ii) both walls uniformly heated with equal temperatures. The non–linear system of governing equations was solved using a Runge–Kutta numerical integration method and results were presented for two values of the radius ratio, $r^* = 0.25$ and 0.5. In all cases studied, an increase in viscous dissipation, characterised by the Eckert number–to–Reynolds number ratio, had little effect on the velocity and temperature profiles but resulted in a reduction in Nusselt number which became more pronounced at higher Rayleigh numbers.

Kim (1985) showed that the general solutions for upward flows in concentric annuli with arbitrarily specified UHF heating imposed at each wall can be expressed as a combination of certain fundamental solutions which are independent of the ratio of the wall heat fluxes. Values of fundamental constants tabulated by Kim (1985) allow Nusselt numbers and pressure drops to be computed for any heat flux ratio over a wide range of radius ratio and Grashof number–to–Reynolds number ratio.

Iannello et al (1988) applied their analysis for azimuthally symmetric, fully–developed combined convection in uniformly heated vertical ducts to the case of aiding flow in an internally heated annulus. Friction factors and Nusselt numbers calculated for radius ratios in the range $r^* = 0.1$ to $r^* = 0.9$ were presented for a limited range of the Grashof number–to–Reynolds number ratio.

2.2.3 Parallel Plate Ducts

Fully–developed combined natural and forced convective flows in vertical parallel plate ducts have been analysed by Ostrach (1954), Hanratty et al (1958), Tao (1960), Rao and Morris (1968), Aung and Worku (1986b), Cheng et al (1990) and Hamadah and Wirtz (1991).

Ostrach (1954) analysed fully–developed combined natural and forced convection in fluids with and without heat sources in a channel with linearly varying wall temperatures. Hanratty et al (1958) presented analytical velocity and temperature profile solutions for buoyancy–opposed flow between parallel plates with UHF boundary conditions. The critical value of Grashof number–to–Reynolds number ratio for the velocity gradient to disappear at the wall agreed approximately with available experimental data. As an illustration of the complex function method, Tao (1960a) treated the case of fully–developed combined convection between equally heated plates having a constant axial wall temperature gradient. The analytical solutions presented, which are only valid for positive Rayleigh numbers, are written in terms of real functions of the Rayleigh number but no numerical results are given.

Rao and Morris (1968) obtained exact solutions for situations with one plate subject to a uniform heat flux and the other thermally insulated. Both buoyancy assisted and buoyancy–opposed flows were considered. Dimensionless velocity and temperature distributions were expressed in terms of the Rayleigh number and a pressure gradient parameter (interpreted as a Reynolds number). For buoyancy–assisted flows, the position of the maximum axial velocity was found to move closer to the heated or cooled wall as the Rayleigh number increased, leading eventually to flow reversal adjacent to the insulated wall for sufficiently high values of Ra. The associated friction factor–Reynolds number modulus f Re and the Nusselt number both increase steadily with Rayleigh number, the latter becoming proportional to $Ra^{\frac{1}{4}}$ at large values of the Rayleigh number. For buoyancy–opposed flows Nu and f Re were both predicted to decrease with Ra. Rao and Morris (1968) conjectured that the usefulness of the steady laminar solutions would be limited either by transition to turbulent flow or the onset of oscillatory flow.

Aung and Worku (1986b) considered the case of heated upward flow in a vertical parallel plate duct with the walls maintained at uniform, but not necessarily equal, temperatures. Under these conditions the fluid temperature varies linearly across the duct for asymmetric wall temperatures and is constant for the symmetric case. A general expression was derived for the axial velocity distribution in terms of the Grashof–to–Reynolds number ratio, expressing the buoyancy effect, and the ratio of the wall temperature differences, defined by $r_T = (T_{w1} - T_o)/(T_{w2} - T_o)$ where $T_{w2} \geq T_{w1}$ so that $0 \leq r_T \leq 1$. Aung and Worku (1986b) showed that for asymmetric wall temperatures (i.e. $r_T < 1$) velocities increase near the hotter wall and decrease near the cooler wall, the degree of profile skewness increasing progressively with increase in the buoyancy effect. The velocity profiles presented show that skewness is also promoted by a smaller value of r_T. A criterion was established for the onset of flow reversal adjacent to the cooler wall and it was deduced that since the duct centreline velocity assumes the value $U = + 1.5$ for all profiles, the transverse width occupied by any flow reversal region could not exceed the duct half–width. Furthermore, it was noted that for $r_T = 1$, the same unidirectional profile as found for pure isothermal forced convection is obtained, indicating that flow reversal is impossible in fully–developed flow for symmetric wall temperatures, irrespective of the strength of the buoyancy effect.

Cheng et al (1990) studied the characteristics of fully–developed buoyancy–assisted flows and presented velocity distributions, flow reversal criteria and Nusselt numbers for different combinations of UHF and UWT boundary conditions at the duct walls. The following combinations were considered: Case 1: UHF–UHF, Case 2: UHF–UWT and Case 3: UWT–UWT. Both symmetric and asymmetric situations were treated for Cases 1 and 3 and for Case 2 both finite and zero values of the UHF were considered. For Case 1 and the heat flux ratio $r_q < 0.053$, it was found that with increase of Gr_q/Re flow reversal first appears adjacent to the cooler wall. As Gr_q/Re is further increased, the fluid velocity adjacent to the wall recovers to be positive and the area of reversed flow moves

towards the duct centreline. For $r_q > 0.053$, reversed flow was only found to exist away from the walls. For Cases 2 and 3 reversed flow always occurs adjacent to the cooler wall. Cheng et al (1990) also found that the fully—developed Nusselt numbers depended on the thermal boundary conditions. For the special cases of equal wall temperatures and zero UHF—UWT, where the fluid temperature profile becomes uniform, the Nusselt numbers take the same values as in fully—developed forced convection. In all other cases, the effect of increasing the Grashof number—to—Reynolds number ratio is to increase the Nusselt number for the hotter wall and decrease the Nusselt number for the cooler wall. Apart from the addition of the Nusselt number information the results presented for Case 3 basically reiterate those obtained by Aung and Worku (1986b).

Hamadah and Wirtz (1991) made a similar study to Cheng et al (1990) for downward heated (i.e. buoyancy—opposed) flows where, in contrast to buoyancy—aided situations, the tendency is for flow reversal to occur near to the hotter wall. The sets of boundary conditions considered included those described as Case 1 and Case 3 above. In addition, the situation of one wall subject to uniform heating and the other maintained at the fluid inlet temperature was treated. Hamadah and Wirtz (1991) showed that the value of the Grashof number—to—Reynolds number ratio for incipient flow reversal in an opposed flow with UWT—UWT boundary conditions is identical to that established for the corresponding aided flow (Aung and Worku, 1986b).

2.3 Developing Combined Convection in Vertical Ducts

The theoretical solutions for fully—developed combined convection in vertical ducts, discussed in Section 2.2 above, are based on essentially one—dimensional treatments for the invariant hydrodynamic and thermal conditions which are postulated to exist far downstream. Nearer the duct entrance or the start of heating a development region exists where velocity and temperature profiles exhibit continuous change in at least two—dimensions. The term "developing" is

employed here to embrace two cases: (i) simultaneous hydrodynamic and thermal development, which in reality is always the case for combined convection, and (ii) the hypothetical case of thermally developing and hydrodynamically developed flow. The first attempts to obtain solutions for developing combined convection considered case (ii) above in order to make the problem amenable to the available analytical methods. However, the advent of computational modelling techniques has reduced the need for simplifications, allowing realistic and accurate numerical solutions to be obtained for flow and heat transfer throughout the development region, taking into account property variations.

Numerical investigations of developing combined natural and forced laminar convection in vertical ducts have been carried out using finite-difference methods. These studies can be broadly divided into the following two types, according to the method of solution employed:

(i)   marching solution methods, using either implicit or explicit finite-difference schemes, in which the solution is advanced step-by-step from the inlet to the exit of the duct.

(ii)   whole-field solution methods, in which the solution is computed at all grid points on the domain simultaneously, usually by an iterative relaxation technique.

Marching methods are usually, but not always, based on governing equations which are parabolic with respect to the marching direction (e.g. the boundary layer equations). Boundary conditions are not required to be specified at the duct exit plane. In general, marching can only be continued for as far as the flow remains unidirectional. However, several investigators have found it possible to march with parabolic equations for some distance beyond a point of flow reversal without failure of the solution. Furthermore, special approximations have been developed to permit marching computation to continue through small regions of recirculation. However, in general, elliptic conservation equations must be solved for recirculating flows or for situations where axial diffusion effects must be taken

into account. Whole—field solution methods are required for elliptic equations and boundary conditions must be specified on all sides of the domain considered.

Previous theoretical and experimental investigations into developing combined convection in circular tubes, concentric annuli and parallel plate ducts are considered in Sections 2.3.1, 2.3.2 and 2.3.3 respectively. For the theoretical studies discussed below, it should be assumed that unless some other duct entrance condition is mentioned the inlet velocity profile was considered to be uniform.

2.3.1 Circular Tubes

Approximate analytical methods were employed in the early attempts to quantify the effects of natural convection on laminar flows in vertical tubes.

Martinelli and Boelter (1942) obtained an approximate solution for aiding flow in a vertical tube maintained at UWT, neglecting inertia forces and convective heat transfer in the radial direction. The tube was considered to comprise an infinite number of short sections, each of which was treated by the method of Lévêque, which in essence assumes that the velocity gradient at the wall controls the rate of heat transfer. An equation was derived giving the average Nusselt number, based on the arithmetic mean temperature difference $(2T_w - T_{b_0} - T_{b_e})/2$, in terms of a Graetz number, defined as $(\pi/4)RePrd/L$, the product Gr_TPrd/L and correction factors for the use of the arithmetic mean temperature difference and the axial variation of buoyant force. Eckert and Diaguila (1954) modified the equation derived by Martinelli and Boelter (1942) for the opposed flow case, noting that this simply leads to a change of sign for the constant multiplying Gr_TPrd/L.

Jackson et al (1958) assumed that average heat transfer coefficients for aided combined convection in a vertical tube heated at UWT could be found from a slug flow approximation, given by $Nu_{lm} = 1.128 (RePrd/x)^{\frac{1}{2}}$, if $RePrd/x$ is calculated by summing contributions for the forced and natural convection effects. The

natural convection contribution, derived from a pressure—buoyancy force balance over the entire heated length L, was found to be proportional to $(Gr_T Pr^2 d/L)^{0.4}$. This simple analysis led to an equation which correlated the average Nusselt numbers (for a heated length from tube inlet to position x) measured by Jackson et al (1958) for upward flow of air in a steam heated tube more satisfactorily than the equation due to Martinelli and Boelter (1942).

Pigford (1955) analysed the same problem as Martinelli and Boelter (1942), using a broadly similar method, but allowed for a linear variation of $1/\mu$ with temperature in addition to density variation. Graphs were presented illustrating the effect of different values of the additional parameter μ_w/μ_0, ranging from 0 to 10, on the average Nusselt number for both pure forced convection and aiding combined convection. Rosen and Hanratty (1961) used the boundary layer integral method in their analysis for upward flow in a circular tube with the wall heated or cooled at UWT. A power series and an exponential series, respectively, were assumed for the velocity and temperature profiles and, following Pigford (1955), ρ and $1/\mu$ were treated as linear functions of temperature. The approximate analysis was found to satifactorily predict the position of flow reversals but, as conceded by Rosen and Hanratty (1961), it was rather poor in predicting heat transfer rates.

Bradley and Entwistle (1965) evaluated velocity and temperature profiles, Nusselt numbers and the friction factor times Reynolds number modulus for developed upward flow of air in a vertical tube cooled at UWT. Allowance was made for variations of all the fluid properties. The solutions were obtained by numerically integrating simplified forms of the momentum and energy equations which neglected the radial velocity component and also, in the first instance, axial conduction and momentum changes. When the latter two effects were included in the solution, axial momentum was found to be more significant than the conduction effect.

The earliest published numerical treatment of developing laminar combined convection in a vertical tube appears to have been made by Lawrence and Chato (1966). Their marching procedure uses an implicit finite–difference scheme and is suitable for both upward and downward flows with either a UHF or a UWT boundary condition. Lawrence and Chato (1966) computed developing velocity and temperature profiles, and the axial pressure variation for upward flow of water in a uniformly heated tube. They found that the inclusion of nonlinear functions to describe the temperature dependence of viscosity and density was necessary to obtain a good correlation with their experimental measurements. No numerical or experimental results are shown for the effect of natural convection on Nusselt number.

Marner and McMillan (1970) used a modified version of the numerical method introduced by Bodoia and Osterle (1962) to investigate vertical buoyancy–aided tube flows subject to UWT boundary conditions. A fully–developed inlet velocity profile was assumed. Arithmetic mean Nusselt numbers predicted for $Pr = 1$ and $Pr = 1000$ were compared with the analysis of Martinelli and Boelter (1942) which neglects inertia terms. As might be expected, the numerical results and the approximate theory agreed more closely for the higher Prandtl number, differences of up to 30% being observed for $Pr = 1$. The results obtained for $Pr = 1000$ also show that natural convection can increase the mean Nusselt number by as much as 52%, compared to the Graetz solution. The typical Nu_x variation presented by Marner and McMillan (1970) exhibits an increase with axial distance near to the position of maximum velocity profile distortion. This unusual behaviour was explained by reference to the developing velocity profiles, which show an increase in the wall gradient up to the point of maximum distortion.

Collins (1972, 1975, 1978, 1980) used a marching solution procedure, based on a set of implicit finite–difference equations, for the computation of developing combined convection in vertical tubes. Upward or downward laminar flows with heating or

cooling at UHF or UWT can be treated using his method which allows fluid property variations to be taken into account. A novel technique, introduced by Collins (1975), is the use of the integral energy equation as part of the analysis. This at once guarantees the energy balance and satisfies the wall thermal boundary condition. Rather unusually for a step—by—step solution method, Collins' model is based on the full elliptic equations for steady laminar axisymmetric flow of a quasi—incompressible fluid. Ingham et al (1988) commented that although the equations used in Collins' method contain terms representing axial diffusion, these effects cannot be adequately accounted for because no downstream information is fed into the marching solution. Notwithstanding this criticism, Collins (1972, 1975,1978,1980) has applied his method successfully to obtain stable solutions comparing favourably with experimental data and other theoretical work for a wide range of fluid and thermal conditions. The papers by Collins et al (1977) and Szpiro et al (1978) describe comparisons between experimental data for oil and water, and numerical solutions obtained by Collins' full treatment and a cylindrical coordinate version of the truncation technique of Allen and Finn (1970), outlined in Section 2.3.3. Both solution methods accommodated temperature—dependence of the fluid properties and the effects of property variations were assessed, both individually and in combination.

Collins' (1975) computer program, originally developed for tube flows, was modified by the present author for numerical studies of combined convection in parallel plate ducts (Szpiro, Lewis and Collins, 1984) and thermosyphon loops (Lewis, Collins and Allen, 1990). Further details of these developments are given in Section 4.1.

Brauer et al (1988) also applied a marching numerical procedure to solve the parabolic energy and momentum equations for upward flow in a vertical tube heated or cooled at UWT. A Crank—Nicolson finite—difference scheme was employed. The inlet velocity profile was considered to be fully—developed so that

the downstream development could be entirely attributed to the effects of natural convection. Axial variations of centreline axial velocity and bulk temperature are presented covering a wide range of Prandtl number from 0.1 to 10 000. The centreline velocity $U_{Y=0}$ versus x* results for aided flow show that an increase in Prandtl number accelerates the development of the central concavity in the axial velocity profile, although the values of x* and $U_{Y=0}$ (for a fixed value of the Grashof number–to–Reynolds number ratio) at maximum distortion appear to be unaffected. Heating of the bulk fluid is also improved by an increase in Pr and this is particularly evident around the point of maximum distortion. Brauer et al (1988) also presented flow reversal criteria for both aided and opposed flow and results in terms of local and mean Nusselt numbers and pressure drop.

The papers by Zeldin and Schmidt (1972), Shadday (1986), Morton et al (1989), Heggs et al (1990) and Kasz (1990) describe numerical investigations in which spatially elliptic equations, including terms for axial diffusion of both heat and momentum, were solved over the whole domain.

Zeldin and Schmidt (1972) employed both theoretical and experimental methods in their study of the effects of natural convection for upward heated flow of air. Their theoretical model assumed an infinitely long tube heated at UWT. Two different hydrodynamic conditions were considered at entrance to the heated tube: (i) uniform and irrotational and (ii) fully–developed. The elliptic governing equations were written in a dimensionless stream function–vorticity form and an axial coordinate transformation was applied so their finite–difference approximations could be solved on a finite computational domain. Comparison of the velocity profiles predicted for the two entry conditions at Re = 500, Gr_T = 240 shows that a central concavity develops in both cases. However, in the case of the fully–developed entry flow the minimum centreline velocity is higher and is reached further downstream. The corresponding local Nusselt number variations from the numerical study are also presented. Zeldin and Schmidt (1972) also

measured velocity and temperature profiles for upward flow of air at four axial locations in a heated vertical tube (L/d ≈ 104) with an inlet designed to produce a uniform velocity profile. The predicted and measured velocity profiles show substantial agreement.

On the basis of the elliptic governing equations and whole–field relaxation technique employed by Zeldin and Schmidt (1972) they should, in principle, have been able to obtain numerical solutions for reversed flows. However, they reported that their iteration algorithm could not be forced to converge in these cases. Furthermore, although axial diffusion of heat and momentum was included in their analysis, the upstream boundary considered in the theoretical model was assumed to coincide with the start of heating (x = 0). Consequently, axial heat conduction was prevented from exerting an influence for x < 0. In the discussion attached to their paper, Marner stated that for the reason given above the Nusselt numbers predicted by Zeldin and Schmidt (1972) for small positive values of x* are probably high. In more recent studies using elliptic conservation equations, discussed below, the latter problem has been overcome by including an adiabatic or isothermal section upstream of the start of heating. In addition, converged solutions have now been obtained for situations involving streamwise flow reversals.

Shadday (1986) used an explicit scheme to solve the time–dependent, Navier–Stokes equations, written in vorticity–stream function form, for upward laminar flow in a heated vertical tube. A heat transfer section approximately 15 diameters long with a UWT boundary condition was considered. The computational domain also included an isothermal entrance region and an adiabatic exit section. Fully–developed velocity profiles were specified at entry and exit. Streamline and isotherm maps are presented for Re = 200 and Pr = 6.5 at two values of Grashof number. In both cases the streamline patterns show a central core of stagnant fluid with net axial fluid transport confined to a thin wall

boundary layer. For the higher Grashof number, the predicted flow field was unsteady, with Tollmein–Schlichting waves clearly evident in the boundary layer. The time–dependent solutions for this case revealed that the vortices which were periodically shed from the boundary layer were eventually dissipated in the central core region. Shadday (1986) stated that the large–scale vortices predicted by his model were, in qualitative terms, strikingly similar to those observed experimentally by Scheele and Hanratty (1962). Local Nusselt number and friction factor distributions, evaluated from the time–averaged temperature and velocity fields, are also presented.

Morton et al (1989) conducted an experimental and numerical investigation into situations where buoyancy–induced recirculation occurs for laminar flow in a vertical tube, with finite axial sections maintained at uniform wall temperatures. Flow visualisation experiments were performed for upward flow of water in a perspex tube with adjacent heated and cooled sections. Two cases were investigated: (i) cooling followed by heating and (ii) heating followed by cooling. The flow patterns were made visible by adding aluminium powder to the water and photographed for comparison with numerically predicted streamline contour plots. As anticipated, for case (i), cooling resulted in a flow reversal near the tube wall. This disappeared further downstream, in the heated section, where a reversed flow occurred near the centre of the tube. For case (ii), heating followed by cooling, the order in which these same effects occurred was reversed. In the parallel numerical study Morton et al (1989) assumed steady axisymmetric laminar flow and used the stream function–vorticity form of the governing elliptic partial differential equations, including axial diffusion terms but ignoring viscous dissipation. In addition to the heat transfer sections, the model included a finite entry section with a UWT equal to that of the fully–developed entry flow. Furthermore, the downstream heat transfer section was extended to infinity, using the same axial coordinate transformation employed by Zeldin and Schmidt (1972), so that the assumed fully–developed isothermal exit conditions would be satisfied.

The location, size and shape of the recirculation regions observed experimentally were quite accurately predicted by the numerical model.

Heggs et al (1990) studied the problem of developing combined convection in a vertical tube with conjugate wall conduction. The case of an upward heated flow was considered and the model studied comprised an entry section of finite length followed by a heated section extending to infinity in the axial coordinate. Fully—developed isothermal conditions were specified at both entry and exit. Thermal boundary conditions of UWT and zero heat flux were applied at the outside surface of the tube wall in the heated section and the entry section respectively. The numerical techniques employed by Morton et al (1989) were extended to allow the elliptic governing equations for the solid and fluid solution domains to be treated simultaneously. Numerical solutions were obtained for water (Pr = 7.0) at Re = 100 and values of k_w/k in the range of 0.5 to 50, and values of d_{w_o}/d_{w_i} in the range 1.1 to 1.4. The Grashof number was fixed at a sufficiently large value so that flow reversals occurred for most cases investigated. The results show that significant upstream heating of the fluid occurs by axial wall conduction at high values of k_w/k, accelerating the onset of flow reversal. In contrast, at low values of k_w/k the wall acts more like an insulator, restricting heating of the fluid and thus resulting in less rapid development of the velocity profile. These effects become more pronounced as the ratio d_{w_o}/d_{w_i} increases.

An unpublished paper by Kasz (1990) gives details of a numerical study made for an upward heated flow subject to a UWT thermal boundary condition. The domain considered for the developing flow was semi—infinite, extending to infinity both upstream and downstream from the start of heating. An axial coordinate transformation was applied to map the governing elliptic equations, formulated in terms of stream function and vorticity, into a finite domain for the finite—difference solution. Unsteady terms were added to the vorticity and energy equations which were then solved using an alternating direction implicit (ADI)

scheme. The stream function was solved for using the successive over-relaxation (SOR) technique. Kasz (1990) presents results for $Pr = 10$, $Re = 1$ and $Gr_T = 1000$. Under these conditions Gr_T/Re is well above the threshhold value for the onset of flow reversal and the results exhibit a recirculation at the entrance to the heated section, which even extends into the unheated entry section. The temperature field results show preheating of the fluid, reflecting the inclusion of axial heat conduction terms in the analysis.

Early experimental investigations into combined natural and forced convection in vertical tubes were conducted with apparatus of the double-pipe heat exchanger type. In this form of equipment, the test fluid flows through the central pipe and is heated (usually by steam) or cooled by a secondary heat transfer fluid supplied to the surrounding annulus at a heat capacity rate sufficient to produce a thermal boundary condition approximating to UWT. Martinelli et al (1942) compared their experimental heat transfer data for upward flow of oil and water in steam heated tubes (L/d from 126 to 602), and the data of Watzinger and Johnson (1939) for downflow of water in a cooled tube ($L/d \approx 20$), with the analytical equation of Martinelli and Boelter (1942). The equation correlated all the data to within $\pm 20\%$ when the $Gr_T Pr d/L$ exponent was raised from the theoretically predicted value of 0.75 to 0.84. The experiments by Jackson et al (1958) and Zeldin and Schmidt (1972), already referred to above, were also designed to furnish information on combined convection under UWT conditions.

Data for laminar combined convection obtained from experiments performed using electrically heated vertical tubes, giving an approximately UHF thermal boundary condition at the wall, are reported by Hallman (1961), Kemeny and Somers (1962), Lawrence and Chato (1966), Petukhov et al (1969), Collins, Allen and Szpiro (1977) and Barozzi, Dumas and Collins (1984).

Hallman (1961) made measurements for water flowing in a vertical uniformly heated test section (L/d ≈ 115). Unheated starting lengths were employed for both upflow (x_a/d ≈ 115) and downflow (x_a/d ≈ 13) tests. Local Nusselt numbers measured near the start of heating verify constant–property analytical predictions for thermally developing and hydrodynamically developed pure forced flow under UHF conditions. Sample Nu_x versus x^* distributions from two upflow tests, presented in Hallman's report, show an increase of Nu_x with Gr_q/Re, at a fixed x^*. This effect of buoyancy becomes more marked as x^* increases. Moreover, instead of decreasing monotonically, in a manner characteristic of pure forced convection, the experimental Nu_x values for each test exhibit a minimum followed by an increase further downstream. Hallman (1961) found that the upflow data obtained for large x^* under steady laminar conditions approached his fully–developed theory (Hallman, 1956) applied locally with all fluid properties evaluated at the local film temperature. His upflow data also show an initial decrease in the length of the thermal entrance region L_{th}^* as Gr_q/Re is increased, followed by a rise in L_{th}^* at higher values of Gr_q/Re. The downflow tests were characterised by asymmetry in wall temperature, which became more severe with increase in either x/d or Gr_q/Re, and at the highest heat fluxes by unsteadiness. Hallman (1961) speculated that these wall temperature variations suggested a cell flow near the bottom of the tube and, not surprisingly, the corresponding experimental Nusselt numbers were underpredicted by his fully–developed analysis.

Kemeny and Somers (1962) obtained pressure drop and local heat transfer data for upward flows of water (Pr ≈ 3 − 6) and transformer oil (Pr ≈ 80 − 170) using four test sections with different diameters (L/d from 64 to 384) and sharp–edged entrances. The data cover Reynolds number ranges from 61 to 3000 for water and 3.4 to 630 for oil. The local Nusselt number, evaluated on the somewhat unconventional basis of local wall–to–inlet bulk temperature difference ($T_{w_x} - T_{b_0}$), were plotted against Gr_q/Re with $1/x^*$ as a parameter on each curve.

The experiments conducted by Lawrence and Chato (1966), alluded to above, included measurements of pressure drops, temperature profiles and tube centreline velocities for water flowing upward in a uniformly heated vertical tube (L/d ≈ 203). The entrance to the heated test section was designed to give a uniform velocity profile. Experimental Nusselt numbers do not appear to have been evaluated.

Petukhov et al (1969) made local heat transfer measurements for heating of distilled water flowing vertically upwards. Two uniformly heated test sections were employed (L/d ≈ 99 and L/d ≈ 80). An isothermal calming length equal to 96 diameters was provided at inlet to the L/d ≈ 99 heated section. The local Nusselt numbers were correlated within ± 8% by an equation which can be written as follows: $[Nu_x/Nu_{x_F}] = [1 + (Gr_q/Re)/B]^{0.27}$, where B is a function of x^*, given by $B(x^*) = 5.4/x^* + 312 x^{*0.25}$ for $x^* \leq 0.07$ and $B(x^*) = 240$ for $x^* \geq 0.07$. In this equation all fluid properties are evaluated at the local bulk temperature. Nu_{x_F} is the local Nusselt number for constant–property, pure forced convection under UHF conditions at the same value of x^* and with the same hydrodynamic inlet condition (i.e. either a fully–developed or a uniform velocity profile). The correlation obtained by Petukhov et al (1969) was stated to be valid for the following parameter ranges covered by the data: $10^3 \leq Gr_q/Re \leq 4 \times 10^5$, $250 \leq Re \leq Re_{cr}$, $4 \leq Pr \leq 6$ and $3 \times 10^{-4} \leq x^* \leq x^*_{cr}$ where Re_{cr} and x^*_{cr} are the critical threshold values measured for instability of the buoyancy–aided flow.

To the present author's knowledge, only a few comparisons between numerical solutions for developing combined convection in vertical circular tubes and experimentally determined local heat transfer data are contained in the literature. The papers by Collins, Allen and Szpiro (1977) and Barozzi, Dumas and Collins (1984) are notable exceptions. As previously mentioned, the study by Collins et al (1977) utilsed two different numerical methods; those due to Collins (1975) and Allen and Finn (1970), which both allowed fully for fluid property changes. Nusselt

number predictions were made for comparison with experimental data from the authors' own tests for upward flow of oil in a uniformly heated vertical tube ($L/d \approx 51$) preceded by an unheated section ($x_a/d \approx 51$). Further comparisons were made with published experimental data, including the measurements of Kemeny and Somers (1962) for oil and those of Scheele and Hanratty (1962) and Lawrence and Chato (1966) for water. Barozzi et al (1984) obtained local Nusselt number data for upflow of water in a uniformly heated vertical tube ($L/d \approx 100$) under strong combined convection conditions. The heat transfer data presented are for $412 \leq Re \leq 938$, $3.78 \leq Pr \leq 4.96$ and $1487 \leq Gr_q/Re \leq 6120$ where all properties are evaluated at the average bulk temperature T_{b_m}. Sample comparisons were made between the experimental data and predictions obtained by Collins' (1975) finite–difference procedure, including variations of both ρ and μ. Close agreement was achieved except at small and large values of x^*, where deviations were attributed to a sharp–edged entry effect and transition from laminar flow respectively.

Additional data for combined natural and forced convection heat transfer in vertical tubes was reported by W.G.Brown (1960) and C.K.Brown and Gauvin (1965a, 1965b), although the wall thermal boundary conditions appear to be less well defined for their experiments. The data obtained by Brown (1960) are for water and cover heating and cooling in upflow and cooling in downflow. Detailed temperature profiles are presented for each case. The two companion papers by Brown and Gauvin (1965a, 1965b) deal with heat transfer to air at low velocities for upward flow and downward flow respectively. They presented limited data for the laminar flow regime.

2.3.2 Concentric Annuli

All theoretical treatments of developing combined natural and forced convection in vertical annular ducts found in the literature utilise some type of marching finite–difference calculation procedure.

Sherwin and Wallis (1970) studied the development of an initially fully–developed downward flow in a $r* = 1/3$ vertical concentric annulus with UHF heating at the inner surface and the outer surface maintained adiabatic. The implicit finite–difference scheme employed was found to remain stable well into the region of reversed flow where a large increase in magnitude of the positive radial velocities was calculated. The predicted axial locations for the onset of reversed flow under developing conditions are in good agreement with the observed behaviour for water reported by Sherwin and Wallis (1968), and for large axial distances the critical value of Gr_q/Re for flow reversal closely approaches the value given by fully–developed combined convection theory (Sherwin, 1968). In a later study, for heated upflow of water with the same initial and boundary conditions, and radius ratio, Sherwin and Wallis (1972) used the same computational method to detect the point where the calculated radial velocity profile became unstable as the gradient of the axial velocity profile on the unheated wall approached zero. They interpreted such an occurrence as indicating the onset of unstable flow and found the predicted positions to be in reasonable agreement with their experimental observations.

In a thesis, Ogunba (1972) presented a marching finite–difference procedure for the computation of developing combined laminar convection flows in vertical annuli. Variations of density, viscosity and thermal conductivity were allowed for throughout the governing equations. Although radial pressure variation was neglected, terms for viscous dissipation and axial diffusion (both momentum and heat) were retained. The inclusion of the latter elliptic influences may in fact have been the reason why the numerical solution failed for $Re < 25$, although Ogunba (1972) attributed this to the neglect of radial pressure variation. In contrast, Ogunba (1972) reported that he was able to obtain stable solutions in the case of an internally heated annulus ($r* = 0.25$) beyond the point where a flow reversal was predicted at the outer wall.

A novel feature of Ogunba's (1972) solution procedure is the piecewise treatment given to the global mass flow constraint equation. The same idea has been adopted and extended for the computational method presented in Chapter 3. The experimental work conducted by Ogunba (1972) is discussed later in this section.

El–Shaarawi and Sarhan (1980) used an implicit scheme in their study of annuli with one wall isothermal and the other adiabatic and also encountered unexpected numerical stability beyond the flow reversal point under certain conditions. The results presented are for $Pr = 0.7$, $r* = 0.9$ and 0.5, and cover both aided and opposed flows, including situations where a flow reversal occurs in the development region near to the insulated wall or the heat transfer surface respectively. For a fixed value of Gr_T/Re, it was found that the axial distance to flow reversal decreases as $r*$ increases and, for a given radius ratio, it has the lowest value when the UWT boundary condition is prescribed at the (larger) outer surface. Computations covering the full development length, until a fully–developed isothermal velocity profile is established, indicate that the hydrodynamic development length increases with the parameter Gr_T/Re. For the boundary conditions considered by El–Shaarawi and Sarhan (1980), the local Nusselt number for fully–developed combined convection is the same value as found for $Gr_T/Re = 0$ (i.e. pure forced convection). However, in the development region the values of Nu_x for aided and opposed flows are respectively higher and lower than for $Gr_T/Re = 0$.

The numerical studies of developing combined convection in vertical annuli made by Malik and Pletcher (1980), Zenen et al (1985), Hashimoto et al (1986) and Aung et al (1991) take account of fluid property variations in addition to the essential density variation in the body force term. Malik and Pletcher (1980) presented an explicit finite–difference scheme for the computation of axisymmetric, variable–property laminar and turbulent convection in annular

passages. Local Nusselt number predictions for laminar upflow with UHF heating at the inner surface only were compared with experimental data obtained by Maitra and Subba Raju (1975) for water in a concentric annulus ($r* = 0.38$) and Joshi and Bergles (1978) for ethylene glycol in a high aspect ratio rectangular duct (see Section 2.3.3). A fully–developed inlet velocity profile was assumed. For water, only density variation in the body force term was considered, whereas, all properties were varied for ethylene glycol. Malik and Pletcher (1980) also predicted the axial position for the onset of reversed flow near the unheated wall, commenting that for ethylene glycol this location appeared to be best correlated by the parameter Gr_q/Re^2 which, unlike Gr_q/Re, remained fairly constant along the duct. Zenen et al (1985) utilised a modified version of the numerical method developed by Collins (1980) for combined convection in circular tubes, discussed in Section 2.3.1 above. Results were obtained for upward heated and downward cooled flows of 37% ethylene glycol–water solution, accommodating variable viscosity and natural convection effects. Axially varying wall temperature boundary conditions were considered at the outer surface with the inner surface insulated. For design purposes, Zenen et al (1985) correlated the predicted Nusselt numbers in terms of Graetz number, Grashof number and further dimensionless functions expressing the effects of entry, viscosity variation and variable wall temperature respectively. Hashimoto et al (1986) obtained numerical solutions for upward and downward flows in a vertical annulus of $r* = 0.9$. The inner wall was subject to UHF or UWT heating and the outer wall was treated as an adiabatic boundary. The fluid, helium gas with $Pr = 0.671$, was treated as incompressible and temperature dependence of the fluid properties, including density, was approximated by power law relations throughout the governing equations. Property variation was represented in terms of an additional problem parameter, either T_w/T_0 (for UWT heating) or $q_w d_h/k_0 T_0$ (for UHF heating), and was found to exert a rather slight influence on heat transfer coefficient and friction factor. However, for a fixed value of the Grashof number–to–Reynolds number ratio, Hashimoto et al (1986) found that with increase in T_w/T_0 or $q_w d_h/k_0 T_0$ flow

reversal is delayed and eventually disappears altogether. Aung et al (1991) studied the effects of temperature–dependent fluid properties on forced and combined convection heat transfer for upward gas flow in a vertical concentric annulus of $r^* = 0.25$. Uniform heat flux heating was prescribed at the inner wall and the outer wall was assumed to be heated at UHF or insulated. The fluid considered was air, which was treated as an ideal gas with $Pr = 0.72$. Accordingly, density was related to temperature and pressure through the equation of state and enthalpy was taken as a function of specific heat and temperature. Viscosity, thermal conductivity and specific heat were approximated by power law functions of temperature. For the UHF boundary conditions studied, it was found that for forced convection the overall effect of fluid property variations is to reduce both radial and axial temperature gradients. However, the consequent increase in local Nusselt number is less marked because of an increase in thermal conductivity. For combined convection with variable properties, Aung et al (1991) showed that buoyancy reduces wall temperatures, and enhances local Nusselt numbers, except near the entrance or far downstream where these effects were found to be negligible. Other results from this study are discussed in the paper by Moghadam et al (1990).

Details of the implicit finite–difference numerical method used by Aung et al (1991) and Moghadam et al (1990) are given by Moghadam and Aung (1990).

Heggs et al (1988) computed local Nusselt and bulk temperature distributions for upward flow, with the fluid ($Pr = 0.72$) entering at a temperature midway between the UWT conditions maintained at the inner and outer walls. The range of conditions investigated includes situations where asymmetry of the wall temperatures is sufficient to cause reversed flow adjacent to the colder wall. The computational method applied was adapted from that originally used by Ingham et al (1988a, 1988b) for combined convection flows in parallel plate ducts containing regions of reversed flow (discussed in Section 2.3.3 below). The cases of the inner wall hotter than the outer wall and vice versa were both considered.

The numerical study performed by Rao and El–Genk (1990) to predict the onset of buoyancy–induced instability in vertical annuli with internal UHF heating included a comparison between solutions based on the boundary layer approximations and other sets of equations involving elliptic terms. Further discussion of this work is deferred to Section 2.4.2.

Although developing combined convection in vertical annuli has been subject to fairly extensive theoretical investigation a comparatively small amount of experimental information is available.

The experimental apparatus used for upflow and downflow tests with water by Sherwin and Wallis (1968, 1972) comprised a vertical annulus of $r* = 1/3$ and $L/d_h \approx 48$, with UHF heating at the inner wall only. Unfortunately, although the heated surface was instrumented for local wall temperature measurements, the experimental Nusselt numbers presented are based on the difference between the mean bulk fluid temperature and the mean heated surface temperature. It does not seem surprising, therefore, that these experimental heat transfer results show a marked increase with Reynolds number, only approaching the theoretical predictions for fully–developed conditions (Sherwin, 1968) at the smallest value of Re used in the tests.

Rao and Barrow (1972) and Ogunba (1972) both obtained local heat transfer data for water in upflow in annular test sections with UHF heating at the inner wall. The experimental set–up used by Rao and Barrow (1972) had a radius ratio close to unity since it was intended to simulate a parallel plate system and consequently their results are discussed in Section 2.3.3. Ogunba (1972) used an annulus of $r* = 0.25$ and $L/d_h \approx 24$. His experimental local Nusselt numbers exhibit a continuous decrease with axial distance for all Grashof numbers, indicating that fully–developed conditions were never attained in the relatively short test section. Furthermore, Ogunba (1972) found that his numerical scheme underpredicted the

experimental Nu_x data, particularly at higher values of Gr_q. Ogunba (1972) also used the hydrogen bubble technique and photographic recording to determine the effect of buoyancy on the velocity distribution at five equally–spaced axial locations in the heated developing flow. The experimental and numerically predicted velocity profiles compare favourably. A description of this velocity measurement technique and some sample velocity profiles and Nusselt numbers are given by Ogunba and Barrow (1979).

Okuno and Sugita (1973) made heat transfer measurements for water flowing upward through a short vertical annular duct ($r* = 0.295$, $L/d_h \approx 16$) preceded by an adiabatic entrance section ($x_a/d_h \approx 11$). The inner surface was cooled by water flowing through the central pipe and the outer surface was heated by a surrounding warm water jacket. Flow length average heat transfer coefficients, based on the net heat transfer to the fluid and the difference between the wall temperatures, determined for positions in the downstream two–thirds of the test section, were correlated by a dimensionless equation giving the mean Nusselt number in terms of Re, Pr, x/d_h, μ_b/μ_{w_1}, μ_b/μ_{w_2} and Grashof number (also based on the difference in the wall temperatures). The data cover a range of Re from 30 to 200 and Grashof numbers from 1.4×10^7 to 9.9×10^7, although the effect of natural convection was stated to be not too pronounced.

The local heat transfer measurements of Maitra and Subba Raju (1975), referred to earlier in this section and in Section 2.2.2, were obtained with water flowing upward in a vertical annulus ($r* = 0.38$, $L/d_h \approx 83$) with UHF heating at the inner wall. Experimental data were obtained for Reynolds numbers from 200 to 1200. The typical local Nusselt numbers presented by Maitra and Subba Raju (1975) show a marked increase with Rayleigh number and indicate that fully–developed conditions are attained at much shorter axial distances for combined convection than for forced convection.

El–Genk et al (1986) reported Nusselt numbers measured at a single axial location ($x/d_h \approx 29$) for upflow of water in a vertical annulus ($r* = 0.854$, $L/d_h \approx 52$) with UHF heating at the inner wall and an adiabatic outer wall. Their data for natural laminar and natural and forced laminar flows, also discussed in the paper by Zaki et al (1985), exhibit a variation with Rayleigh number in reasonable agreement with the fully–developed combined convection theory of Maitra and Subba Raju (1975), but also show a clear dependence of Nu on Re. In a later series of experiments, El–Genk and Rao (1989) used another internally heated annular test section ($r* = 0.5$, $L/d_h \approx 71$) to collect local heat transfer data for water at seven axial locations for developing upflows and at four axial locations for developing downflows. The new data for $r* = 0.5$ and the data for $r* = 0.854$ obtained in the earlier study (Zaki et al, 1985; El–Genk et al, 1986) were used to develop a general correlating equation for the natural, combined and forced laminar convection regimes.

2.3.3 Parallel Plate Ducts

Early theoretical treatments of developing combined convection flows in vertical parallel plate ducts used approximate analytical methods. Savkar (1970) neglected the inertia terms in the momentum equation and linearised the convective terms of the energy equation as $\gamma^2\theta$, where γ depends on the axial coordinate only. Upward fully–developed flow was assumed at entry and situations with UHF heating imposed at both plates or at one plate with the other adiabatic were considered. The results exhibit some non–physical behaviour but are consistent with fully–developed solutions (e.g. Rao and Morris, 1968) and indicate that the axial distances required for thermal development and for a point of inflexion to form in the velocity profile reduce as Rayleigh number increases. Quintiere and Mueller (1973) used a slug–flow linearisation of the convective terms in the momentum and energy equations to obtain a tractable problem for upward flow with symmetric UWT heating. Results were presented relating the average Nusselt number and the applied pressure gradient to the flow rate and the Rayleigh

number for $Pr = 0.7$. Sitharamarao and Barrow (1972) modelled the entry region between vertical plates at uniform wall temperature by considering the effects of natural convection on a flow parallel to a single vertical plate in an infinite medium. A varying free–stream velocity of the form $u_\infty \propto u_0 x^m$ was assumed, where m is a constant chosen to simulate the acceleration of the potential core in the duct. Similarity solutions were obtained for both aiding and opposed flows, with $Pr = 0.72$, 1.0 and 5.0, by taking the first–order approximation given by perturbing the solution of the pure forced convection problem. The solutions only apply for a marginal natural convection contribution. More recently, Yao (1983) analysed combined convection for upward flow in the entry region of a heated vertical duct by considering the effect of buoyancy as a perturbation on the developing flow in an unheated channel. This analysis is only valid near the duct entrance where the influence of natural convection is small. Axial length scales were identified for the various regions traversed by developing flows under symmetric UWT and symmetric UHF boundary conditions.

Allen and Finn (1970) devised an approximate numerical technique to calculate developing temperature and velocity profiles for high Prandtl number fluids flowing through uniformly heated ducts, making due allowance for the effects of property variations, including buoyancy forces. In this approach, which utilises only fully–developed forms of the momentum and energy equations, thermal boundary layer development is approximated by a series of truncated versions of the fully–developed temperature profile. The corresponding velocity profiles are subsequently computed by a finite–difference method and axial distances are found from the energy balance equation using the bulk temperature rise. Predictions made for transformer oil flowing upward in a short duct, heated from one side only, are in excellent agreement with the average wall temperature measurements of Allen and Finn (1970).

Dalbert (1982) investigated the natural, combined and forced convection regimes of developing, laminar, upward and downward flows in a vertical duct with uniform heating at one or both walls. A fully–implicit finite–difference technique developed in earlier work (Dalbert et al, 1981) was used. The results presented are mainly for the symmetric heating case and give the dimensionless pressure drop over a wide range of Reynolds number and Grashof number. The Prandtl number is not stated. Szpiro, Lewis and Collins (1984)[1] compared the approximate numerical method of Allen and Finn (1970), described above, with a modified version of the marching finite–difference procedure for tube flows developed by Collins' (1980) (see Section 2.3.1). The modifications, which were required to allow computations for the parallel plates geometry, were made by the present author. Numerical solutions were obtained for two upward flows: ethylene glycol ($Pr_0 = 172.2$) with symmetric UHF heating and transformer oil ($Pr_0 = 406.4$) with UHF heating at one plate only. Temperature dependence was allowed for in all fluid properties. Good agreement was achieved for the developing velocity profiles but the approximate method gave consistently lower Nusselt numbers, which could be attributed to the truncated temperature profiles assumed. Habchi and Acharya (1986) used the Spalding–Patankar marching procedure for parabolic systems (see Patankar, 1988) to compute developing temperature and axial velocity profiles and local Nusselt number distributions for air flowing upward in a parallel plate duct. Symmetric UWT heating as well as the case of one plate heated at UWT and the other adiabatic were treated. The computations spanned the complete development region from extreme entry, through maximum velocity profile distortion up to fully–developed conditions. No flow reversals were predicted for the range of parameters considered.

The results of an important study of developing laminar combined convection for vertically upward flow in a parallel plate duct were described in two parts; dealing

---

[1]A copy of this paper is included in Appendix G.

separately with UWT (Aung and Worku, 1986a) and UHF (Aung and Worku, 1987) boundary conditions. The numerical results presented, which are for $Pr = 0.72$ and cover symmetric and asymmetric heating for both kinds of boundary conditions, were obtained by a marching finite–difference procedure developed for pure natural convection duct flows (Aung et al, 1972). The results obtained by Aung and Worku (1986a) for UWT boundary conditions show that buoyancy can strongly distort the axial velocity profile in the development region, with a central concavity forming as the less–dense fluid near the heated walls is accelerated. For equal wall temperatures, this concavity is gradually eliminated downstream as the velocity profile assumes the fully–developed parabolic form. Aung and Worku (1986a) found, however, that the corresponding hydrodynamic development length under combined convection conditions is longer than for pure forced convection and increases dramatically with an increase in the Grashof number–to–Reynolds number ratio. For asymmetric wall temperatures ($r_T < 1$) the velocity profiles presented also exhibit skewness as the fluid is drawn toward the hotter wall. Aung and Worku (1986a) state that for $r_T < 1$ profile distortion eventually reduces with increase in X, although the concavity never completely disappears. For cases where a flow reversal was predicted in the developing flow, the point of separation occurred at shorter axial distances as r_T was reduced for a fixed value of the buoyancy effect parameter. For conditions where the marching procedure used by Aung and Worku (1986a) permitted stable solutions to be obtained up to large axial distances, including one particular situation where the fully–developed flow was mildly bidirectional, the predicted velocity profiles and axial pressure gradient are in excellent agreement with the fully–developed theory of Aung and Worku (1986b). In contrast to the predicted increase in the hydrodynamic development length, the heat transfer results show that an increase in buoyancy reduces the thermal entry length, as indicated by a more rapid rise in bulk temperature, but only mildly affects the average Nusselt numbers at both walls.

In contrast to UWT boundary conditions, for which the fluid temperature profile develops to become either uniform or linearly varying between the walls, UHF conditions give rise to a continuous axial variation of fluid temperatures, albeit that $\partial T/\partial x$ eventually becomes constant. The numerical study made by Aung and Worku (1987) of developing combined convection for UHF conditions showed the influence of buoyancy on developing velocity profiles, axial pressure distribution and heat transfer to be less than for UWT conditions. Aung and Worku (1987) concluded that flow reversal is more prone to occur for UWT than UHF conditions and reported that no flow reversals were predicted for the latter case in the range of Gr_q/Re investigated, at any value of r_q. This finding was supported by Cheng et al (1990) who noted that for the ranges of parameters studied by Aung and Worku (1987) no flow reversals occur in fully–developed combined convection.

Cebeci et al (1982) and Ingham et al (1988a) developed numerical methods for handling vertical duct flows containing a buoyancy–induced flow reversal. Both methods are based on parabolic equations. In order to allow forward–marching computation to proceed stably either the FLARE approximation (see Cebeci and Bradshaw, 1984; Anderson et al, 1984) is incorporated (Cebeci et, 1982), whereby streamwise convective terms are neglected for the reverse flow region, or a similar technique is used which insists that no negative streamwise velocities are used in the marching calculations (Ingham et al, 1988a). Cebeci et al (1982) and Ingham et al (1984a) considered the development of aiding and opposed flows under symmetric UWT boundary conditions for $Pr = 0.72$. For a sufficiently strong buoyancy effect these flows can be bidirectional in the developing region but, as shown by Aung and Worku (1986b) and also noted above, the fully–developed velocity profile for symmetric wall temperatures is unidirectional and parabolic. In other respects, different approaches were used in these two studies. Cebeci et al (1982) employed a modified Falkner–Skan transformation of the governing boundary layer equations near the duct entrance, changing to physical coordinates

before the calculated shear layers merged. An inverse boundary layer finite–difference procedure employing the Box differencing scheme (see Cebeci and Bradshaw, 1984; Anderson et al, 1984) was used. The results presented by Cebeci et al (1982) only feature flow reversal situations for opposed flow. In these situations a more rapidly decreasing Nusselt number and a more rapidly increasing pressure drop were predicted downstream of the flow separation point which moved upstream with an increase in buoyancy. This study is also described in the book by Cebeci and Bradshaw (1984). Ingham et al (1988a) formulated the problem in terms of a dimensionless stream function, vorticity and temperature and expressed the governing parabolic equations in an implicit finite–difference scheme. For situations where the developing flow remains unidirectional, a straightforward marching solution procedure was used and Ingham et al (1988a) obtained results in good agreement with Aung and Worku (1986a). A modified technique was employed for situations where buoyancy–induced recirculation occurs over some portion of the duct length, near either the duct centreline (aided flow) or the duct walls (opposed flow). When flow reversal was encountered, Ingham et al (1988a) invoked the approximation mentioned above to maintain stability as the marching solution was advanced thoughout and a few extra steps beyond the reversed flow region. The approximate solution formed in this manner was refined by applying an iterative procedure over the recirculation region. This calculation involved marching backwards in the reverse flow region only and forwards in the forward flow region only until convergence was achieved. Numerically predicted velocity profiles, Nusselt numbers, friction factors and bulk temperature distributions are presented. Ingham et al (1988b) carried out a similar study for asymmetric UWT boundary conditions using the same numerical technique. In this case the fully–developed flow can be bidirectional, and for such situations it was necessary to continue marching well into the fully–developed region before the iterative procedure was carried out.

The three studies discussed next were based on spatially elliptic governing equations. Tjelflaat and Ytrehus (1981) studied a downward cooled flow between walls at different but uniform temperatures and with a discontinuity in the inlet fluid temperature profile at the duct centreline. This flow contained a region of reversed flow and was described by the Navier–Stokes equations in quasi–incompressible, constant property form. Asymptotic (steady–state) solutions were obtained by the artificial compressibility method (see Anderson et al, 1984) using an explicit, time–marching finite–difference scheme. Chow et al (1984) studied the simultaneous effects of natural convection and axial diffusion (heat and momentum) for low Peclet number upward flows in a short vertical duct subject to symmetric UWT thermal boundary conditions. The problem was formulated in terms of vorticity and stream function and solved using a finite–difference method over a region incorporating adiabatic entry and exit lengths. Buoyancy effects were shown to enhance axial conduction near the start of a cooled section, whereas the opposite was found for heating. Baek et al (1990) made numerical predictions for air flowing upward between vertical parallel plates of finite length; one heated at UWT and the other maintained at the inlet air temperature. The elliptic equations considered allowed situations with reversed flow at the cooler wall to be treated and were solved in finite–difference form using the TEACH code. Developing axial velocity profiles, including flow reversals, predicted on the basis of the laminar, two–dimensional model compare well with LDV measurements made by Baek et al (1990), apart from at high Grashof numbers when transition to turbulent flow was observed. The changes in the flow structure with increase in the Grashof number, observed by Baek et al (1990), are described in Section 2.4.3. Viscous dissipation was neglected in all three numerical studies described above.

Experimental data available for laminar buoyant flows in vertical ducts approximating to a parallel plates system are mainly for pure natural convection of air through open–ended ducts. Measurements for combined natural and forced

convection are rare for this geometry.

Rao and Barrow (1972) made heat transfer measurements for upward flow of water in a vertical concentric annulus of $L/d_h \approx 231$ and radius ratio nearly equal to unity ($r* = 0.931$) with UHF heating at the inner surface. Joshi and Bergles (1978) obtained data for the heating of ethylene glycol flowing upward in a high aspect ratio rectangular duct of $L/d_h \approx 39$ at wall heat flux ratios of 0.0, 0.5 and 1.0. Local Nusselt numbers determined in these two experimental studies were found to be in good agreement with constant–property, pure forced convection predictions near the entrance. However, at greater axial distances the experimental values were severely underpredicted, this discrepancy being attributed to the aiding effect of buoyancy. The data of Rao and Barrow (1972), in particular, show that with increase in the Rayleigh number the Nu_x versus $x*$ distribution, away from the entrance, falls progressively higher than the forced convection line, eventually developing a pronounced "tail–up" appearance. Their local Nu_x values for $x* > 0.05$ are, however, underestimated by the fully–developed combined convection analysis of Rao and Morris (1968).

Wirtz and McKinley (1985) investigated the effect of buoyancy for air in downward laminar flow through a one–side heated duct of length–to–spacing ratio equal to 20. Velocity profiles and temperature profiles were measured by laser velocimetry and thermocouple traverses respectively. Local wall temperatures and heat fluxes were determined using holographic interferometry. The measurements revealed that an increase in Grashof number, at a fixed value of the pressure gradient, reduced the flow rate in the duct and shifted the flow profile further away from the heated wall. A corresponding decrease in local Nusselt number was noted for low Grashof numbers. Further increase of the wall heat flux eventually resulted in a reversal of this trend, coinciding with a marked increase in measured turbulence intensities adjacent to the heated wall. The recent measurements for heating of air in upflow with asymmetric wall temperatures, made by Baek et al

(1990), are referred to earlier in this section.

2.4 Instability and Transition for Combined Convection in Vertical Ducts

It is evident from perusal of the early literature on non—isothermal laminar flow in vertical ducts that it was known that heat transfer could result in instability of the flow, leading to transition at lower Reynolds numbers than normally associated with isothermal flow. For example, Martinelli et al (1942) in discussing data for water obtained at high wall temperature and showing points of unstable flow stated that "Under this condition $\cdots$ which probably induced turbulence in the fluid stream, the rates of heat transfer were much higher than predicted by viscous flow heat transfer theory". Also, in a comparison of theory with experimental data, Pigford (1955) commented that " $\cdots$ the strong natural convection currents near the wall $\cdots$ could have caused the appearance of incipient turbulence, even though the criterion of flow stability usually applied in isothermal flow indicates that laminar flow would exist".

Systematic attempts to understand buoyancy—induced flow instability for combined convection in vertical ducts and the conditions under which it occurs commenced in the 1950s and both experimental and theoretical investigations have subsequently been made. In the former approach, flow visualization experiments and measurements of heated wall and fluid temperature fluctuations have been employed. In parallel with these observations theoretical studies have been performed, using contemporary methods of analysis for steady, laminar combined convection, to provide predictions of velocity and temperature profiles near to transition as an aid in interpreting experimental results. More recently, linear stability analysis has been applied to gain insight into the dominant modes of disturbance for a number of problems of fully—developed combined convection in vertical ducts.

Contributions to the literature on the stability of laminar combined convection in vertical ducts are described in Sections 2.4.1–2.4.3, dealing with circular tubes, concentric anuuli and parallel plate ducts respectively.

2.4.1 Circular Tubes

The effect of buoyancy on the stability of an upward laminar flow in a uniformly heated vertical tube has been studied experimentally by several workers. Scheele et al (1960) utilised an upstream dye injection technique to visualize transition. Observations could only be made at the heated test section outlet ($L/d = 114.3$) and transition was detected by noting when the dye filament first deviated from streamline flow and became slightly sinuous or burst into turbulence. Scheele and Hanratty (1962) tested various heated lengths up to $L/d = 762$ and defined transition as the condition for which fluid temperature fluctuations were first detectable ($\approx 0.1°C$) at the tube outlet. According to Scheele and Hanratty (1962), the transition data collected in these two studies indicate that the value of Gr_q/Re at transition asymptotically approaches a lower limit of 340 at low values of Re. In order for fluid temperature fluctuations to be detected at the tube outlet for higher flow rates, a higher value of Gr_q/Re was required and the data also exhibited an influence of L/d. By considering the experimentally determined values of Gr_q/Re needed for transition in relation to velocity profiles predicted by fully–developed theory (Hallman, 1956; Hanratty et al, 1958) Scheele et al (1962) concluded that flow instability is initiated when a concavity develops in the buoyancy–distorted axial velocity profile at the centreline. A laminar velocity profile possessing such a point of inflexion is known to be unstable (e.g. Schlichting, 1968) and to favour the growth of disturbances which eventually lead to transition.

Hallman (1961), Kemeny and Somers (1962), Lawrence and Chato (1966) and Petukhov (1969) reported fluid and/or wall temperature fluctuations for combined convection in vertical tubes with UHF heating, indicating departure from steady laminar conditions. For upflow of water, Hallman (1961) recorded temperature

fluctuations on the upper portion of his heated test section indicating transition to a slow, apparently randomn, eddy flow. For a constant flow rate, the point where fluctuations were first noted moved nearer to the tube entrance as heat flux was increased. Hallman (1961) provided a correlation for the location of the transition point x^*_{cr}, which can be written as $GrPr = 2664 (x^*_{cr})^{1\cdot83}$, where $Gr = g\beta\rho^2 d^3 (T_w - T_b)/\mu^2$ and all fluid properties are to be evaluated at the local film temperature. Hallman's (1961) wall temperature measurements for upflow show some circumferential variations towards the top of the heated section, indicating some asymmetry of the flow. As heat flux was increased this asymmetry was observed to worsen and, in addition, an unexplained dip in the wall–to–bulk temperature difference was seen near the tube exit. However, Hallman (1961) does not appear to have interpreted this dip as an improvement in heat transfer due to transition from laminar flow. He also obtained wall temperature data for heating of water in downflow, which in general exhibited a much greater degree of asymmetry than for upflow. The asymmetry was particularly noticeable towards the exit (bottom) of the test section for high heat fluxes and suggested the existence of a cell flow in this region. At the highest heat fluxes, the wall temperatures on the lower part of the test section varied in an approximately periodic fashion, with typical frequencies of about 12 mHz.

Kemeny and Somers (1962) used wall temperature variations and fluid temperature fluctuations to infer the occurrence of "non–laminar" conditions for upflow of oil and water with UHF heating. For water, such a transition was reported to occur only for Re greater than about 200, but for oil non–laminar conditions were observed even at Reynolds numbers below 10. Transition was found to be accompanied by either a drop in wall temperature, or a smaller rise than expected, in going from one wall thermocouple position to the next in the downstream direction. Fluid temperature fluctuations were measured by a probe inserted axially from the top of the tube. At the axial position where the largest fluctuations were found, the frequency was approximately 0.25 Hz, with

amplitudes of between 0.9 K and 14.4 K measured near the tube centreline. Close to the tube wall the amplitudes of the fluctuations were found to be up to 21.6 K. Nusselt numbers for non—laminar conditions were found to be much larger than those for steady laminar flow (by as much as 30% for oil), although Kemeny and Somers (1962) were unable to obtain a consistently satisfactory heat transfer correlation for these results. In addition, observations were made of non—laminar flow in a separate transparent apparatus where instabilities were observed to lead to a rolling or wave—type flow that originated in the boundary layer and dissipated in the main stream.

Metais and Eckert (1964)[2] provided a convection regime diagram for flow through vertical tubes intended to give guidance on when the combined effects of natural convection and forced convection have to be considered. The diagram is based on information taken from both theoretical and experimental sources (mainly the latter), including work by Watzinger and Johnson (1939), Martinelli and Boelter (1942), Brown (1960), Hallman (1961) and Kemeny and Somers (1962).

Lawrence and Chato (1966) used fluid temperature fluctuation measurements to indicate the transition point location for upflow of water in a vertical tube (L/d ≈ 203) heated at UHF. For each heat flux used in their tests, flow rate was varied so that the transition point could be located at a number of different axial measurement positions. Although large and irregular fluctuations were reported for regions with "gross turbulence", only small periodic fluctuations, with frequencies of the order of 5 to 10 Hz were observed nearer to the transition point. Lawrence and Chato (1966) defined the point indicating the initiation of turbulence, said to be near the beginning of laminar instability, as the location where fluctuations of the order of 0.09 K were first detected. Their transition data show a strong

---

[2]Further information on the Metais and Eckert (1964) convection regime diagram is given in Section 7.2.1, where a comparison with experimental data collected in this research is presented.

functional relationship between the buoyancy parameter Gr_q/Re and the nondimensional distance to transition x_{cr}^*; with scatter being attributed to the different inlet temperatures used in the tests. Developing axial velocity profiles were calculated using the authors' finite—difference model (see Section 2.3.1) for conditions correponding to specific tests. These confirmed that transition always occurred downstream of the position where a point of inflexion developed in the distorted velocity profile. Lawrence and Chato (1966) also attempted to devise a characteristic shape parameter, based on features of the predicted transition point velocity profiles, which could be related to inlet Reynolds number and used as a transition criterion. Using the present nomenclature, their tentative shape parameter is given by $\mu_w(U_{max} + U_{cl})/(1 - R_{max})$. However, Collins (1975, 1978) concluded that it was difficult to justify the form of this dimensional parameter on analytical grounds and found that it did not correlate the results of Scheele et al (1960).

Petukhov et al (1969) performed experiments for upflow of water with UHF heating and used wall temperature fluctuations to detect the critical axial distance x_{cr}^* at which instability of laminar combined convection occurs. Their correlation for x_{cr}^*, which reflects the effect of different hydrodynamic inlet conditions, can be written as follows: $x_{cr}^* = 12.9 \, C(Gr_q/Re)^{-0.8}$ where $C = 1$ in the presence of a calming section and $C = 1 + 10 \exp(-0.0025 \, Re)$ without a calming section.

Local Nusselt numbers for upflow of water in a uniformly heated tube, measured by Barozzi et al (1984), exhibited a steep increase for large x^*, providing strong evidence of transition from laminar flow. The data were compared with numerical predictions, obtained using Collins' (1975) finite—difference method for developing combined convection, showing good agreement up to the position of minimum Nu_x, but thereafter the experimental values were much higher. The predictions confirmed the development of a point of inflexion in the axial velocity profile upstream of the minimum Nu_x position. The feasibility of using a correlation

between Gr_q/Re and x^* at the minimum Nu_x position as a transition criterion was examined. Barozzi et al (1984) compared their experimental data and a large number of predicted cases with the transition data correlation presented by Lawrence and Chato (1966) on the basis of fluid temperature fluctuation measurements. It was found that the position of minimum Nu_x does correlate in a manner similar to that for the onset of measurable fluid temperature fluctuations.

A linear stability analysis by Yao (1987a), of fully–developed buoyancy–aided flow in a vertical tube heated at UHF, revealed flow instability boundaries indicating that the flow can become unstable for $Gr_q/Re > 300$ and $Re > 80$. Furthermore, it was found that, except in the range of Reynolds numbers $Re \approx 100 - 300$, the most unstable mode corresponds to two plane symmetric spiral flows. Yao (1987b) used the same method of analysis to study buoyancy–opposed flow for the same boundary condition. The numerical results indicate that for $Re > 100$, opposed flow is unstable for $Gr_q/Re > 400$. The type of disturbance associated with the dominant unstable mode predicted for this case is two counter–rotating spirals. However, Yao (1987b) considered that since opposing flow is subcritical this flow pattern is unlikely to be detected in practice.

2.4.2 Concentric Annuli

Both experimental and theoretical approaches have been employed to study the stability of laminar combined convection in vertical annuli. Not surprisingly, attention has mainly focussed on the internally heated annulus as this allows the flow to be observed without experimental complications.

Sherwin and Wallis (1968) used dye injection to indictate flow patterns for downflow of water in a concentric annulus ($r^* = 1/3$) with UHF heating at the inner surface. Their experiments showed that increase of the buoyancy force opposing the main flow did lead to reversed flow adjacent to the heated wall, and a consequent fall in Nusselt number, but that this situation only remained stable

over a limited range of heat input. Further increase in heat flux, eventually resulted in flow instability associated with the development of radial velocity components across the annulus, though the flow did not appear to be asymmetric. A pattern of alternate unstable and stable flow sections was observed, with the instabilities growing in size and frequency as the heat flux was increased. A considerable improvement in heat transfer was measured beyond the onset of unstable flow; with Nu increasing with Gr_q/Re. In later experiments (Sherwin and Wallis, 1972) for heating of water in upflow using the same apparatus, onset of flow instability was observed as the velocity gradient approached zero at the outer unheated wall. An associated increase in the radial flow was seen in this case also and, in addition, some asymmetry was evident near the transition to the unstable region which was not found in the downflow experimemts. As Gr_q/Re was increased in the upflow experiments, the onset of flow instability occurred at progressively smaller values of $x*$. The observed locations agreed reasonably well with developing flow predictions made using the finite—difference model of Sherwin and Wallis (1970).

Ogunba and Barrow (1979) used the hydrogen bubble technique and photography in a visual study of combined convection for upflow of water (Re $\approx$ 450) in the entry region of a concentric annulus ($r* = 0.25$) heated internally at UHF. They reported that the photographs showed the onset of turbulence near the outlet ($x/d \approx$ 20) at larger heat inputs but no details of the critical value of Gr_q were given.

In a two—part study of buoyancy—induced instability of laminar flow in a vertical annulus flow visualization and heat transfer experiments (El—Genk and Rao, 1990) were complemented by a numerical study (Rao and El—Genk, 1990). Upflow and downflow tests were performed for water in a vertical annulus ($r* = 0.5$, $L/d_h \approx$ 71) with UHF heating of the inner wall only. Incipient flow instability was taken as the point where, for each test condition, oscillations of an injected dye

filament began; the reported axial locations being determined from video images of the flow field. For downflow, bulk flow mixing was observed to occur almost immediately downstream of the location of incipient instability. The flow in this mixing region was referred to as turbulent by El—Genk and Rao (1990). For upflow, transition from stable laminar flow to a bulk mixing flow occurred more gradually, over a short region, characterised by a moderate rate of mixing and by the formation of vortices near the outer unheated wall. The onset of flow instability was also detected by recording the accompanying fluctuations of the heated wall and fluid temperatures, which were found to be less frequent and much less intense for upward flow than for downward flow.

In the companion numerical study, Rao and El—Genk (1990) compared three numerical schemes for predicting the axial location of incipient instability, x_{cr}, defined as the axial distance at which $\partial u/\partial r$ vanishes at either the outer wall (for upflow) or the inner wall (for downflow). The three schemes were based on different forms of the equations for steady, laminar, two—dimensional axisymmetric flow, namely: (i) elliptic equations, including both the axial and the radial momentum equations, with axial momentum (but not heat) diffusion represented; (ii) the same as (i) but omitting the axial momentum diffusion term; in essence a partially parabolic set of equations; and (iii) the boundary layer equations. Viscosity and density variations were considered. Solution was effected by a marching finite—difference procedure in the main flow direction for each scheme, except that additional sweeps were made with scheme (i) above to achieve a higher order of accuracy. The numerical predictions for x_{cr} obtained by schemes (i) and (ii) were almost identical, indicating that the effect of axial momentum diffusion on x_{cr} is negligible. Furthermore, these predictions gave reasonable agreement with the authors' (El—Genk and Rao, 1990) measurements, and also with the downflow data of Sherwin and Wallis (1968, 1970). In contrast, the solutions based on the boundary layer equations were found to underpredict x_{cr} by up to 45% at higher values of Gr_q/Re, as a result of neglecting radial momentum

transfer. This was confirmed by comparing the developing velocity profiles for the three schemes; with scheme (iii) showing a more rapid development and hence predicting an earlier onset of instability. Based on the experimental data and the results of a parametric numerical study, including the effects of Gr_q/Re, $r*$, inlet temperature and inlet velocity profile shape, Rao and El–Genk (1990) proposed equations for estimating the nondimensional axial distance to the onset of instability, x^*_{cr}, in terms of Gr_q/Re and $r*$, for upward and downward flows in vertical annuli with internal UHF heating. The time–averaged wall–to–bulk temperature difference measurements made by El–Genk and Rao (1990) show a decrease at axial positions downstream of the onset of instability, indicating an improvement in heat transfer consistent with the mixing observed in this region. Nusselt number correlations for combined convection in vertical annuli under stable laminar flow and unstable flow conditions, based on experimental data for water obtained in the experiments of El–Genk and co–workers, are given by El–Genk and Rao (1989, 1990).

Yao and Rogers (1989) carried out a linear stability analysis for fully–developed combined convection in a vertical annulus with the walls kept at different temperatures. A very large aspect ratio was considered so that a two–dimensional channel was approximated. Results were obtained for an aspect ratio of 100 ($r* = 100/101 = 0.990$) and $Pr = 0.71$. Although both axial and azimuthal disturbances were investigated, the marginal stability boundary was found to be sufficiently determined by the former, since the first few azimuthal modes became unstable at the same time. In the range of values of Re up to about 4000, where the flow is susceptible to so–called thermal instability in which the buoyancy forces play an important role, the critical ratio of Grashof number (based on the difference in wall temperatures and the hydraulic diameter) to the Reynolds number reduced from 720 at $Re = 300$ to 480 at $Re = 4000$. At higher Reynolds numbers other types of hydrodynamic instability (shear, interactive) are important. In a subsequent paper, Rogers and Yao (1990) determined the limit of

stability for upward flow ($Pr = 6.0$) in an annulus ($r^* = 0.375$) with UHF heating at the inner wall and the outer wall insulated. Linear stability theory showed the most unstable disturbance to be axisymmetric in this case. Thermal instability was predicted to occur at an almost constant value of Gr_q/Re equal to 1305 for $Re > 200$, but at lower Reynolds numbers this critical value was found to increase sharply due to the minimal inertia forces. Rogers and Yao (1990) pointed out that the critical value $Gr_q/Re = 1305$ is less than that predicted by steady fully–developed combined convection theory for a point of inflexion to form in the velocity profile, given as $Gr_q/Re = 1408$. The results from the linear stability analysis were used together with energy balances, representing the redistribution of the disturbance energy between the thermal and kinetic components, to determine the shape and amplitudes of the disturbances. It was shown that the disturbances consist of a set of counter–rotating cells, tilted slightly upward towards the insulated wall. Nusselt numbers, calculated from the distorted mean velocity and temperature profiles, demonstrated increases due to the disturbances in line with the large positive deviations from steady fully–developed combined convection theory exhibited by the experimental data of Maitra and Subba Raju (1975).

2.4.3 Parallel Plate Ducts

Only a few papers can be found giving information on flow stability and transition for combined natural and forced convection in vertical parallel plate ducts, despite the practical importance of this geometry. This can be understood from an experimental viewpoint, because of the practical difficulties of maintaining a two–dimensional base flow, especially when the flow is unstable. The experiments for air by Fukui et al (1982), Wirtz and McKinley (1985) and Baek et al (1990) are relevant.

Fukui et al (1982) used smoke to visualize upward flow at a section approximately 42 hydraulic diameters downstream from the entrance in a vertical rectangular duct with an aspect ratio of nearly 17:1. Reynolds number was varied from 0 to

200 and different Grashof numbers were fixed by maintaining asymmetric UWT conditions at the opposite spanwise walls. Above a critical Grashof number, which was found to increase as the square of Reynolds number, unstable flow was observed with moving transverse vortex rolls at regular axial spacing. These disturbances were aligned with their axes in the spanwise direction and travelled in the flow direction at 0.855 times the mean velocity in the duct. These observations were in good agreement with the predictions of an accompanying linear stability theory. Fukui et al (1982) also employed a quasi—linear approximation to determine the amplitudes of the disturbances affecting the primary flow field and the resulting augmentation of heat transfer and pressure gradient.

Bearing in mind the flow structure observed by Fukui et al (1982), it is of interest to note that, at about the same time, Yao (1983) hypothesised that the fully—developed flow field for buoyancy—aided convection in a vertical two—dimensional channel under symmetric UHF conditions may take the form of pairs of recirculating cells moving downstream in order to satisfy the mass continuity principle.

Wirtz and McKinley (1985) made LDV measurements for downward flow in a parallel plate duct (aspect ratio ≈ 20:1) with UHF heating at one plate only. When the Grashof number was increased beyond a certain level (dependent on the Reynolds number) a sharp increase in streamwise turbulence intensity was detected adjacent to the heated plate, suggesting production of turbulence by destabilizing buoyancy forces. Nusselt numbers were correspondingly improved, reversing the decline seen at lower Grashof numbers, which was characteristic of laminar buoyancy—opposed convection. Smoke experiments made by Wirtz and McKinley (1985) showed that at higher Grashof numbers the flow adjacent to the heated plate first became unsteady and sinuous, and eventually three—dimensional with an upward reversed flow near the duct side walls and a downward flow at the plate centrespan.

Baek et al (1990) used LDV measurements and flow visualization to examine the effect of buoyancy on the structure of an upward flow between parallel plates of finite length; one heated at UWT and the other maintained at the fluid inlet temperature (i.e. $r_T = 0$). At low heating rates, the flow became skewed towards the heated wall but remained unidirectional throughout the duct. As heating was increased, stable laminar bidirectional flow was observed at the duct exit plane; with air entering the top of the duct along the colder wall. The reversed flow region penetrated further down the duct as the heating rate was further increased until, above a critical Grashof number, it was replaced by a three–dimensional recirculation bubble. The bubble divided the upstream laminar flow region from a developing unidirectional turbulent flow downstream and its appearance was taken to indicate the onset of transition. Baek et al (1990) established empirical relationships, in terms of Gr_T and Re, delineating the boundaries between the unidirectional laminar, bidirectional laminar and turbulent flow regimes.

PART 2

ANALYSIS AND COMPUTATIONAL WORK

CHAPTER 3

ANALYSIS OF LAMINAR COMBINED CONVECTION IN VERTICAL DUCTS

3.1 Introduction

In this chapter the theoretical model and governing equations underlying the present analysis of developing combined natural and forced laminar convection in vertical ducts are presented.

In the analysis the governing equations are written in a generalized axisymmetric form which is suitable for the treatment of flows between parallel plates and in circular tubes and concentric annuli. Following a discussion of various forms of the basic conservation equations, attention is focussed on the variable—property boundary layer forms used in this study. The finite difference approximations of the governing equations and the marching procedure used in their solution are then described.

3.2 Description of Theoretical Model

3.2.1 Initial Assumptions

The following theoretical analysis is applicable to steady, laminar, two—dimensional duct flows under developing hydrodynamic and thermal conditions. Both plane and non—swirling axisymmetric situations are considered. The duct walls are assumed to be parallel, smooth and impermeable. Any thermal boundary conditions imposed on these boundaries are considered to be either of the uniform temperature type or the uniform heat flux type. It is assumed that the fluid can be treated as a single chemical species and behaves as a continuum. Only Newtonian fluids are considered, so that a shear stress exhibits a linear dependence on the rate of strain, and no phase change is allowed. Internal thermal energy generation within the fluid, such as that due to electrical heating or nuclear reactions, is excluded and thermal radiation is negligible.

As the combined effects of thermally–induced buoyancy and forced convection are being studied, variation of the fluid density with temperature is necessarily considered, but subject to the following two restrictions:

(i)   Density variation is accounted for in the gravitational body force only. Elsewhere in the equations a constant density ρ_0 is used. This is essentially the well–known Boussinesq approximation, but instead of the usual linear dependence of the density on temperature, ρ is treated as a polynomial function of temperature in this work.

ii)   The main duct flow is aligned in the same or opposite direction as the gravitational acceleration vector. Thus the inclusion of density variation is restricted to vertically upward or vertically downward duct flows. To extend consideration of buoyancy effects to other duct orientations would generally require a three–dimensional approach. Consequently, horizontal and inclined duct flows are embraced by the present treatment only for the forced convection limit.

Furthermore, each thermophysical property of the fluid, including density in the restricted sense discussed above, is considered to be a function of the local fluid temperature alone. Fluid property variations due to pressure differences are considered negligible.

3.2.2 Duct Geometries and Coordinate System

Figure 3.1 depicts the cylindrical polar coordinate system (x, r, ϕ) and the associated notation used to unify the presentation of the analysis for the three common duct geometries studied here; namely, the circular tube, the concentric annulus and the parallel plate duct.
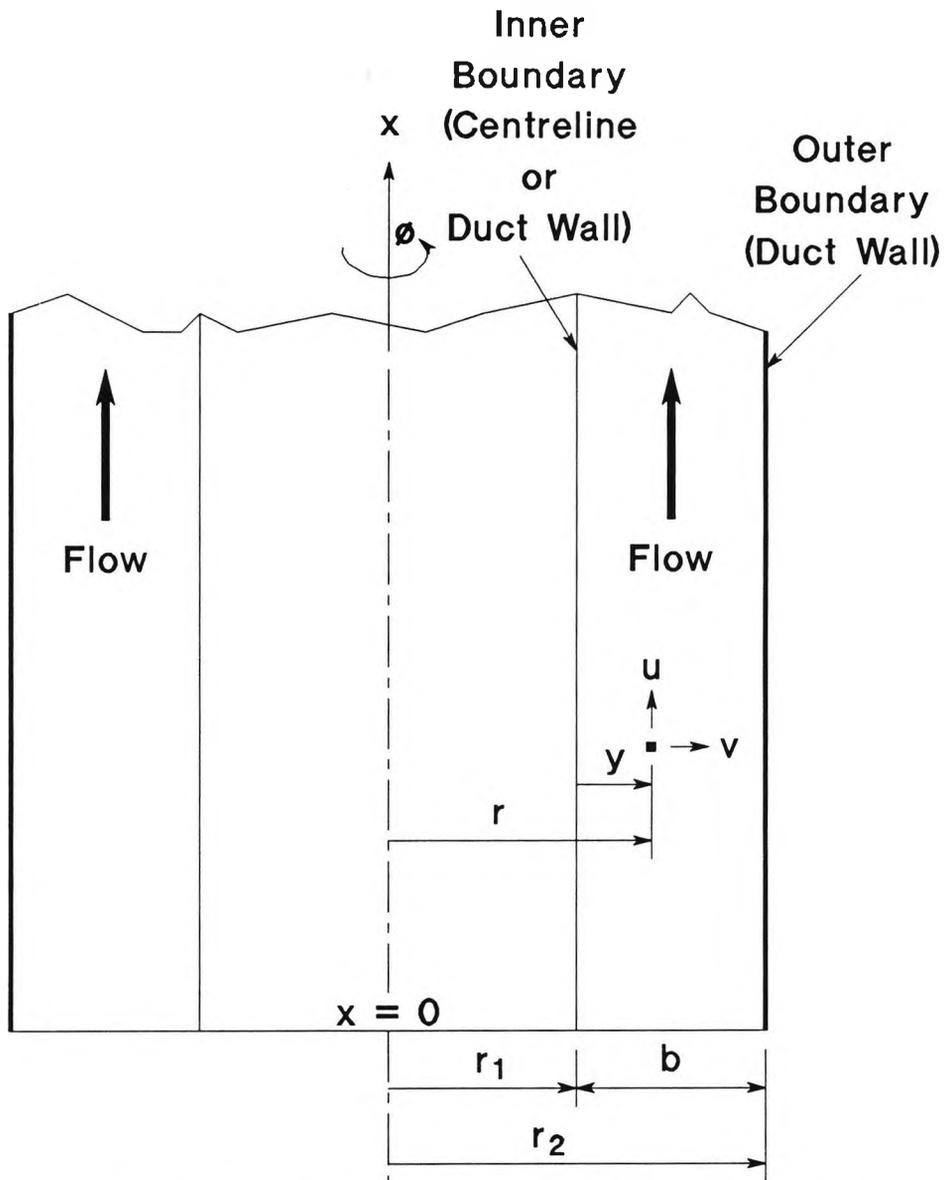
Figure 3.1 Coordinate system for axisymmetric ducts.

The x–coordinate axis is directed downstream in the main flow direction and can be at any angle to the gravitational acceleration vector for pure forced convection. However, as explained earlier, only vertical flows are considered for natural or combined convection conditions. The origin of the x–coordinate axis is usually taken at the duct entrance position, although for comparison a fully–developed velocity distribution may be specified at $x = 0$ as an alternative to a uniform flow entry. Heat transfer to or from a duct wall is assumed to commence at $x = 0$ unless an adiabatic entry length is introduced to investigate the effect of a partially developed velocity profile on the subsequent thermal and hydrodynamic development.

For axially symmetric situations, variations with respect to the azimuthal coordinate ϕ are negligible and attention is confined to the remaining axial (x) and radial (r) coordinate directions. Obviously this provides a suitable framework for developing flow and heat transfer in circular tubes and concentric annuli. However, plane flow between parallel plates is also two–dimensional and can be treated as axisymmetrical, if it is regarded as a special case in which the distance to the symmetry axis is very much greater than the (radial) spacing of the plates. These common features: two–dimensionality and axial symmetry, are exploited in the unified treatment presented here.

Thus, for each geometry considered, flow and temperature solutions are sought for a defined two–dimensional region on the x–r plane between an inner boundary at $r = r_1$ and an outer boundary at $r = r_2$. The radial width b of this region and its distance from the symmetry axis are defined by

$$b = r_2 - r_1 \tag{3.1}$$

and
$$r^* = \frac{r_1}{r_2} \tag{3.2}$$

where r* is the radius ratio. Conventionally, r* is used as a geometric similarity parameter for concentric annuli, but its use is extended to cover all the geometries considered here. Shah and London (1978) pointed out that the parallel plates geometry and also the circular tube can be viewed as limiting cases of the concentric annulus. From equations (3.1) and (3.2) we obtain $r^* = 1 - b/r_2$, from which it follows that $r^* = 1$ for parallel plates, since r_2/b is infinite. For the circular duct $r_1 = 0$ and therefore $r^* = 0$ from equation (3.2). However, it should be noted that the circular tube centreline boundary conditions are not the same as those at $r = 0$ in a concentric annulus of $r^* = 0$.

For the convenience of restricting attention to the region between the inner and

outer boundaries, a new transverse coordinate y is defined (see Figure 3.1). Originating at the inner ($r = r_1$) boundary, the y–coordinate axis defines the positive transverse flow direction, which is taken outward in the same sense as r, so that

$$r = r_1 + y \qquad (3.3)$$

Moreover, as $\delta y = \delta r$ this change of origin does not affect transverse derivatives.

Physically, the outer ($y = b$) boundary is always a duct wall, although the inner ($y = 0$) boundary may be either a duct wall or a duct centreline. The centreline inner boundary condition applies for a circular tube and can also be used for a parallel plate duct with symmetrical thermal boundary conditions, since only the duct semi–width need be considered. Note that for a circular tube the centreline coincides with the symmetry axis of the coordinate system. The duct wall inner boundary condition must be used for a concentric annulus or a parallel plate duct with asymmetric thermal boundary conditions.

The physical nature and radial position of the transverse boundaries for each duct geometry and sub–geometry considered are summarised in Table 3.1. The ratio of the duct hydraulic diameter d_h to the transverse width b is also given. In all cases the hydraulic diameter is taken as $4A_f/P_w$, where A_f is the flow cross–sectional area and P_w is the wetted perimeter. Specific hydrodynamic and thermal boundary conditions for the inner and outer boundaries are discussed in Section 3.3.2.

Table 3.1 Physical nature and radial position of transverse boundaries.

Duct geometry (radius ratio)	d_h/b	Inner boundary ($y = 0$)	Outer boundary ($y = b$)
Circular tube ($r* = 0$)	2	centreline ($r = 0$)	wall ($r = b$)
Concentric annulus ($0 < r* < 1$)	2	inner wall ($r = r_1$)	outer wall ($r = r_2 = r_1 + b$)
Parallel plates ($r* = 1$)			
symmetric thermal bc's	4	centreline ($r = \infty$)	wall ($r = \infty$)
asymmetric thermal bc's	2	wall ($r = \infty$)	wall ($r = \infty$)

3.3 Mathematical Formulation

3.3.1 Conservation Equations in Differential Form

For the previously stated assumptions the following partial differential equations expressing conservation of mass, momentum and energy are appropriate:

(i) Mass Continuity Equation

$$\frac{\partial}{\partial x}(r^\kappa u) + \frac{\partial}{\partial y}(r^\kappa v) = 0 \tag{3.4}$$

(ii) Axial Momentum Equation

$$\rho_0 \left[u\frac{\partial u}{\partial x} + v\frac{\partial u}{\partial y} \right] = -\frac{\partial \hat{p}}{\partial x} - Sg(\rho(T) - \rho_0) + \frac{1}{r^\kappa}\frac{\partial}{\partial y}\left[r^\kappa \mu(T)\frac{\partial u}{\partial y} \right]$$

$$+ \frac{\partial}{\partial x}\left[\mu(T)\frac{\partial u}{\partial x} \right] + \frac{\partial \mu(T)}{\partial y}\frac{\partial v}{\partial x} + \frac{\partial \mu(T)}{\partial x}\frac{\partial u}{\partial x} \qquad (3.5)$$

(iii) Transverse Momentum Equation

$$\rho_0 \left[u\frac{\partial v}{\partial x} + v\frac{\partial v}{\partial y} \right] = -\frac{\partial \hat{p}}{\partial y} + \frac{1}{r^\kappa}\frac{\partial}{\partial y}\left[r^\kappa \mu(T)\frac{\partial v}{\partial y} \right] - \kappa\mu(T)\frac{v}{r^2}$$

$$+ \frac{\partial}{\partial x}\left[\mu(T)\frac{\partial v}{\partial x} \right] + \frac{\partial \mu(T)}{\partial y}\frac{\partial v}{\partial y} + \frac{\partial \mu(T)}{\partial x}\frac{\partial u}{\partial y} \qquad (3.6)$$

(iv) Energy Equation

$$\rho_0 c(T)\left[u\frac{\partial T}{\partial x} + v\frac{\partial T}{\partial y} \right] = \frac{1}{r^\kappa}\frac{\partial}{\partial y}\left[r^\kappa k(T)\frac{\partial T}{\partial y} \right] + \frac{\partial}{\partial x}\left[k(T)\frac{\partial T}{\partial x} \right] + \mu(T)\Phi \quad (3.7)$$

where the viscous dissipation function Φ in equation (3.7) is given by

$$\Phi = 2\left[\left[\frac{\partial u}{\partial x}\right]^2 + \left[\frac{\partial v}{\partial y}\right]^2 + \left[\frac{\kappa v}{r}\right]^2 \right] + \left[\frac{\partial v}{\partial x} + \frac{\partial u}{\partial y}\right]^2 \qquad (3.8)$$

In equations (3.4)–(3.8), u and v denote the velocity components in the x and y directions respectively and κ is a flow index which determines the correct forms for two–dimensional and axisymmetric flows. It takes the following values:

$$\kappa = 0, \ (r^\kappa = 1) \qquad \text{for two–dimensional flow}$$

and
$$\kappa = 1, \ (r^\kappa = r) \qquad \text{for axisymmetric flow.}$$

The factor S multiplying the buoyancy term of equation (3.5) distinguishes between upward (S = +1) and downward (S = −1) vertical flows. Putting S = 0 is

suitable for pure forced convection at any duct inclination since it has the same effect as omitting density variation altogether. To emphasise that the density, dynamic viscosity, thermal conductivity and specific heat capacity are functions of the local temperature T, they are denoted by $\rho(T)$, $\mu(T)$, $k(T)$ and $c(T)$ respectively.

The pressure variable $\hat{p}$ appearing in the momentum equations (3.5) and (3.6) deserves some additional explanation since it is not simply the local static pressure p. The latter is considered to be split into two parts

$$p = \hat{p} - \rho_0 gz \tag{3.9}$$

where g is the magnitude of the gravitational acceleration, z is the height measured above some arbitrary horizontal datum and $-\rho_0 gz$ represents the change in hydrostatic pressure corresponding to an increase in elevation equal to z in a static fluid of constant density ρ_0. The pressure $\hat{p}$ is the contribution due to the motion of the fluid. Upon differentiation with respect to z, equation (3.9) produces two terms: $\partial \hat{p}/\partial z$ and the hydrostatic pressure gradient $-\rho_0 g$. The x–direction and y–direction components of these two gradients are included in the respective momentum equations. For a strictly incompressible fluid, the hydrostatic gradient cancels with the body force per unit volume, whereas these two quantities combine to give the buoyancy force per unit volume when density variation is admitted in the body force term.

The set of partial differential equations (3.4)–(3.7) are coupled and contain nonlinear terms. The coupling arises from the assumed temperature dependence of density (included in the buoyancy generation term only) and viscosity. Consequently, the solutions of the velocity and temperature fields are interdependent and must be pursued simultaneously. Nonlinearities occur in the equations wherever functions of the dependent variables or their derivatives occur

as products, as for example in the first—order convective acceleration terms in the momentum equations. The corresponding terms in the energy equation are similarly nonlinear since the velocity components depend on temperature because of the coupling. Further nonlinearities are introduced through the temperature dependent fluid properties which can also be regarded as dependent variables of the flow.

Equations (3.5)—(3.7) represent the fullest forms of the momentum and energy equations for the assumptions stated so far and have an elliptic mathematical character. Elliptic flows must be solved over a closed domain and require boundary conditions to be specified on all sides. The physical interpretation of this classification is that, in general, local effects may be transmitted in all directions, including the upstream direction, and thus may influence the conditions at any other point. Molecular diffusion processes and the pressure field both exhibit such elliptic behaviour. In the numerical treatment of these elliptic equations, it follows that solutions must be obtained for all points over the entire domain simultaneously. Elliptic solution procedures are therefore expensive in terms of computer time and a further implication is that storage must be provided simultaneously for each of the dependent variables (i.e. u, v, $\hat{p}$ and T) at every discrete point considered.

Fortunately, equations (3.5)—(3.7) can be simplified for the two—dimensional and axisymmetric duct flows studied here, allowing considerable computational advantages to be enjoyed. Attention is confined to unidirectional flows (i.e. no regions of reverse flow), so that the axial velocity component u always remains positive, ensuring that convection can only convey information about local conditions in one direction. Elliptic influences in the equations are partially eliminated by assuming that the Reynolds numbers are sufficiently high for the terms representing axial diffusion of momentum and heat to be neglected in comparison to the corresponding convection and transverse diffusion terms. In

addition, pressure variations are considered to be absent in the transverse direction, so that $\hat{p}$ becomes a function of the x—coordinate only. The latter assumption removes any remaining elliptic influence in the main flow direction.

The above assumptions will not be strictly observed in practice for a small region close to a duct entrance where transverse pressure gradients and axial momentum diffusion are known to be present. Based on solutions to the full elliptic equations, Shah and London (1978) offer some guidance on the extent of this region for laminar forced convection. According to Anderson et al (1984) it is negligibly small for Reynolds numbers greater than about 75. A similar region might be expected near to the start of wall heat transfer where axial diffusion of heat would occur. To completely resolve these effects the only option is to use a full elliptic treatment covering the upstream and downstream affected zones. However, for present purposes it is considered that the neglect of axial diffusion and transverse pressure gradient is a reasonable approximation for laminar duct flows throughout any region of hydrodynamically and/or thermally developing flow. Together, these simplifications transform the momentum and energy equations, so that they become parabolic with respect to the main flow direction. For the so—called parabolic flows governed by these equations, downstream events are prevented from propogating upstream. Consequently, local behaviour is determined only by upstream conditions and numerical solutions can be obtained by a "once through" marching procedure, starting from known conditions at the upstream boundary and proceeding in the main flow direction. It is implied that conditions are not required to be specified at the downstream boundary.

The use of a step—by—step marching process, permitted by the simplification of the elliptic equations to parabolic form, considerably reduces the time for computation. A saving in computer storage is also achieved, because solutions are computed for only one transverse section at a time using known values at the immediately—upstream section. Therefore, storage for the dependent variables

need only be provided for the two sections currently involved.

The set of parabolic partial differential equations used in this work follow from equations (3.4)–(3.7) when the approximations discussed above are made. They are

$$\frac{\partial}{\partial x}(r^{\kappa}u) + \frac{\partial}{\partial y}(r^{\kappa}v) = 0 \tag{3.10}$$

$$\rho_0\left[u\frac{\partial u}{\partial x} + v\frac{\partial u}{\partial y}\right] = -\frac{\partial \hat{p}}{\partial x} - Sg(\rho(T) - \rho_0) + \frac{1}{r^{\kappa}}\frac{\partial}{\partial y}\left[r^{\kappa}\mu(T)\frac{\partial u}{\partial y}\right] \tag{3.11}$$

$$\frac{\partial \hat{p}}{\partial y} = 0 \tag{3.12}$$

$$\rho_0 c(T)\left[u\frac{\partial T}{\partial x} + v\frac{\partial T}{\partial y}\right] = \frac{1}{r^{\kappa}}\frac{\partial}{\partial y}\left[r^{\kappa}k(T)\frac{\partial T}{\partial y}\right] + \mu(T)\left[\frac{\partial u}{\partial y}\right]^2 \tag{3.13}$$

The axial momentum equation (3.11) is obtained by dropping all viscous diffusion terms containing partial derivatives with respect to the axial coordinate. Equation (3.12) gives the degenerate form of the transverse momentum equation, which simply states that transverse pressure variations are neglected. In the energy equation (3.13), axial diffusion is omitted and only the largest of the viscous dissipation terms from equation (3.8) is included. The incompressible continuity equation (3.10) remains unchanged.

It is noted that the parabolic flow equations (3.10)–(3.13) are identical to those obtained under the classical boundary layer approximations. Velocity and thermal boundary layers can be viewed as slender regions adjacent to a heat transfer surface in which large normal gradients of velocity and temperature occur. Outside of these layers it is imagined that uniform free stream conditions prevail. This traditional concept of a boundary layer is of limited applicability to duct flow heat transfer situations, except perhaps over a relatively short distance downstream of a duct entrance where the boundary layers have not yet grown to fill the entire duct

cross–section. Nowadays it is common for the term boundary layer to be used more generally to refer to any situations for which the parabolic flow equations apply.

3.3.2 Boundary and Initial Conditions

As discussed in the previous section, numerical solutions to equations (3.10)–(3.13) can be computed by a step–by–step procedure in the main flow direction, starting from initial conditions supplied at the upstream boundary or the duct entrance. At each step the solutions must simultaneously satisfy specified conditions at the transverse boundaries. In general, the number of boundary conditions which must be specified for each dependent variable, with respect to a particular coordinate direction, is given by the order of the highest derivative. As equations (3.10)–(3.13) contain only first derivatives with respect to x, the specification of initial conditions at $x = 0$ is sufficient for the marching direction, and hence boundary conditions are not required at the duct outlet. In contrast, the axial momentum equation (3.11) and the energy equation (3.13) retain elliptic characteristics in the transverse direction, as evidenced by the second derivatives of u and T. Consequently, boundary conditions are needed at $y = 0$ and at $y = b$ for both these variables. Strictly, only a single boundary condition is required for v in the transverse direction, since its highest derivative in the governing differential equations is $\partial v / \partial y$ (in the mass continuity equation). Nevertheless, $v = 0$ is shown below for both transverse boundaries, because both conditions are employed in the numerical solution. For completeness, it is noted that a boundary condition is not required for pressure in the transverse direction since, as follows from equation (3.12), $\hat{p}$ only depends on the axial coordinate x.

Only conditions of the Dirichlet (i.e. dependent variable specified) and Neumann (i.e. normal gradient of dependent variable specified) types are involved here. In terms of the thermal boundary conditions at the duct walls, this effectively means

that either the wall temperature T_w or the wall heat flux q_w is prescribed. Although in principle any axial distribution $T_w(x)$ or $q_w(x)$ could be specified, it is assumed that heat transfer to or from a duct wall occurs under either axially uniform wall temperature (UWT) or axially uniform wall heat flux (UHF) conditions. Adiabatic walls represent a special case of the UHF condition where q_w, and hence $(\partial T/\partial y)_w$, are equal to zero. As all situations are assumed to be two–dimensional, it is implied that the wall thermal boundary conditions must also be peripherally uniform.

The boundary conditions at the two transverse boundaries and the initial conditions are elaborated separately below:

i) Boundary Conditions at $y = 0$

As shown in Table 3.1, the boundary at $y = 0$ can be formed by either a duct centreline or a duct wall. Different boundary conditions apply in each case.

For a duct centreline at $y = 0$, symmetry is expressed by the following conditions:

$$\text{at } y = 0 \,,\, x > 0 : \qquad \frac{\partial u}{\partial y} = 0 \,,\, v = 0 \,,\, \frac{\partial T}{\partial y} = 0 \qquad\qquad (3.14)$$

For a duct wall at $y = 0$, the no–slip and no–blowing or suction conditions are expressed as follows:

$$\text{at } y = 0 \,,\, x > 0 : \qquad u = 0 \,,\, v = 0 \qquad\qquad (3.15)$$

Allowing for an optional adiabatic entry length x_{a_1}, so that

$$\text{at } y = 0 \,,\, 0 < x \leq x_{a_1} : \qquad \frac{\partial T}{\partial y} = 0 \qquad\qquad (3.16)$$

the two alternative thermal boundary conditions at the duct wall over the

remaining length are

at $y = 0$, $x > x_{a_1}$:
$$T = T_{w_1} \qquad \text{(UWT)} \qquad (3.17)$$

$$\text{or} \quad k\frac{\partial T}{\partial y} = -q_{w_1} \qquad \text{(UHF)}[1] \qquad (3.18)$$

It is noted that equation (3.18) is a nonlinear boundary condition since the fluid thermal conductivity k is a function of the local wall temperature.

ii) Boundary Conditions at $y = b$

The outer boundary is formed by a duct wall in all cases (see Table 3.1), so the appropriate boundary conditions are similar to those stated above for a duct wall at the inner boundary. That is

at $y = b$, $x > 0$:
$$u = 0 \text{ , } v = 0 \qquad (3.19)$$

at $y = b$, $0 < x \leq x_{a_2}$:
$$\frac{\partial T}{\partial y} = 0 \qquad (3.20)$$

at $y = b$, $x > x_{a_2}$:
$$T = T_{w_2} \qquad \text{(UWT)} \qquad (3.21)$$

$$\text{or} \quad k\frac{\partial T}{\partial y} = +q_{w_2} \qquad \text{(UHF)} \qquad (3.22)$$

where k must also be evaluated at the local wall temperature.

Finally, it should be mentioned that the ranges specified above, for the wall boundary conditions, are deliberately written to avoid contradictions associated with the leading edge singularity and positions where the thermal boundary

---

[1]The usual thermodynamic sign convention is adopted here, so that q_w is treated as positive when heat transfer is from the duct wall to the fluid.

conditions undergo step changes. In general, the upstream condition is assumed to prevail at such points, thus reflecting the manner in which the boundary conditions are applied in the discretized numerical procedure.
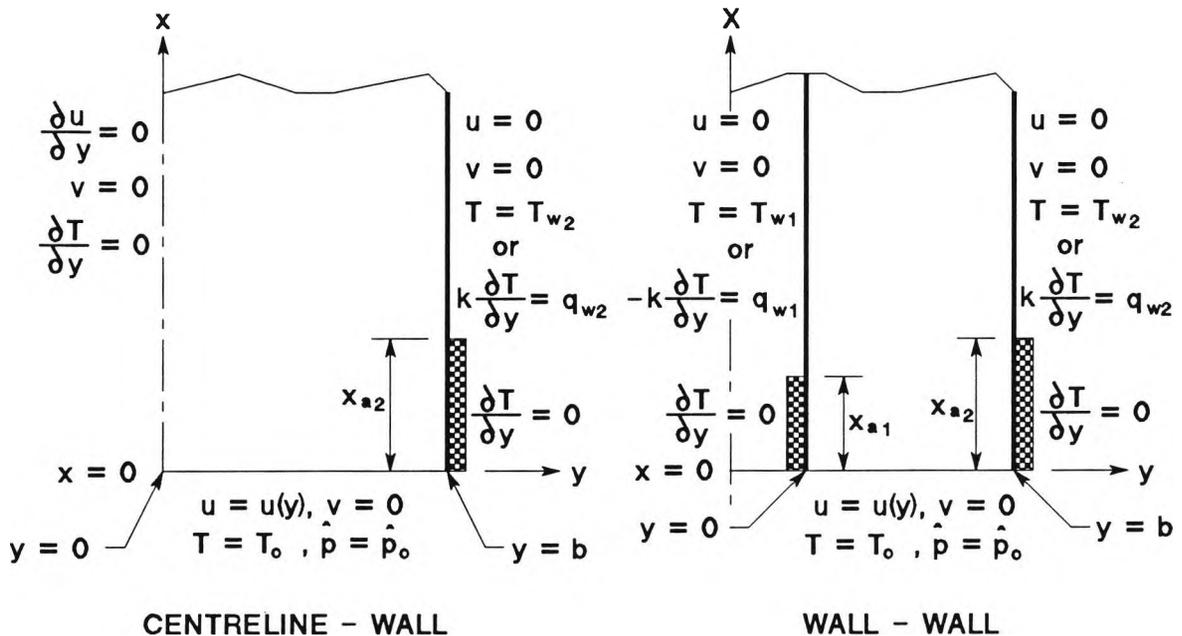
Figure 3.2   Initial and boundary conditions for centreline—wall and wall—wall problems.

iii) Initial Conditions at $x = 0$

Initial distributions of both the axial velocity u and the transverse velocity v are supplied at $x = 0$. Two alternative kinds of axial velocity profile are considered at $x = 0$: uniform and fully—developed. From the mathematical viewpoint, an initial condition is not required for v, since no axial derivatives of v appear in the governing equations. In the numerical treatment, however, a starting distribution is supplied as part of the artifice used to deal with the nonlinear term $v(\partial u/\partial y)$. By definition, the transverse velocity is exactly zero for an assumed fully—developed profile at $x = 0$. In contrast, large values of v occur in the vicinity of the duct wall leading edges at a duct entry, due to the rapid deceleration of the

fluid necessary to comply with the no—slip condition. Notwithstanding this difference in the initial distributions of v, numerical marching techniques frequently assume v = 0 along x = 0 for a uniform flow entry and this practice is also followed here. From the discussions of Hornbeck (1973) and Anderson et al (1984), it can be concluded that the errors caused by this assumption will be confined to a small region near the duct inlet if suitably small axial marching steps are used initially.

The uniform entry profile with zero transverse velocity approximates conditions for flow entering a duct via a well designed, smooth contraction. These conditions are stated as follows:

$$\text{at } x = 0 \text{ , } 0 \leq y \leq b : \qquad u = u_m \text{ , } v = 0 \qquad\qquad (3.23)$$

where u_m is the mean axial velocity in the duct.

Alternatively, the axial velocity profile may be considered to take the form for fully—developed, constant—property forced convection at $x = 0$, as would result from a sufficiently long length of identical ducting upstream of this position. Fully developed velocity distributions for each of the duct geometries (and sub—geometries) considered can be derived in analytical form. This is achieved by solving the following reduced form of the axial momentum equation subject to the appropriate boundary conditions for u at y = 0 and y = b (see above):

$$\frac{1}{r^\kappa} \frac{\partial}{\partial y} \left[r^\kappa \frac{\partial u}{\partial y} \right] = \frac{1}{\mu} \frac{\partial \hat{p}}{\partial x} \qquad\qquad (3.24)$$

The right—hand side of equation (3.24) is constant since the fluid viscosity and the axial pressure gradient are both constant. The resulting initial conditions are

at $x = 0$, $0 \leq y \leq b$:

circular tube:
$$u = 2\,u_m\left[1 - \left[\frac{y}{b}\right]^2\right] \;,\; v = 0 \tag{3.25}$$

concentric annulus:

$$u = 2\,u_m\left[\frac{1 - (r/r_2)^2 + 2(r_{max}/r_2)^2\,\ln(r/r_2)}{1 + r^{*\,2} - 2(r_{max}/r_2)^2}\right] \;,\; v = 0 \tag{3.26}$$

where $(r/r_2) = (r^* + (1 - r^*)y/b)$. The radius r_{max}, where the maximum velocity occurs in a concentric annular duct, is given by $(r_{max}/r_2) = [(r^{*2} - 1)/(2\,\ln r^*)]^{\frac{1}{2}}$.

parallel plates:

— symmetric problems
$$u = 1.5\,u_m\left[1 - \left[\frac{y}{b}\right]^2\right] \;,\; v = 0 \tag{3.27}$$

— asymmetric problems
$$u = 6\,u_m\left[\frac{y}{b} - \left[\frac{y}{b}\right]^2\right] \;,\; v = 0 \tag{3.28}$$

Initial conditions are also provided for the fluid temperature and pressure. The temperature is assumed to be uniform along $x = 0$, and since the only pressure distribution consistent with equation (3.12) is also uniform, we have

at $x = 0$, $0 \leq y \leq b$:
$$T = T_0 \;,\; \hat{p} = \hat{p}_0 \tag{3.29}$$

The various initial and boundary conditions discussed in this section are summarised in Figure 3.2.

3.3.3 Integral Mass and Energy Balances

In addition to the partial differential equations, given in Section 3.3.1, integral equations are utilised which express familiar mass and energy balance principles for duct flows with heat transfer under steady conditions. The integral equations place global constraints on the solution and may be derived by integrating the

corresponding conservation equations in differential form over some convenient space.

i) Integral Mass Balance Equation

For a duct flow the axial pressure gradient cannot be specified a priori. The additional information provided by the integral mass balance equation allows the pressure to be computed as part of the solution.

Integration of equation (3.10) between $y = 0$ and $y = b$ and insertion of the boundary condition $v = 0$ at both limits, from equations (3.14) or (3.15) and (3.19), gives

$$\frac{d}{dx} \int_0^b r^\kappa u \, dy = 0 \qquad \text{or} \qquad \int_0^b r^\kappa u \, dy = \text{constant} \qquad (3.30)$$

where $\kappa = 0$ for two–dimensional plane flow and $\kappa = 1$ for axisymmetric flow. Equation (3.30) is a statement of the well–known continuity condition for steady flow in a duct. Since both transverse boundaries are streamline surfaces, it follows that the volume flow rate between these boundaries remains constant for an incompressible fluid. The corresponding mean axial velocity u_m is simply the right–hand side of equation (3.30) multiplied by a constant. For the general axisymmetric case

$$u_m = \frac{2}{r_2^2 - r_1^2} \int_0^b r u \, dy \qquad (3.31)$$

The geometric relationships (3.1)–(3.3) can be used to rearrange equation (3.31) in the following form:

$$u_m = \frac{2}{(1 + r^*)b} \int_0^b \left[r^* + (1 - r^*)\frac{y}{b} \right] u \, dy \qquad (3.32)$$

As may easily be confirmed by substituting the appropriate value of r^*, equation (3.32) is applicable to all of the duct geometries considered, including circular tubes ($r^* = 0$) and parallel plates ($r^* = 1$).

ii) Integral Energy Balance Equation

The differential form of the energy equation (3.13) represents conservation of thermal energy on a local scale. At each step of a marching numerical solution, discretized versions of equation (3.13) are written for individual locations spanning the flow region. By incorporating specified boundary conditions where necessary, sufficient equations can be provided to solve for the temperature at each location (assuming that the required velocities are either known or can be determined by solving the momentum and continuity equations).

In his numerical study of forced and combined convection in axisymmetric ducts, Collins (1975) omitted the discretization equation for one location and instead made use of an integral form of the energy equation applying to the whole flow. The aim of this alternative approach, which is also provided as an option in the present work, is to enforce global energy conservation for the duct flow.

The derivation of the relevant equation from equation (3.13), for the general axisymmetric case, is explained below. The convective transport terms are first expressed in terms of the specific internal energy (denoted by e), using the incompressible fluid relation, $de = c\, dT$. Then, after multiplication by the radius r, the left–hand side is put into the so–called conservation form and the result is integrated over the transverse domain width b. Noting that $v = 0$ at both boundaries, the following equation is obtained:

$$\rho_0 \frac{d}{dx} \int_0^b rue\, dy = r_2 \left[k\frac{\partial T}{\partial y} \right]_{y=b} - r_1 \left[k\frac{\partial T}{\partial y} \right]_{y=0} + \int_0^b r\mu \left[\frac{\partial u}{\partial y} \right]^2 dy \qquad (3.33)$$

Equation (3.33) clearly shows that two mechanisms are responsible for changes to the internal energy transported by an incompressible fluid from section to section: heat transfer to or from the fluid across the transverse boundaries and conversion of mechanical to thermal energy by viscous dissipation.

The specific internal energy in equation (3.33) can be replaced, using $(e - e_0) = c_m(T - T_0)$, where c_m is the mean specific heat capacity over the range T_0 to T. For the bulk temperature rise $(T_b - T_0)$, c_m is given by

$$c_{m_b} = \frac{\int_{T_0}^{T_b} c \, dT}{(T_b - T_0)} \tag{3.34}$$

where the bulk temperature T_b is defined by

$$T_b - T_0 = \frac{2 \int_0^b ruc_m(T - T_0) \, dy}{u_m c_{m_b}(r_2{}^2 - r_1{}^2)} \tag{3.35}$$

Using equations (3.1)–(3.3) and (3.35) the integral energy equation (3.33) can be expressed in the form

$$\frac{d}{dx}\left[c_{m_b}(T_b - T_0)\right] = \frac{2}{\rho_0 u_m(1 + r^*)b}\left[\left[k\frac{\partial T}{\partial y}\right]_{y=b} - r^*\left[k\frac{\partial T}{\partial y}\right]_{y=0}\right]$$

$$+ \frac{2}{\rho_0 u_m(1 + r^*)b}\int_0^b \left[r^* + (1 - r^*)\frac{y}{b}\right]\mu\left[\frac{\partial u}{\partial y}\right]^2 dy \tag{3.36}$$

On substitution of the appropriate value of r*, equation (3.36) reduces to the correct form for a circular tube (r* = 0) and a parallel plate duct (r* = 1).

For a duct centreline and a duct wall subjected to a uniform heat flux (UHF), the corresponding boundary values of $(k\partial T/\partial y)$ in equation (3.36) are given explicitly by the thermal boundary conditions (3.14) and either (3.18) or (3.22) respectively.

Although the use of equation (3.36) is comparatively straightforward for UHF thermal boundary conditions, two difficulties arise where a uniform wall temperature (UWT) is imposed. Firstly, the normal temperature gradient at the wall is initially unknown, and must be represented implicitly in the solution. Secondly, because the wall heat flux varies axially under the UWT thermal boundary condition, an average value of $(k\partial T/\partial y)_w$ is required when equation (3.36) is integrated over an axial step length Δx. Both these matters are further discussed when the finite–difference treatment of the integral energy equation is presented in Section 3.4.2.

3.3.4 Fluid Property Variations

To solve the governing equations in variable property form, supplementary relations are required giving the dependence of the thermophysical properties on temperature.

Lilley (1987) lists sixteen common functional representations of a property (denoted generally by ψ) in terms of the temperature, including low degree polynomial functions. Here it is assumed that, in most circumstances, the property variation over the required temperature range can be adequately described by the nth–degree polynomial

$$\psi = a_0 + a_1 T + a_2 T^2 + \cdots + a_n T^n \tag{3.37}$$

which can also be written in the form

$$\psi = \psi_0[1 + a_{\psi 1}(T - T_0) + a_{\psi 2}(T - T_0)^2 + \cdots + a_{\psi n}(T - T_0)^n] \tag{3.38}$$

where ψ_0 is evaluated at the inlet temperature T_0. The derivation of equation (3.38) is given in Appendix A, where the relationships between the

coefficients $a_{\psi 1}$, $a_{\psi 2}$ $\cdots$ $a_{\psi n}$ and those in equation (3.37) are listed for polynomials up to the 5th–degree. Setting $a_{\psi i} = 0$ for $i \geq 2$ in equation (3.38) allows a linear property variation to be selected. For example, the linear density variation expressed by

$$\rho = \rho_0[1 + a_{\rho 1}(T - T_0)] \tag{3.39}$$

is simply the usual Boussinesq approximation, where the constant thermal expansion coefficient $\beta = - a_{\rho 1}$.

An alternative equation for the dynamic viscosity, given by the power law

$$\mu = \mu_0 \left[\frac{T + c_1}{T_0 + c_1} \right]^{- c_2} \tag{3.40}$$

may be selected in the computer implementation instead of the polynomial form. Equation (3.40) reduces to the simpler form, $\mu = \mu_0[T/T_0]^{- c_2}$, for $c_1 = 0$ and using $c_2 = 0$ delivers the constant property form. The constants c_1 and c_2 are independent of T_0.

When their diffusion terms are fully expanded, the axial momentum equation (3.11) and the energy equation (3.13) contain the derivatives $\partial \mu / \partial y$ and $\partial k / \partial y$ respectively. As both μ and k are assumed to be functions of the temperature alone, these spatial derivatives can be replaced by

$$\frac{\partial \mu}{\partial y} = \frac{d \mu}{d T} \frac{\partial T}{\partial y} \qquad \text{and} \qquad \frac{\partial k}{\partial y} = \frac{d k}{d T} \frac{\partial T}{\partial y} \tag{3.41}$$

respectively. The polynomial and power law forms discussed above are both easily differentiable, thus allowing $d\mu/dT$ and dk/dT in equations (3.41) to be expressed in terms of the local temperature.

The mathematical formulation is now basically complete. To summarise, it is noted that the variable–property boundary layer equations (3.10)–(3.13) and the integral mass balance equation (3.32) form a system of simultaneous equations for the four primitive variables: u, v, $\hat{p}$ and T. Empirical equations of polynomial or power law form, equations (3.38) and (3.40) respectively, relate the thermophysical properties of the quasi–incompressible fluid to the temperature. Optionally, the integral energy balance equation (3.36) may be used in concert with its differential form to ensure global conservation.

The theory presented in this chapter is appropriate for steady, laminar duct flow heat transfer situations exhibiting planar or axisymmetric two–dimensionality. The governing equations have been developed primarily for the purpose of studying combined convection heat transfer in vertical ducts with peripherally and axially uniform thermal boundary conditions. However, they are also applicable to the corresponding natural convection problem and to forced flows with or without heat transfer. In view of the numerous possible combinations of duct geometry (circular, concentric annular and parallel plates), thermal boundary conditions (uniform wall temperature or uniform heat flux) and inlet flow profile (uniform or fully–developed) catered for by the present analysis, it is clear that a wide range of related problems can be investigated.

3.3.5 Dimensionless Variables and Parameters

Before proceeding to describe the solution procedure, the governing equations and the boundary and initial conditions are recast in terms of dimensionless variables and parameters. The objectives of nondimensionalization are to reveal the dimensionless parameters on which the solutions depend and to simplify the equations as far as possible. Although a dimensionless formulation is not an essential requirement of the solution procedure, it is noted that solutions obtained in dimensionless form will be immediately applicable to all physically similar

conditions. Nondimensional parameters give useful insights into the relative importance of the various competing physical processes represented in the governing equations and are also important in the design of experiments and subsequently in the presentation of results.

Many different nondimensionalizing procedures are possible. The nondimensional variables adopted here are easily related to their dimensional counterparts. Lengths and velocity components are made dimensionless in a straightforward manner by referring them to the domain width b in the y–direction and the mean axial velocity u_m respectively. That is

$$X = \frac{x}{b} \qquad\qquad Y = \frac{y}{b}$$

$$(3.42)$$

$$U = \frac{u}{u_m} \qquad\qquad V = \frac{v}{u_m}$$

The nondimensional radius is similarly defined and the following useful replacement is derived from equations (3.1)–(3.3) and (3.42):

$$R = \frac{r}{b} = \frac{r^* + (1 - r^*)Y}{(1 - r^*)} = \frac{F(Y)}{(1 - r^*)} \qquad\qquad (3.43)$$

where the function $F(Y)$ is defined for compactness.

The transverse coordinate is normalised so that Y will vary between 0 (inner boundary) and 1 (outer boundary), whereas in a long slender duct the dimensionless axial distance increases from $X = 0$ at the duct entrance to $X \gg 1$ far downsteam. From the global mass flow constraint we can anticipate that in the absence of streamwise flow reversals the dimensionless axial velocity U will take positive values of order of magnitude 1, except at duct walls where $U = 0$ (i.e. no slip). The dimensionless transverse velocity V may be positive or negative but will be zero at duct walls and throughout any region of fully–developed flow. Treating

developing duct flows as boundary layers leads to the conclusion that transverse velocities will typically be much smaller than axial velocities, or $V \ll O(1)$. However, transverse velocities will be large locally in a small region near a duct entrance where rapid growth of the viscous layer occurs and where the boundary layer approximation is acknowledged to be poor (e.g. Anderson et al, 1984: p.382).

For a strictly incompressible fluid, thermodynamic expansion and compression processes are absent, so that pressure changes are as a result of dynamic processes only. This suggests $\rho_0 u_m^2$ (i.e. twice the dynamic pressure) as a suitable scale to nondimensionalize the pressure. This practice is also followed in the present quasi—incompressible treatment, albeit the buoyant force originates from a thermal expansion process. Moreover, because the pressure variable $\hat{p}$ only appears under a derivative in the axial momentum equation (3.11), its level is immaterial and a constant value may be subtracted without any effect on the solution. Based on the foregoing arguments the nondimensional pressure variable is defined as

$$ P = \frac{\hat{p} - \hat{p}_0}{\rho_0 u_m^2} \qquad (3.44) $$

where $\hat{p}_0$ is the value of $\hat{p}$ at $x = 0$.

Conventionally, a dimensionless temperature variable is defined by referring the local fluid temperature rise $(T - T_0)$ to some convenient reference temperature difference ΔT_r impressed on the flow. That is

$$ \theta = \frac{T - T_0}{\Delta T_r} \qquad (3.45) $$

For the cases of a uniform wall temperature (UWT) T_w and a uniform wall heat flux (UHF) q_w the obvious definitions for ΔT_r are $(T_w - T_0)$ and $(q_w b / k_0)$ respectively. The aim of the present analysis is to allow any combination of

heating or cooling and UWT or UHF conditions at a duct wall. Consequently, mixed thermal boundary conditions can be envisaged and ΔT_r is defined by one of equations (3.46)–(3.48) below[1].

For UWT conditions:
$$\Delta T_r = \left[\, |T_{w_1} - T_0|,\, |T_{w_2} - T_0|\, \right] \qquad (3.46)$$

For UHF conditions:
$$\Delta T_r = \left[\, |q_{w_1}b/k_0|,\, |q_{w_2}b/k_0|\, \right] \qquad (3.47)$$

where the compact notation $[A,B]$ is defined to denote the larger of the quantities A and B.

For a parallel plate duct or concentric annular duct, where a UWT condition is imposed at one wall and a non–zero uniform heat flux q_w is imposed at the other wall, ΔT_r is arbitrarily defined as follows:

For mixed UWT/UHF conditions:
$$\Delta T_r = |q_w b/k_0| \qquad (3.48)$$

The physical properties are nondimensionalized by using the corresponding values at temperature T_0. The resulting physical property ratios are all functions of θ and are denoted by the following asterisked quantities:

$$\mu^*(\theta) = \frac{\mu}{\mu_0} \qquad\qquad \rho^*(\theta) = \frac{\rho}{\rho_0}$$

$$ \qquad (3.49)$$

$$c^*(\theta) = \frac{c}{c_0} \qquad\qquad k^*(\theta) = \frac{k}{k_0}$$

---

[1]The above θ definitions do not cater for situations where the duct walls are either adiabatic or are maintained at the fluid inlet temperature T_0. However, in both circumstances an energy equation solution would only be required if viscous dissipation alone were of interest, when $\mu_0 u_m^2/k_0$ could serve as a suitable reference value for ΔT_r. Such matters are not pursued further in this thesis.

In addition to the dimensionless variables defined above, the following dimensionless parameters may appear in the nondimensional form of the governing equations:

$$Br = \frac{\mu_0 u_m^2}{k_0 \Delta T_r} \qquad = \text{Brinkmann number} \qquad (3.50)$$

$$G = \frac{g b^3}{\nu_0^2} \qquad = \text{gravitational parameter} \qquad (3.51)$$

$$Gr_b = \frac{g b^3 \beta \Delta T_r}{\nu_0^2} \qquad = \text{Grashof number} \qquad (3.52)$$

$$Pr = \frac{c_0 \mu_0}{k_0} \qquad = \text{Prandtl number} \qquad (3.53)$$

$$Re_b = \frac{\rho_0 u_m b}{\mu_0} \qquad = \text{Reynolds number} \qquad (3.54)$$

In equations (3.50)–(3.54), all physical properties are evaluated at the fluid inlet temperature and Gr_b and Re_b are based on the domain width b (rather than the duct hydraulic diameter d_h). As both the Grashof and the Brinkmann numbers involve ΔT_r, it is evident that the thermal boundary conditions determine whether these parameters are based on a wall temperature or a wall heat flux.

3.3.6 Governing Equations in Nondimensional Form

The following nondimensional forms of the governing equations are obtained when equations (3.42) – (3.45) are used to substitute for the dimensional variables:

i) Partial Differential Equations

The boundary layer equations are now written for the general axisymmetric case with the diffusion terms fully expanded and the spatial property derivatives replaced by equations (3.41). In nondimensional form they become

$$\frac{\partial}{\partial X}\left[F(Y)U\right] + \frac{\partial}{\partial Y}\left[F(Y)V\right] = 0 \qquad (3.55)$$

$$U\frac{\partial U}{\partial X} + V\frac{\partial U}{\partial Y} = -\frac{\partial P}{\partial X} - \frac{SG}{Re_b{}^2}(\rho* - 1)$$

$$+ \frac{1}{Re_b}\left[\mu*\left[\frac{\partial^2 U}{\partial Y^2} + \frac{(1-r*)}{F(Y)}\frac{\partial U}{\partial Y}\right] + \frac{d\mu*}{d\theta}\frac{\partial\theta}{\partial Y}\frac{\partial U}{\partial Y}\right] \qquad (3.56)$$

$$\frac{\partial P}{\partial Y} = 0 \qquad (3.57)$$

$$U\frac{\partial\theta}{\partial X} + V\frac{\partial\theta}{\partial Y} = \frac{1}{c*Re_bPr}\left[k*\left[\frac{\partial^2\theta}{\partial Y^2} + \frac{(1-r*)}{F(Y)}\frac{\partial\theta}{\partial Y}\right]\right.$$

$$\left. + \frac{dk*}{d\theta}\left[\frac{\partial\theta}{\partial Y}\right]^2\right] + \frac{\mu*Br}{c*Re_bPr}\left[\frac{\partial U}{\partial Y}\right]^2 \qquad (3.58)$$

Equations (3.55)–(3.58) can be used for all possible values of r*. The mass continuity equation (3.55) has been multiplied by $(1 - r*)$ to avoid division by zero when $r* = 1$.

It is noted that when the dependence of density on the temperature is given by the linear (Boussinesq) equation (3.39), then the buoyancy term $G(\rho* - 1)/Re_b^2$ in the axial momentum equation (3.56) can be written simply as $-Gr_b\theta/Re_b^2$.

ii) Boundary Conditions at $Y = 0$

The duct centreline conditions, equations (3.14), become

at $Y = 0$, $X > 0$: $\qquad \frac{\partial U}{\partial Y} = 0$, $V = 0$, $\frac{\partial\theta}{\partial Y} = 0$ $\qquad (3.59)$

The inner duct wall conditions, equations (3.15)–(3.18), become

at $Y = 0$, $X > 0$: $\qquad U = 0$, $V = 0$ $\qquad (3.60)$

at $Y = 0$, $0 < X \leq X_{a_1}$: $\qquad \frac{\partial\theta}{\partial Y} = 0$ $\qquad (3.61)$

at $Y = 0$, $X > X_{a_1}$: $\qquad\qquad\qquad \theta = \theta_{w_1}$ $\qquad$ (UWT) $\quad$ (3.62)

or $\quad k_* \dfrac{\partial \theta}{\partial Y} = -\dfrac{q_{w_1}}{q_r} = -r_{q_1}$ $\qquad$ (UHF) $\quad$ (3.63)

where r_{q_1} denotes the ratio of the wall heat flux to the absolute value of the reference heat flux q_r, given by $q_r = [\,|q_{w_1}|\,,\,|q_{w_2}|\,]$.

iii) Boundary Conditions at $Y = 1$

The outer wall conditions, equations (3.19)–(3.22), become

at $Y = 1$, $X > 0$: $\qquad\qquad\qquad U = 0$, $V = 0$ $\qquad\qquad$ (3.64)

at $Y = 1$, $0 < X \leq X_{a_2}$: $\qquad\qquad \dfrac{\partial \theta}{\partial Y} = 0$ $\qquad\qquad$ (3.65)

at $Y = 1$, $X > X_{a_2}$: $\qquad\qquad\qquad \theta = \theta_{w_2}$ $\qquad$ (UWT) $\quad$ (3.66)

or $\quad k_* \dfrac{\partial \theta}{\partial Y} = +\dfrac{q_{w_2}}{q_r} = +r_{q_2}$ $\qquad$ (UHF) $\quad$ (3.67)

iv) Initial Conditions at $X = 0$

The uniform entry profile conditions, equations (3.23), become

at $X = 0$, $0 \leq Y \leq 1$: $\qquad\qquad U = 1$, $V = 0$ $\qquad\qquad$ (3.68)

Equations (3.25)–(3.28), the fully–developed velocity profiles for the various duct geometries considered, become

at $X = 0$, $0 \leq Y \leq 1$:

circular tube: $\qquad\qquad\qquad U = 2\,[1 - Y^2]$, $V = 0$ $\qquad\qquad$ (3.69)

concentric annulus:

$$U = 2 \left[\frac{1 - F(Y) + 2[(r^{*2} - 1)/(2\ln r^*)]\ln F(Y)}{1 + r^{*2} - 2(r^{*2} - 1)/(2\ln r^*)} \right] , V = 0 \qquad (3.70)$$

parallel plates:

— symmetric problems $\qquad\qquad U = 1.5\left[1 - Y^2\right] , V = 0 \qquad\qquad (3.71)$

— asymmetric problems $\qquad\qquad U = 6\left[Y - Y^2\right] , V = 0 \qquad\qquad (3.72)$

The initial conditions for the temperature and the pressure, given by equations (3.29), become

at $X = 0 , 0 \leq Y \leq 1$: $\qquad\qquad \theta = 0 , P = 0 \qquad\qquad\qquad (3.73)$

v) Integral Balance Equations

Introducing the definitions of U and Y, given by equations (3.42), into the integral mass balance equation (3.32), we obtain

$$\frac{(1 + r^*)}{2} = \int_0^1 F(Y) \, U \, dY \qquad\qquad (3.74)$$

The integral energy balance equation (3.36) can also be expressed in nondimensional form as

$$\frac{d}{dX}(c_{mb} \theta_b) = \frac{2}{Re_b Pr(1 + r^*)} \left[\left[k^* \frac{\partial \theta}{\partial Y} \right]_{Y=1} - r^* \left[k^* \frac{\partial \theta}{\partial Y} \right]_{Y=0} \right]$$

$$+ \frac{2 \, Br}{Re_b Pr(1 + r^*)} \int_0^1 F(Y)\mu^* \left[\frac{\partial U}{\partial Y} \right]^2 dY \qquad (3.75)$$

The dimensionless equivalents of equation (3.34) and equation (3.35) are, respectively:

$$c_{m\bar{b}}^* = \frac{c_{\underline{m}b}}{c_o} = \frac{1}{\theta_b} \int_0^\theta c^* \, d\theta \tag{3.76}$$

and
$$\theta_b = \frac{2}{c_{m\bar{b}}^*(1 + r^*)} \int_0^1 F(Y) \, U c_m^* \theta \, dY \tag{3.77}$$

vi) Property Relations

The physical property ratios, defined by equations (3.49), and the derivatives $d\mu^*/d\theta$ and $dk^*/d\theta$ appearing in equation (3.56) and equation (3.58) respectively, can be expressed in terms of the dimensionless temperature θ.

When a polynomial function gives the dependence on temperature of a property ψ, the expression is given by the dimensionless form of equation (3.38). That is

$$\psi^* = \frac{\psi}{\psi_0} = [1 + A_{\psi 1}\theta + A_{\psi 2}\theta^2 + \cdots + A_{\psi n}\theta^n] \tag{3.78}$$

where $A_{\psi i} = a_{\psi i}/\Delta T_r^i$, from which we obtain

$$\frac{d\psi^*}{d\theta} = [A_{\psi 1} + 2A_{\psi 2}\theta + \cdots + nA_{\psi n}\theta^{n-1}] \tag{3.79}$$

The corresponding results for the power law equation (3.40) are

$$\mu^* = [C_1\theta + 1]^{-C_2} \tag{3.80}$$

and
$$\frac{d\mu^*}{d\theta} = -C_1 C_2 [C_1\theta + 1]^{-(C_2+1)} \tag{3.81}$$

where $C_1 = \Delta T_r/(T_0 + c_1)$ and $C_2 = c_2$.

3.4 Numerical Methods

The governing equations presented in Section 3.3 are too formidably complex to contemplate an analytical solution, except under restrictive simplifying assumptions. In contrast, numerical methods allow the maximum generality to be retained in these equations. They also offer the flexibility to obtain tractable solutions of acceptable accuracy for a wide range of duct geometries, initial and boundary conditions and fluid property variations.

Since the partial differential equations governing flow and heat transfer for unidirectional duct flows are parabolic in nature, they can be integrated by a step–by–step marching procedure. Starting from given initial data at the upstream boundary, the equations are solved by marching in the downstream direction. The numerical technique employed here is a fully–implicit finite–difference method.
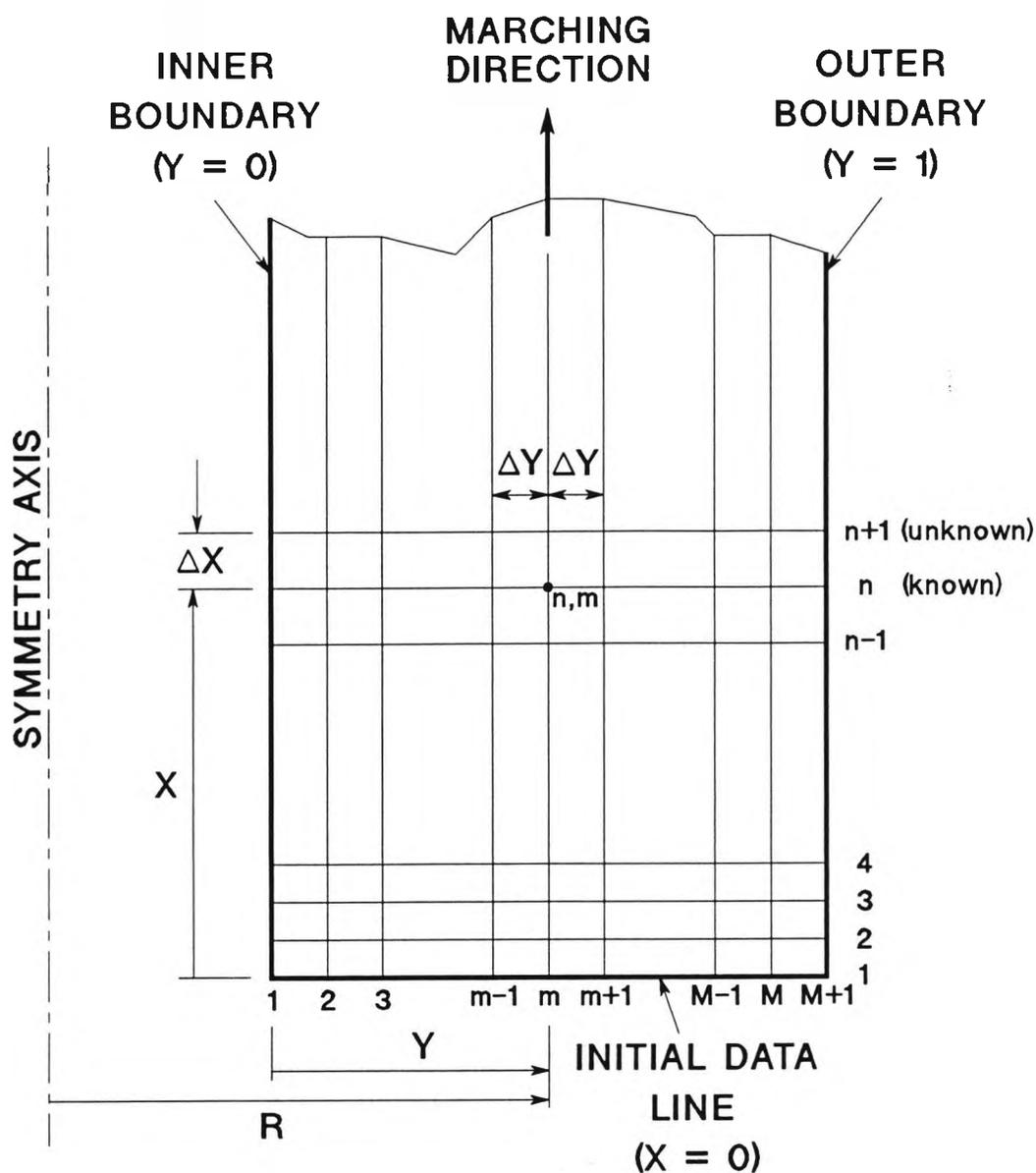
Figure 3.3 Finite–Difference Grid.

3.4.1 Discretization of the Problem Domain

An essential step in the finite–difference method is the replacement of the continuous physical domain by a finite number of discrete grid points forming a finite–difference grid. Partial derivatives are approximated locally by differences between dependent variable values at adjacent grid points, thus reducing the governing equations to a system of algebraic equations.

The finite—difference grid for the present problem is illustrated in Figure 3.3. The grid point locations in the axial (or marching) direction and the transverse direction are given by the general subscripts n and m respectively. It is assumed that n = 1 at X = 0 (the upstream boundary or initial data line) and m = 1 at Y = 0 (inner boundary). The number of transverse grid divisions is denoted by M, so that m = M + 1 at Y = 1 (outer boundary). A uniform grid spacing is used in the transverse direction. To allow certain cross—stream integrals (e.g. bulk temperature) to be evaluated using Simpson's one—third rule, M is always taken to be even. The uniform transverse grid spacing ΔY and the dimensionless transverse coordinate value Y_m at the grid point (n, m), are respectively

$$\Delta Y = \frac{1}{M} \tag{3.82}$$

and
$$Y_m = (m - 1)\Delta Y \tag{3.83}$$

The marching step size for the finite—difference method is the axial grid spacing ΔX. Stability analyses, such as those presented by Bodoia (1959) and Hornbeck (1973), indicate that a fully—implicit finite—difference representation of the boundary layer equations will be unconditionally stable for all values of ΔX if the axial velocity U remains positive. Nevertheless, Hornbeck (1973) recommended that very small values of ΔX should be used near X = 0 to restrict the downstream spread of the effect of the mathematical singularity represented by the uniform flow profile initial condition. Anderson et al (1984) note that reduction of ΔX, at any location, helps to reduce the truncation errors associated with the finite—difference approximation of the derivatives and the linearization of coefficients. To economise on computation time, progressively larger values of ΔX are normally utilised as the solution is advanced downstream, because the dependent variables change less rapidly. If desired, the present scheme allows ΔX

to be changed at every forward step. In practice, however, an even number of equal–sized intervals is employed between axial step size changes, to allow Simpson's one–third rule to be used for the calculation of length–averaged quantities (e.g. mean friction factor) at every other step. The dimensionless axial coordinate value X_n at the grid point (n,m) can be found from

$$X_n = \sum_{i=1}^{n-1} \Delta X_i \tag{3.84}$$

where i denotes the axial step number.

Finally, it should be stated that to establish that the solutions obtained are independent of the grid spacings ΔX and ΔY, numerical experiments should be performed for progressively finer grids.

3.4.2 Finite–Difference Approximations

The fully–implicit method is so named because transverse derivatives in the governing equations are replaced by finite–difference approximations involving unknown values at the n + 1 level (see Figure 3.3). Furthermore, special measures must be taken to deal with the nonlinearities inherent in the governing equations. These are due to the convective terms in the partial differential equations and the variation of the fluid properties with temperature. The computational procedure described here includes iteration within each axial marching step to handle these difficulties. The resulting set of linear algebraic equations, written for all grid points at the n + 1 level, must be solved simultaneously to obtain the unknowns.

In the following exposition of the fully–implicit scheme, axial (X–direction) and transverse (Y–direction) partial derivatives are replaced by the finite–difference approximations given below:

$$\left[\frac{\partial F}{\partial X}\right]_{n+1,m} \approx \frac{F_{n+1,m} - F_{n,m}}{\Delta X} \tag{3.85}$$

$$\left[\frac{\partial F}{\partial Y}\right]_{n+1,m} \approx \frac{F_{n+1,m+1} - F_{n+1,m-1}}{2\Delta Y} \tag{3.86}$$

$$\left[\frac{\partial^2 F}{\partial Y^2}\right]_{n+1,m} \approx \frac{F_{n+1,m+1} - 2F_{n+1,m} + F_{n+1,m-1}}{(\Delta Y)^2} \tag{3.87}$$

where F is used to represent any of the dependent variables U, V, P and θ. The approximations (3.85)–(3.87) can be developed from Taylor series expansions for $F_{n+1,m+1}$, $F_{n+1,m-1}$ and $F_{n,m}$ about the unknown level grid point (n + 1, m). Corresponding expressions are found for other expansion points.

The difference between a partial derivative and its finite–difference approximation is called the truncation error (TE_{pd}) and is determined by the sum of the discarded terms originating from the infinite Taylor series. In the derivation of the backward–difference formula (3.85), terms involving ΔX and higher powers of ΔX are truncated, and therefore it is said to have a truncation error of order ΔX, written as $O(\Delta X)$. It should be understood that $O(\Delta X)$ indicates the behaviour of the truncation error as ΔX tends to zero. For consistency, the truncation error associated with approximation (3.85) should satisfy $\lim_{\Delta X \to 0}(TE_{pd}) = 0$, which is clearly true. The central–difference approximations (3.86) and (3.87) both have truncation errors of $O[(\Delta Y)^2]$, thus establishing their consistency with the corresponding partial derivatives.

The notions of truncation error and consistency are also applicable to the finite–difference representation of an entire partial differential equation. If each

derivative is approximated at the same grid point, the individual truncation errors can be added to give the truncation error of the complete equation, denoted by (TE_{pde}). For consistency, this should also vanish under grid refinement, i.e. $\lim_{\Delta X \to 0, \Delta Y \to 0}(TE_{pde}) = 0$.

In the finite–difference formulation, it is often necessary to express the value of a dependent variable at a boundary when only the normal derivative is given explicitly by the boundary conditions or vice versa. Implicit replacements for the the missing quantities are provided by suitably rearranging the following 3–point, one–sided approximations:

at $Y = 0$:
$$\left[\frac{\partial F}{\partial Y}\right]_{m=1} \approx \frac{1}{2\Delta Y}\left[-3F_{m=1} + 4F_{m=2} - F_{m=3}\right] \tag{3.88}$$

at $Y = 1$:
$$\left[\frac{\partial F}{\partial Y}\right]_{m=M+1} \approx \frac{1}{2\Delta Y}\left[3F_{m=M+1} - 4F_{m=M} + F_{m=M-1}\right] \tag{3.89}$$

where the X–coordinate subscripts have been omitted for clarity. The approximations (3.88) and (3.89) provide consistent representations of the first derivatives with a truncation error $O[(\Delta Y)^2]$ and the boundary values with a truncation error of $O[(Y)^3]$. They are also used to recover local boundary values and normal gradients from the velocity and temperature solutions in order to calculate heat transfer and wall friction parameters[3].

---

[3]For comparison, these quantities are also calculated using 4–point and 5–point, one–sided derivative approximations, with $O[(\Delta Y)^3]$ and $O[(\Delta Y)^4]$ truncation errors respectively, in the computer implementation. At the $Y = 0$ boundary, for example, these alternative approximations are:

$$\left[\frac{\partial F}{\partial Y}\right]_{m=1} \approx \frac{1}{6\Delta Y}\left[-11F_{m=1} + 18F_{m=2} - 9F_{m=3} + 2F_{m=4}\right]$$

$$\left[\frac{\partial F}{\partial Y}\right]_{m=1} \approx \frac{1}{12\Delta Y}\left[-25F_{m=1} + 48F_{m=2} - 36F_{m=3} + 16F_{m=4} - 3F_{m=5}\right]$$

The finite–difference representation of the governing partial differential and integral equations are considered separately below.

i) Mass Continuity Equation

In the solution procedure the differential continuity equation is not solved simultaneously with the momentum equations. Instead, equation (3.55) is integrated over one transverse grid spacing to develop the following auxiliary equation for $V_{n+1,m}$:

$$V_{n+1,m} = \frac{1}{F(Y)_m}\left[F(Y)_{m-1}V_{n+1,m-1} - \int_{Y_{m-1}}^{Y_m}\frac{\partial}{\partial X}\left[F(Y)U\right]dY\right] \qquad (3.90)$$

The integral in equation (3.90) is evaluated by the trapezoidal rule with the integrand replaced at each end of the interval using the backward–difference approximation (3.85). This gives

$$(V_{n+1,m})_{1-2} = \frac{1}{F(Y)_m}\left[F(Y)_{m-1}V_{n+1,m-1} - \frac{\Delta Y}{2\Delta X}\left[F(Y)_m(U_{n+1,m} - U_{n,m})\right.\right.$$

$$\left.\left. + F(Y)_{m-1}(U_{n+1,m-1} - U_{n,m-1})\right]\right] \qquad (3.91)$$

If equation (3.91) is derived using Taylor series expansions about some convenient point, such as the off–grid position $(n + 1, m - \frac{1}{2})$, it can be shown that its truncation error is $O[\Delta X, (\Delta Y)^2]$.

At each marching step, the transverse velocity components are calculated at each grid position on the $n + 1$ level after the axial velocities have been solved for. Equation (3.91) is applied recursively to calculate the $V_{n+1,m}$ values in the sequential order $V_{n+1,2}, V_{n+1,3} \cdots V_{n+1,m}$, moving outward from the inner boundary (see Figure 3.3), invoking the boundary condition $V_{n+1,1} = 0$ to start the process. Since $V_{n+1,M+1} = 0$, the transverse velocities can also be found in the

reverse order, starting at the outer boundary and moving inward. The corresponding version of equation (3.91) is

$$(V_{n+1,m})_{2-1} = \frac{1}{F(Y)_m}\left[F(Y)_{m+1}V_{n+1,m+1} + \frac{\Delta Y}{2\Delta X}\left[F(Y)_m(U_{n+1,m} - U_{n,m})\right.\right.$$

$$\left.\left. + F(Y)_{m+1}(U_{n+1,m+1} - U_{n,m+1})\right]\right] \qquad (3.92)$$

The additional subscripts 1–2 and 2–1 indicate the direction of calculation for equation (3.91) and equation (3.92) respectively.

Separate numerical tests were performed during this research to compare values of $V_{n+1,m}$ calculated from equations (3.91) and (3.92) for the case of hydrodynamically developing flow in a circular tube. Very close agreement was found at all axial and transverse positions when the trapezoidal rule was used to evaluate the integral continuity equation. Initially, Simpson's rule was employed, resulting in differences of magnitude (and sign in some cases) between the $V_{n+1,m}$ values for the two directions of calculation. These were particularly severe for the first few marching steps, but this appeared to have little effect on the axial velocity profile development and the pressure drop. Recalling that the derivation of equation (3.91) was based on the trapezoidal rule, this experience emphasises the need to use the same approximation for its integral form, if reliable predictions of transverse velocities are to be obtained. Dalbert et al (1981) also observed that the trapezoidal rule is the only integral approximation compatible with equation (3.91).

In their study of asymmetric free convection between vertical parallel plates Aung et al (1972) calculated $V_{n+1,m}$ using equation (3.91) on one side of the duct centreline and equation (3.92) on the other side. The centreline value was obtained by fitting a third order polynomial through adjacent points on both sides. Miyatake and Fujii (1972) and Aihara (1973) used a combination of equation

(3.91) and equation (3.92), involving the transverse coordinate Y as a local weighting factor. Their equation can be written as

$$V_{n+1,m} = (1 - Y_m)(V_{n+1,m})_{1-2} + Y_m(V_{n+1,m})_{2-1} \tag{3.93}$$

Equation (3.93) satisfies the boundary conditions V = 0 at Y = 0 and 1 irrespective of numerical errors and for this reason was adopted for this work.

ii) Axial Momentum Equation

Using the approximations (3.85)–(3.87) to replace the derivatives in equation (3.56) results in the following finite–difference equation which has a truncation error of $O[\Delta X, (\Delta Y)^2]$:

$$U_{n+1,m}^{\bullet}\left[\frac{U_{n+1,m} - U_{n,m}}{\Delta X}\right] + V_{n+1,m}^{\bullet}\left[\frac{U_{n+1,m+1} - U_{n+1,m-1}}{2\Delta Y}\right] = -\left[\frac{P_{n+1,m} - P_{n,m}}{\Delta X}\right]$$

$$-\frac{SG}{Re_b^2}\left[(\rho^*)_{n+1,m}^{\bullet} - 1\right] + \frac{1}{Re_b}\left[(\mu^*)_{n+1,m}^{\bullet}\left\{\left[\frac{U_{n+1,m+1} - 2U_{n+1,m} + U_{n+1,m-1}}{(\Delta Y)^2}\right]\right.\right.$$

$$\left.+ \frac{(1 - r^*)}{F(Y)_m}\left[\frac{U_{n+1,m+1} - U_{n+1,m-1}}{2\Delta Y}\right]\right\}$$

$$+ \left[\frac{d\mu^*}{d\theta}\right]_{n+1,m}^{\bullet}\left[\frac{\theta_{n+1,m+1}^{\bullet} - \theta_{n+1,m-1}^{\bullet}}{2\Delta Y}\right]\left[\frac{U_{n+1,m+1} - U_{n+1,m-1}}{2\Delta Y}\right]\right] \tag{3.94}$$

At each marching step, equation (3.94) is used within an iterative procedure, involving all the governing equations, to obtain the values of $U_{n+1,m}$ and $P_{n+1,m}$. To make equation (3.94) algebraically linear the superscripted quantities (denoted by a bullet •) are approximated by their most recently calculated values. Initially, the corresponding values obtained at the previous step (n level) are utilised. Subsequently, these are updated to the values found in the previous iteration at the n + 1 level. As the superscripted quantities in general depend on the temperature, it is implied that a solution of the energy equation must be included

in each iteration. For constant–property, forced convection situations the iterative procedure just described is not usually employed and the values of $U^{\bullet}_{n+1,m}$ and $V^{\bullet}_{n+1,m}$ in the inertia terms are simply approximated by the corresponding values at level n. The resulting errors should not be serious if the axial step size ΔX is not too large.

For the matrix solution, equation (3.94) is written in the form

$$A^{(1)}_m U_{n+1,m-1} + A^{(2)}_m U_{n+1,m} + A^{(3)}_m P_{n+1,m} + A^{(4)}_m U_{n+1,m+1} = B^{(1)}_m \qquad (3.95)$$

where

$$A^{(1)}_m = -\frac{V^{\bullet}_{n+1,m}}{2\Delta Y} - \frac{1}{Re_b(\Delta Y)^2}\left[(\mu^*)^{\bullet}_{n+1,m}\left[1 - \frac{(1 - r^*)\Delta Y}{2F(Y)_m}\right]\right.$$

$$\left. - \frac{1}{4}\left[\frac{d\mu^*}{d\theta}\right]^{\bullet}_{n+1,m}\left[\theta^{\bullet}_{n+1,m-1} - \theta^{\bullet}_{n+1,m+1}\right]\right]$$

$$A^{(2)}_m = \frac{U^{\bullet}_{n+1,m}}{\Delta X} + \frac{1}{Re_b(\Delta Y)^2}\left[2(\mu^*)^{\bullet}_{n+1,m}\right]$$

$$A^{(3)}_m = \frac{1}{\Delta X} \qquad (3.96)$$

$$A^{(4)}_m = \frac{V^{\bullet}_{n+1,m}}{2\Delta Y} - \frac{1}{Re_b(\Delta Y)^2}\left[(\mu^*)^{\bullet}_{n+1,m}\left[1 + \frac{(1 - r^*)\Delta Y}{2F(Y)_m}\right]\right.$$

$$\left. + \frac{1}{4}\left[\frac{d\mu^*}{d\theta}\right]^{\bullet}_{n+1,m}\left[\theta^{\bullet}_{n+1,m-1} - \theta^{\bullet}_{n+1,m+1}\right]\right]$$

$$B^{(1)}_m = \frac{U^{\bullet}_{n+1,m} U_{n,m}}{\Delta X} + \frac{P_{n,m}}{\Delta X} - \frac{SG}{Re_b^2}\left[(\rho^*)^{\bullet}_{n+1,m} - 1\right]$$

All the quantities involved in the coefficients A_m and the right–hand sides B_m are either known or can be approximated by previously calculated values. The integer

superscripts in parentheses identify the variable each A_m associates with and the equation respectively.

Equation (3.96) can be used in exactly the form presented for the interior grid points $m = 3$ to $m = M - 1$. For the grid points $m = 2$ and $m = M$, adjacent to the inner and outer boundaries respectively, some minor modifications are made to accommodate the relevant boundary conditions for U. For a duct centreline at the inner boundary, the velocity $U_{n+1,1}$ can be expressed in terms of $U_{n+1,2}$ and $U_{n+1,3}$ by using the approximation (3.88) to write the symmetry boundary condition for U, given by equation (3.59), in finite–difference form. The modified coefficients (indicated by a tilde ~) to be used in equation (3.95) for $m = 2$ are as follows:

$$\tilde{A}_{m=2}^{(1)} = 0 \ , \ \tilde{A}_{m=2}^{(2)} = A_{m=2}^{(2)} + \frac{4}{3} A_{m=2}^{(1)} \ , \ \tilde{A}_{m=2}^{(4)} = A_{m=2}^{(4)} - \frac{1}{3} A_{m=2}^{(1)} \qquad (3.97)$$

After the velocity solution has been obtained the reverse procedure is used to obtain $U_{n+1,1}$. When the inner boundary is formed by a duct wall the no–slip condition $U_{n+1,1} = 0$, given by equation (3.60), is enforced by setting $\tilde{A}_{m=2}^{(1)} = 0$. Since the outer boundary is always a duct wall it follows that $\tilde{A}_{m=M}^{(4)} = 0$ in all cases.

iii) Transverse Momentum Equation

In the present formulation of the algebraic finite–difference equations, pressure is treated as an unknown quantity[4], which is solved for with the help of the integral mass balance equation.

---

[4]An alternative approach employed with implicit schemes, exemplified by the Patankar–Spalding method (see Patankar (1988) for a recent description) is to use an estimate of the pressure gradient at each stage of the calculation. The resulting velocities will not in general satisfy the global mass flow constraint and the imbalance is used to adjust the pressure gradient for the next step or iteration. Anderson et al (1984) review several methods of this type.

The degenerate form of the transverse momentum equation (3.57) is a reminder that pressure variations are neglected for the transverse direction under the boundary layer simplifications. Thus the pressure is regarded as a function of the X—coordinate only and at any cross—section it is characterized by a single value. However, in the computational method used here, the pressures at all interior grid points on the n + 1 level are included as separate unknowns. To ensure that $\partial P/\partial Y = 0$ is satisfied, these pressures are linked using the following exact difference representation for m = 2 to m = M:

$$A_m^{(5)} P_{n+1,m} + A_m^{(6)} P_{n+1,m+1} = B_m^{(2)} \tag{3.98}$$

where $A_m^{(5)} = 1$, $A_m^{(6)} = -1$ and $B_m^{(2)} = 0$.

Although the use of equation (3.98) is open to the criticism that it introduces $M - 2$ redundant pressures, it nevertheless appears to work satisfactorily. Its main advantage is that it allows the finite—difference equations for the velocity—pressure solution to be assembled in band matrix form. When equation (3.98) is not used and a single unknown pressure is considered at each step, the system of equations obtained is sparse and unbanded. Although solution can be effected using conventional Gaussian elimination, this will not be computationally efficient for a large number of transverse grid points. For this reason, Bodoia (1959) and later Bodoia and Osterle (1962) used a special elimination method to take advantage of the sparseness. In contrast, the band matrix formulation allows solution by standard techniques and requires less storage and fewer arithmetic operations, despite the larger number of equations.

iv) Energy Equation

The treatment of the energy equation (3.58) is the same as for the corresponding terms in the axial momentum equation and the resulting truncation error is also

$O[\Delta X, (\Delta Y)^2]$. The finite–difference representation is written as

$$U^{\bullet}_{n+1,m}\left[\frac{\theta_{n+1,m} - \theta_{n,m}}{\Delta X}\right] + V^{\bullet}_{n+1,m}\left[\frac{\theta_{n+1,m+1} - \theta_{n+1,m-1}}{2\Delta Y}\right]$$

$$= \frac{1}{Re_b Pr(c^*)^{\bullet}_{n+1,m}}\left[(k^*)^{\bullet}_{n+1,m}\left\{\left[\frac{\theta_{n+1,m} - 2\theta_{n+1,m} + \theta_{n+1,m-1}}{(\Delta Y)^2}\right]\right.\right.$$

$$\left.+ \frac{(1 - r^*)}{F(Y)_m}\left[\frac{\theta_{n+1,m+1} - \theta_{n+1,m-1}}{2\Delta Y}\right]\right\}$$

$$+ \left[\frac{dk}{d\theta}\right]^{\bullet}_{n+1,m}\left[\frac{\theta^{\bullet}_{n+1,m+1} - \theta^{\bullet}_{n+1,m-1}}{2\Delta Y}\right]\left[\frac{\theta_{n+1,m+1} - \theta_{n+1,m-1}}{2\Delta Y}\right]\right]$$

$$+ \frac{Br}{Re_b Pr}\left[\frac{\mu^*}{c^*}\right]^{\bullet}_{n+1,m}\left[\frac{U^{\bullet}_{n+1,m+1} - U^{\bullet}_{n+1,m-1}}{2\Delta Y}\right]^2 \tag{3.99}$$

As before, equation (3.99) is linearized by using the latest estimates of the superscripted quantities (indicated by a bullet •). Since the velocity solution is obtained first during each iteration, estimates of $U_{n+1,m}$ and $V_{n+1,m}$ are already available when the temperature distribution is solved for at the n + 1 level. All the other superscripted quantities in equation (3.99) must initially be evaluated at the n level before being updated to the n + 1 level.

The unknown $\theta_{n+1,m}$ values can be found by simultaneous solution of the set of M − 1 algebraic equations obtained by rearranging equation (3.99) for each interior grid point and incorporating suitable modifications for the thermal boundary conditions. This system can be written as

$$A_m^{(7)}\,\theta_{n+1,m-1} + A_m^{(8)}\,\theta_{n+1,m} + A_m^{(9)}\,\theta_{n+1,m+1} = B_m^{(3)} \tag{3.100}$$

for m = 2 to m = M. The coefficients in equation (3.100) form a tridiagonal matrix and for m = 3 to m = M − 1 are given by

$$A_m^{(7)} = -\frac{V_{n+1,m}^{\bullet}}{2\Delta Y} - \frac{1}{Re_b Pr(\Delta Y)^2(c^*)_{n+1,m}^{\bullet}}\left[(k^*)_{n+1,m}^{\bullet}\left[1 - \frac{(1 - r^*)\Delta Y}{2F(Y)_m}\right]\right.$$

$$\left.- \frac{1}{4}\left[\frac{dk^*}{d\theta}\right]_{n+1,m}^{\bullet}\left[\theta_{n+1,m-1}^{\bullet} - \theta_{n+1,m+1}^{\bullet}\right]\right]$$

$$A_m^{(8)} = \frac{U_{n+1,m}^{\bullet}}{\Delta X} + \frac{1}{Re_b Pr(\Delta Y)^2(c^*)_{n+1,m}^{\bullet}}\left[2(k^*)_{n+1,m}^{\bullet}\right] \qquad (3.101)$$

$$A_m^{(4)} = \frac{V_{n+1,m}^{\bullet}}{2\Delta Y} - \frac{1}{Re_b Pr(\Delta Y)^2(c^*)_{n+1,m}^{\bullet}}\left[(k^*)_{n+1,m}^{\bullet}\left[1 + \frac{(1 - r^*)\Delta Y}{2F(Y)_m}\right]\right.$$

$$\left.+ \frac{1}{4}\left[\frac{dk^*}{d\theta}\right]_{n+1,m}^{\bullet}\left[\theta_{n+1,m-1}^{\bullet} - \theta_{n+1,m+1}^{\bullet}\right]\right]$$

The right—hand side of equation (3.99) is given by

$$B_m^{(3)} = \frac{U_{n+1,m}^{\bullet}\theta_{n,m}}{\Delta X} + \frac{Br}{4Re_b Pr(\Delta Y)^2}\left[\frac{\mu^*}{c^*}\right]_{n+1,m}^{\bullet}\left[U_{n+1,m+1}^{\bullet} - U_{n+1,m-1}^{\bullet}\right]^2 \qquad (3.102)$$

The coefficients (3.101) and the right—hand side (3.102) must be modified for m = 2 and m = M, according to the type of thermal boundary condition at the adjacent boundary. For a uniform wall temperature (UWT), either $\theta_{n+1,1} = \theta_{w_1}$ or $\theta_{n+1,M+1} = \theta_{w_2}$, as given by the boundary conditions (3.62) and (3.66) respectively. In either case, the term containing the given θ_w value is moved to the right—hand side of equation (3.100) and the coefficients are modified accordingly, as follows:

UWT at Y = 0: $\qquad \tilde{A}_{m=2}^{(7)} = 0$, $\tilde{B}_{m=2}^{(3)} = B_{m=2}^{(3)} - A_{m=2}^{(7)}\theta_{w_1}$ $\qquad\qquad$ (3.103)

UWT at Y = 1: $\qquad \tilde{A}_{m=M}^{(9)} = 0$, $\tilde{B}_{m=M}^{(3)} = B_{m=M}^{(3)} - A_{m=M}^{(9)}\theta_{w_2}$ $\qquad\qquad$ (3.104)

Where a normal derivative type thermal boundary condition applies (i.e. for a uniform wall heat flux, an adiabatic wall or for thermal symmetry at a duct

centreline), approximation (3.88) or (3.89), as appropriate, is used to substitute for θ at the boundary. For the uniform heat flux (UHF) conditions, given by equations (3.63) and (3.67), the modified coefficients are as follows:

UHF at Y = 0: $\qquad \tilde{A}_{m=2}^{(7)} = 0 \, , \, \tilde{A}_{m=2}^{(8)} = A_{m=2}^{(8)} + \frac{4}{3} A_{m=2}^{(7)}$

$$(3.105)$$

$$\tilde{A}_{m=2}^{(9)} = A_{m=2}^{(9)} - \frac{1}{3} A_{m=2}^{(7)} \, , \, \tilde{B}_{m=2}^{(3)} = B_{m=2}^{(3)} - \frac{2}{3} A_{m=2}^{(7)} \, r_{q1} \frac{\Delta Y}{(k^*)}\!\!\!\!\!{}^{\bullet}_{n+1,1}$$

UHF at Y = 1: $\qquad \tilde{A}_{m=M}^{(7)} = A_{m=M}^{(7)} - \frac{1}{3} A_{m=M}^{(9)} \, , \, \tilde{A}_{m=M}^{(8)} = A_{m=M}^{(8)} + \frac{4}{3} A_{m=M}^{(9)}$

$$(3.106)$$

$$\tilde{A}_{m=M}^{(9)} = 0 \, , \, \tilde{B}_{m=M}^{(3)} = B_{m=M}^{(3)} - \frac{2}{3} A_{m=M}^{(9)} \, r_{q2} \frac{\Delta Y}{(k^*)}\!\!\!\!\!{}^{\bullet}_{n+1,M+1}$$

The boundary values of the temperature dependent thermal conductivity ratio k^* appearing in equations (3.105) and (3.106) are re-evaluated at each iteration after the provisional $\theta_{n+1,m}$ solution has been obtained. The required boundary temperatures are calculated from approximations (3.88) and (3.89). Equations (3.105) and (3.106) can also be used for thermal symmetry and adiabatic boundary conditions when r_{q1} and r_{q2} are set to zero.

v) Integral Mass Balance

As previously explained, the integral mass balance equation (3.74) should be evaluated using the trapezoidal rule for compatibility with the finite-difference treatment of the differential continuity equation considered in (i) above.

The quadrature is performed in a piecewise manner over each of the M equal grid spacings between Y = 0 and Y = 1, so that equation (3.74) is approximated by

$$\frac{(1 + r^*)}{2} = \frac{\Delta Y}{2} \sum_{m=2}^{m=M+1} \left[F(Y)_{m-1} U_{n+1,m-1} + F(Y)_m U_{n+1,m} \right] \qquad (3.107)$$

In a similar fashion to Ogunba (1972), a new variable W is now introduced, defined by

$$W_{n+1,m} = W_{n+1,m-1} + \frac{\Delta Y}{2} \left[F(Y)_{m-1} U_{n+1,m-1} + F(Y)_m U_{n+1,m} \right] \qquad (3.108)$$

By comparing equations (3.107) and (3.108) it can be deduced that $W_{n+1,m}$ is simply the trapezoidal approximation to the continuity integral, evaluated over the range $Y = 0$ to Y_m. The appropriate boundary conditions are

at $Y = 0$: $\qquad\qquad\qquad\qquad W_{n+1,1} = 0 \qquad\qquad\qquad\qquad (3.109)$

at $Y = 1$: $\qquad\qquad\qquad W_{n+1,M+1} = \frac{(1 + r^*)}{2} \qquad\qquad\qquad (3.110)$

Using the additional variable W, which Barrow et al (1974) referred to as a pseudo stream function, equation (3.107) is replaced by M linear algebraic equations in W and U. This set of equations, which is suited to a band matrix formulation, is formed by writing equation (3.108) as

$$A_m^{(10)} W_{n+1,m-1} + A_m^{(11)} U_{n+1,m-1} + A_m^{(12)} W_{n+1,m}$$
$$+ A_m^{(13)} U_{n+1,m} + A_m^{(14)} U_{n+1,m+1} = B_m^{(4)} \qquad (3.111)$$

for $m = 2$ to $m = M+1$, where

$$A_m^{(10)} = 1 , \ A_m^{(11)} = F(Y)_{m-1} \frac{\Delta Y}{2} , \ A_m^{(12)} = -1$$

$$(3.112)$$

$$A_m^{(13)} = F(Y)_m \frac{\Delta Y}{2} , \ A_m^{(14)} = 0 , \ B_m^{(4)} = 0$$

To accommodate the various boundary conditions on W and U, the modifications detailed below are necessary.

Duct wall at Y = 0:
$$\tilde{A}_{m=2}^{(10)} = 0 \;,\; \tilde{A}_{m=2}^{(11)} = 0 \tag{3.113}$$

Duct centreline at Y = 0:
$$\tilde{A}_{m=2}^{(10)} = 0 \;,\; \tilde{A}_{m=2}^{(13)} = A_{m=2}^{(13)} + \frac{4}{3} A_{m=2}^{(11)} \tag{3.114}$$

$$\tilde{A}_{m=2}^{(11)} = 0 \;,\; \tilde{A}_{m=2}^{(14)} = -\frac{1}{3} A_{m=2}^{(11)}$$

Outer boundary wall (Y = 1):
$$\tilde{A}_{m=M+1}^{(12)} = 0 \;,\; \tilde{A}_{m=M+1}^{(13)} = 0 \tag{3.115}$$

$$\tilde{B}_{m=M+1} = \frac{(1 + r^*)}{2}$$

vi) Integral Energy Balance

Optionally, the integral (or global) energy balance equation (3.75) can be used to replace one of the set of finite–difference equations (3.100) representing the differential (or local) energy balance equations. Although in principle any one of these equations can be substituted for, the programming complexity is less if the finite–difference equation for a grid point immediately adjacent to one or other of the boundaries is eliminated. In this work, the grid point (n + 1, M) next to the outer boundary has normally been selected[5].

---

[5]During the computer program development an odd numbered grid point (n + 1, J), where J = 2∗INT(M/4) + 1, mid–way between the inner and outer boundaries, was also tried. The rationale for choosing a grid point position removed from either boundary was to minimise any possible error in the temperature solution near a heat transfer surface caused by not enforcing a differential (local) energy balance. The calculated temperature distribution exhibited a lack of smoothness around the point (n + 1, J) which has not been further investigated and the approach has been temporarily abandoned.

To apply equation (3.75) it is first integrated over one axial step and equation (3.77) is used to substitute for θ_b at the n + 1 level. This gives

$$\left[\int_0^1 F(Y)Uc_m{}^*\theta\,dY\right]_{n+1} = \frac{(1\ +\ r^*)}{2}(c_{mb}^*\theta_b)_n$$

$$+ \frac{\Delta X}{Re_b Pr}\left[\left[k*\frac{\partial\theta}{\partial Y}\right]_{Y=1} - r^*\left[k*\frac{\partial\theta}{\partial Y}\right]_{Y=0}\right]$$

$$+ \frac{Br\ \Delta X}{Re_b Pr}\overline{\int_0^1 F(Y)\,\mu^*\left[\frac{\partial U}{\partial Y}\right]^2 dY} \qquad (3.116)$$

where $(c_{mb}^*\theta_b)_n$ is known from the previous step. In equation (3.116), the overbars denote that the relevant quantities should strictly be averaged over the interval ΔX, but in the present treatment they are simply evaluated at the end of the interval (i.e. n + 1 level). This assumption will cause no error for a uniform wall heat flux, since $(k*\partial\theta/\partial Y)_w$ is constant anyway and given by either equation (3.63) or equation (3.67) as appropriate. It should also be adequate for the viscous dissipation term, which in most cases is negligible. However, for a uniform duct wall temperature $(k*\partial\theta/\partial Y)_w$ is not axially uniform and some error might be expected if ΔX is made too large.

The discretized version of equation (3.116) is obtained by evaluating the integrals numerically. Here, the integral on the left—hand side is evaluated piecewise, using Simpson's one—third rule over each two adjacent intervals. Proceeding in a manner similar to that used for the integral mass balance equation, a further new variable E is introduced. For the even numbered (i.e. m = 2, 4 $\cdots$ M) grid points

$$E_m = E_{m-1} + \frac{\Delta Y}{3}\left[\left[F(Y)Uc_m{}^*\theta)\right]_{n+1,m-1} + 4\left[F(Y)Uc_m{}^*\theta\right]_{n+1,m}\right.$$

$$\left. + \left[F(Y)Uc_m{}^*\theta\right]_{n+1,m+1}\right] \qquad (3.117)$$

and for the odd numbered (i.e. $m = 3, 5 \cdots M - 1$) internal grid points

$$E_m = E_{m-1} \tag{3.118}$$

To comply with equation (3.116), use is made of the following boundary conditions:

at $Y = 0$:
$$E_{n+1,1} = \frac{\Delta X \; r^*}{Re_b Pr}\left[k^* \frac{\partial \theta}{\partial Y}\right]_{n+1,1} \tag{3.119}$$

at $Y = 1$:
$$E_{n+1,M+1} = E_{n+1,M} = \frac{(1 + r^*)}{2}(c_{m_b}^* \theta_b)_n + \frac{\Delta X}{Re_b Pr}\left[k^* \frac{\partial \theta}{\partial Y}\right]_{n+1,M+1}$$

$$+ \frac{Br \; \Delta X}{Re_b Pr}\left[\int_0^1 F(Y)\mu^* \left[\frac{\partial U}{\partial Y}\right]^2 dY\right]_{n+1} \tag{3.120}$$

Using equations (3.119) and (3.120), equation (3.116) can be formed into a set of $M - 1$ algebraic equations, written generally as

$$A_m^{(15)} \theta_{n+1,m-1} + A_m^{(16)} E_{n+1,m-1} + A_m^{(17)} \theta_{n+1,m} + A_m^{(18)} E_{n+1,m}$$

$$+ A_m^{(19)} \theta_{n+1,m+1} = B_m^{(5)} \tag{3.121}$$

where for the even numbered grid points

$$A_m^{(15)} = F(Y)_{m-1}\dot{U}_{n+1,m-1}(c_m^*)\dot{}_{n+1,m-1}\frac{\Delta Y}{3} \; , \quad A_m^{(16)} = 1$$

$$A_m^{(17)} = 4\, F(Y)_m \dot{U}_{n+1,m}(c_m^*)\dot{}_{n+1,m}\frac{\Delta Y}{3} \; , \quad A_m^{(18)} = -1 \tag{3.122}$$

$$A_m^{(19)} = F(Y)_{m+1}\dot{U}_{n+1,m+1}(c_m^*)\dot{}_{n+1,m+1}\frac{\Delta Y}{3} \; , \quad B_m^{(5)} = 0$$

and for the odd numbered grid points

$$A_m^{(15)} = 0 \ , \ A_m^{(16)} = 1 \ , \ A_m^{(17)} = 0$$

$$(3.123)$$

$$A_m^{(18)} = -1 \ , \ A_m^{(19)} = 0 \ , \ B_m^{(5)} = 0$$

The necessary modifications to the above A_m and B_m expressions for the grid points adjacent to the boundaries depend on the thermal boundary conditions and are given below. Use is made of the one–sided, derivative approximations (3.88) and (3.89) to provide implicit replacements for either $\partial\theta/\partial Y$ or θ, whichever is not specified, at the boundaries.

For normal derivative type thermal boundary conditions (e.g. uniform heat flux)

UHF at Y = 0: $\quad \tilde{A}_{m=2}^{(15)} = 0 \ , \ \tilde{A}_{m=2}^{(16)} = 0 \ , \ \tilde{A}_{m=2}^{(17)} = A_{m=2}^{(17)} + \dfrac{4}{3} A_{m=2}^{(15)}$

$$\tilde{A}_{m=2}^{(19)} = A_{m=2}^{(19)} - \dfrac{1}{3} A_{m=2}^{(15)} \qquad\qquad (3.124)$$

$$\tilde{B}_{m=2}^{(5)} = r_{q1}\left[\dfrac{r^* \, \Delta X}{Re_b P r} - \dfrac{2}{3} A_{m=2}^{(15)} \dfrac{\Delta Y}{(k^*)_{n+1,1}} \right]$$

UHF at Y = 1: $\quad \tilde{A}_{m=M}^{(18)} = 0 \ , \ \tilde{A}_{m=M}^{(19)} = 0$

$$\tilde{B}_{m=M}^{(5)} = \dfrac{(1 + r^*)}{2}(c_{mb}^*\theta_b)_n + \dfrac{\Delta X}{Re_b Pr} r_{q2} \qquad (3.125)$$

$$+ \dfrac{Br \, \Delta X}{Re_b Pr}\left[\int_0^1 F(Y)\mu^* \left[\dfrac{\partial U}{\partial Y}\right]^2 dY \right]_{n+1}$$

Equations (3.124) and (3.125) can be simplified for thermal symmetry or an adiabatic wall by setting r_{q1} or r_{q2} equal to zero, as appropriate. Furthermore, $A_{m=2}^{(15)} = 0$ in all cases apart from the symmetric parallel plates problem.

For uniform duct wall temperature conditions

UWT at $Y = 0$: $\tilde{A}_{m=2}^{(15)} = 0$, $\tilde{A}_{m=2}^{(16)} = 0$

$$\tilde{A}_{m=2}^{(17)} = A_{m=2}^{(17)} + \frac{2r^*(k^*)_{n+1,1}^{\bullet} \, \Delta X}{Re_b Pr \, \Delta Y}$$

(3.126)

$$\tilde{A}_{m=2}^{(18)} = A_{m=2}^{(18)} - \frac{r^*(k^*)_{n+1,1}^{\bullet} \, \Delta X}{2 \, Re_b Pr \, \Delta Y}$$

$$\tilde{B}_{m=2}^{(5)} = \frac{3r^*(k^*)_{n+1,1}^{\bullet} \, \Delta X}{2 \, Re_b Pr \, \Delta Y} \, \theta_{w1}$$

UWT at $Y = 1$: $\tilde{A}_{m=M}^{(15)} = A_{m=M}^{(15)} - \frac{(k^*)_{n+1,M+1}^{\bullet} \, \Delta X}{2 \, Re_b Pr \, \Delta Y}$

$$\tilde{A}_{m=M}^{(17)} = A_{m=M}^{(17)} + \frac{2(k^*)_{n+1,M+1}^{\bullet} \, \Delta X}{Re_b Pr \, \Delta Y}$$

$$\tilde{A}_{m=M}^{(18)} = 0 \ , \ \tilde{A}_{m=M}^{(19)} = 0$$

(3.127)

$$\tilde{B}_{m=M}^{(5)} = \frac{(1 + r^*)}{2}(c_{mb}^* \theta_b)_n + \frac{3(k^*)_{n+1,M+1}^{\bullet} \, \Delta X}{2 \, Re_b Pr \, \Delta Y} \, \hat{\theta}_{w2}$$

$$+ \frac{Br \, \Delta X}{Re_b P \, r}\left[\int_0^1 F(Y)\mu^* \left[\frac{\partial U}{\partial Y}\right]^2 dY\right]_{n+1}^{\bullet}$$

The integral of the viscous dissipation appearing in $\tilde{B}_{m=M}^{(5)}$ above must be evaluated numerically from the previously calculated velocity profile using, for example, the trapezoidal rule approximation

$$\left[\int_0^1 F(Y) \, \mu^* \left[\frac{\partial U}{\partial Y}\right]^2 dY\right]_{n+1}^{\bullet}$$

$$= \frac{\Delta Y}{2} \sum_{m=2}^{m=M+1}\left[\left[F(Y) \, \mu^{*\bullet}\left[\frac{\partial U^{\bullet}}{\partial Y}\right]^2\right]_{n+1,m-1} + \left[F(Y) \, \mu^{*\bullet}\left[\frac{\partial U^{\bullet}}{\partial Y}\right]^2\right]_{n+1,m}\right]$$

(3.128)

where $(\partial U^\bullet / \partial Y)$ is approximated using the central difference formula (3.86) at the interior points and the one—sided differences (3.88) and (3.89) at the boundaries.

3.4.3 Solution Procedure

In Section 3.4.2, each of the finite—difference versions of the governing equations used in the present scheme is put in a form suitable for direct solution using band matrix methods. This has been done to obviate the need for dealing with the unbanded, sparsely populated matrices that would otherwise occur. An immediate advantage of the band matrix formulation is that storage need only be allocated for the diagonal band containing the non—zero coefficients. The band matrices met in this work are generally unsymmetric and have different upper and lower bandwidths, except that a tridiagonal matrix is obtained when the differential energy equation is solved alone. The associated systems of equations are solved using a variant of Gaussian elimination with partial pivoting or the tridiagonal matrix algorithm for the single case mentioned above. It is well known (e.g. Jennings, 1977) that with these methods it is possible to accommodate any additional non—zero elements formed during elimination within the diagonal band storage. Moreover, since arithmetic operations are only performed on the band structure, solution is faster and less prone to round—off error than for a comparable unbanded, sparse system.

The basic unit of the marching solution procedure is one axial step. At the start of computation for each new step, the values of the dependent variables (including the physical property ratios) are available for all transverse grid points at the end of the previous step (i.e. n level). In the case of the first step, this information is provided by the initial conditions.

Because the finite—difference equations are linearized by approximating the coefficients, the solution is advanced to n + 1 level via a series of iterations in which the coefficients are progressively updated. A further consequence of this

linearization technique is that, although the axial momentum equation and the energy equations are coupled through the temperature dependence of the fluid properties, the discretized equations need not be solved simultaneously at each iteration. This separation of the flow and temperature solutions is practised in this work and appears to have the following two advantages. Firstly, more accurate values of $U^{\bullet}_{n+1,m}$ and $V^{\bullet}_{n+1,m}$ become available earlier for the evaluation of the coefficients in the difference forms of the energy equations. Secondly, separate coding for the two solutions allows each segment to be called independently, so that the computer program can be used for problems where either temperature or flow solutions alone are required. Examples are, the calculation of developing temperature profiles for a constant–property, fully–developed flow and the calculation of flow profiles for zero heat transfer and negligible viscous dissipation. However, in general, each iteration comprises both a flow solution, to obtain improved predictions of the $U_{n+1,m}$, $P_{n+1,m}$ and $V_{n+1,m}$ values, and subsequently a solution for $\theta_{n+1,m}$. At the end of each iteration, new estimates of the fluid property ratios at each grid point on the $n + 1$ level are found using the $\theta_{n+1,m}$ solution just obtained. The process is then repeated using updated coefficients. The end of the computation for each axial step is marked by the termination of these iterations. In the present computer implementation only one iteration is performed at each marching step for variable–property computations, the option of calculation without iteration being reserved for constant–property cases.

Further information on the sequence of the solution procedure is given below. Matrices are shown illustrating how the various coefficients can be assembled in band form. However, it should be realised that these are purely symbolic since storage is only provided for the diagonal band during computation. The subscript and superscript notations used here are the same as in Section 3.4.2 where the definitions of the coefficients A_m and the right–hand sides B_m are presented. In the following, a tilde (~) indicates that a coefficient or right–hand side constant may need modification to accommodate the relevant boundary conditions.

i) Solution for $U_{n+1,m}$ and $P_{n+1,m}$

The solution for the axial velocities and the pressure at the n + 1 level is based on a system of $3M - 3$ algebraic equations. These are the $M - 1$ equations (3.95) expressing local axial momentum conservation at the grid points m = 2 to m = M, the $M - 2$ equations (3.98) equalizing the pressures at these positions and the M equations (3.111) representing the piecewise treatment of the integral mass balance. The resulting system of linear equations can be written in matrix form as

$$\mathbf{A\ Z = B} \tag{3.129}$$

where the coefficient matrix $\mathbf{A}$ in equation (3.129) has the following banded form:

$$
\begin{bmatrix}
A_2^{(12)} & \tilde{A}_2^{(13)} & & & \tilde{A}_2^{(14)} & & & & & \\
\tilde{A}_2^{(2)} & A_2^{(3)} & & & \tilde{A}_2^{(4)} & & & & & \\
 & A_2^{(5)} & & & A_2^{(6)} & & & & & \\
\ddots & \ddots & \ddots & \ddots & \ddots & \ddots & \ddots & & & \\
 & A_m^{(10)} & A_m^{(11)} & & A_m^{(12)} & A_m^{(13)} & & & & \\
 & & A_m^{(1)} & & & A_m^{(2)} & A_m^{(3)} & & A_m^{(4)} & \\
 & & & & & A_m^{(5)} & & & A_m^{(6)} & \\
 & & & \ddots & \ddots & \ddots & \ddots & \ddots & \ddots & \ddots \\
 & & & & A_M^{(10)} & A_M^{(11)} & & A_M^{(12)} & A_M^{(13)} & \\
 & & & & & & A_M^{(1)} & A_M^{(2)} & A_M^{(3)} \\
 & & & & & & & A_{M+1}^{(10)} & A_{M+1}^{(11)} \\
\end{bmatrix}
$$

$$\tag{3.130}$$

Note that the coefficient $\tilde{A}_{m=2}^{(14)}$ is only non–zero for the parallel plates geometry under symmetrical thermal boundary conditions, when the inner boundary is taken at the duct centreline. The column matrix $\mathbf{B}$ contains the constants that appear on

the right–hand sides of the system of equations (3.129) and Z is a column matrix of the $3M - 3$ unknown $U_{n+1,m}$, $P_{n+1,m}$ and $W_{n+1,m}$ values. They are written as follows:

$$
Z = \begin{bmatrix}
W_{n+1,2} \\
U_{n+1,2} \\
P_{n+1,3} \\
\vdots \\
\vdots \\
W_{n+1,m} \\
U_{n+1,m} \\
P_{n+1,m} \\
\vdots \\
W_{n+1,M} \\
U_{n+1,M} \\
P_{n+1,M}
\end{bmatrix} \quad (3.131) \qquad
B = \begin{bmatrix}
0 \\
B_{m=2}^{(1)} \\
0 \\
\vdots \\
\vdots \\
0 \\
B_m^{(1)} \\
0 \\
\vdots \\
0 \\
B_{m=M}^{(1)} \\
\tilde{B}_{m=M+1}^{(4)}
\end{bmatrix} \quad (3.132)
$$

For a duct centreline at $Y = 0$, the duct centreline velocity $U_{n+1,1}$ is found after the system of equations (3.129) has been solved, by approximating the symmetry condition given in equations (3.59) using the derivative approximation (3.88).

ii) Calculation of $V_{n+1,m}$

Following the solution of the axial velocities the transverse velocities at all internal grid points on the $n + 1$ level are found from equations (3.91)–(3.93) after setting V to zero at both boundaries.

iii) Solution for $\theta_{n+1,m}$

When the solution of the unknown $\theta_{n+1,m}$ values is based solely on the differential energy equation, a tridiagonal system of $M - 1$ difference equations (3.100) is obtained. In matrix form, this system can be written as

$$\mathbf{A}\,\theta = \mathbf{B} \tag{3.133}$$

or

$$
\begin{bmatrix}
\tilde{A}_2^{(8)} & \tilde{A}_2^{(9)} & & & & & \\
A_3^{(7)} & A_3^{(8)} & A_3^{(9)} & & & & \\
& \cdot & \cdot & \cdot & & & \\
& & A_m^{(7)} & A_m^{(8)} & A_m^{(9)} & & \\
& & & \cdot & \cdot & \cdot & \\
& & & & A_{M-1}^{(7)} & A_{M-1}^{(8)} & A_{M-1}^{(9)} \\
& & & & & \tilde{A}_M^{(7)} & \tilde{A}_M^{(8)}
\end{bmatrix}
\begin{bmatrix}
\theta_{n+1,2} \\
\theta_{n+1,3} \\
\vdots \\
\theta_{n+1,m} \\
\vdots \\
\theta_{n+1,M-1} \\
\theta_{n+1,M}
\end{bmatrix}
=
\begin{bmatrix}
\tilde{B}_2^{(3)} \\
B_3^{(3)} \\
\vdots \\
B_m^{(3)} \\
\vdots \\
B_{M-1}^{(3)} \\
\tilde{B}_M^{(3)}
\end{bmatrix}
$$

$$\tag{3.134}$$

If the option is taken of replacing the finite–difference version of the differential energy equation for the grid location $m = M$ with the system of $M - 1$ equations (3.121) representing the piecewise treatment of the integral energy equation, then $\mathbf{A}$ is no longer tridiagonal. The column matrices are also changed by the inclusion of the additional variable E and its boundary conditions. The new forms can be written in matrix form as

$$\mathbf{A}\,\mathbf{Z} = \mathbf{B} \tag{3.135}$$

where the coefficient matrix $\mathbf{A}$ has the banded form shown below:

$$
\begin{bmatrix}
\tilde{A}_2^{(8)} & & \tilde{A}_2^{(9)} \\
\tilde{A}_2^{(17)} & A_2^{(18)} & \tilde{A}_2^{(19)} \\
\ddots & \ddots & \ddots & \ddots & \ddots \\
\ddots & A_m^{(7)} & & A_m^{(8)} & & A_m^{(9)} \\
& A_m^{(15)} & A_m^{(16)} & A_m^{(17)} & A_m^{(18)} & A_m^{(19)} \\
& & A_{m+1}^{(7)} & & A_{m+1}^{(8)} & & A_{m+1}^{(9)} \\
& & A_{m+1}^{(16)} & & A_{m+1}^{(18)} \\
& & & \ddots & \ddots & \ddots & \ddots & \ddots \\
& & & & A_{M-1}^{(7)} & & A_{M-1}^{(8)} & & A_{M-1}^{(9)} \\
& & & & A_{M-1}^{(16)} & & A_{M-1}^{(18)} \\
& & & & & A_M^{(15)} & A_M^{(16)} & \tilde{A}_M^{(17)}
\end{bmatrix}
$$

$$(3.136)$$

$\mathbf{Z}$ is column matrix of the unknown $\theta_{n+1,m}$ and $E_{n+1,m}$ values and $\mathbf{B}$ is a column matrix of the right–hand side constants. They are written as

$$
\mathbf{Z} =
\begin{bmatrix}
\theta_{n+1,2} \\
E_{n+1,2} \\
\vdots \\
\theta_{n+1,m} \\
E_{n+1,m} \\
\theta_{n+1,m+1} \\
E_{n+1,m+1} \\
\vdots \\
\theta_{n+1,M-1} \\
E_{n+1,M-1} \\
\theta_{n+1,M}
\end{bmatrix}
\quad (3.137)
\qquad
\mathbf{B} =
\begin{bmatrix}
\tilde{B}_{m=2}^{(3)} \\
\tilde{B}_{m=2}^{(5)} \\
\vdots \\
B_m^{(3)} \\
B_m^{(5)} \\
B_{m+1}^{(3)} \\
B_{m+1}^{(5)} \\
\vdots \\
B_{m=M-1}^{(3)} \\
B_{m=M-1}^{(5)} \\
\tilde{B}_{m=M}^{(5)}
\end{bmatrix}
\quad (3.138)
$$

Following solution of either of the systems of equations (3.134) or (3.135), any unknown boundary temperatures at the n + 1 level are found using the derivative approximations (3.88) and (3.89).

CHAPTER 4

COMPUTER PROGRAM AND NUMERICAL STUDIES

4.1 Evolution of Computer Program

One of the main tasks completed during this research was the development of a new computer program embodying the numerical procedures presented in Chapter 3. Before describing the new program some of the background leading to its development is explained.

Experience in the application of marching finite–difference methods to solve duct flow heat transfer problems was initially gained using the program developed by Collins (1975). In his algorithm the integral mass balance equation and the partial differential equations expressing conservation of mass, axial momentum and radial momentum are solved simultaneously (by Gaussian elimination) at each forward step to obtain the unknown values of the velocity components $U_{n+1,m}$ and $V_{n+1,m}$ and the pressures $P_{n+1,m}$ at each each grid point on the $n + 1$ level. This is followed by a solution for the unknown temperatures $\theta_{n+1,m}$, based on both the differential and integral balance forms of the energy equation. Allowance for property variation is made by repeating the above procedure, using updated property values, before advancing the solution to the next axial position. Collins' computational method uses the fullest axisymmetric coordinate forms of the conservation equations for a quasi–incompressible fluid, including both the axial and the radial momentum equations, thereby admitting the possibility of pressure variation in both coordinate directions. All axial diffusion terms are retained and approximated by backward difference formulae, thus requiring 3–level storage for U, V and θ. Strictly, a space–marching method is not well–posed for a solution of this set of equations, since they permit axial transmission of elliptic influences through the pressure field and diffusion processes. For non–recirculating duct flows, however, elliptic effects are confined to a small region near the entrance. Collins (1975) found that provided an initial marching step size ΔX greater than

0.625 is used his forward marching procedure remained stable. It is noted that the technique of restricting the minimum axial step size is also employed in the marching solution of the (partially) parabolised Navier–Stokes equations used for the prediction of steady, supersonic flow fields (Anderson et al, 1984). These equations allow elliptic–type behaviour, associated with the pressure field, when subsonic regions exist in the flow. By using a minimum marching step size it is found possible to overstep the zone of influence of the upstream elliptic effect and thus maintain a stable marching solution.

Initially, some numerical investigations were conducted by the author using suitably modified versions of Collins' (1975) program. The changes made are summarised below in the order of increasing extent of modification required to the program:

i)   The circular tube program was modified by omitting the axial diffusion terms from the momentum and energy equations. However, because the equations allowed pressure to vary in both the axial and the transverse directions (i.e. elliptic behaviour), it was still found that computation only remained stable if the minimum value of the initial axial step was restricted. [No restriction of the marching step was necessary when computation was eventually based on the parabolic flow equations which neglect transverse pressure variation.]

ii)   Coding was included for the calculation of the spatially averaged cross–sectional temperature of the fluid at each axial position. The modified version was used to make flow rate predictions for a closed loop thermosyphon comprising heated and cooled vertical tubes. This work is outlined in Section 4.3.3 below.

iii)   Modified versions were developed for symmetric and asymmetric parallel plate duct flows by changing from an axisymmetric cylindrical coordinate system to a two—dimensional rectangular coordinate system. For the asymmetric case, modifications to the inner boundary conditions were also required since a centreline was no longer appropriate. The modified programs were used to obtain solutions for combined convection of viscous liquids between uniformly heated parallel plates. This study is outlined in Section 4.3.2 below.

iv)   The parallel plate programs were subsequently modified so that the coefficients of the finite—difference equations for the velocity—pressure solution were assembled in band matrix form. This change markedly improved computational efficiency, in terms of both storage and time, and the approach was later extended to the treatment of the energy equations.

Eventually, a completely new computer program was developed with a view to improving computational efficiency and flexibility. The new program implements the computational procedure described in Chapter 3 for the unified treatment of forced convection and combined convection (vertical ducts only) flows in circular, concentric annular and parallel plate ducts. Although use is restricted to laminar unidirectional flows (no flow reversals), the program is capable of handling both hydrodynamic and thermal development and either an upward or a downward vertical flow can be specified when density variation is admitted in the body force term. The program defaults to pure forced convection, applicable to any flow orientation, when a constant density is specified. A uniform or a fully—developed initial flow profile can be chosen and either a uniform heat flux (UHF) or a uniform wall temperature (UWT), with an optional adiabatic starting length, can be independently set along each duct wall. Further options allow the effects of

viscous dissipation[1] and temperature dependence for any fluid property to be included in a computation. For appropriate situations, computation of the flow field alone or the temperature field alone is allowed.

A few features of Collins' (1975) program have survived, notably the option of using the integral energy balance equation in the temperature profile solution, but the new program is substantially different in the following ways:

i)   Instead of using the full elliptic equations the solutions are now based on the parabolic flow equations which neglect axial diffusion and transverse pressure variation. The latter difference, in particular, removed the restriction of a minimum axial step size.

ii)   As mentioned above, Collins (1975) solved for $U_{n+1,m}$, $V_{n+1,m}$ and $P_{n+1,m}$ by a simultaneous solution of both momentum equations and both the integral and differential mass continuity equations. The velocity–pressure solution is now carried out in two steps:

         1)   First the axial momentum, transverse momentum and integral mass balance equations, equations (3.94), (3.98) and (3.107) repectively, are solved simultaneously for the axial velocities $U_{n+1,m}$ and the pressures $P_{n+1,m}$. Equation (3.98) is simply used to enforce the equality of pressures in the transverse direction.

---

[1]For completeness, viscous dissipation is retained throughout the analysis presented in Chapter 3 and is also incorporated as an option in the computer program given in Appendix F. Collins and Keynejad (1983) concluded that the effect of viscous dissipation on simultaneously developing laminar flow and heat transfer in a uniformly heated tube is negligible for $Pr < 200$. Viscous heating was in fact neglected in all the numerical studies for which results are reported in this thesis.

2)   Using the values of $U_{n+1,m}$ found in the previous step the transverse velocities $V_{n+1,m}$ are explicity calculated from the differential continuity equation, given by equations (3.91)–(3.93).

iii)   Use of band matrix methods, rather than Gaussian elimination, to solve the finite–difference equations.

A full listing of the new program is given in Appendix F.

4.2 Numerical Studies

4.2.1 Constant–Property, Forced Convection

To establish confidence in the accuracy of the new computer program numerical solutions have been obtained for a number of constant–property, forced convection problems. Details of the computations and the results obtained for the following two cases are given below:

i)   hydrodynamic development in a circular tube;

ii)   thermal development of a hydrodynamically fully–developed flow in a circular tube maintained at a uniform wall temperature (UWT) different from the fluid entry temperature (i.e. the well–known Graetz problem).

Comparisons are made with published solutions and analytically derived asymptotes for fully–developed conditions. Similar checks, not discussed here, have been conducted for parallel plate duct flows using the new program and its antecedents. As yet, the new program has not been systematically tested for flows in concentric annular ducts. However, the correct working of the program for circular tubes and ducts formed by two parallel plates is considered to demonstrate its capacity to handle situations exhibiting the same general features as a concentric annulus (i.e. axial symmetry and a duct wall at both the inner and

outer transverse boundaries). Recalling that in this work annular ducts problems are treated within the same general framework as circular ducts and parallel plate ducts, and in fact utilize the same coding sequences during a computation, it is not anticipated that any unique problems will be encountered.

i) Hydrodynamic development in a circular tube

In the hydrodynamically developing flow of an incompressible fluid in a duct the axial velocity profile develops from an initially flat (uniform) entrance profile to achieve a fully–developed form, given by equations (3.25) and (3.69) for a circular tube, which is independent of axial distance. The approach to fully–developed conditions is asymptotic and it is conventional to define the dimensionless hydrodynamic entrance length L_{hy}^{*} [$= (L_{hy}/d)/Re$] based on the distance L_{hy} from the tube entrance required to achieve a maximum velocity equal to 99% of the fully developed value. Numerical results obtained for the development of the axial
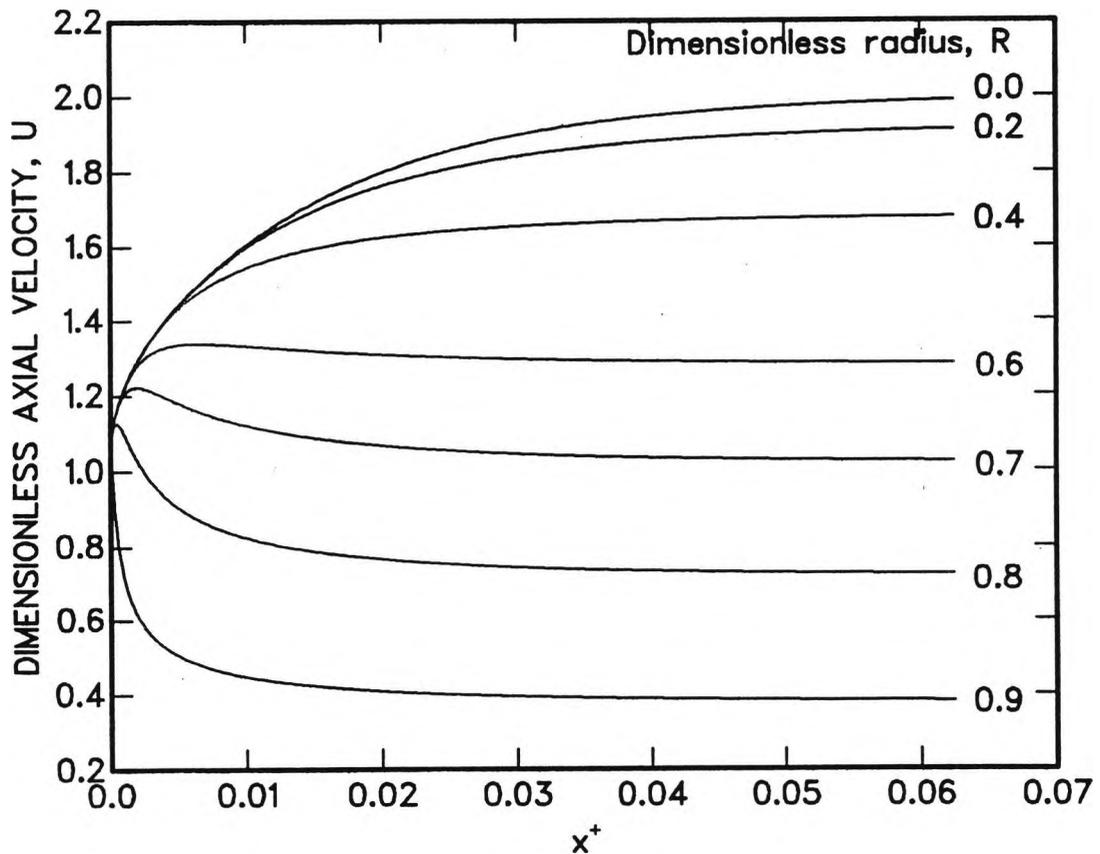
Figure 4.1   Predicted axial velocity profile development in the entrance region of a circular tube for constant–property, laminar flow.
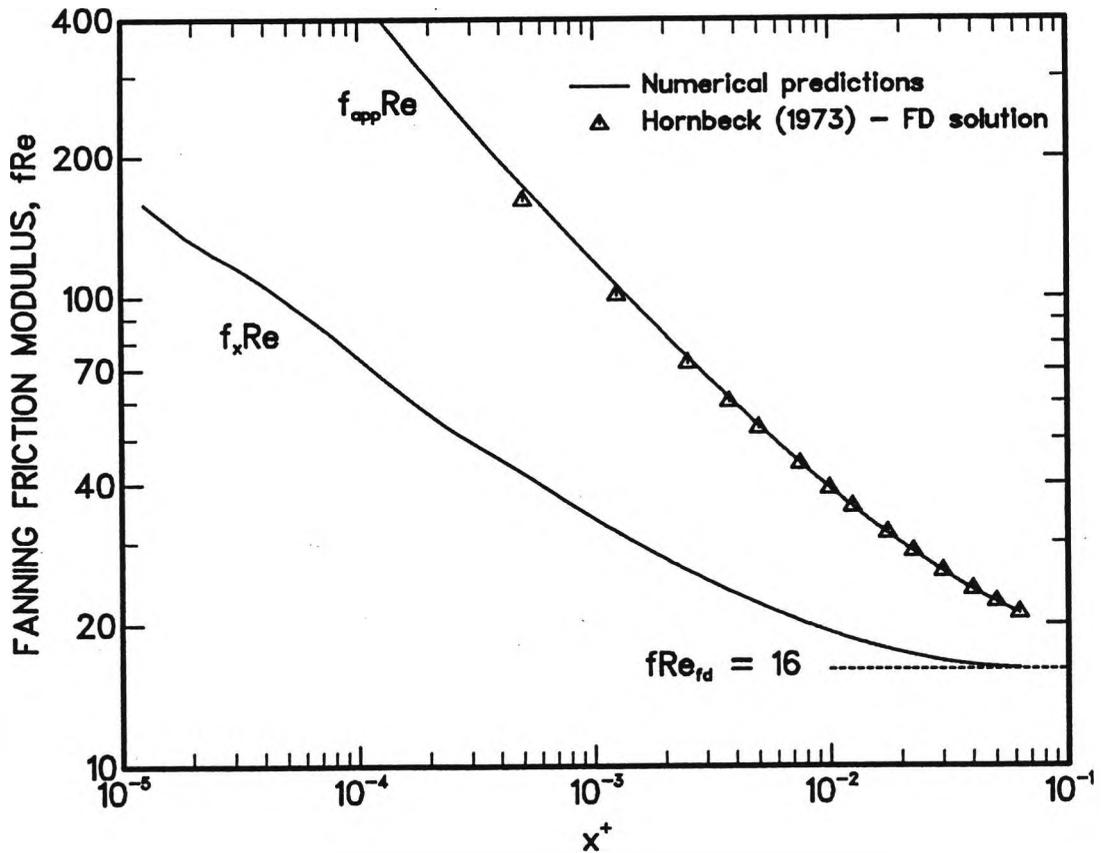
Figure 4.2   Predicted local and apparent Fanning friction factors for hydrodynamically developing laminar flow in a circular tube. (constant properties)

velocity profile with the dimensionless axial distance x^+ [$= (x/d)/Re$] are shown in Figure 4.1 and the corresponding variations of the local and apparent Fanning friction factor moduli, $f_x Re$ [$= -4(\partial U/\partial R)_{R=1}$] and $f_{app} Re$ [$= -P/x^+$] respectively, are shown in Figure 4.2. The computation utilised a finite–difference grid with 40 uniform radial divisions (i.e. $M = 40$, $\Delta Y = \Delta R = 0.025$) and the following nonuniform axial grid requiring a total of 274 marching steps to reach $x^+ = 0.0625$: $\Delta x^+ = 6.25 \times 10^{-6}$ for $0.0 \le x^+ \le 5.0 \times 10^{-5}$, $\Delta x^+ = 2.50 \times 10^{-5}$ for $5.0 \times 10^{-5} < x^+ \le 2.5 \times 10^{-4}$, $\Delta x^+ = 1.25 \times 10^{-4}$ for $2.5 \times 10^{-4} < x^+ \le 2.5 \times 10^{-3}$, $\Delta x^+ = 2.50 \times 10^{-4}$ for $2.5 \times 10^{-3} < x^+ \le 6.25 \times 10^{-2}$. The results shown in Figures 4.1 and 4.2 can be compared with the finite–difference solutions obtained by Hornbeck (1973) using the same axial grid spacings as listed above. In the radial direction, however, Hornbeck (1973) used only 16 nonuniform divisions with $\Delta R = 0.1$ in the range $0 \le R \le 0.8$ and $\Delta R = 0.025$ in the range $0.8 < R \le 1.0$. Differences between the axial velocity profile development shown in Figure 4.1 and

the tabulated results of Hornbeck (1973) are less than 1% at $x^+ = 5$ x 10^{-4} and diminish to around 0.1% at $x^+ = 5$ x 10^{-2}. The predicted value of L_{hy}^* is 0.0545, which is about 3.5% shorter than reported by Hornbeck (1973). Figure 4.2 confirms that $f_x Re$ converges to the theoretical fully–developed asymptote. However, the $f_{app} Re$ predictions of this work are slightly higher than Hornbeck's by 7.8% at $x^+ = 5$ x 10^{-4}, 1.4% at $x^+ = 5$ x 10^{-3} and 0.03% at $x^+ = 5$ x 10^{-2}.

ii) Graetz Problem

Figure 4.3 shows the effect of the number of radial grid divisions M on the predicted local Nusselt number for the circular tube Graetz problem. The same nonuniform axial grid, involving a total of 2681 steps to reach $x^* = 0.1$, was used for all values of M. The axial step size Δx^* used in each range of the axial coordinate x^* [$= (x/d)/RePr$] is bracketed in the following list: 0 (1 x 10^{-7}) 10^{-6}, 1 x 10^{-6} (2 x 10^{-7}) 1 x 10^{-5}, 1 x 10^{-5} (4 x 10^{-7}) 5 x 10^{-5}, 5 x 10^{-5} (1 x 10^{-6}) 1 x 10^{-4},
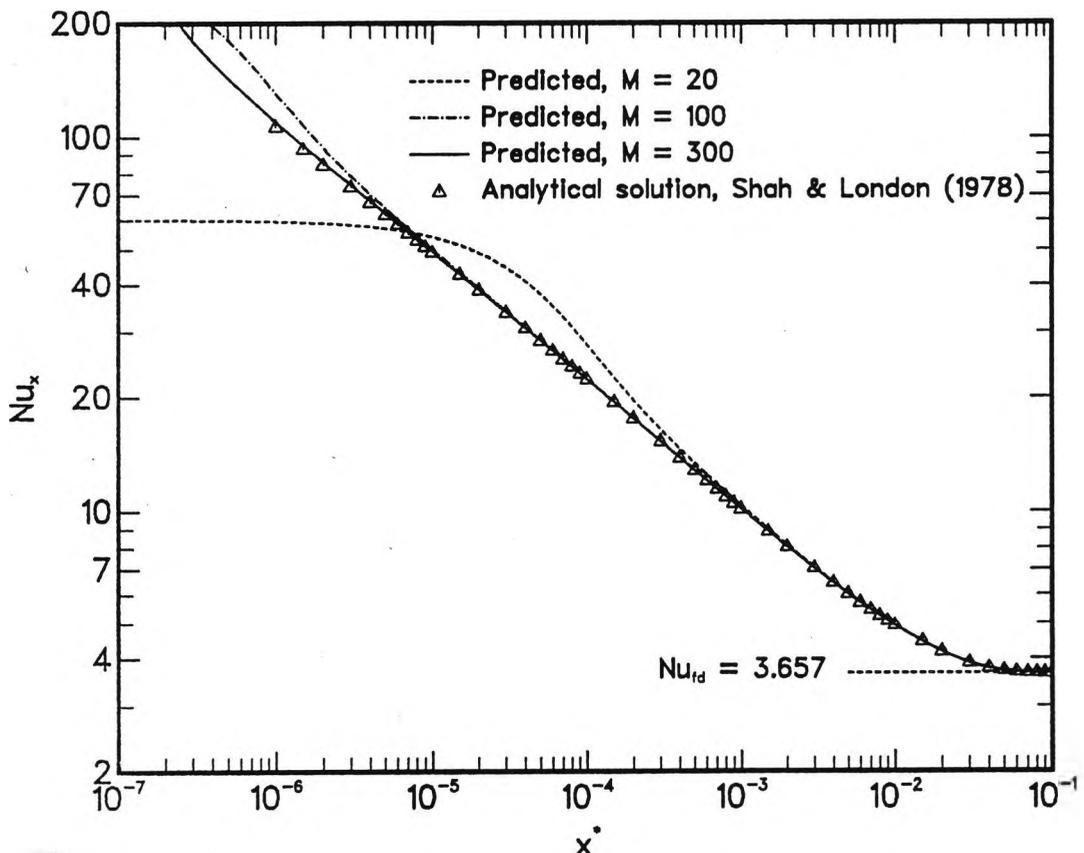
Figure 4.3   Local Nusselt number predictions for thermally developing laminar flow in a circular tube at uniform wall temperature (Graetz problem). Effect of radial grid spacing.

1 x 10⁻⁴ (2 x 10⁻⁶) 5 x 10⁻⁴, 5 x 10⁻⁴ (4 x 10⁻⁶) 1 x 10⁻³, 1 x 10⁻³ (1 x 10⁻⁵) 5 x 10⁻³, 5 x 10⁻³ (2 x 10⁻⁵) 1 x 10⁻², 1 x 10⁻² (4 x 10⁻⁵) 5 x 10⁻², 5 x 10⁻² (1 x 10⁻⁴) 1 x 10⁻¹. The numerical predictions are based solely on the solution of the tridiagonal system of equations (3.134) representing the energy equation. The results for M = 300 agree closely (error is 0.5% at $x^* = 10^{-5}$ reducing to 0.03% at $x^* = 0.1$) with the analytical results tabulated by Shah and London (1978). For M = 20 and 100 some rather large deviations are seen at low values of x^*. Conley et al (1985) conducted a similar grid dependence study for the Graetz problem and obtained results which are in almost exact agreement with those shown in Figure 4.3.

4.2.2 Combined Convection

i)   As noted is Section 4.1 a numerical study has been made of combined convection between vertical uniformly heated parallel plates. Predictions were obtained for the developing axial velocity profile and the local Nusselt number for symmetric heating of ethylene glycol and asymmetric heating of transformer oil. These results were compared with those obtained by a more approximate numerical method (Allen and Finn, 1970). Appendix G contains the full text of a paper describing this study.

ii)   Heat transfer predictions for the upward flow of water through a uniformly heated circular tube have been made for comparison with the experimental data collected in the present study. The computational details and results are presented in Chapter 7.

4.2.3 Thermosyphon Loop Study

A numerical investigation has been conducted to predict the steady–state circulation rate in a closed–loop thermosyphon comprising two vertical tubes, one uniformly heated and the other uniformly cooled, joined by upper and lower plenums. The working fluid was water (Pr = 4.3). A copy of the paper describing this work is included in Appendix G.

PART 3

EXPERIMENTAL WORK

CHAPTER 5

EXPERIMENTAL APPARATUS AND PROCEDURE

5.1 Rationale for Test Configuration

The apparatus described in this chapter was designed for the purpose of obtaining experimental data against which the numerical predictions could be compared. Although the computational method developed could be applied to several duct geometries and to uniform heat flux (UHF) as well as uniform wall temperature (UWT) boundary conditions it was necessary, in view of time and resource constraints, to limit the scope of the experimental investigation to one duct shape and one kind of thermal boundary condition.

The configuration selected for the laboratory tests was a vertical circular tube subject to uniform heat flux (UHF) heating. The following factors influenced this choice of duct geometry and thermal boundary condition:

i)   design simplicity and ease of construction;

ii)   less likelihood of departure from two–dimensional flow and heat transfer conditions than for other candidate duct geometries (annular duct or high aspect ratio rectangular duct);

iii)   convenience of using direct electrical resistive heating of the test section wall to approximate a UHF boundary condition.

The tubular test apparatus developed could be operated over a wide range of heat flux and flow rate and was instrumented to allow local entrance region heat transfer measurements to be made. The experimental work described in this thesis refers only to tests made with upward flows of water. However it was envisaged that modification of the experimental apparatus to allow the use of other working fluids or operation with downward flow could easily be accomplished.

The equipment and the techniques employed in the experimental programme are described in detail in the following sections of this chapter.

5.2 Description of Test Rig Construction

The test rig essentially consisted of a open circuit flow system, incorporating the vertical tubular test section, and an electrical power system for heating the test tube. These principal parts are described separately below. The instrumentation of the test rig is described in Section 5.3.

5.2.1 Flow System

The main features of the flow system are shown schematically in Figure 5.1.

All the tests were performed using ordinary tap water taken from the laboratory main. A filter unit (METALife model FL.3/4–40), fitted with a 40 micron stainless steel mesh filter cartridge, was installed to prevent suspended particulate matter from this supply entering the rig flow system. The filter unit could be back–flushed periodically to remove accumulated deposits from the cartridge.

The flow system was constructed so that, by opening or closing suitably positioned valves, filtered water could be made to flow to the test section either directly, utilizing the pressure in the supply main, or by gravity from an atmospheric header tank mounted above the test section. This tank provided a constant static head difference of 1.05 m to overcome the flow system losses. As there appeared to be no difference in the steadiness of the flows generated by these two alternative feed methods, it was eventually decided to use the mains pressure feed system for all tests, as higher flow rates could be achieved with this arrangement. In comparison to the pressure losses caused by flowmeters, control valves and flow mixing devices the test section pressure loss was minor. Consequently, the flow rate was virtually unaffected by the magnitude of the buoyant head generated by heating in the test section and, once set, remained very constant.
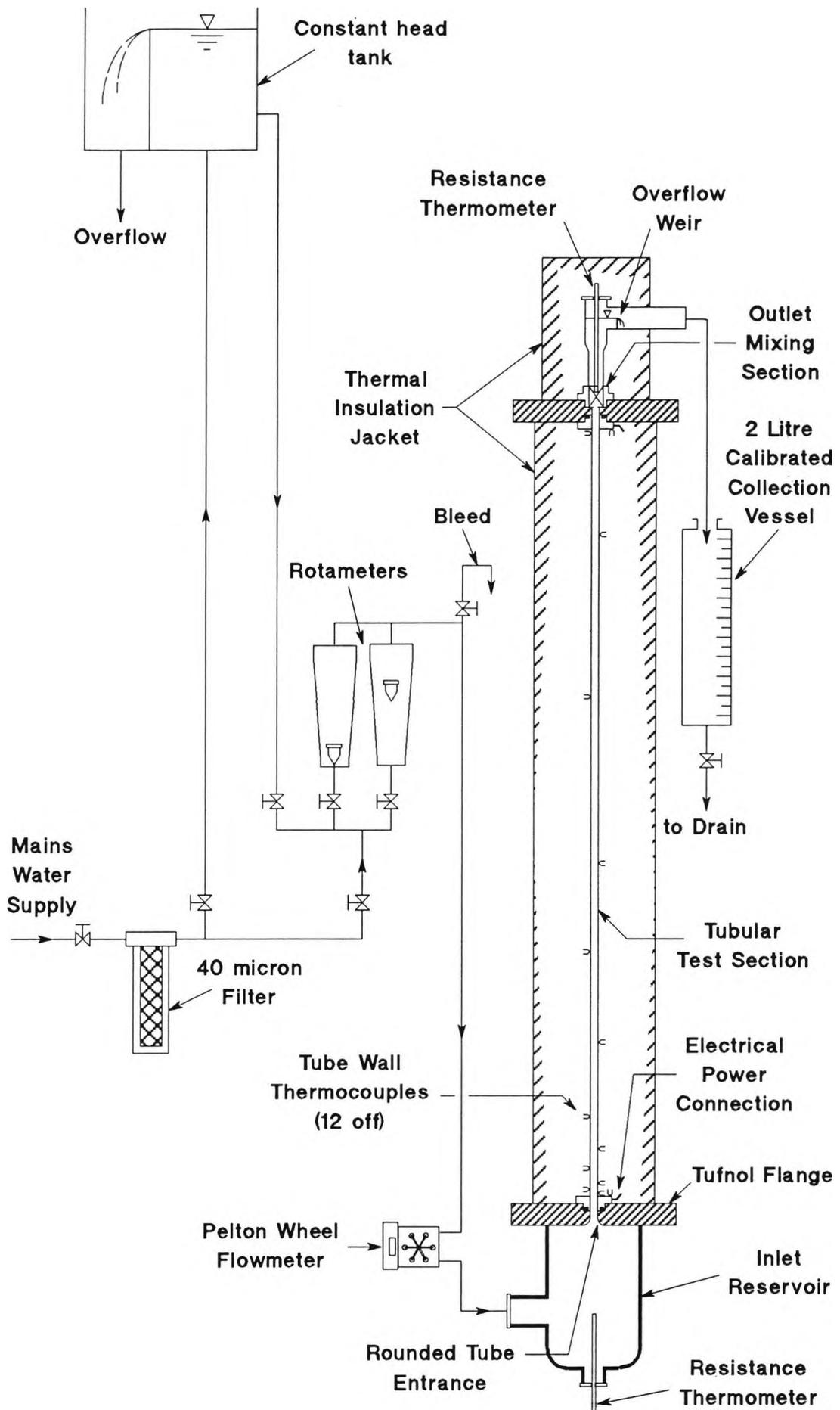
Figure 5.1   Schematic of flow system and test section.

A maximum volume flow rate of about 1 litre/minute could be obtained, corresponding to a test section Reynolds number of approximately 1800 at 20°C. The flow rate of water through the test section was adjusted by using hand valves situated upstream of the rotameters. Bleed valves were provided at positions in the feed piping where air bubbles might collect, although there proved to be only occasional need for these after the circuit was filled with water and the entrapped air vented.

After flow metering the water passed into an inlet reservoir immediately upstream of the tube entrance where the inlet bulk temperature was measured. This reservoir was intended to still inlet flow disturbances and utilized a borosilicate glass vessel, approximately 100 mm bore and 175 mm deep, with a side inlet connection and a base of roughly hemispherical shape. The inlet reservoir was completed by a top cover, made from 32 mm thick phenolic resin and paper laminated sheet (Tufnol — Heron brand), which was bolted to the glass vessel. A rounded tube entrance, with a leading edge radius of approximately 7 mm, was machined centrally in the lower face of this cover. Thus, water flowed smoothly upward from the inlet reservoir into the heated test section which was flanged to the upper face of the cover. The area contraction ratio from the inlet reservoir to the test section tube was about 70 to 1 and the flow development length between the end of the contraction and the start of the heated section was equal to approximately 2.5 tube diameters.

A second Tufnol flange, almost identical to that described above, connected the top of the heated tube to the test section outlet pipe, which was mounted co—axially with the test section and vented to atmosphere at its upper end. The measurement of exit bulk temperature was made in this pipe and to ensure temperature uniformity, the flow leaving the heated tube was first made to negotiate flow mixing elements inserted in the flow. Water discharged from the rig by spilling over a small weir plate fitted in a side branch of the outlet pipe and

passed to drain through a 2 litre graduated glass vessel. A shut—off valve fitted at the outlet from this vessel allowed water to be collected during flowmeter calibrations.

Only stainless steel, non—ferrous metals, rubber and plastic materials were employed in the construction of the flow circuit. The connecting pipework was mostly assembled from either 15 mm (nominal o.d.) copper pipe, joined with compression or soldered fittings, or plastic tubing of a similar size. Short sections of larger or smaller diameter were used in a few places.

5.2.2 Test Section

The central component of the experimental set—up was the electrically heated test section which consisted of a 1.92 m length of seamless stainless steel (type 316) tube of circular cross—section. The internal diameter and wall thickness of this tube were 11.9 mm and 0.30 mm repectively.

At each end of the test tube a rectangular copper flange, 60 mm x 40 mm and 10 mm thick, was silver soldered to the outer surface to carry the heating current. This left a heated tube length of 1.9 m (or almost 160 tube diameters) between the flanges. Copper strips, approximately 35 mm long and 25 mm x 1.5 mm cross section, were soldered to the outer edge of the copper flanges to provide convenient terminals to which the power cables and the test section voltage tappings could be connected. Details of the electrical circuit used for the test section power supply are given in Section 5.2.3.

As mentioned in Section 5.2.1, the lower and upper ends of the test section were connected to the inlet reservoir and the outlet pipe respectively via Tufnol flanges. The flange material, phenolic—paper laminate sheet, provided electrical isolation of the test section and also helped to reduce heat conduction losses because of its low thermal conductivity. The lower flange also incorporated the tube entry, making

accurate alignment with the test section essential in order to prevent disturbance of the entering flow. This was ensured by a circular spigot, 38 mm diameter and 4 mm long machined on the outer face of each copper flange which located in a complementary recess in the mating Tufnol flange. The copper test section flanges were fastened to the Tufnol flanges by set screws. A rubber O—ring was fitted in a groove in the face of each copper flange to prevent leakage.

Prior to assembly in the test rig the test section tube was cleaned and polished internally. The attachment of thermocouples for the measurement of surface temperatures on the test section is described in Section 5.3.5.

5.2.3 Electrical Power Supply

As stated earlier, the object of the experiments was to obtain local heat transfer data for a uniform heat flux (UHF) distribution at the inner surface of the heated tube wall. In the experimental set—up the tube wall was heated by the power dissipation of an alternating current passing through the tube. This direct electrical resistance heating technique, also known as Joule or ohmic heating, produced a wall heat flux which was virtually constant and approximated the UHF thermal boundary condition.

A circuit diagram of the test section power supply is shown in Figure 5.2. The low—voltage, high—current supply demanded by the test section was derived from a 240 V, 50 Hz single—phase supply by stepping down the voltage in two stages. A 3 kVA, two—winding, core—type transformer gave a voltage transformation ratio of nearly 12:1. The voltage applied to the primary winding was adjustable by a 25 A autotransformer (Berco Regavolt, type 121AE) to allow the heating power to the test section to be varied. The test section formed a purely resistive load which was connected to the transformer secondary winding by heavy copper cables bolted to the copper terminal strips at each end of the test section.
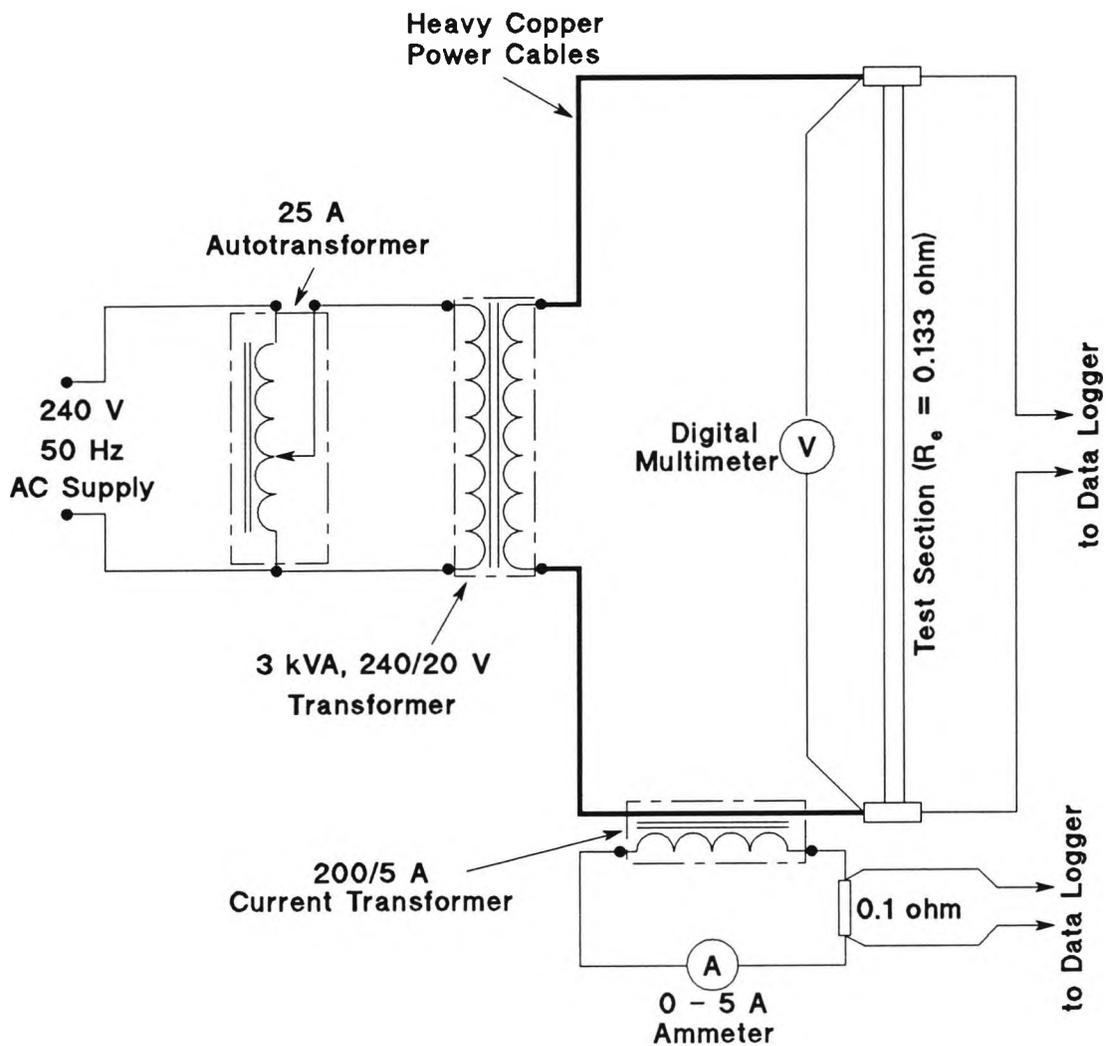
Figure 5.2   Test section electrical power supply system.

The electrical resistance of the test section, measured between the terminals at room temperature, was 0.133 ohm. A maximum current of 150 A could be drawn from the transformer, although during the experiments the test section current did not exceed 122 A. The corresponding maximum rate of heat generation due to the $\tilde{I}^2 R_e$ effect was around 2 kW; equivalent to a wall heat flux of about 28 kW/m². The measurements required for determining the test section power input are described in Section 5.3.3.

5.2.4 Thermal Insulation

After assembly of the rig and testing for leaks, the test section was thermally insulated to minimise, as far as practical, heat losses to the ambient air. Residual losses were allowed for by applying a correction based on empirical data from heat loss tests, as described in Section 5.4.1.

Insulation of the heated tube was provided mainly by two layers of preformed glass fibre sections fitted over the whole length. To exclude air gaps between the tube surface and the glass fibre insulation, the tube was first wrapped with a few layers of asbestos paper tape. The inner glass fibre layer was of approximately 25 mm thickness, covered with an aluminium foil and paper laminate. The outer glass fibre layer was of approximately 50 mm thickness and was clad by a thin aluminium sheet jacket secured by toggle clips and self—tapping screws. This jacket gave a low emissivity finish and served to prevent mechanical damage and the ingress of moisture to the insulation system. The connections between the test section terminals and the power cables were buried within the glass fibre insulation.

The test section outlet pipe assembly was also encased by glass fibre insulation and an aluminium jacket. However, no insulation was applied to the the test section inlet reservoir, since it was expected that the inlet bulk temperature in this thick—walled glass vessel would be within a few degrees of the surrounding air temperature and hence remain rather uniform.

5.2.5 Structural Support

The test section and the components of the flow system, described in Sections 5.2.2 and 5.2.1 respectively, were mounted on a rectangular frame, approximately 2.8 m high and 0.25 m x 0.3 m cross—section, fabricated from 40 mm square hollow steel sections. A smaller frame, approximately 0.65 m high, was sited on top of the main frame to support the atmospheric header tank. The base of the main frame

incorporated four adjustable feet, used for levelling the frame, each sitting on a pad of cork material ($\approx$ 12 mm thick) to reduce the transmission of floor vibrations to the test rig.

The test section assembly; comprising the heated test section, the inlet reservoir and the outlet pipe, was supported from the main frame at the lower and upper ends of the test section. It was calculated that the thermal expansion of the 1.9 m long stainless steel heated tube would be about 1.5 mm for an average tube wall temperature rise of 50 K. To accommodate such expansion the test section was held under light axial tension provided by coil springs at the upper support.

After erection in the support frame, and before thermal insulation was fitted, the verticality of the test section was checked using a plumb line and the necessary adjustments made by levelling the frame.

5.3 Measurement Systems and Calibration Procedures

For each set of test conditions, evaluation of the independent test variables (i.e. Reynolds number and wall heat flux) and the dependent quantities (e.g. local Nusselt numbers) involved the measurement of several different quantities. The primary quantities measured were water flow rate, inlet and exit bulk temperatures, wall temperatures at various axial locations along the heated tube and test section heating current and voltage drop.

It was decided at an early stage of the experiment planning to use an electronic data acquisition system to integrate the measurement and recording of all the necessary quantities and render the data in a form suitable for further processing by computer. The data acquisition system and the measurement devices installed in the test rig to sense the required physical quantities are described in detail in the following sections. The instrumentation calibration procedures used are also explained below.

5.3.1 Data Acquisition System

In outline, the data acquisition system comprised a programmable multi—channel data logger (Solartron, 3530A Orion) interfaced to an IBM—XT compatible microcomputer.

The various flow, temperature and electrical power measurements totalled 20 analogue voltage signals, including both AC and DC voltages. These voltages were connected to separate channels of the data logger for periodic scanning and conversion to digital form. In the main test series the data logger was programmed to scan and measure all of the inputs every 15 s. A channel measurement rate of 40 channels per second was selected, allowing each input to be averaged over a 20 ms integration time. This rate afforded the best possible resolution for the analogue—to—digital conversion process and ensured virtual elimination of mains frequency (50 Hz) interference. Statistical processing routines, available on—board the data logger, calculated the mean value, $\bar{x} = \frac{1}{n} \sum_1^n x_i$, and standard deviation, $\sigma = \left[\frac{1}{n-1} \sum_1^n (x_i - \bar{x})^2 \right]^{\frac{1}{2}}$, of measurements accumulated for each channel over the previous 5 minutes (20 scans). In a few tests all input channels were scanned every second for a period of 4 minutes to investigate fluctuations of the input signals.

Software linearization, provided by the microprocessor in the data logger, gave automatic conversion to degrees Celsius for all temperature sensors. Calibration and scaling equations were stored in the logger to allow the magnitudes of certain measured quantities to be calculated in the appropriate engineering units from the sensor output voltages.

An RS—232—C serial cable link transmitted the converted data to the microcomputer from the data logger after each scan of the input channels. The data transfer protocols were set up using communications software installed on the microcomputer. The same software also displayed the received data on the monitor screen and, when requested, controlled the logging of the same information to a

specified file (TESTn.LOG) on the hard disk of the computer. The monitor display was refreshed as soon as a new set of measured data was received (usually at 15 second intervals), thus providing informative and frequent visual checks on the state of operation of the test rig. A sample set of data is shown in Figure 5.3. A permanent record of logged results could also be obtained from a small paper tape printer incorporated in the data logger.

```
LOG TO PC+PRINTER RUN    16:21:09 18-04
VERTICAL TUBE TESTS T 1 16:25:49.8
:LOWER CLAMP TEMP   C 062 0015.65  dgC    :TUBE WALL TEMP     C 064 0020.18  dgC
:TUBE WALL TEMP     C 065 0020.77  dgC    :TUBE WALL TEMP     C 066 0024.25  dgC
:TUBE WALL TEMP     C 067 0027.56  dgC    :TUBE WALL TEMP     C 068 0031.00  dgC
:TUBE WALL TEMP     C 069 0035.15  dgC    :TUBE WALL TEMP     C 070 0039.85  dgC
:TUBE WALL TEMP     C 071 0043.93  dgC    :TUBE WALL TEMP     C 072 0048.92  dgC
:TUBE WALL TEMP     C 073 0053.97  dgC    :TUBE WALL TEMP     C 074 0059.10  dgC
:TUBE WALL TEMP     C 075 0058.62  dgC    :UPPER CLAMP TEMP   C 076 0053.30  dgC
:TEST SECTION AMPS  C 082 0081.50  AMP    :TEST SECTION VOLTSC 084 011.198  Vac
:VOLUME FLOWRATE    C 086 0.76333  L/M    :INLET BULK TEMP    C 093 0013.05  dgC
:OUTLET BULK TEMP   C 095 0029.26  dgC    :AMBIENT TEMP       C 097 0021.65  dgC
```

Figure 5.3   Sample measurement data set for one data logger scan.

The data acquisition system provided a reliable and rapid means of data capture, with consequent savings in the time and labour required for testing compared to a manual system of recording observations. Information could be obtained about the temporal variation of the measured quantities by sampling at rates which could not have been achieved manually. Furthermore, the risk of errors associated with manual data recording and re—entry to a computer were eliminated.

A spreadsheet program was specially developed to import, parse and process the experimental data log files obtained by the data acquisition system. The spreadsheet could rapidly perform all the necessary data reduction calculations, thus allowing results to be viewed during the progress of a test.

As the data logger was central to all the measurements its state of calibration was an obvious concern at the outset. However, since common circuitry (e.g. same

analogue–to–digital converter) was used it is noted that this issue possibly merited less concern than if each quantity had been measured using a completely independent system. Nevertheless, the calibration of DC voltage conversion was checked over the ranges $0 - 10$ mV and $0 - 10$ V using a DC voltage source (Time Electronics, model 2003N) to generate known inputs of both polarities. Excellent agreement was achieved; the maximum discrepancies for the two ranges being 7 μV and 1.2 mV respectively. Such systematic checking was not undertaken with AC voltage inputs, but impromptu comparisons with other laboratory meters confirmed that the data logger could be used with confidence.

5.3.2 Flow Rate Measurement

The water flow rate passing through the test section was measured using a Pelton wheel type flowmeter (LitreMeter, size LM.05) installed upstream of the test section inlet reservoir (see Figure 5.1). This flowmeter featured a six–lobe turbine rotor, formed in nylon with a stainless steel shaft, supported on tungsten carbide ball bearings running in sapphire bearing cups. Each lobe contained a ferrite core and the speed of rotation of the turbine was detected by a sensing coil as the ferrites passed by. The resulting stream of output pulses was fed to a signal conditioning unit (LitreMeter, LM.EI 30) for conversion to a DC voltage analogue signal $(0 - 20$ V$)$ suitable for input to the data logger.

To ensure the best possible measurement accuracy, the voltage output from the flowmeter signal conditioning unit was calibrated against the measured flow rate with the flowmeter in situ. The volume flow rate was determined from the time taken to collect 1 litre of water in a previously calibrated graduated glass vessel situated at the test rig outlet. Calibration runs were carried out at 17 flow rates in the range $0.022 - 1.03$ litre/minute, which was within the manufacturer's recommended range $(0.02 - 1.3$ litre/minute$)$ and encompassed the range of flow rates covered in the tests $(0.045 - 0.82$ litre/minute$)$. Two collections were made at each flow rate and the results averaged. Voltage outputs recorded by the data

acquisition system at regular intervals throughout each calibration run (typically 15 − 60 readings) were also averaged. The calibration data obtained in this manner indicated an almost linear relationship between the volume flow rate and the voltage. A best straight line fitted to the data by least squares regression was programmed into the data logger to perform the subsequent conversions from voltage to volume flow rate.

In addition to the Pelton wheel flowmeter, two rotameters (G.A.Platon, GapMeters sizes A6 and B6) were installed to give a convenient visual indication of the flow rate when setting−up test conditions. These auxiliary flowmeters were fitted in parallel and covered a range up to approximately 0.8 litre/minute. They were also calibrated by the collection method described above.

During the main test series the same technique was used to make occasional checks on the state of the Pelton wheel flowmeter calibration at randomly selected flow rates. In 9 (out of 12) of these checks the measured flow rate was within ± 1.2% of that predicted by the original calibration equation. The maximum discrepancy found was + 3.2%.

Transient records taken of the flowmeter output signal exhibited apparently random fluctuations at all flow rates, regardless of whether heating was applied to the test section. The magnitude of the fluctuations was typically ± 1.5% of the mean value used in the data reduction calculations. Efforts made to discover if these fluctuations resulted from actual flow rate variations or some effect introduced by the flowmeter or signal conditioning unit were inconclusive. No flow rate fluctuations could be detected by observing the rotameters.

5.3.3 Evaluation of Test Section Electrical Power

The average rate of heat generation due to the power dissipation of the alternating current passing through the purely resistive test section was calculated from the

product $\tilde{I}\tilde{V}$, where $\tilde{I}$ and $\tilde{V}$ are the rms values of the current and the impressed voltage respectively. Figure 5.2 shows the arrangement of the instrumentation used to determine the electrical power input to the test section.

The applied rms voltage between the power cable connection points on the test section terminals was measured directly using the data logger. Voltages ranging between 3.5 V and 17.2 V were recorded during the main test series. It was confirmed, by calculation, that the contribution to the measured voltage drop due to the resistance of the terminals was negligible. The test section voltage drop was also monitored by a true rms digital multimeter (Thurlby, model 1504) connected between the same tapping points. The voltages displayed on this auxiliary instrument were within ± 1% of the corresponding data logger measurements in nearly 90% of the tests and the maximum difference observed was − 1.8%.

The rms value of heating current drawn by the test section was measured with the aid of a Class B current transformer arranged with one of the test section power cables forming a single primary inserted turn. A calibrated 0 − 5 A moving iron ammeter and a 0.1 ohm precision resistance were connected in series in the secondary circuit of the current transformer. For data acquisition purposes the required current was inferred from the voltage measured across the 0.1 ohm resistance. The appropriate scaling factor was programmed into the data logger so that the result of the test section current measurement was presented in amperes. The ammeter was mainly used for setting−up test conditions and gave a visual indication equal to the test section current divided by the turns ratio (40:1) of the current transformer. Where the resolution of the ammeter scale permitted a sufficiently accurate reading, the indicated test section current (after applying any calibration correction) was within ± 1% of the value recorded by the data acquisition system.

5.3.4 Fluid Bulk Temperature Measurements

The bulk (or mixed—mean) temperatures of the water entering and leaving the test section and the room air temperature close to the test rig were measured using identical commercially available platinum resistance thermometer probes. Each probe incorporated a 15 mm long, 100 ohm (at 0°C) wire—wound platinum resistance element with a quoted tolerance of 1/10 of the Class B sensor (BS 1904:1984 or DIN 43760:1980) value: equivalent to 0.03°C at 0°C. The overall length and diameter of the stainless steel probe sheath were 150 mm and 3/16" ($\approx$ 4.75 mm) repectively.

Measurements were made using the data logger by the four—wire connection method; in which the voltage developed across the platinum resistance element is measured when a known current is passed through it. A constant 100 μA current was supplied from the transducer energization module in the data logger for this purpose. Conversion to temperature units was performed automatically by the microprocessor in the data logger.

A proper calibration of the resistance thermometers could not be undertaken because no traceable temperature standard was available. Instead, the outputs of these sensors were compared when the probes were fastened together and immersed in melting ice, saturated steam at atmospheric pressure and, for intermediate temperatures, a thermostatically controlled bath of ethanediol. Differences in the indicated temperatures were less than 0.1 K in the majority of cases. On the basis of these checks and the manufacturer's quoted tolerance for the detector elements the resistance thermometers were considered sufficiently accurate to be used as a standard in producing a calibration for the thermocouple cable used in wall temperature measurements (see Section 5.3.5).

The water inlet bulk temperature was measured in the test section inlet reservoir with the platinum resistance thermometer probe installed vertically through a

compression gland fitted in an opening at the base of the reservoir. The probe was mounted co–axially with the test section with the sensing tip about 120 mm below the rounded tube entrance, giving an immersed probe length equivalent to approximately 25 sheath diameters. As the inlet reservoir temperature was essentially uniform and close to the ambient temperature, measurement errors due to probe positioning and heat conduction loss were considered to be negligible.

Although not used for the evaluation of experimental Nusselt numbers, the water exit bulk temperature was measured to indicate the level of overall energy balance achieved in each test. A platinum resistance thermometer probe was mounted vertically downward along the centreline of the test section outlet pipe to a depth of immersion of about 23 sheath diameters with its sensing tip approximately 50 mm downstream of the heated tube outlet. Preliminary rig tests exhibited measured exit bulk temperatures lower than expected from the test section power inputs. These apparent energy balance errors (up to 44% in one case) could be attributed to the non–uniform temperature profile of the water leaving the heated tube, with the warmest water flowing near the tube wall by–passing the sensing tip of the resistance thermometer. The situation was rectified by inserting simply fashioned devices into the emerging flow to cause mixing. A piece of stainless steel expanded mesh ($\approx$ 12% open area) was fitted normal to the flow and immediately downstream of the tube exit. This was followed by two short sections of convoluted copper strip, 15 mm and 12 mm long respectively. The 12 mm copper section was in the shape of an eight–pointed star and push–fitted over the sensing tip of the platinum resistance thermometer to form a set of high–conductivity radial fins.

The high blockage and thermal conduction caused by these mixing elements tended to produce radial temperature uniformity in the test section outlet pipe, thus enabling the resistance thermometer to respond to the proper mixed–mean exit temperature. A fuller discussion is deferred to Section 6.3, but it is noted here

that the overall energy balance error was reduced to tolerable levels in the tests performed subsequent to the installation of the mixing elements.

The third platinum resistance thermometer was mounted at mid—height on the test rig support frame and about 50 mm from the outside of the test section insulation jacket. The air temperature measured at this position was used in the estimation of the test section heat losses as discussed in Section 5.4.1.

5.3.5 Surface Temperature Measurements

A total of 14 Type K (nickel—chromium / nickel—aluminium) thermocouples were attached to the test section for the measurement of surface temperatures. All the thermocouples were manufactured from the same bobbin of glass fibre insulated thermocouple cable, which comprised a pair of 40 swg ($\approx$ 0.12 mm diameter) wires. The exposed measuring junctions were formed using a capacitance discharge thermocouple welding unit (Spembley Technical Products).

The measuring junctions of 12 thermocouples were spot—welded to the outer surface of the stainless steel tube using the capacitance discharge welder. As the axial temperature gradient on the tube wall was expected to be steep at the upstream end of the heated section, thermocouples were spaced at less than one tube diameter in this region. Axial spacing was gradually increased in the downstream direction up to a maximum of about 34 tube diameters. Alternate junctions were attached to diametrically opposite sides of the tube in an attempt to detect possible circumferential temperature variations. The axial locations of all the thermocouples used for tube wall temperature measurement are given in Table 5.1.

After spot—welding, the thermocouples were secured to the tube using self—adhesive patches and epoxy resin adhesive. The thermocouple wires leading from the junctions were wrapped around the tube circumference for a short

Table 5.1 Axial locations of wall temperature measurement thermocouples.

thermocouple position number	axial distance from start of heated section mm	equivalent length–to–diameter ratio
1	3.7	0.31
2	10.1	0.85
3	29.1	2.45
4	67.2	5.65
5	118	9.92
6	194	16.3
7	397	33.4
8	601	50.5
9	804	67.6
10	1210	101.7
11	1617	135.9
12	1896	159.3

distance, following a roughly isothermal path, to minimise measurement errors due to heat conduction along the wires. Care was taken to ensure that exposed thermocouples wires were not touching each other or the tube surface, apart from at the measuring junction.

The two remaining thermocouples were used to monitor the temperatures of the copper flanges at each end of the test section. They were attached to the flanges approximately 20 mm from the outer surface of the tube.

The output voltages from thermocouples were measured and converted to temperature units by the data logger. Each thermocouple was routed to the logger via a connection box mounted on the test rig support frame, where a separate ice

point reference junction[1] was joined into the circuit. Type K thermocouple materials were used throughout, including the terminal block connectors in the junction box. All the reference junctions were held near the bottom of a stoppered test tube which was partly filled with silicone fluid. The test tube was immersed to a depth of approximately 140 mm in a mixture of melting ice and water contained in a wide–necked ($\approx$ 90 mm diameter) vacuum flask fitted with a thick cork lid. Preliminary checks, using mercury–in–glass thermometers verified that the temperature of the reference junctions closely approached $0°$ C.

Because the measuring junctions of the thermocouples were in direct contact with the alternating current heated tube, two precautionary measures were taken to combat potential signal interference from this source. Partial rejection of common mode noise was achieved by providing links between the LO side of each thermocouple input signal and the floating internal guard section of the data logger. In addition, an integration period of 20 ms was selected for the analogue–to–digital conversion process, thereby virtually eliminating 50 Hz interference by averaging over one full cycle.

A sample thermocouple, made from Type K cable taken from the same bobbin, was calibrated against the resistance thermometer used for the ambient air temperature measurements (see Section 5.3.4). Both sensors were connected to the data logger and an ice point reference junction was provided for the thermocouple as described above. Comparisons were carried out at the ice and steam points and also at ten intermediate temperatures in a stirred constant temperature bath of ethanediol. The difference between the temperatures indicated by the resistance

---

[1]Initially, reference junction compensation was based on the temperature sensed by thermistors at the data logger input terminals. Extensive checks established that this method introduced unacceptably high errors ($\approx$ 1 to $2°$ C) in the indicated temperatures and so it was abandoned in favour of using a separate external reference junction in each thermocouple circuit.

thermometer and the thermocouple varied between + 0.13 K (in ice) and + 0.56 K (in steam). A 5th–degree polynomial was fitted to the calibration data representing this temperature difference as a function of the thermocouple reading. The polynomial was included in the experimental data reduction spreadsheet for calculating the corrections to be applied to the thermocouple measurements.

Evaluation of local heat transfer coefficients and Nusselt numbers strictly required the inside surface temperature of the tube wall, T_{w_i}, rather than the measured outside surface temperature, T_{w_o}. The temperature difference across the heated tube wall can be estimated from the following expression:

$$\Delta T_w = T_{w_o} - T_{w_i} = \frac{q_w d_i}{2k_w}\left[\frac{d_o{}^2}{(d_o{}^2 - d_i{}^2)}\ln\left[\frac{d_o}{d_i}\right] - \frac{1}{2}\right] \qquad (5.1)$$

where q_w is the heat flux at the inside surface of the tube and k_w is the thermal conductivity of the tube material. Equation (5.1) assumes steady radial heat conduction only (i.e. no axial or circumferential temperature gradients), perfect thermal insulation at the outer surface, uniform k_w and uniform volumetric heat generation throughout the tube wall. In the experiments heat fluxes of between 1.64 kW/m² and 28 kW/m² were supplied. The corresponding range of values for ΔT_w across the stainless steel ($k_w \approx 16$ W/m K) wall was about $0.015 - 0.25$ K. As the wall temperature differences were always less than 1% of the difference between the average wall temperature and the arithmetic mean bulk temperature they were ignored in the data reduction calculations.

5.4 Factors Affecting the Experimental Thermal Boundary Condition

Direct resistance heating, as employed in the experimental tubular test section, attempts to simulate a thermal boundary condition of uniform heat flux (UHF) at the wall–fluid interface. Ideally, heat generation within the tube wall is envisaged to be peripherally and axially uniform, with heat transfer to the fluid inside the

tube taking place by radial conduction, without loss or axial redistribution.

The characteristic wall temperature distribution for axisymmetric convection through a heated tube subjected to a UHF boundary condition is peripherally uniform, but varies in the flow direction due to the rising fluid bulk temperature and the nonuniform distribution of heat transfer coefficient associated with thermal and hydrodynamic development. Paradoxically, axial wall temperature variation gives rise to effects which prohibit the achievement of a strictly uniform surface heat flux in practice. In reality, the heat generated in each element of length of a conductive tube wall of finite thickness is, at steady state, balanced by heat transfer to the fluid inside the tube, heat losses to the surroundings and net axial heat conduction along the tube wall. The purpose of the following sections is to provide either quantitative or qualitative information on the effects of test section heat losses, temperature dependence of the tube wall resistivity and axial wall conduction on the magnitude and uniformity of the wall–fluid heat flux. The empirical heat loss data given here were used directly in the data reduction calculations, whereas the other factors are discussed to provide some background for the interpretation of the experimental results.

The possibility of temporal variation of the tube wall temperature due to the use of alternating current heating is considered in Section 5.4.4.

5.4.1 Test Section Heat Loss

In order to determine the surface heat flux into the fluid from the electrical power input measurements, some estimate of the test section heat loss was required. This information was provided by heat loss tests in which the electrical power inputs were measured for a range of test section temperature rises with no flow passing through the test section. In preparation for these tests, the rig was drained and a length (≈ 2 m) of softwood dowelling, sanded to give a sliding fit in the tube bore, was inserted to eliminate air convection inside the heated tube. All electrical and

pipe connections, thermal insulation and instrumentation were replaced for the heat loss tests.

A total of seven heat loss tests were performed, covering a range of tube wall temperatures up to approximately 93° C. When steady conditions were attained (usually 1 to 2 hours), the data acquisition system recorded the measurements required to determine the heat loss and the average temperature rise of the test section. The quantities measured were the test section heating current and voltage drop, the ambient air temperature, T_{amb}, measured by a platinum resistance thermometer mounted near to the test section and the surface temperatures indicated by thermocouples attached at various axial locations along the heated test section. In the absence of convective cooling inside the heated tube electrical power input was minimal, allowing the heating current to be checked directly using a calibrated $0 - 10$ A ammeter connected in series with the test section. An independent check on the voltage drop was given by a digital multimeter connected across the test section terminals. The power input determined from these auxiliary measurements was always within 1.4% of that indicated by the data acquisition system measurements.

Figure 5.4 shows a typical distribution of surface temperature measured along the test section in the heat loss tests, taken from the test with the highest power dissipation. The temperature is reasonably uniform, apart from at the ends of the test section, where strong conduction pathways to the power connection flanges are evident. However, for the purposes of heat loss estimation, it was considered sufficiently accurate to represent the test section temperature by an average value, T_{w_m}, given by the simple rectangular integral approximation

$$T_{w_m} = \frac{1}{L}\sum_{j=1}^{12} T_{wj}\frac{(x_{j+1} - x_{j-1})}{2} \tag{5.2}$$
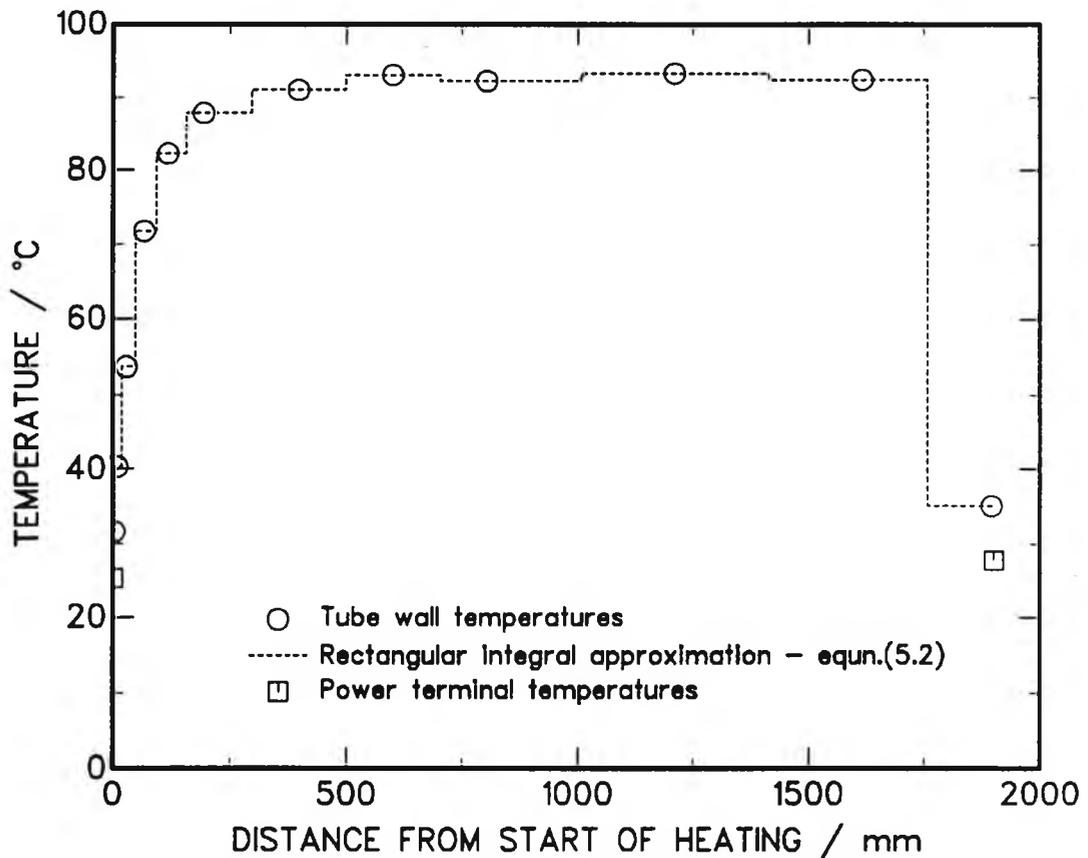
Figure 5.4   Typical axial temperature distribution along test section in heat loss tests. ($\dot{Q}_{loss} = 12.84$ W).

In equation (5.2), L is the heated length of the test section, j denotes the thermocouple position number and x_{j-1} and x_{j+1} are the axial distances from the upstream end of the heated test section given in Table 5.1. Results for the rate of heat loss from the test section, $\dot{Q}_{loss}$, (taken equal to the power input) for all the heat loss tests are plotted against the average test section temperature rise, $(T_{w_m} - T_{amb})$, in Figure 5.5. Linear regression was used to derive the following straight line equation representing the heat loss test results:

$$\dot{Q}_{loss} = 0.436 + 0.192 \, (T_{w_m} - T_{amb}) \quad \text{W} \tag{5.3}$$

where the temperature difference is in kelvin. The small error in $\dot{Q}_{loss}$ caused by not constraining equation (5.3) to pass through the origin is extremely small compared to the power input, which ranged from 120 W to over 2 kW in the main test series. The reciprocal value of the slope in equation (5.3) can be interpreted as

an effective thermal resistance for heat losses; equal to $1/0.192 = 5.2$ K/W. This value is approximately half that estimated for pure radial heat loss from the heated tube, based on the thickness and thermal conductivity of the glass fibre insulation alone. The difference is believed to reflect the additional loss caused by axial heat conduction to the attachments at each end of the test section. Although it combines both radial heat loss and axial end losses, it is emphasised that equation (5.3) is based on data from heat loss tests where the ratio of axial to radial losses and the wall temperature distributions were not truly representative of normal operating conditions. For example, with convective cooling inside the tube, the wall temperature increased continuously in the flow direction, giving a greater driving force for radial heat loss at the top of the test section than at the bottom. However, in the absence of other information allowing the separate characterization of radial and axial heat losses on a local basis, equation (5.3) was used to estimate the total test section heat loss for each experiment.
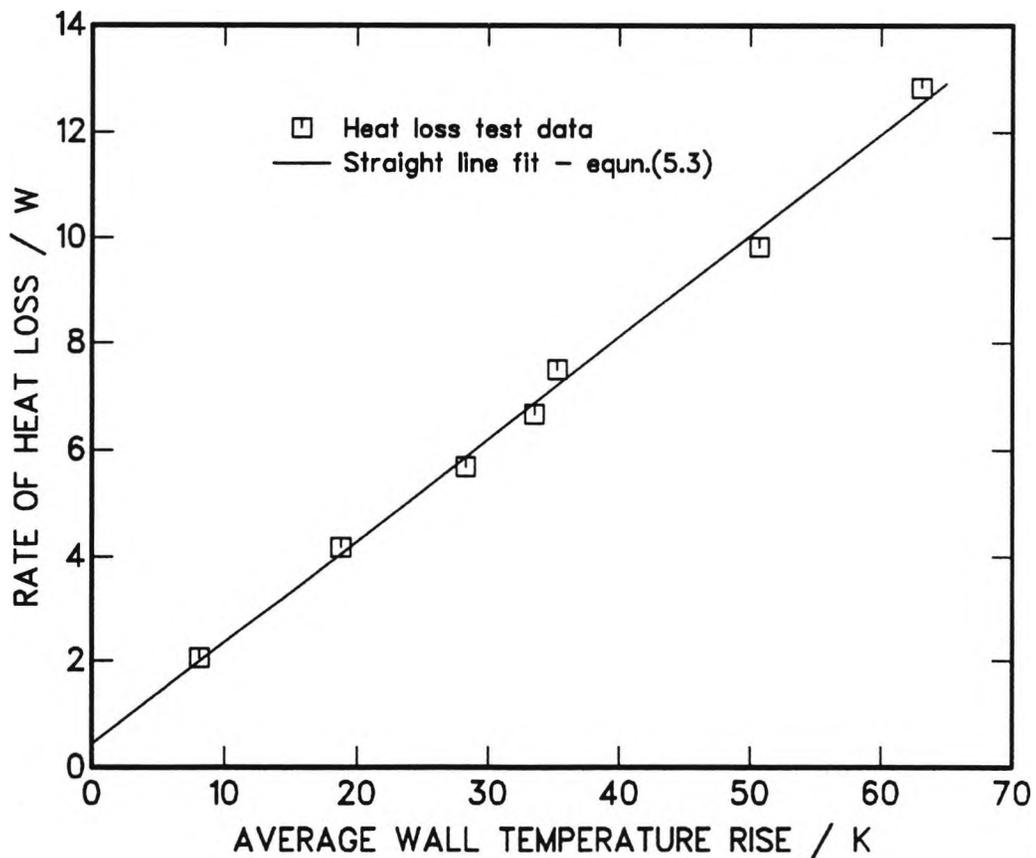
Figure 5.5 Variation of test section heat loss with average temperature rise in heat loss tests.

This loss was applied as an overall correction in calculating the average surface heat flux, q_w, from the expression

$$q_w = \frac{\tilde{I}\tilde{V} - \dot{Q}_{loss}}{\pi dL} \qquad (5.4)$$

where πdL is the inside surface area of the heated test length and $\tilde{I}$ and $\tilde{V}$ are the rms values of the heating current and the voltage drop for the test section respectively. As the correction was less than 1.5% of the electrical power input in over 90% of the tests, the error caused by spatial averaging of heat losses was not considered to be serious. The heat loss correction assumed a greater importance ($\approx$ 3%) for the lowest flow rate tests (Re $\approx$ 100), since the power input required to produce a given test section temperature rise was less than at higher flow rates.

5.4.2 Temperature Dependence of Tube Wall Resistivity

Spatial uniformity of internal energy generation in the test section wall was of primary importance to the practical realization of a uniform heat flux boundary condition. The effect of the resistance temperature coefficient for the tube wall material on the local heat generation rate is considered below for the experimental conditions of this work. Nonuniformity of heat generation due to local variations of either wall thickness or material composition was considered negligible for the precision drawn stainless steel tube used in the experiments.

For ohmic heating, the local rate of energy generation per unit inside surface area is given by

$$q_{gx} = \frac{\tilde{I}^2}{\pi d} \left[\frac{dR_e(x)}{dx} \right] \qquad (5.5)$$

where $\tilde{I}$ is the rms electric current and $dR_e(x)$ is the electrical resistance of an elemental length of tube dx.

Assuming the electrical resistivity of the tube wall material to vary linearly with temperature and neglecting the radial temperature variation in the wall

$$dR_e(x) = \epsilon_0[1 + \alpha(T_{w_x} - T_0)] \frac{dx}{A_w} \qquad (5.6)$$

where ϵ_0 is the value of the resistivity at temperature T_0, α is the temperature coefficient of the resistivity and A_w is the cross–sectional area of the tube wall. Substitution of equation (5.6) in equation (5.5) produces a relation between q_{w_x} and T_{w_x} which can be integrated to obtain the corresponding equation giving the length–averaged rate of energy generation per unit surface area q_{g_m} in terms of the average wall temperature T_{w_m}.

The degree of nonuniformity in the rate of energy generation can be expressed as the ratio of the difference between the local and average values of q_g to the average value, given by

$$\frac{q_{g_x} - q_{g_m}}{q_{g_m}} = \frac{\alpha(T_{w_x} - T_{w_m})}{1 + \alpha(T_{w_m} - T_0)} \qquad (5.7)$$

Equation (5.7) confirms the expected result that the percentage variation of the heat generation rate is greater when there is a large variation in the tube wall temperature. Such conditions can occur at either high flow rate or at low flow rate. In general, since the temperature coefficient α is positive, q_{g_x} takes its minimum value at the heated test section inlet where the wall temperature is lowest. Downstream of the start of heating q_{g_x} increases, steeply at first, and eventually exceeds the average value q_{g_m} at axial positions where $T_{w_x} > T_{w_m}$. Furthermore, the nonuniformity depends not only on the difference between the extreme temperatures and the average temperature but also on the shape of the wall temperature distribution. This is illustrated by the two cases discussed below which were both characterised by a large variation of wall temperature.

In one extreme case (Test 13A) the test section wall temperature increased from 28.4°C at the thermocouple position nearest to the start of heating ($x/d = 0.31$), reaching a maximum of approximately 85°C around $x/d = 100$, before falling and then rising again towards the end of the tube (see Figure 6.6(c)). The average wall temperature was 73°C. Using $\alpha = 0.001$ K^{-1} for stainless steel, it can estimated from equation (5.7) that the local rate of energy generation in the tube wall varied from approximately 4% below (at $x/d = 0.31$) to 1% above (at the position of the maximum temperature) the average value. In contrast, the wall temperature variation was reasonably linear in Test 15A (see Figure 6.3(b)) where minimum and maximum values of 21.9°C (at $x/d = 0.31$) and 92.7 °C (at $x/d = 159.3$) were measured. The average wall temperature for the heated test section was 58.3°C in this case and equation (5.7) indicates that q_{gx} varied within ± 3.5% of its average value.

5.4.3 Axial Wall Heat Conduction

Even if internal heat generation within the wall of an electrically heated tubular test section is substantially uniform, the heat flux at the wall–fluid interface can still suffer significant nonuniformity, particularly over a short length at the start of the thermal entry section. The mechanism responsible for this redistribution of energy is axial heat conduction along the tube wall.

In mathematical terms, axial wall conduction is directly proportional to dT_w/dx, whereas, the departure from uniformity of the thermal boundary condition depends on the rate at which the axial flux varies with distance along the tube and is therefore governed by d^2T_w/dx^2. Consequently, the strongest influence of axial wall conduction is encountered at positions near to the start of the thermal entrance region where the axial wall temperature gradient changes most rapidly. In this region the wall–fluid heat transfer is less than the electrical heat input due to net upstream conduction along the tube wall. The surface heat flux increases rapidly with downstream distance and approaches the expected uniform value as

the effect of axial wall conduction diminishes. For thermally developed conditions a strictly UHF boundary condition is achieved since a constant axial wall temperature gradient prevails.

In order to clarify the influence of axial wall conduction on the surface heat flux distribution, and also to reveal important parameters, the energy balance equation for the heat generating wall is derived below. In the following development, the tube wall is assumed to be sufficiently thin for radial temperature variation across the thickness, denoted by δ_w, to be neglected. Internal heat generation within the tube wall is treated as a uniform heat source term, equal to q_g per unit inside surface area. The outside surface of the tube is considered to be perfectly insulated and the wall is cooled by convection at the inside surface.

Adopting the same axisymmetrical coordinate system used elsewhere in this work, with x taken axially and y radially, yields the following energy balance equation for conduction in the tube wall:

$$k_w \delta_w \frac{d^2 T_w}{dx^2} - k\left[\frac{\partial T}{\partial y}\right]_{y=b} + q_g = 0 \qquad (5.8)$$

where k is thermal conductivity, b is tube radius and the subscript w refers to the tube wall. When the dimensionless variables $X = x/b$, $Y = y/b$ and $\theta = (T - T_o)/(q_g b/k)$ are introduced, equation (5.8) becomes

$$K \frac{d^2 \theta_w}{dX^2} - \left[\frac{\partial \theta}{\partial Y}\right]_{Y=1} + 1 = 0 \qquad (5.9)$$

In equation (5.9), the first term represents axial wall conduction and $K = (k_w \delta_w/kb)$. A reduction in the value of the parameter K, by the use of a thin tube wall or a wall material of low thermal conductivity, helps to reduce the wall conduction effect, thus yielding a more uniform surface heat flux. The latter option is, however, clearly contradictory for an electrically conducting metal wall. The

second and third terms in equation (5.9) represent the unknown local heat flux at the wall–fluid interface and internal heat generation respectively. Equation (5.9) emphasizes the coupling between wall heat conduction and convective heat transfer in the fluid. Although no attempt is made here to solve this conjugate conduction–convection problem, it is noted that equation (5.9) and the energy equation for the fluid region must be solved together, subject to the condition that $\theta_w = \theta_{Y=1}$ for all X. For the simultaneously developing conditions met in combined convection situations the complete problem formulation requires the parameters Pe, Pr and Gr_q/Re to be specified in addition to the axial wall conduction parameter K.

The effect of axial wall conduction on thermally developing forced convection with a parabolic velocity profile in a uniformly heated circular tube was investigated numerically by Faghri and Sparrow (1980) and Cotton and Jackson (1985); the first of these two contributions also considering the simultaneous effect of axial conduction in the fluid. The tube wall temperature distribution was taken to be one–dimensional, as described by equation (5.9), and the tube wall was treated as effectively infinite so that heat could be propogated upstream of the start of direct heating by axial conduction, thereby causing preheating of the fluid. These studies show that axial wall conduction can cause significant departures from UHF conditions for a short length immediately downstream of the start of direct heating. In broad terms, the solutions presented for this region are characterized by a reduction in the convective heat flux and the local Nusselt number and an increase in the fluid bulk and wall temperatures. Although their numerical results are not directly applicable, the findings of Faghri and Sparrow (1980) and Cotton and Jackson (1985) are nevertheless considered to have important implications for this work.

As mentioned in Section 5.2.2, a copper flange almost one tube diameter thick was attached to each end of the tubular test section to act as an electrical power

connection. During the experiments it was evident that the upstream flange assumed a temperature higher than the water bulk temperature measured in the inlet reservoir and it is presumed that this warming was the result of axial heat conduction from the resistively heated tube. No corrections were made to the local bulk temperatures and wall—fluid heat fluxes to account for this wall conduction effect when calculating the experimental Nusselt numbers and this must be borne in mind when examining the results.

5.4.4 Wall Temperature Oscillations Due to AC Heating

Alternating current, rather than direct current, was chosen for resistance heating of the test section, partly for the convenience of using the mains supply to generate the required heavy heating current. A further factor influencing this choice was the capability of the measurement system to reject mains frequency AC interference which would otherwise have caused errors in the temperatures indicated by the thermocouples attached to the test section.

The volumetric heat generation rate of a sinusoidally varying electric current varies between zero and twice its average value, at two times the supply frequency. It is of interest to know if significant temporal variation of the test section temperatures resulted from thermal energy storage in the tube wall over each half cycle, even if not reported by the data acquisition system because of time averaging.

For a given conductor (i.e. fixed dimensions and material properties) the magnitude of the temperature oscillations depends on the convective heat transfer coefficient at the cooled surface. A lumped—system analysis of the wall temperature oscillations experienced by a thin wall heated by alternating current, insulated on one surface and convectively cooled at the other is presented in Appendix C. This simple analysis indicates that the amplitude of tube wall temperature oscillations was negligible (normally much smaller than 0.25% of the

wall–to–bulk temperature difference) under all experimental conditions in this work. This conclusion is confirmed by the results of the distributed analysis made by Jeglic et al (1980) for the same problem.

5.5 Test Procedure and Precautions

The procedure listed below was followed throughout the main test series:

i)   A flow of mains water was established through the test rig flow circuit, with no heating applied to the test section, and the bleed valves were operated to release any entrapped air.

ii)   The vacuum flask housing the thermocouple reference junctions was filled with a fresh mixture of melting ice and water and left to equilibrate. During this period the outputs of the tube wall thermocouples were monitored to check that they approached the inlet bulk temperature of the water measured by the resistance thermometer in the test section inlet reservoir. This provided a check on the consistency of the temperature measurements.

iii)   The desired test flow rate was set using the graduations on the rotameters as a guide. Occasionally at this stage, a check was made on the Pelton wheel flowmeter calibration using the collection method described in Section 5.3.2.

iv)   To commence a test, electrical power to the test section was switched on and increased to the desired level. To prevent boiling the maximum power used at each flow rate was limited so that the wall temperatures near the exit from the heated test section did not exceed 95°C.

v) During a test, all the measured quantities were scanned automatically by the data logger every 15 seconds and the readings were directed to the microcomputer to refresh the display on the monitor screen. At any stage, a set of readings could be stored in a disk file which could be imported into a spreadsheet program for a full data reduction; including calculation of the energy balance error.

vi) A period of not less than $1\frac{1}{4}$ hours (usually over 2 hours) was allowed to elapse before a final set of readings was taken. It should be emphasised that, irrespective of the time allowed for steady conditions to be achieved, tube wall and exit bulk temperatures continued to exhibit fluctuations (about a mean value) in many tests. For this reason, the practice was adopted of logging 20 readings for each measured quantity at 15 s intervals over a 5 minute period from which an average value was found.

vii) During testing, the ice point reference was frequently checked and melted ice was replenished to ensure that the reference temperature was maintained.

viii) In an attempt to randomise extraneous variable influences, both the flow rate and the test section power input were normally changed for each test, except in the sequences Tests 26A − 30A and Tests 31A − 34A where the flow rate was kept approximately constant in each case (see Table E.1).

CHAPTER 6

EXPERIMENTAL RESULTS

6.1 Range of Tests

This chapter documents the experimental results obtained in a series of tests performed to measure the axial variation of local Nusselt number for water flowing vertically upward through a uniformly heated circular tube, almost 160 diameters long, at low values of the Reynolds number. The experimental apparatus, which is fully described in Chapter 5, was operated over a range of flow rates and wall heat fluxes, creating aiding combined forced and natural convection conditions inside the tube with simultaneously developing hydrodynamic and thermal fields.

The primary intention of the experimental programme was to obtain representative test data to allow comparison with the numerical predictions, rather than to develop empirical correlations. Consequently, the amount of data collected is somewhat limited. The main test series comprised 35 individual tests, covering seven nominal flow rates and normally four or five heat flux levels at each flow rate. For the lowest flow rate (≈ 0.045 litre/minute), however, a wall–to–bulk temperature difference of approximately 6 K was sufficient to raise the the wall temperature to over 90° C near the tube exit. To prevent boiling of the water and also to maintain reasonable accuracy in the determination of the local temperature driving force, testing was restricted to only two values of heat flux at this minimum flow rate. Tests $6A - 35A$[1] provide the main heat transfer results reported in Section 6.4 below. The results for the first five tests in the series have been omitted because the measurement data recording technique used was not fully established at the time these tests were made. Moreover, the same test conditions were repeated later in the series.

---

[1]The test number indicates the chronological order of testing and the appended A is a reminder that the results for these tests are based on averages of 20 readings taken for each measured quantity at 15 s intervals over a 5 minute period.

The ranges of the operating conditions investigated in Tests 6A − 35A are shown below:

Volume flow rate: $\dot{V} = 0.045 - 0.78$ litre/minute

Wall heat flux: $q_w = 1.64 - 28.7$ kW/m²

Inlet bulk temperature: $T_{b_0} = 11.9 - 17.6°$ C

The values of $\dot{V}$, q_w and T_{b_0} for each test are given in Appendix E, Table E.1.

The range of inlet bulk temperature given above simply reflects the test−to−test differences in the temperature of the mains water supply connected to the open−circuit flow system, since no provision was made for independently setting T_{b_0}. Consequently, although remaining virtually constant for each test, the Prandtl number (denoted by Pr) of the water entering the test section was not exactly the same for all tests. More significantly, the change of Prandtl number corresponding to the bulk temperature rise along the heated tube was, in the majority of tests, greater than (by a factor of over 4 times in extreme cases) the range of inlet Prandtl number encountered in the tests.

The temperature sensitivity of the dimensionless parameter values, due mainly to the viscosity change for water, is further emphasised in Table 6.1, where the ranges of Reynolds number, Prandtl number, the heat flux based Grashof number, defined as $Gr_q = g\beta\rho^2 d^4 q_w/\mu^2 k$, and the buoyancy parameter Gr_q/Re are tabulated. Table 6.1 lists three values for both the minimum and the maximum limits of each parameter, corresponding to the use of the following different reference temperatures for the evaluation of fluid properties:

i) T_{b_0} −   inlet bulk temperature;

ii) T_{b_m} −   arithmetic mean of the inlet and exit bulk temperatures;

iii) T_{f_m} −   arithmetic mean of T_{b_m} and the average tube wall temperature T_{w_m}.

Table 6.1		Ranges of Reynolds number, Prandtl number, heat flux based Grashof number and buoyancy parameter Gr_q/Re for Tests 6A − 35A.	
Dimensionless Parameter	Property Reference Temperature	Minimum Value (Test No.)	Maximum Value (Test No.)
Re	T_{b_o}	75 (15A)	1181 (20A)
	T_{b_m}	119 (10A)	1784 (13A)
	T_{f_m}	124 (10A)	2606 (3A)
Pr	T_{b_o}	7.42 (24A)	8.77 (16A)
	T_{b_m}	3.42 (15A)	8.22 (16A)
	T_{f_m}	3.03 (32A)	7.34 (16A)
Gr_q	T_{b_o}	6.72×10^4 (19A)	1.16×10^6 (30A)
	T_{b_m}	1.07×10^5 (16A)	7.97×10^6 (25A)
	T_{f_m}	1.49×10^5 (21A)	1.77×10^7 (30A)
Gr_q/Re	T_{b_o}	70.8 (16A)	2.07×10^3 (15A)
	T_{b_m}	92.1 (16A)	1.02×10^4 (15A)
	T_{f_m}	134 (16A)	1.11×10^4 (15A)

Table 6.1 also lists the corresponding test number against each extreme value to illustrate that, in some cases, this is not independent of the reference temperature adopted. The information given in Table 6.1 is extracted from Tables E.2 − E.4 in Appendix E, which summarise the values of various dimensionless parameters for Tests 6A − 35A, with fluid properties evaluated at T_{b_o}, T_{b_m} and T_{f_m} respectively.

As shown in Table 6.1, the tests covered a wide range of the nominally laminar flow regime. Notwithstanding the magnitude of the Reynolds number, strong fluctuations of the tube wall and exit bulk temperatures were noticed in some tests conducted during the main test series (Tests 6A − 35A). Additional tests (Tests 36 − 43) were carried out to obtain transient records of the fluctuating

quantities at various operating conditions and examples of these measurements are shown in Section 6.5.

6.2 Experimental Data Reduction

For each test, the raw measurement data values captured by the data acquisition system were saved in a data file (TESTn.LOG). This log file was of a similar format to that shown in Figure 5.3, but also contained information on the mean value and standard deviation for each of the 20 measured quantities, calculated (by the data logger) from readings accumulated over a specified number of scans.

The experimental data reduction calculations were reasonably straightforward and were based on the average values referred to above. A special spreadsheet program was developed to import and interpret the data files and perform all the necessary computations. The data reduction procedure, including all the formulae used, is illustrated by a specimen calculation in Appendix D, where a sample spreadsheet output is also shown. Equations (B.1), (B.3) and (B.5)–(B.7) of Appendix B were used to evaluate the fluid properties μ, k, c, ρ and β respectively.

It is emphasised that the wall heat flux used to calculate the local Nusselt number Nu_x was based on the electrical energy input to the test section (corrected for heat losses) and not on the measured energy rise of the water. Futhermore, the wall–fluid thermal boundary condition was assumed to conform to a uniform heat flux (UHF) and taken equal to the corrected energy input averaged over the inside surface area of the heated tube. Accordingly, no attempt was made to correct for the effects of axial wall conduction or for nonuniform heat generation in the tube wall due to temperature dependence of the tube material resistivity.

6.3 Energy Balance Results

An apparent energy balance error can be defined as the difference between the energy rise of the fluid, indicated by the measured bulk temperature rise

$(\Delta T_b)_{meas}$, and the energy input to the test section (corrected for heat losses). In percentage terms, this error is given by

$$\% \text{ energy balance error} = 100 \, [\dot{Q}_{meas} - \dot{Q}_{corr}]/\dot{Q}_{corr} \qquad (6.1)$$

where $\dot{Q}_{meas} = \rho_o \dot{V} c_{b_m} (\Delta T_b)_{meas}$. The corrected rate of energy input, denoted by $\dot{Q}_{corr}$, was found from $\dot{Q}_{corr} = \tilde{I}\tilde{V} - \dot{Q}_{loss}$, where the product $\tilde{I}\tilde{V}$ gives the test section electrical power input and $\dot{Q}_{loss}$ is the rate of heat loss estimated from the empirically determined equation (5.3).

Values of the percentage energy balance error for Tests $6A - 35A$, calculated from equation (6.1), varied between $+ 3.2\%$ and $- 12.5\%$ and are shown in Appendix E, Table E.1. Infact, the error was within $\pm 4\%$ for almost two–thirds of the tests. A plot of $\dot{Q}_{meas}$ versus $\dot{Q}_{corr}$ for all the tests is shown in Figure 6.1.
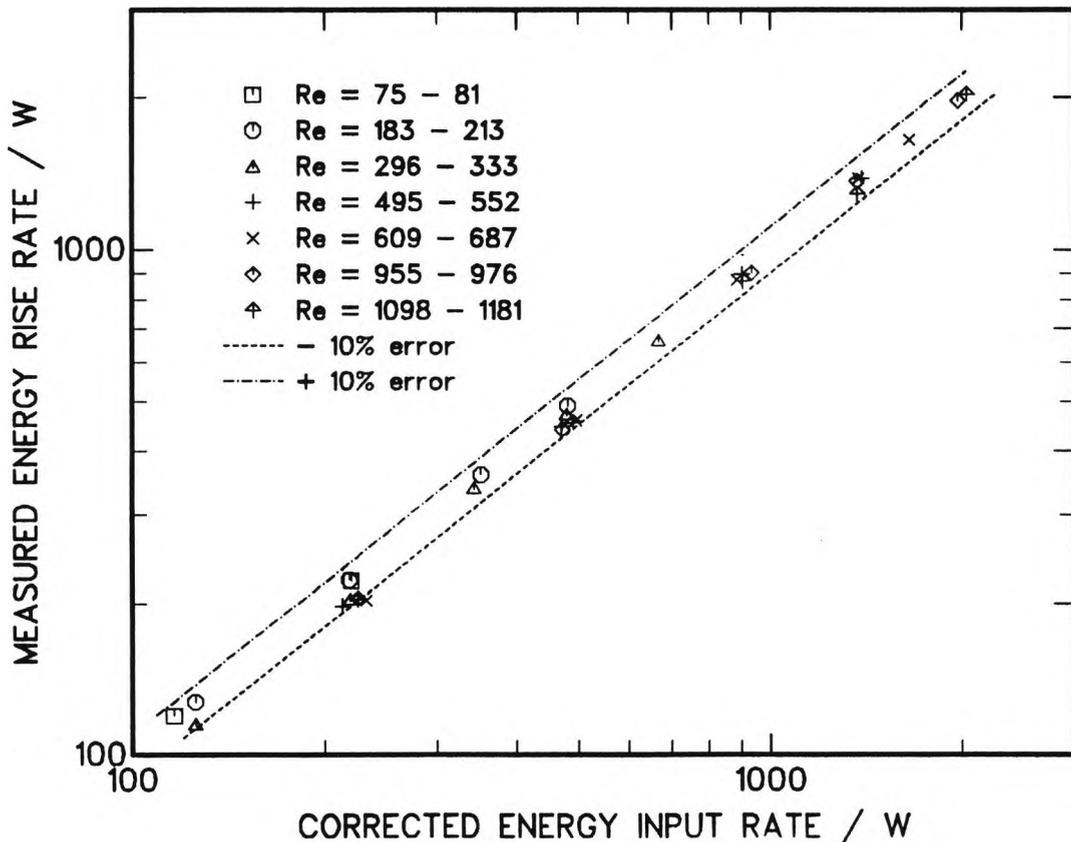
Figure 6.1   Comparison of measured fluid energy rise with corrected energy input for Tests $6A - 35A$.

The level of agreement achieved in the energy balance (see Figure 6.1) is considered to be satisfactory, particularly in view of the earlier problem experienced with the measurement of exit bulk temperature discussed in Section 5.3.4. Closer examination of Table E.1 reveals that, at all flow rates other than the two lowest, the energy balance error tended to become increasingly negative as the heat flux was decreased. The equivalent trend is also seen in Figure 6.2, where the percentage energy balance error is plotted against the bulk temperature rise based on the corrected rate of energy input. The reason for this behaviour, suggesting a systematic error that assumes greater importance as ΔT_b decreases, is unknown.
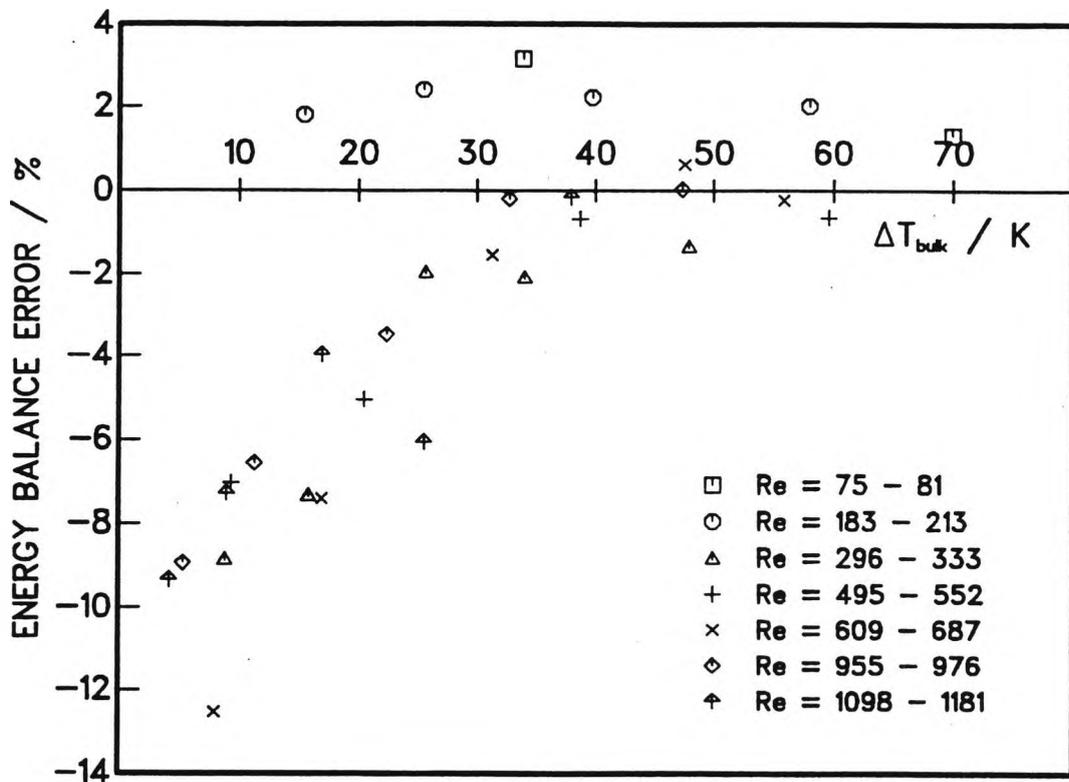
Figure 6.2   Energy balance error versus corrected bulk temperature rise for Tests 6A − 35A.

As shown in Figure 6.2, rather unrealistic positive energy balance errors were found for the tests at the lowest two flow rates and no particular pattern can be discerned with regard to the effect of heat flux in these cases. This is, at least

partly, attributable to the straight line calibration law used for the turbine flowmeter, which is known to have overestimated the flow rate, and hence $\dot{Q}_{meas}$, for small values of $\dot{V}$.

Finally, it is stressed that the measured exit bulk temperature was only employed in the calculation of the energy balance error, as discussed above, and was not used to determine local Nusselt numbers.

6.4 Heat Transfer Results

Experimental results of two types are presented in graphical form in this section:

i)   Measured tube wall temperature profiles. Selected plots of the local tube wall temperatures versus dimensionless axial distance x/d are shown in Section 6.4.1.

ii)   Local Nusselt number variations with dimensionless axial distance $x*$. The local experimental Nu_x results for Tests $6A - 35A$ are summarised in Section 6.4.2.

Both the dimensionless axial distances, x/d and $x*$ [$= (x/d)/RePr$], referred to above are based on the distance x measured from the start of the heated section. In each of the graphs presented in this section the values of the Reynolds number Re and the heat flux based Grashof number Gr_q are given with the fluid properties evaluated at the inlet bulk temperature.

6.4.1 Local Tube Wall Temperature

Sequences of graphs are shown below to illustrate the influence of heat flux on the wall temperature profile for approximately constant flow rates. Only four different flow rates are considered, the intention being to cover the range of parameters rather than to be exhaustive. Figures 6.3(a) and (b) and Figures 6.6(a)–(c) relate to the lowest and the highest flow rate tests respectively and Figures 6.4(a)–(c)

and Figures 6.5(a)–(c) present the same type of information for two intermediate flow rates. For each flow rate, graphs are presented for the minimum and maximum heat flux values and in the case of Figures 6.4 – 6.6 one intermediate heat flux. All these graphs are plotted to the same scale to aid comparison and also show the linear variation of fluid bulk temperature appropriate to the assumed UHF boundary condition in each case. In addition, the measured bulk temperatures at inlet and exit are plotted for comparison with the corrected bulk temperature rise, giving a further illustration of the magnitude of the energy balance error. Apart from the application of thermocouple calibration corrections the local wall temperatures plotted in Figures 6.3 – 6.6 are basically the measured data values and, although time–averaged, they have not been subjected to any spatial smoothing.

From inspection of Figures 6.3 – 6.6 the following observations are noted:

i)   The measured wall temperatures do not appear to approach the fluid bulk temperature at $x = 0$, as ideally expected for a UHF boundary condition. This is believed to be due to the influence of axial heat conduction from the heated tube to the upstream power connection flange. As mentioned in Section 5.4.3, the temperatures measured on this flange (not plotted on Figures 6.3 – 6.6), also exceeded the measured inlet bulk temperature, indicating that preheating of the fluid occurred upstream of the $x = 0$ position.

ii)   With the exception of the departure noted in i) above, the measured wall temperatures in the low heat flux tests are seen to vary with axial distance in a manner resembling that expected for forced convection under uniform heat flux conditions. Initially, the wall temperature rises steeply and eventually a wall temperature gradient is established that is roughly parallel to the linear bulk temperature rise. The figures clearly

show, as expected, that the axial distance necessary for this development increases with the Reynolds number.

iii)   At higher heat fluxes, the wall—to—bulk temperature differences undergo a pronounced decrease in the downstream portion of the tube, indicating an improvement in heat transfer. This is evident from the local Nusselt number variations which are presented in the next section. On reflection, it is considered that closer spacing of the thermocouples in this region would have been helpful in resolving the shape of the wall temperature profiles for these tests.

Finally it is noted that the measured wall temperature profiles shown in Figures 6.5(a)–(c) are compared with numerical predictions in Section 7.1.2.
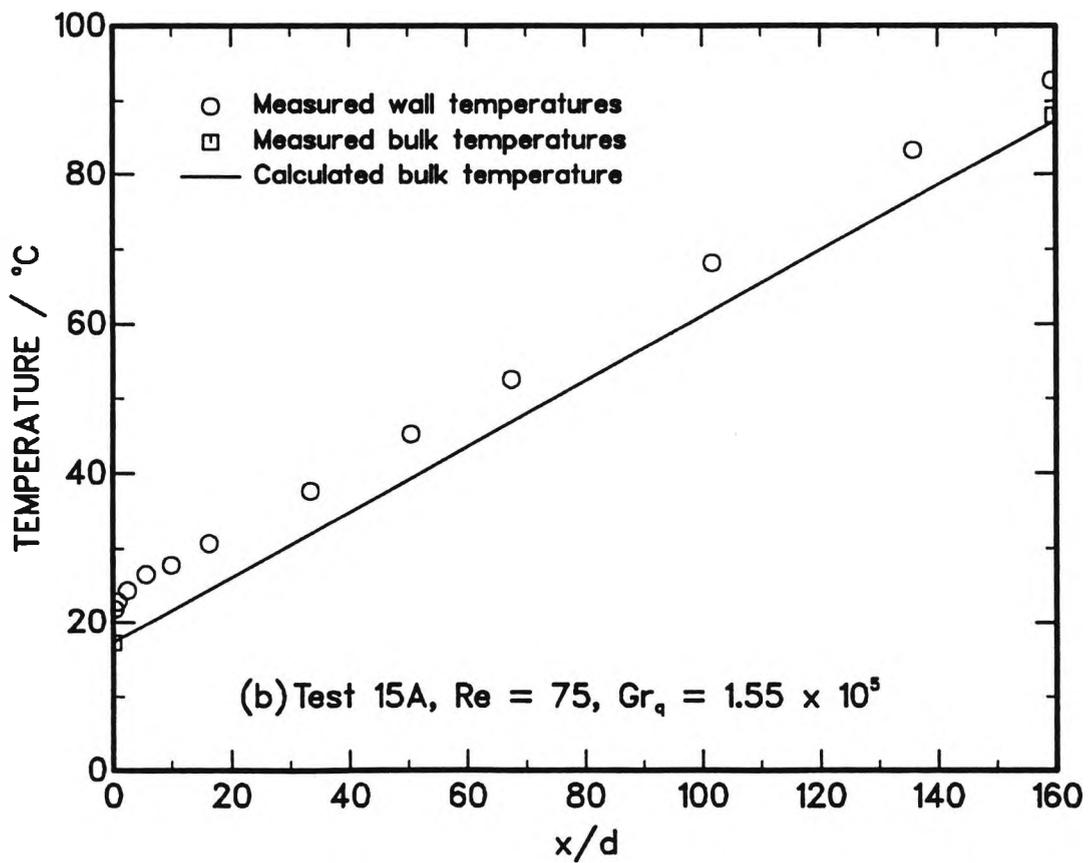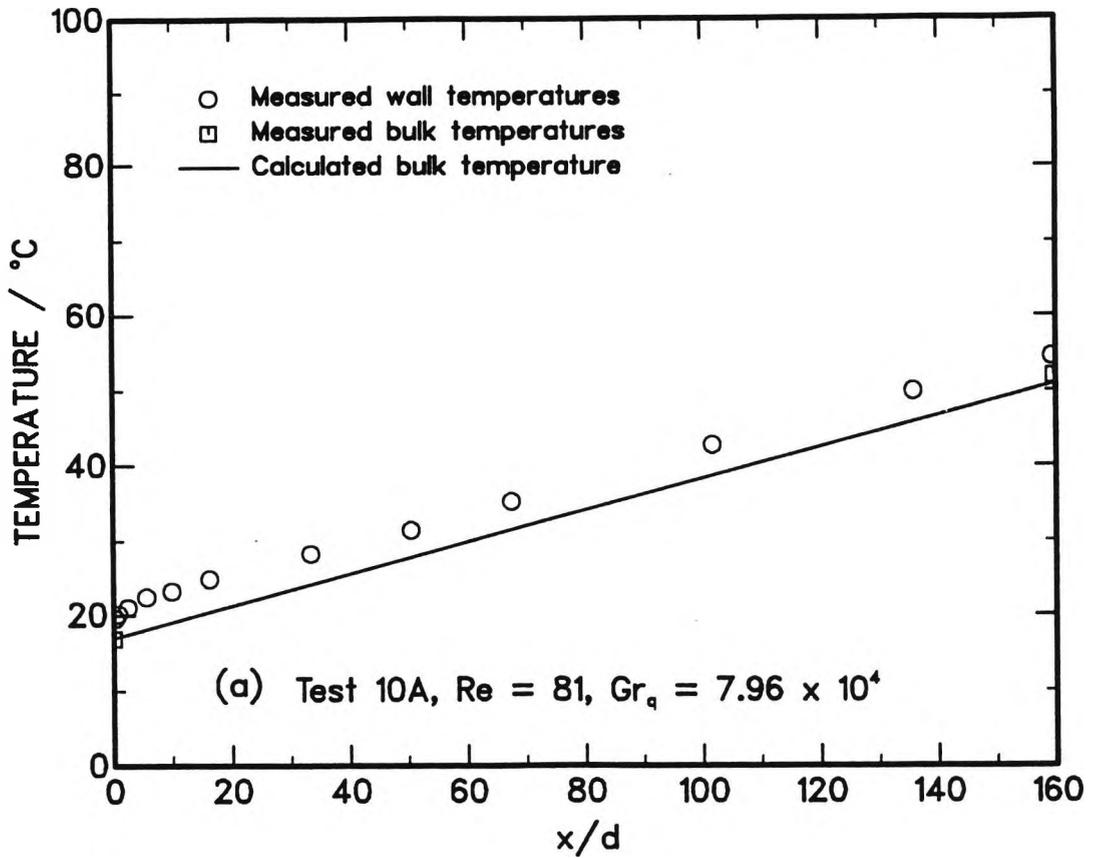
Figure 6.3   Effect of heat flux on wall and bulk temperatures, (Re = 75 − 81): (a) Gr_q = 7.96 x 10⁴, (b) Gr_q = 1.55 x 10⁵.
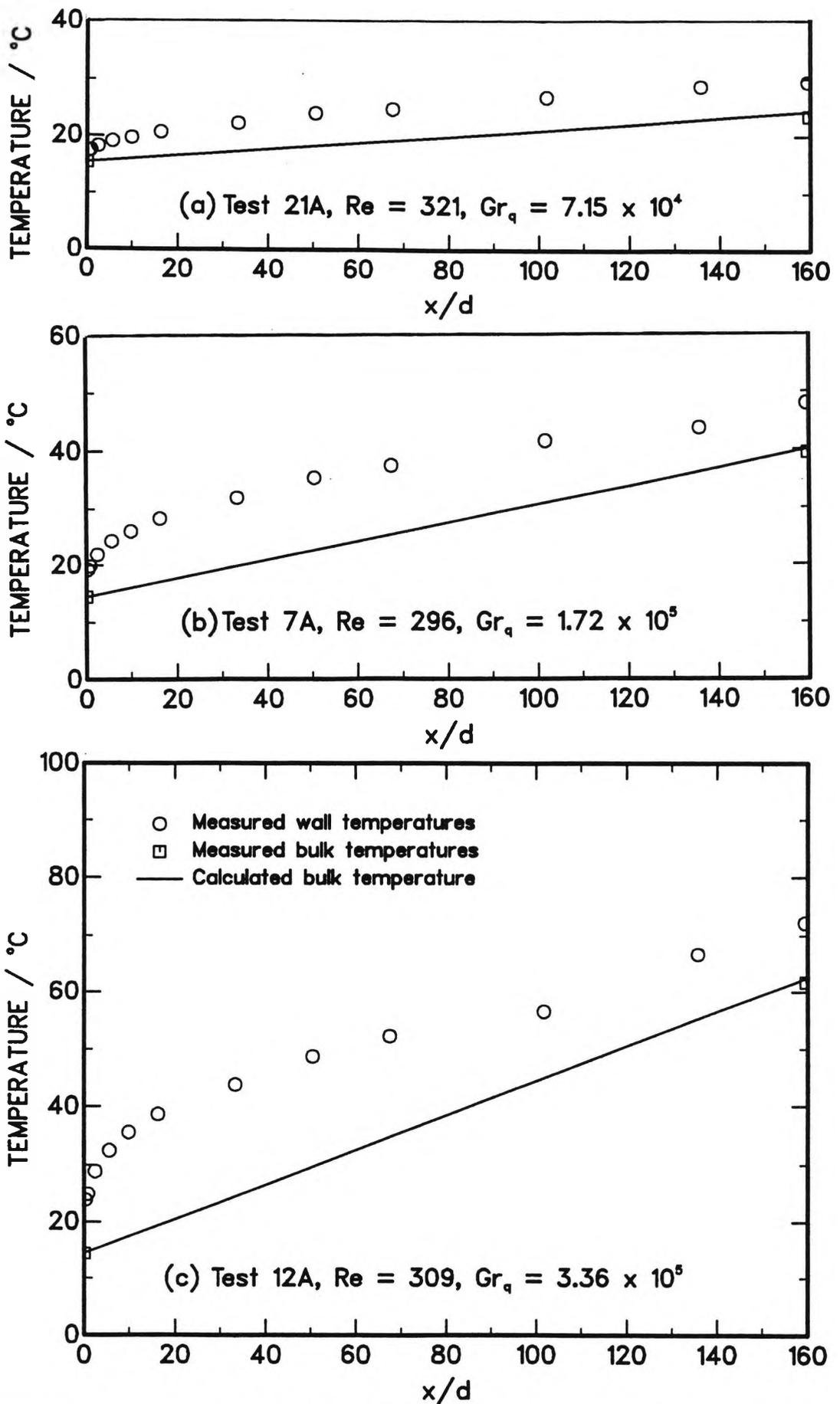
Figure 6.4 Effect of heat flux on wall and bulk temperatures, (Re = 296 − 321). (a) $Gr_q = 7.15 \times 10^4$, (b) $Gr_q = 1.72 \times 10^5$, (c) $Gr_q = 3.36 \times 10^5$.
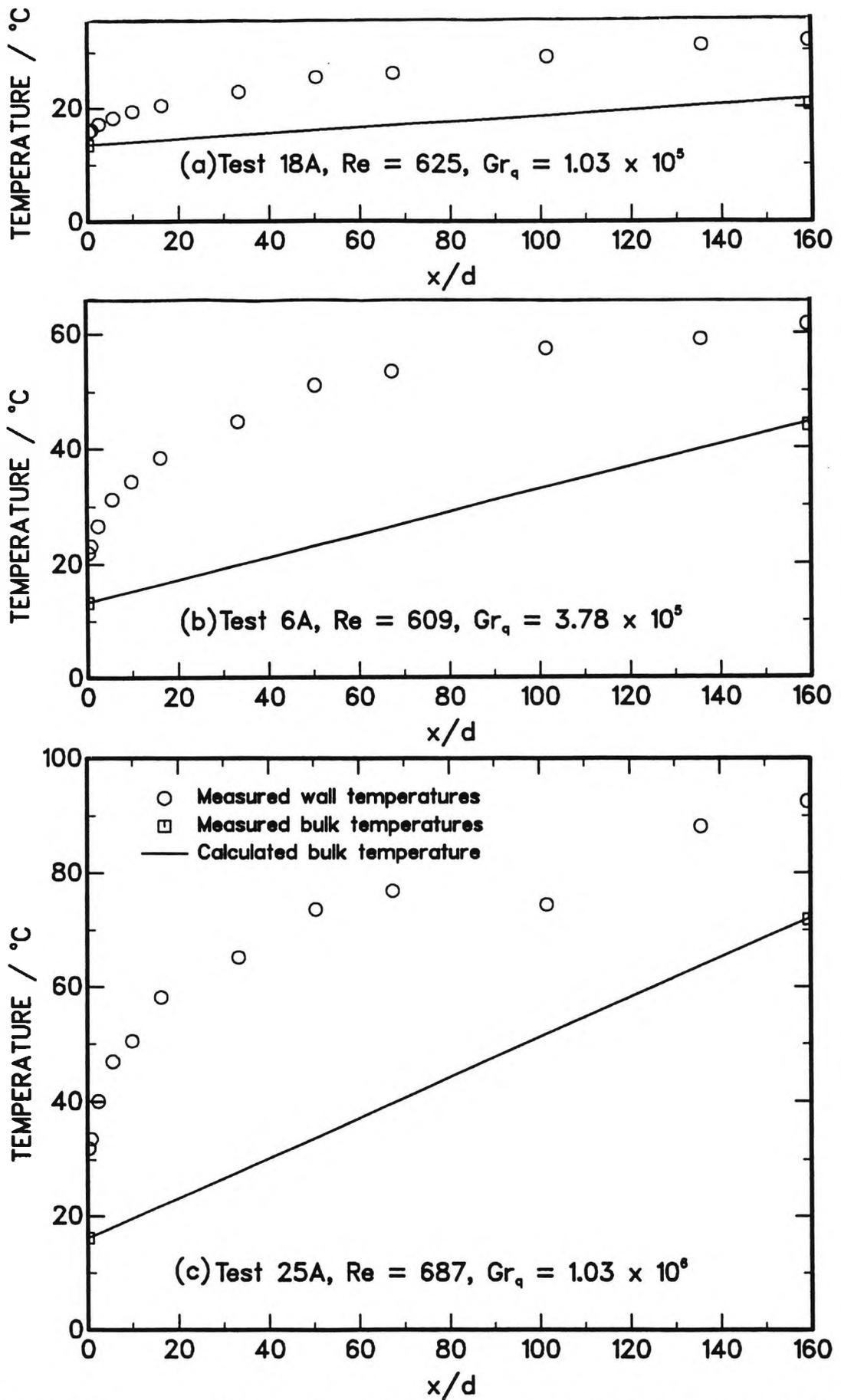
Figure 6.5   Effect of heat flux on wall and bulk temperatures, (Re = 609 − 687). (a) $Gr_q = 1.03 \times 10^5$, (b) $Gr_q = 3.78 \times 10^5$, (c) $Gr_q = 1.03 \times 10^6$.
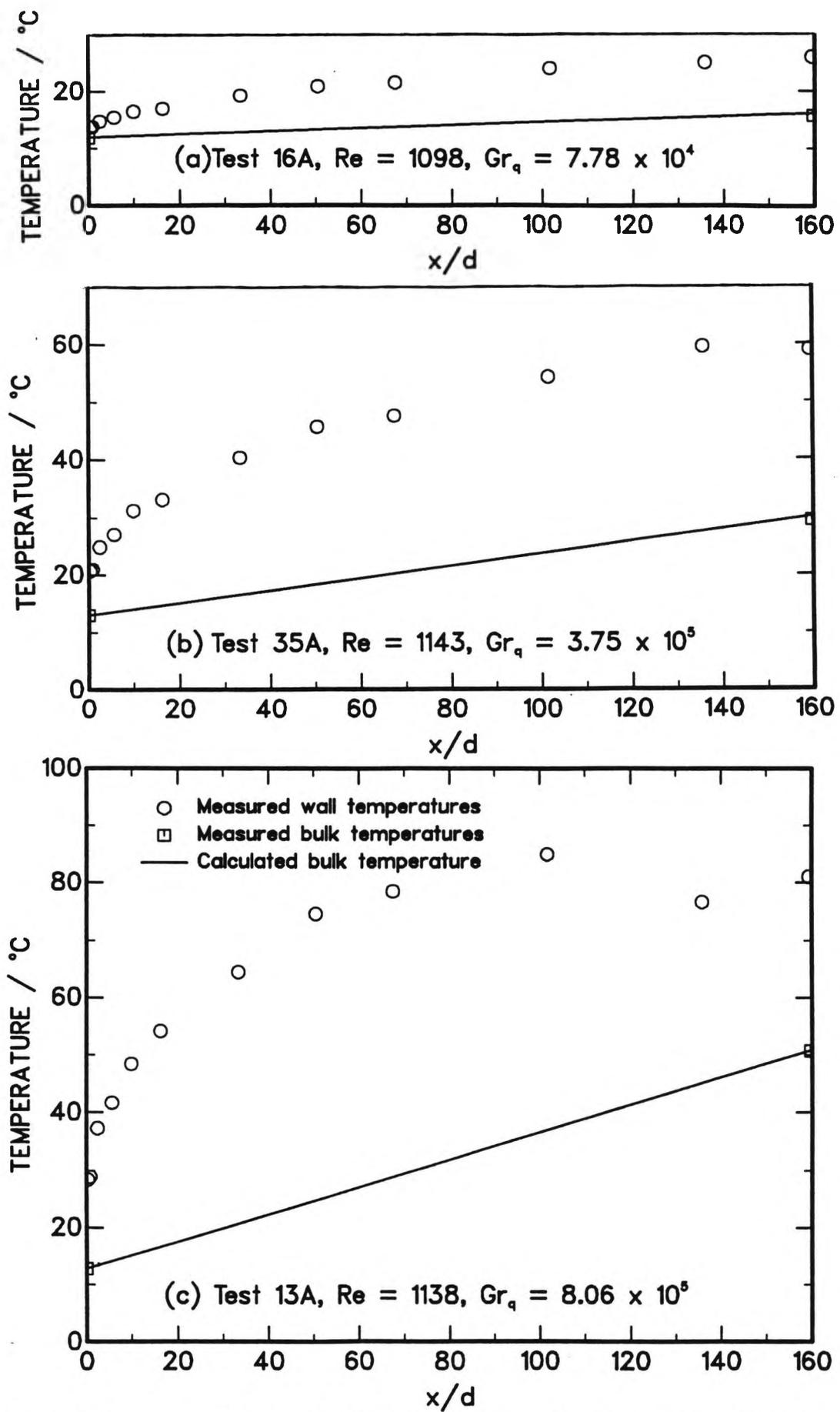
Figure 6.6 Effect of heat flux on wall and bulk temperatures, (Re = 1098 − 1143). (a) $Gr_q = 7.78 \times 10^4$, (b) $Gr_q = 3.75 \times 10^5$, $Gr_q = 8.06 \times 10^5$.

6.4.2 Local Nusselt Number

Figures 6.7 − 6.13 show how the local Nusselt number Nu_x varied with the dimensionless coordinate x∗ in Tests 6A − 35A. Each figure summarises the effect of increasing the Grashof number for one of the seven different flow rates covered by the test series. The inlet Reynolds number is therefore approximately the same for the graphs on each figure. In Figures 6.7 − 6.13 all fluid properties are evaluated at T_{b_0}, the inlet bulk temperature, although, as demonstrated by Barozzi et al (1982), the choice of reference temperature does not strongly affect the position of the plotted points for water.

For a constant flow rate, the experimental Nu_x values for the different Grashof numbers decline along approximately the same line at low x∗, in a manner similar to that for pure forced convection. As the dimensionless axial distance x∗ increases the data show a strong influence of Grashof number; Nu_x increasing with Gr_q at a fixed x∗. For sufficiently large values of Gr_q, the decline in Nu_x with x∗ is arrested and followed by a "tail−up" behaviour.

Numerical predictions of Nu_x made for some of the test conditions are compared with the experimental results in Section 7.1.1.
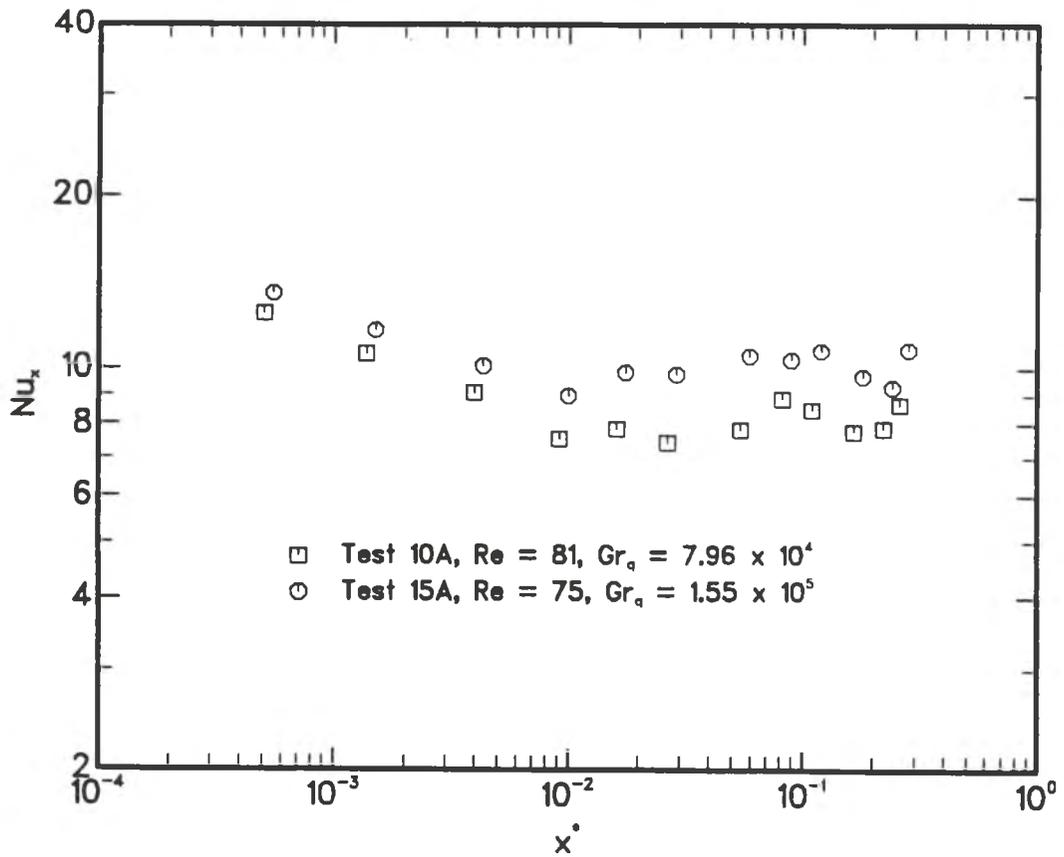
Figure 6.7 Variation of local Nusselt number with x* for two values of Grashof number, (Re = 75 − 81).
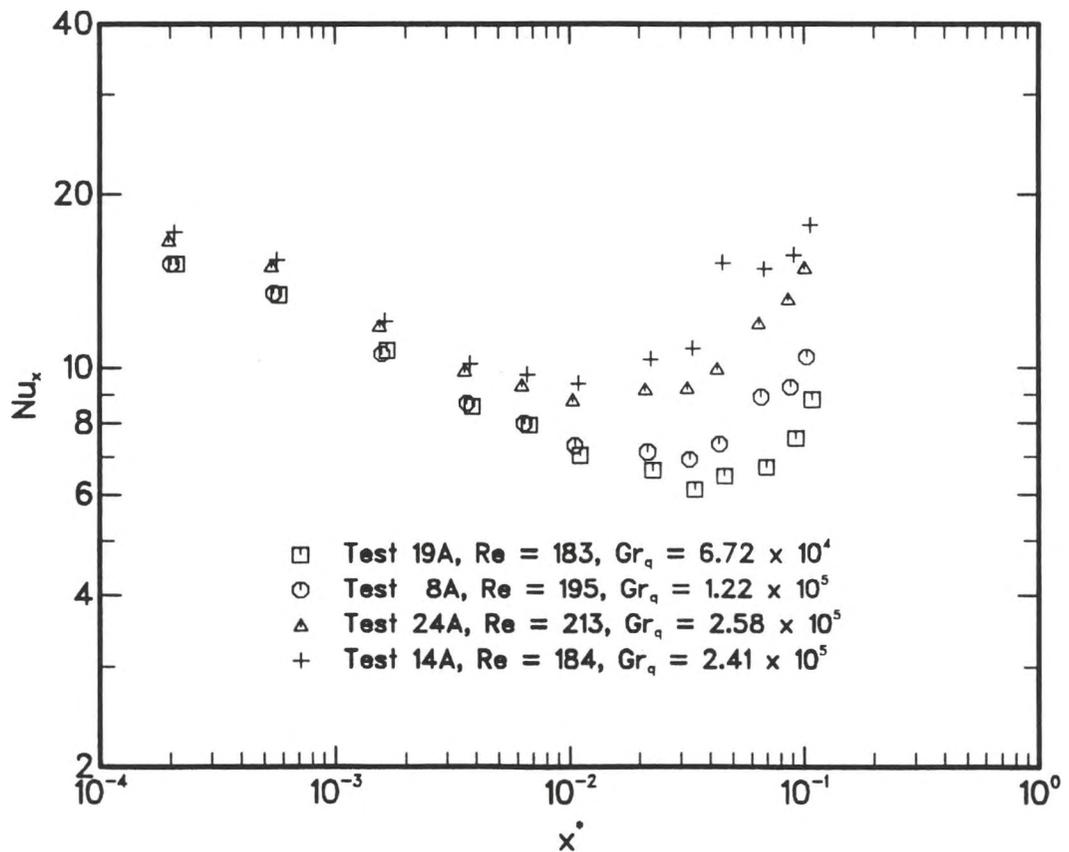
Figure 6.8 Variation of local Nusselt number with x* for four values of Grashof number, (Re = 183 − 213).
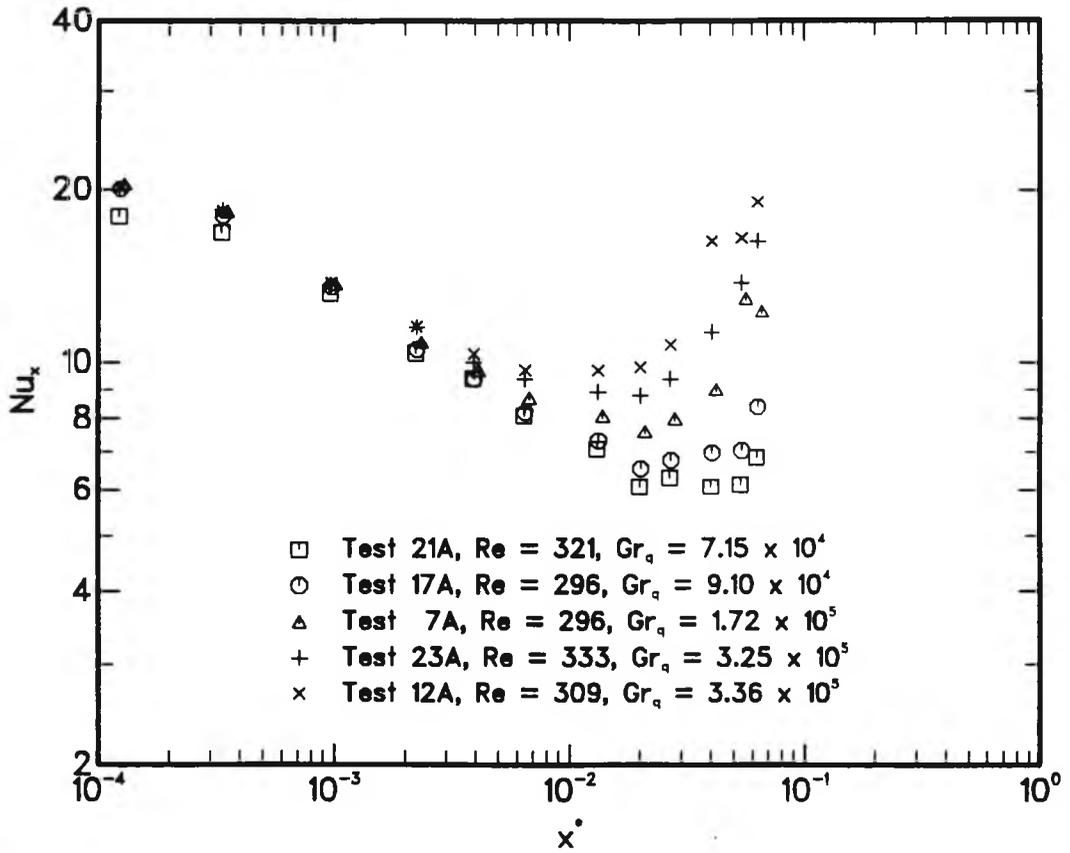
Figure 6.9   Variation of local Nusselt number with x* for five values of Grashof number, (Re = 296 − 333).
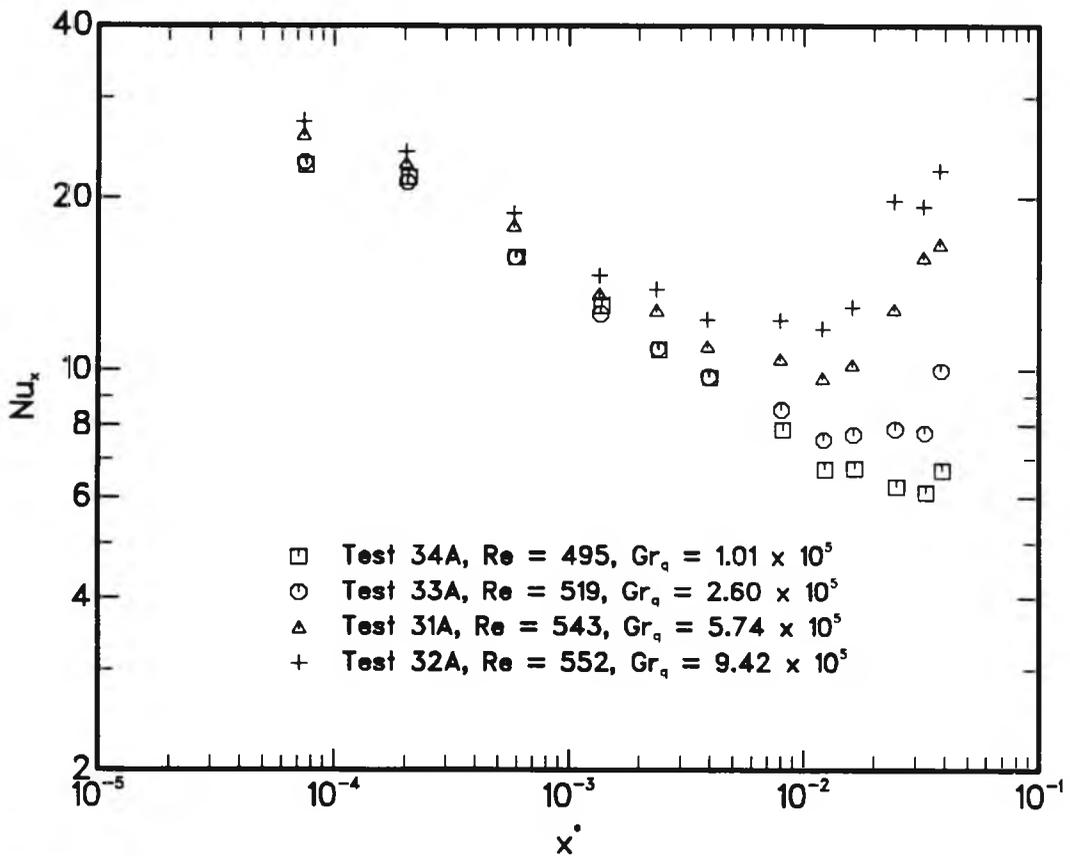
Figure 6.10   Variation of local Nusselt number with x* for four values of Grashof number, (Re = 495 − 552).
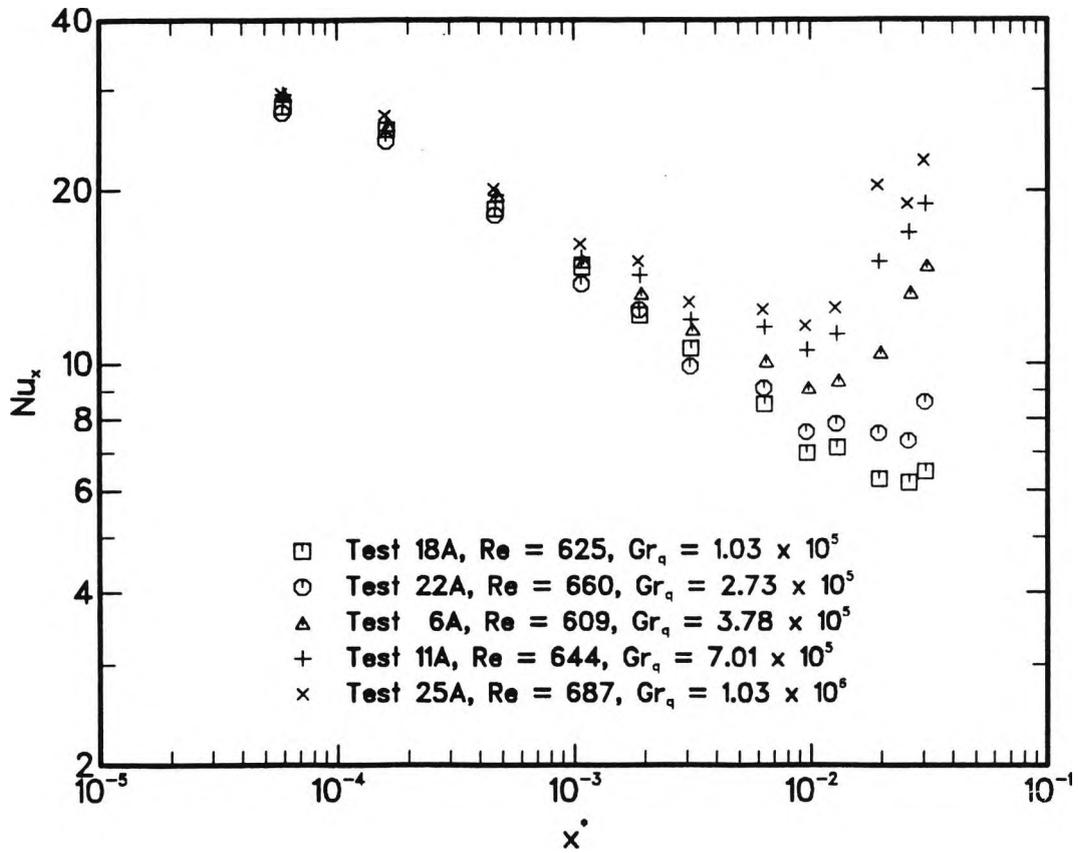
Figure 6.11   Variation of local Nusselt number with x* for five values of Grashof number, (Re = 609 − 687).
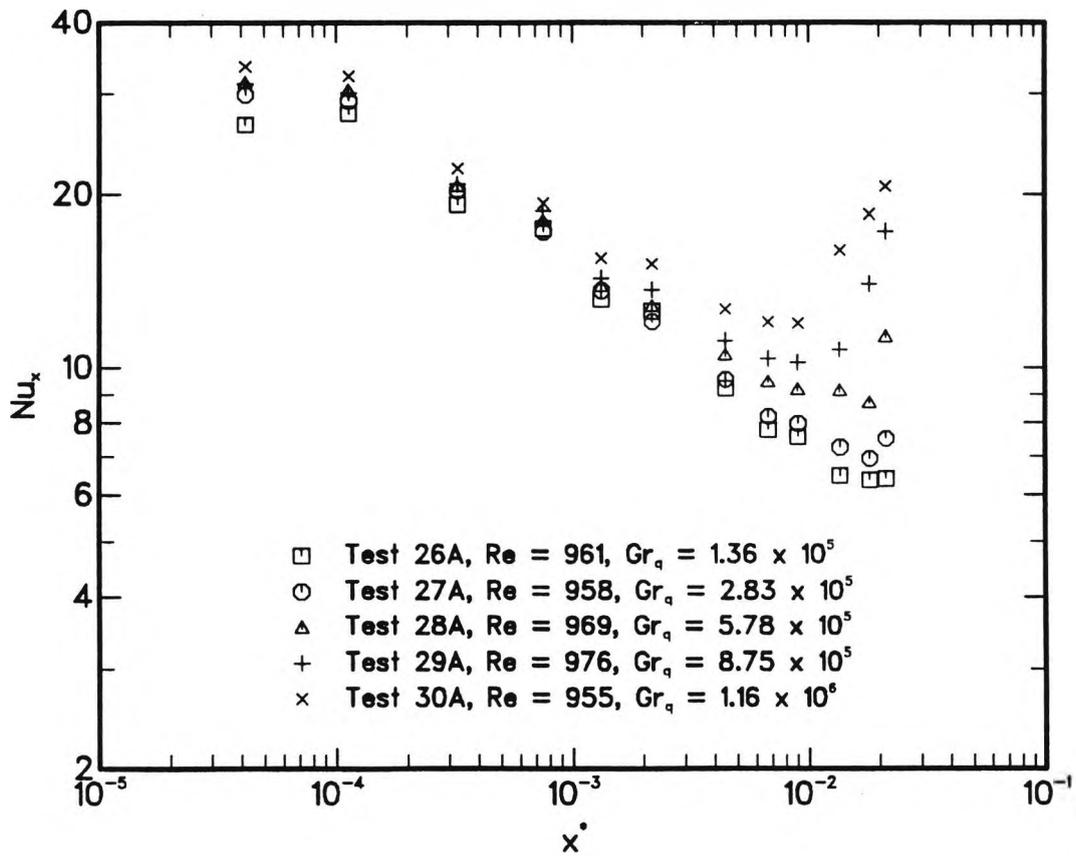
Figure 6.12   Variation of local Nusselt number with x* for five values of Grashof number, (Re = 955 − 976).
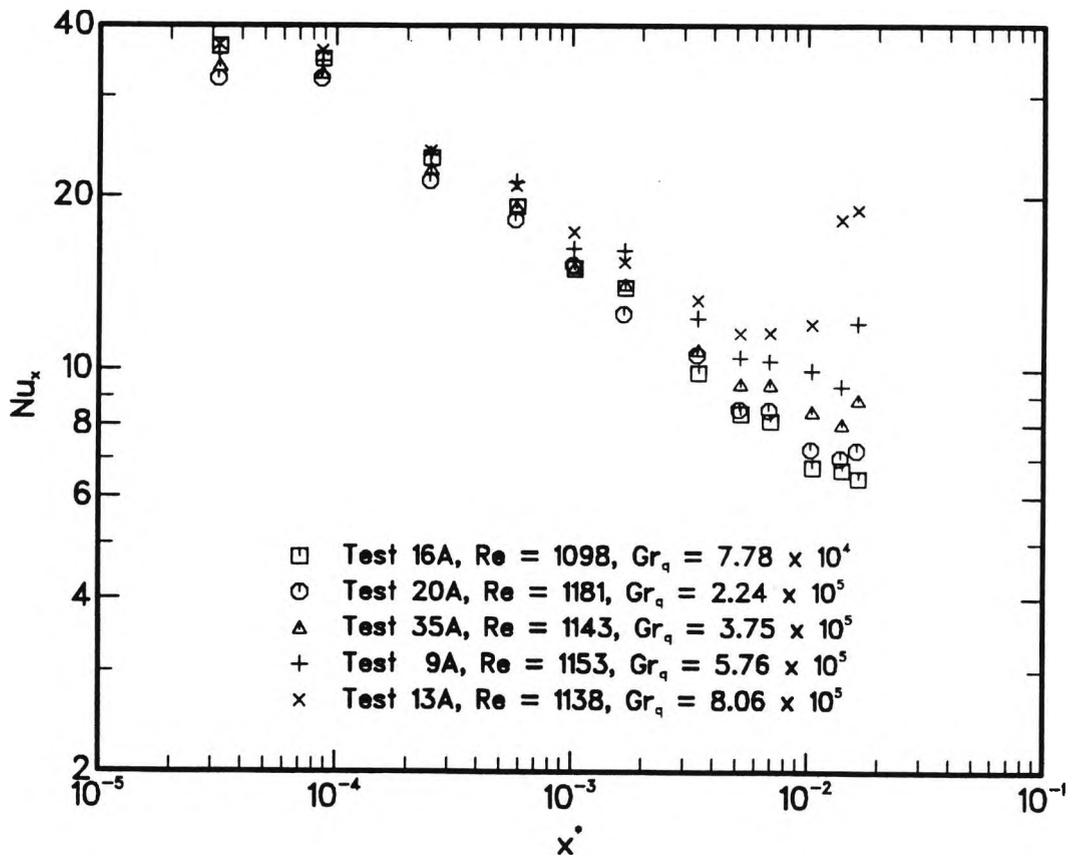
Figure 6.13   Variation of local Nusselt number with x* for five values of Grashof number, (Re = 1098 − 1181).

6.5 Wall and Fluid Temperature Fluctuations

To obtain additional information about the fluctuating temperatures observed during the main test series, a further 8 tests (Tests 36 − 43) were performed. In these tests, all inputs to the data acquisition system were scanned and the measurements recorded every 1 s for a period of 4 minutes. Although the data logger was capable of much faster scanning rates, the scanning interval of 1 s was chosen to allow sufficient integration time for the best possible measurement accuracy to be achieved. The 4 minute scanning period was dictated by the maximum number of readings per channel which could be stored and averaged by the data logger.

Three different flow rates ($\dot{V}$ = 0.055, 0.44 and 0.82 litre/minute) were used in Tests 36 − 43, covering approximately the same overall range as the main test series. At the maximum and minimum flow rates, measurements were made at one

"low" value of the heat flux and one "high" value. For the intermediate flow rate, four heat flux levels were employed. Only the results for Test 36, from the middle of the flow rate–heat flux range, are included here. To avoid overlapping traces, Figure 6.14 shows a separate plot of the local wall temperature variations with time for each of the 12 thermocouple positions along the test section. The corresponding fluctuations of the exit bulk temperature for Test 36 are shown in Figure 6.15. Figures 6.14 and 6.15 were constructed by simply linking the 241 values recorded for each temperature during the scanning period to produce a quasi–continuous record. In each case, the position at which the abscissa crosses the ordinate is used to indicate the mean value and the standard deviation is shown on the plot. In Figure 6.14, successive plots should be staggered by 25 ms (undetectable on the scale plotted) to account for the time difference between the individual measurements at 40 channels per second.

The sample wall temperature records shown in Figure 6.14 exhibit fluctuations characteristic of those seen over a range of conditions. However, the magnitude of the fluctuations observed in Tests 36 − 43 varied considerably, generally increasing with both heat flux and flow rate.

Although shorter wavelength fluctuations of small magnitude also appear to be present, the wall temperature records for the lower half of the heated tube in Test 36, shown in Figure 6.14, are dominated by occasional large excursions below the average value. Over this length of the tube the fluctuations initially increase with axial distance and then decay to their original level. Furthermore, a strong correlation can be seen between the temperature records obtained for the thermocouples positioned at $x/d = 0.85$, 5.65, 16.3 and possibly 50.5 also. A correlation is also evident between the records for $x/d = 2.45$, 9.92 and 33.4. Recalling that alternate thermocouples were attached to diametrically opposite sides of the tube, these correlations are taken to provide strong evidence of asymmetric flow in the tube.
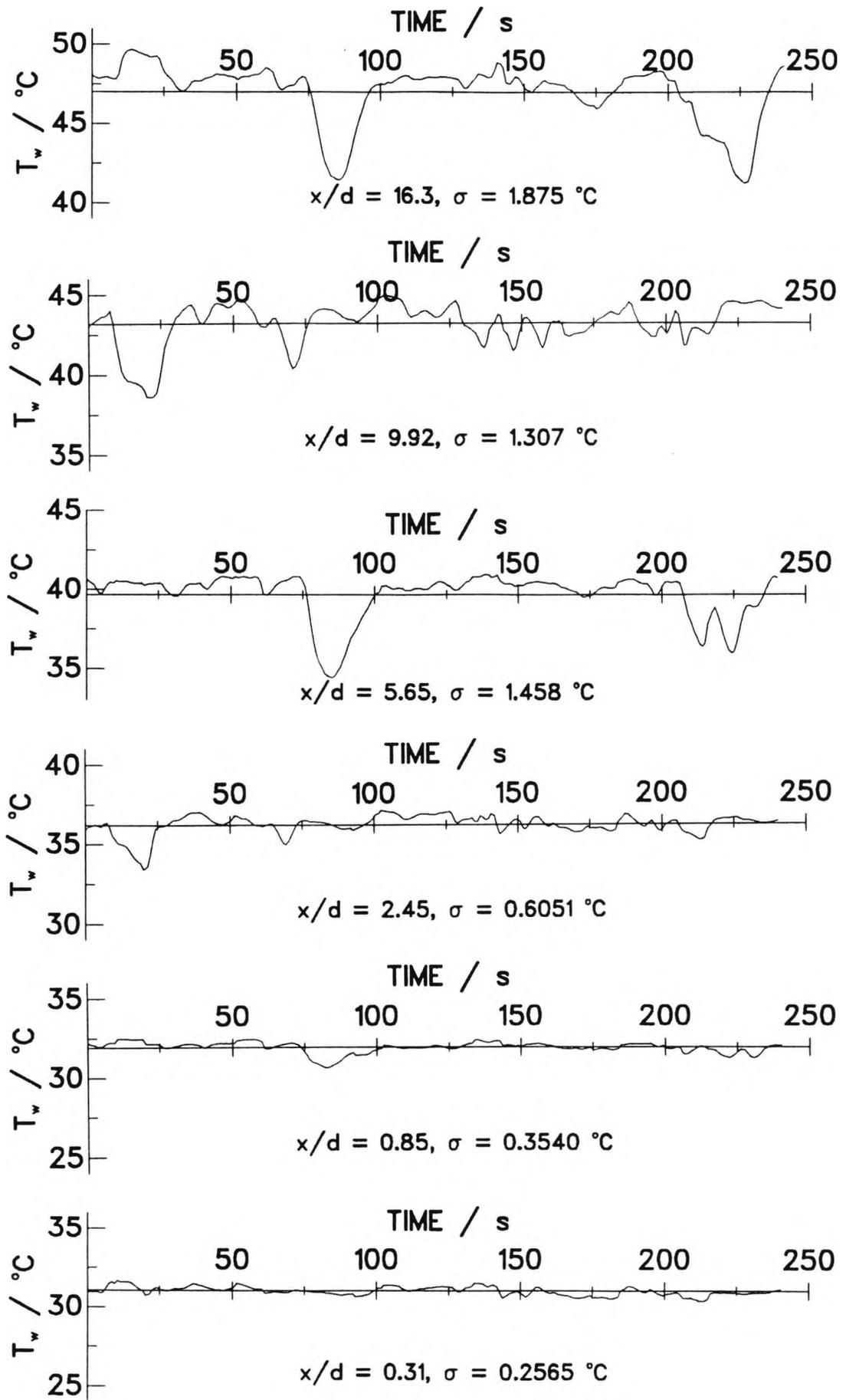
Figure 6.14   Local wall temperature fluctuations for Test 36, Re = 824 and $Gr_q = 1.06 \times 10^6$ (inlet bulk properties).

x/d = 159.3, σ = 2.120 °C

x/d = 135.9, σ = 3.677 °C

x/d = 101.7, σ = 1.916 °C

x/d = 67.6, σ = 0.3639 °C

x/d = 50.5, σ = 0.7341 °C

x/d = 33.4, σ = 0.8691 °C
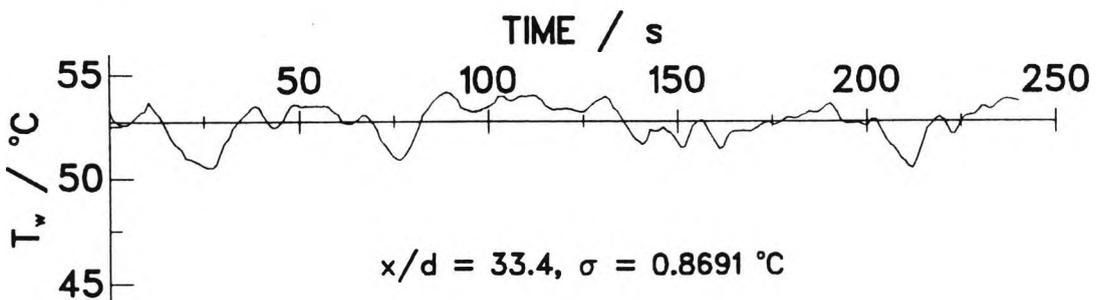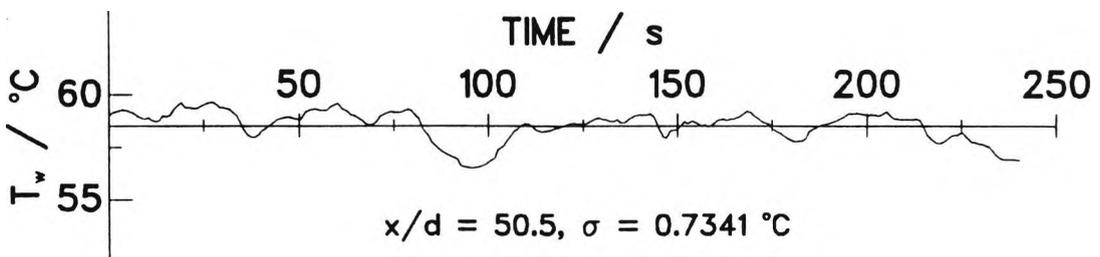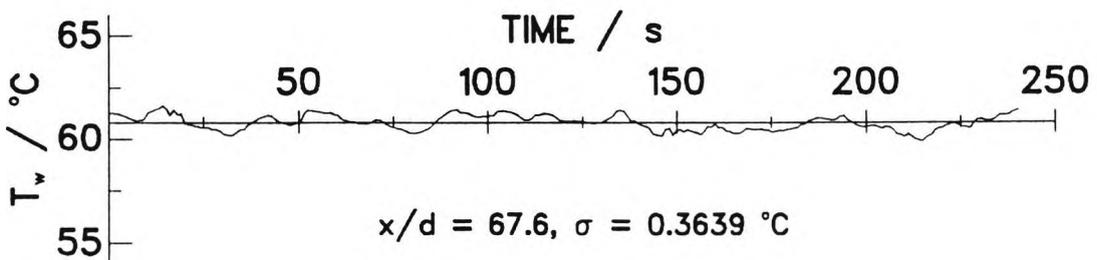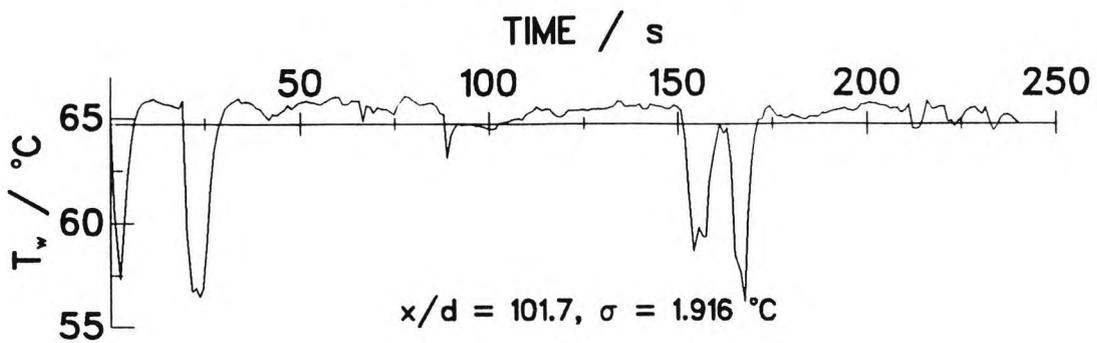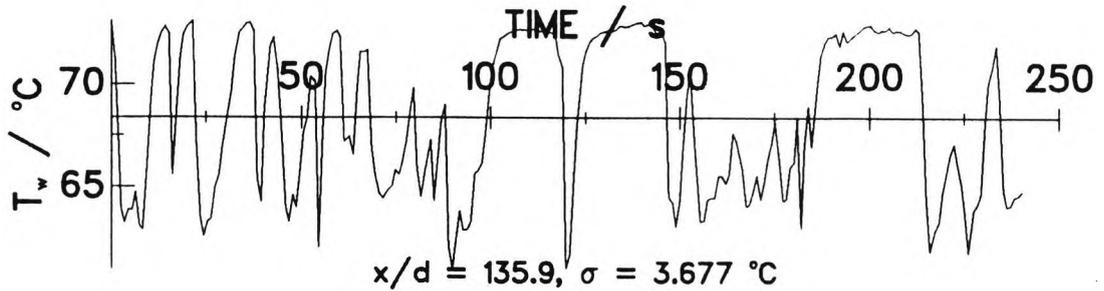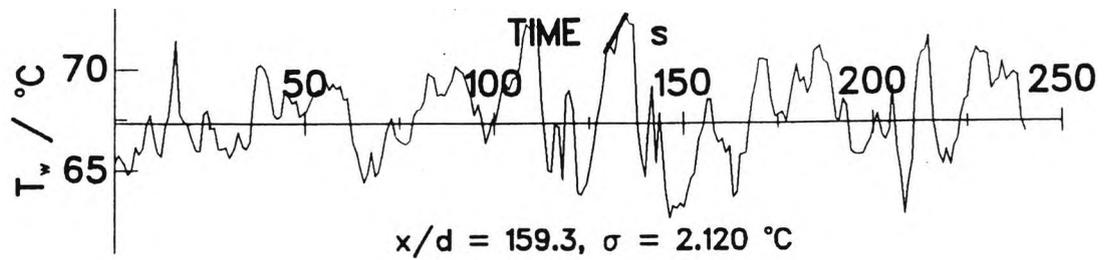
Figure 6.14 (continued)
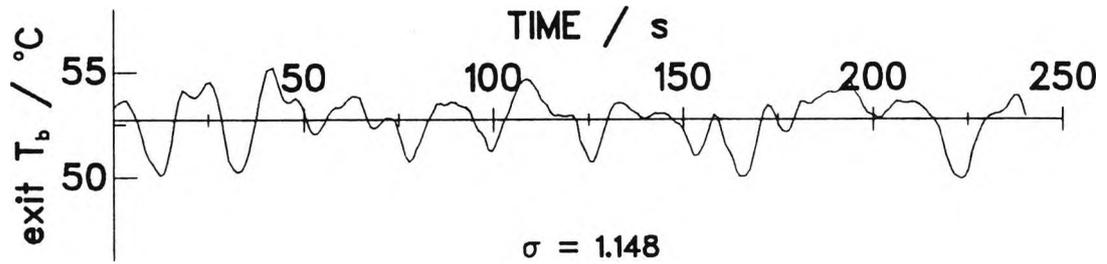
Figure 6.15   Exit bulk temperature fluctuations for Test 36, Re = 824 and $Gr_q = 1.06 \times 10^6$ (inlet bulk properties).

For the upper half of the tube, rapid and irregular wall temperature fluctuations of larger amplitude, exemplified in Figure 6.14, were observed in many tests.

The wall temperature fluctuation measurements made are considered to be of only a preliminary nature. Nevertheless, they demonstrate the feasibility of the technique employed, which could be exploited in subsequent work.

PART 4

INTERPRETATION

CHAPTER 7

DISCUSSION OF RESULTS

7.1 Comparison of Numerical Predictions with Experimental Results

Numerical solutions for thermally and hydrodynamically developing upflow of water through a uniformly heated circular tube have been obtained for selected conditions corresponding to specific tests conducted in the experimental programme. Predicted axial variations of local Nusselt number and tube wall temperature are compared with experimentally determined values in Sections 7.1.1 and 7.1.2 respectively.

All the computations were performed using the computer program listed in Appendix F, which embodies the marching finite–difference procedure described in Chapter 3. Because of its particular appropriateness to the assumed UHF thermal boundary condition, the integral energy balance equation (3.36 or 3.75) was invoked for the solution of the temperature profile at each axial step. This ensured rigid adherence to the correct bulk temperature variation along the tube. Viscous dissipation was neglected in all cases. The option to include in the solution the effect of fluid property variation with temperature was chosen for all properties. Polynomial equations describing the property variations of liquid water, given in Appendix B, were used.

The same finite–difference grid was used for all computer runs corresponding to experimental conditions. A uniform grid spacing with 80 divisions was used in the transverse (radial) direction. In the axial direction a nonuniform grid spacing was used to locate more grid points in the region from the tube entrance to beyond the start of heating. As mentioned in Section 5.2.1, the axial position of the commencement of thermal development was not coincident with that for hydrodynamic development in the experimental set–up. A short adiabatic starting length, equal to 2.5 tube diameters, was allowed in each computation for partial

development of the initially uniform entrance flow upstream of the heated section. Notwithstanding this addition to the total marching length, the dimensionless axial distances x/d and x* [= (x/d)/RePr] used here are based on the distance measured in the marching direction from the start of the heated section.

An initial axial marching step size ΔX [= x/b] of 0.1 was used; equivalent to 1/20 of the tube diameter. This was increased to 0.125 after 5 steps. Thereafter, ΔX was doubled at axial positions 5.0, 20.0 and 52.5 tube diameters from the start of marching. Thus, the largest axial step was equal to half the tube diameter and 551 steps in total were required to reach the end of the heated tube.

7.1.1 Local Nusselt Number Comparisons

Predicted and experimental data for the variation of local Nusselt number with the dimensionless axial distance x* are compared in Figures 7.1 — 7.4. The experimental Nu_x versus x* data shown in this series of figures were selected to span the ranges of Re and Gr_q covered in the experimental programme and constitute only about one—third of the available test data (see Figures 6.7 — 6.13). Tests for approximately equal inlet Reynolds numbers are grouped on each figure. To improve clarity, the comparisons presented for each Reynolds number are limited to the minimum and maximum values, and also one intermediate value in Figures 7.2 — 7.4, of the Grashof number range covered in the experiments. The fluid properties used to evaluate Nu_x, x* and the parameters Re and Gr_q displayed in Figures 7.1 — 7.4 were taken at the inlet bulk temperature of the water.

In some computations, for conditions corresponding to specific tests, it was predicted that flow reversal would occur along the tube centreline at some axial position within the heated tube. As might be expected, the predicted axial position of flow reversal moved nearer to the start of heating when the Grashof number was increased for the same Reynolds number. For conditions corresponding to the two lowest Reynolds number tests (Re = 75 and 81), shown in Figure 7.1, flow reversal
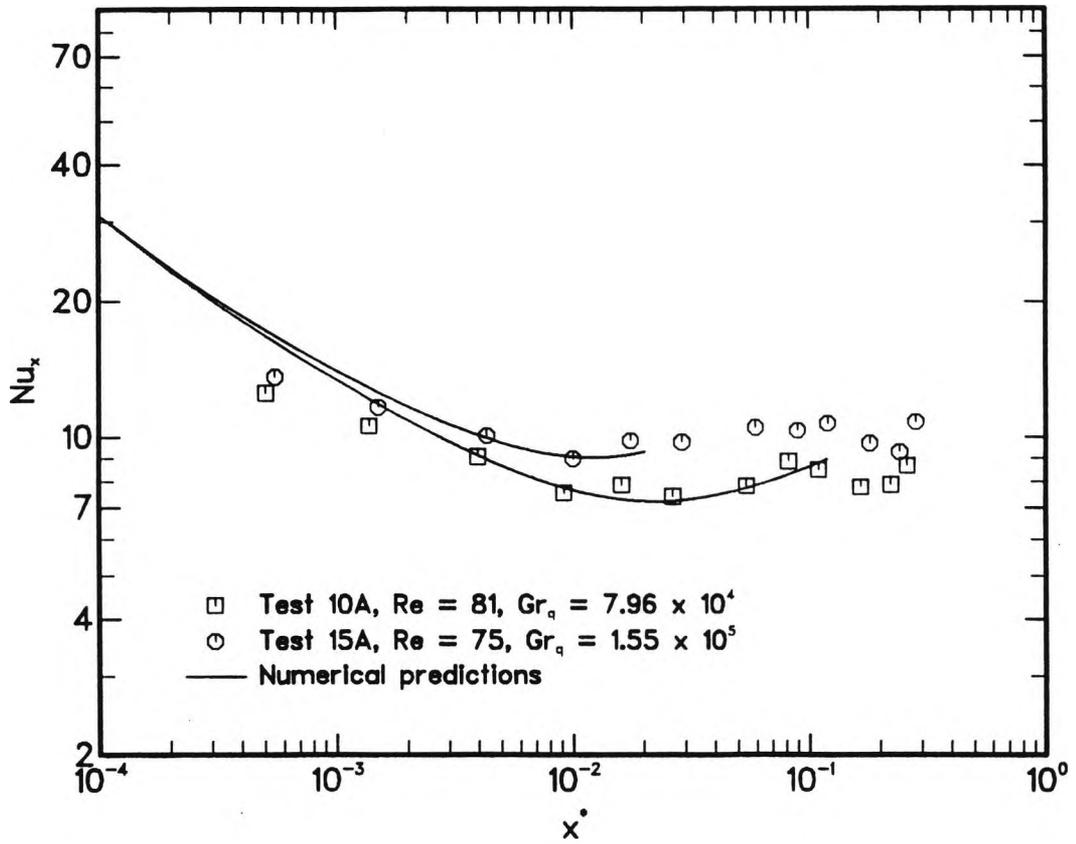
Figure 7.1   Comparison of predicted and experimental Nusselt numbers for two values of Grashof number, (Re = 75 − 81).
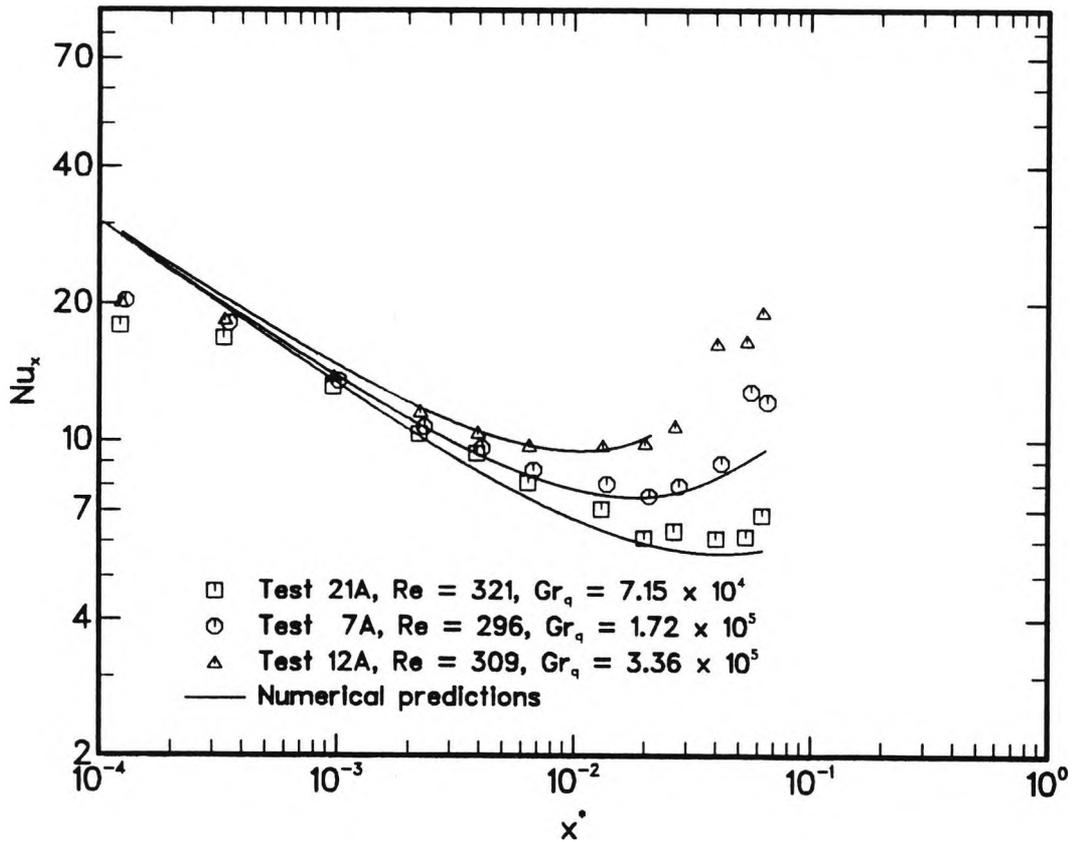
Figure 7.2   Comparison of predicted and experimental Nusselt numbers at three values of Grashof number, (Re = 296 − 321).

was predicted in both cases: at $x/d = 73.5$ for $Gr_q = 7.96 \times 10^4$ (Test 10A) and at $x/d = 11.5$ for $Gr_q = 1.55 \times 10^5$ (Test 15A). The corresponding values of the buoyancy parameter Gr_q/Re for these two tests were 980 and 2069 respectively. For the conditions considered in Figures 7.2 and 7.3 flow reversals were only found for the two highest Grashof numbers in each case. No flow reversals were predicted within the heated tube for the conditions considered in Figure 7.4. The axial positions of the predicted flow reversals for the cases illustrated in Figures 7.1 – 7.3 are summarised in Table 7.1, where the results are arranged in order of increasing values of Gr_q/Re. All the dimensionless groups in Table 7.1 are evaluated at the inlet bulk temperature T_{b_0}, although the same order is preserved when either T_{b_m} or T_{f_m} is used.

Table 7.1   Predicted axial distances to flow reversal for conditions corresponding to specific experiments.

Test No.	Re	Gr_q	Gr_q/Re	$(x/d)_{flow\ reversal}$
7A	296	1.72×10^5	581	157.0
6A	609	3.78×10^5	620	134.5
10A	81.2	7.96×10^4	980	73.5
12A	309	3.36×10^5	1090	54.0
25A	687	1.03×10^6	1500	69.0
15A	74.9	1.55×10^5	2070	11.5

In common with previous workers (Sherwin and Wallis, 1970; Ogunba, (1972); Collins, 1978; El–Shaarawi and Sarhan, 1980; Aung and Worku, 1986a), it was found that marching computations of combined convection duct flows could be continued for some distance beyond the onset of flow reversal before becoming unstable. However, the Nu_x versus x^* predictions shown in Figures 7.1 – 7.4 are truncated at the axial position where negative values of the axial velocity first appeared.
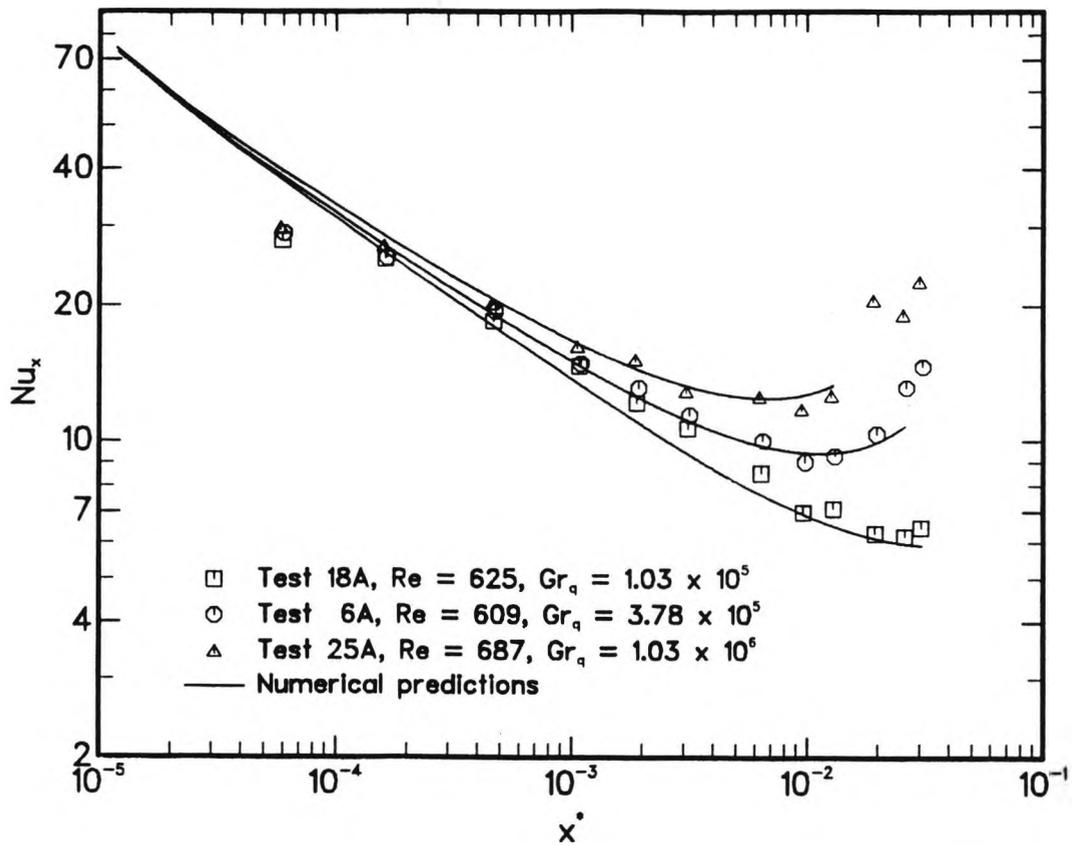
Figure 7.3 Comparison of predicted and experimental Nusselt numbers at three values of Grashof number, (Re = 609 − 687).
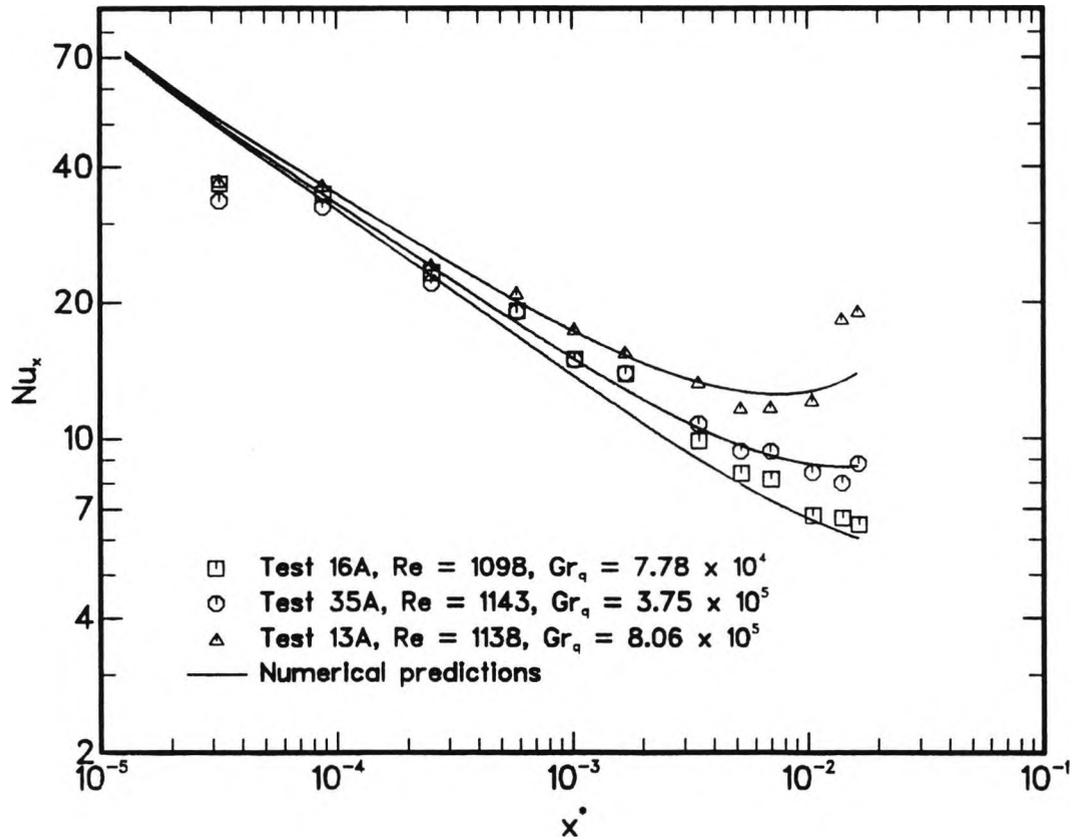
Figure 7.4 Comparison of predicted and experimental Nusselt numbers at three values of Grashof number, (Re = 1098 − 1143).

Considering the comparisons shown in Figures 7.1 – 7.4 collectively, the numerical solutions show pleasing agreement with respect to both the magnitudes and the trends found experimentally. In each figure, for only a slight variation in the Reynolds number, the predicted local Nusselt numbers at any axial location demonstrate a consistent increase for a progressively increasing buoyancy effect. All the predicted curves exhibit an initial decrease in Nu_x with x^*, although the decline is less rapid than for pure forced convection with constant properties. This departure is as expected for solutions including the effects of the viscosity and density variations of water with temperature. In all cases other than Test 16A (Figure 7.4) and Test 18A (Figure 7.3), the predicted Nu_x versus x^* variation falls to a minimum and then rises until either the end of the heated tube or a flow reversal is encountered. The axial positions of the predicted Nu_x minima are in reasonable agreement with the experimental results and move closer to the start of heating as Gr_q increases for a constant Reynolds number.

The marked overprediction of the experimental Nu_x results at the two measurement positions located within one tube diameter of the start of heating ($x/d = 0.31$ and $x/d = 0.85$) deserves comment. Similar differences noted by Shumway and McEligot (1971) for laminar gas flow in a resistively heated tube were attributed to upstream heating caused by axial wall conduction and radiation. Barozzi et al (1982, 1984) also found that numerically predicted Nusselt numbers exceeded their experimental data near to the start of a simultaneously developing flow of water in a vertical tube subjected to a uniform heat flux distribution. They hypothesised that the lower values of Nu_x found in practice were caused by a vena contracta formed immediately downstream of the sharp—edged tube entry used in their experiment. This seems a less plausible explanation for the present experimental set—up, where a rounded tube entry followed by a parallel section 2.5 tube diameters long preceeded the start of heating. Although the presence of a separated flow region cannot be entirely discounted without further evidence, the influence of axial conduction seems to be

a more likely reason for the deviations seen in this work for x/d < 1.0. A brief introduction to the topic of finite axial wall conduction is given in Section 5.4.3.

Axial conduction causes upstream heating of the tube wall, which preheats the fluid above the inlet bulk temperature in the region for x ≤ 0. This preheating is of course achieved at the expense of maintaining a uniform heat flux immediately downstream of the x = 0 position. As clearly shown by the numerical studies of Faghri and Sparrow (1980) and Cotton and Jackson (1985), the effective upstream shift in the origin of thermal development due to axial conduction results in a significant initial decrease in the local Nusselt number in the directly heated section. This is consistent with the deviations seen in Figures 7.1 − 7.4, thus tending to confirm the preferred explanation given here.

The above discussion highlights the difficulty of achieving a strict UHF thermal boundary condition experimentally, pointing to differences between the conditions assumed in making the predictions and those obtaining in the physical experiment. As already noted in Section 6.2, no corrections were made for axial wall conduction in the experimental local Nusselt numbers, which are based on an averaged wall heat flux and assume a linear rise in fluid bulk temperature between x = 0 and x = L. Should any adjustments have been made to the experimental results to correct the local bulk temperatures and heat fluxes for the effects of axial conduction then corresponding modification of the theoretical model would have been necessary in order to make a valid comparison. The effects of axial wall conduction are further discussed in Section 7.1.2.

It is probable that the accuracy of the experimental Nu_x results evaluated for the furthest downstream position (thermocouple position 12), located approximately 1/3 of a tube diameter from the end of the heated section, is also impaired by axial conduction because of heat loss through the adjacent power connection flange.

Where the predictions extend sufficiently far downstream of the minimum Nu_x position to allow comparison with the experimental data, a divergence is noted at higher Grashof numbers, with the latter achieving significantly larger values near to the end of the heated tube. This is most clearly illustrated by Tests 6A, 7A and 13A. Barozzi et al (1984) noticed a similar "tail–up" behaviour with very high experimental Nu_x, relating this to transition from laminar flow brought about by instability of the buoyancy–distorted axial velocity profile. In an earlier study Kemeny and Somers (1962) reported increases in local heat transfer coefficients for combined convection flows of water and transformer oil (up to 30% in the latter case) under conditions referred to as nonlaminar, evidenced by wall temperature variations and fluid temperature fluctuations. These nonlaminar conditions were reported for Reynolds numbers in excess of 200 in the case of water and down to below 10 for the oil. The large wall temperature fluctuations and the sharply increased local Nusselt numbers found towards the end of the test section in this work are qualitatively consistent with the findings of the previous researchers mentioned above. A fuller discussion of the wall temperature fluctuations is presented in Section 7.1.2.

For the low Reynolds number (Re = 75 and 81) test results shown in Figure 7.1, the experimental numbers follow a markedly different pattern downstream of the minimum Nu_x position; showing a limited increase to a second turning point then decreasing over the remainder of the heated length. It should be noted that this description disregards the higher experimental Nu_x values displayed for the measurement position closest to the end of the heated tube (x/d =159.3), which are considered suspect for the reasons given earlier.

7.1.2 Wall Temperature Comparisons

For a given uniform heat flux boundary condition, determination of the resulting wall temperature distribution is of interest from an engineering viewpoint.

A sample comparison of predicted and measured wall temperatures is provided in Figures 7.5(a)–(c) covering three values of the Grashof number for an approximately constant inlet Reynolds number (Re $= 609 - 687$). Flow reversals were predicted for the intermediate and highest values of the Grashof number and the marching solutions presented are truncated accordingly: at $x/d = 134.5$ for Gr_q $= 3.78 \times 10^6$ and at $x/d = 69$ for $Gr_q = 1.03 \times 10^6$ (inlet bulk properties).

The level of agreement between predicted and experimental wall temperature profiles in Figures 7.5(a)–(c) appears satisfactory, especially in view of the uncertainties attaching to the measured values; notably due to under–sampling of the fluctuating thermocouple signals. However, it should be borne in mind that, regardless of the method of presentation (i.e. linear or logarithmic), the ratio of the predicted and experimental wall–to–bulk temperature differences is exactly equal to the inverse ratio of the corresponding Nusselt numbers. For example, the overprediction of local Nusselt numbers at $x/d = 0.31$ and $x/d = 0.85$, seen in Figures $7.1 - 7.4$, results directly from an underprediction of the wall temperatures at these axial positions. Such differences are present in Figures 7.5(a)–(c) but cannot be easily detected because of the horizontal scale. In the predicted variations the tube wall temperature falls steeply to the inlet bulk temperature at $x = 0$. In contrast, scrutiny of the temperatures recorded for the lower power connection flange indicates that the tube wall temperature at $x = 0$ was invariably higher (by $0.5 - 5.7°C$ depending on the heat flux) than the measured inlet bulk temperature of the water. This is taken as direct confirmation of axial conduction from the heated tube as suggested in Section 7.1.1. Since the power connection flange was of copper and 10 mm thick it is safe to assume that it achieved an approximately uniform temperature. This would have caused preheating of the water for almost one diameter upstream of the start of the directly heated section, giving a bulk temperature at $x = 0$ somewhat higher than the measured inlet temperature T_{b_0}. In the experimental data reduction, no account was taken of this temperature rise or of the reduced heat flux in the region immediately downstream
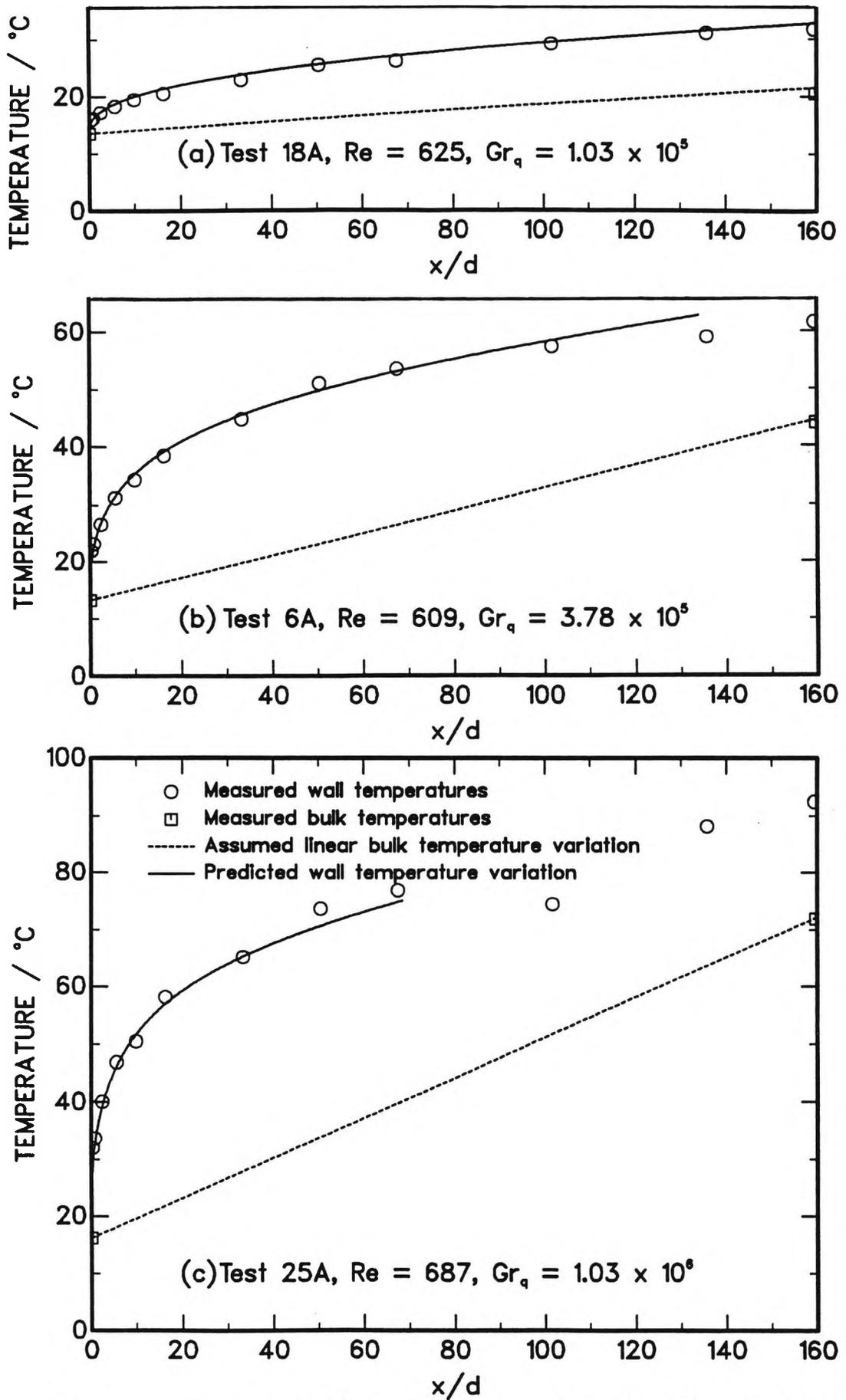
Figure 7.5   Comparison of predicted and measured wall temperature distributions, (Re = 609 − 687). (a) $Gr_q = 1.03 \times 10^5$, (b) $Gr_q = 3.78 \times 10^5$, (c) $Gr_q = 1.03 \times 10^6$.

of the start of heating arising from axial wall conduction. However, it is pointed out that these two effects contributed errors of opposite sign in the evaluation of local Nusselt number. In future work, it is intended to make modifications to the computer program to permit variable wall temperature boundary conditions to be specified. Measured wall temperatures could then be used as input data, thereby ensuring that the conditions assumed in the predictions are consistent with the experiments. For full comparability, however, correction of the local bulk temperature and heat flux values will be necessary in determining the experimental Nu_x values.

In Figures 7.5(b) and (c) the difference between the measured wall temperature and the fluid bulk temperature (i.e the local temperature driving force) undergoes a marked reduction in the downstream half of the test section, reflected by the higher downstream Nu_x values seen in Figure 7.3. From a perusal of Figures 7.5(b) and (c), and other experimental wall temperature data presented in Figures 6.4 – 6.6, it can be deduced that for the Reynolds numbers where a reduction in the wall–to–bulk temperature difference is apparent, this effect becomes more dramatic with increase of Gr_q. Moreover, the reduction appears to coincide with a portion of the tube where strong wall temperature fluctuations, exemplified in Figure 6.14, were evident in some tests. The magnitude of the temperature fluctuations and the length of the affected zone both showed a general tendency to increase with Gr_q. When the fluctuations were sufficiently large the exit bulk temperature also varied, as shown in Figure 6.15. It is surmised that associated fluid fluctuations were responsible for enhancing the heat transfer and hence the wall cooling. Where the predictions extend into the downstream region affected by strong temperature fluctuations they tend to overestimate the measured wall temperatures. This should not be surprising, however, as the predictive model assumes steady laminar flow and therefore cannot represent the flow and temperature fluctuations.

Wall temperature fluctuations were also reported by Hallman (1961) who employed a thin–walled resistively heated tube similar to that used in this work. It was suggested that these temperature fluctuations were caused by transition from laminar flow. Hallman (1961) also reported an unexplained dip in his measured wall temperature profiles around $x/d = 95$ for heating of water under upflow conditions at Peclet numbers of 1500 or greater. Barozzi et al (1984) explained the high downstream Nu_x values found in their experiments in terms of transition, but made no mention of wall temperature fluctuations. A relatively thick–walled copper pipe wrapped by a resistance heating wire was used in this latter study, however, and it seems probable that fluid fluctuations occurred, but were not apparent because potential wall temperature fluctuations were damped by the heat capacity of the tube wall.

Recalling that the experimental values shown in the figures are each based on an average of 20 readings taken at 15 s intervals, we can obtain a rough idea of the magnitude of the downstream wall temperature fluctuations from the sample standard deviations calculated during the data acquisition process. For Tests 6A and 25A, considered in Figures 7.5(b) and (c) respectively, large fluctuations were noted for $x/d > 100$. The maximum standard deviations found for these tests were $3.09°C$ (at $x/d = 135.8$) and $4.32°C$ (at $x/d = 101.7$) respectively. For the lower Grashof number test at this same flow rate, Test 18A shown in Figure 7.5(a), much smaller wall temperature fluctuations ($\sigma < 0.11°C$) were obtained at these downstream axial positions. This is qualitatively consistent with the smaller degree of axial velocity profile distortion predicted in this case.

The peak value of the fluctuations would of course be larger than the sample standard deviation. Confirmation of this point can be obtained by referring to the transient records given for $Re = 824$ and $Gr_q = 1.06 \times 10^6$ in Figure 6.14. The values of σ shown in Figure 6.14 are presumably very accurate measures of the fluctuations since they are based on samples of 241 readings (compared to the 20

readings used in the main test series). A further point to consider in judging the importance of the wall temperature fluctuations is their magnitude relative to the local wall–to–bulk temperature difference.

Mention should be made that some wall temperature fluctuation could be detected at most axial positions along the heated tube wall and under virtually all test conditions, even at the lowest Reynolds numbers. This attests to the sensitivity of the measurement technique. The inlet Reynolds number in Tests 10A and 15A was approximately 80 which would be expected to lead to a strictly parallel laminar flow under isothermal conditions. However, a strong influence of buoyancy was experienced in both these tests and the corresponding numerical solutions indicate that flow reversal was expected to occur within the lower half of the tube length (see Figure 7.1). The development of a point of inflexion in the inverting axial velocity profile is known to destabilize the flow, favouring the growth of fluctuations which lead eventually to transition from laminar flow.

An interesting phenomenon, not mentioned by previous workers, was observed with respect to the wall temperature fluctuations measured on the lower part of the heated tube. With the exception of the tests at the lowest Reynolds numbers, moderate wall temperature fluctuations, which increased in magnitude with both Gr_q and Re, were noted at axial positions on the lower one–third of the heated test section. Further downstream the magnitude of fluctuations decreased before increasing sharply in the latter half of the tube as described previously. The reason for this apparent decay of fluctuations, clearly demonstrated in Figure 6.14, is not known. One possible explanation is that these fluctuations were caused by some inlet disturbance effect.

7.2 Comparison of Experimental Data with Published Correlations

In this section experimental data collected in this study are compared with existing correlations for predicting the flow regime and the Nusselt number. In view of the limited data available there is no intention to suggest new correlations.

7.2.1 Metais and Eckert (1964) Convection Regime Diagram

Nearly 30 years ago, Metais and Eckert (1964) contributed a short paper summarising their work to establish tentative limits classifying the various regimes of laminar and turbulent convection encountered with internal flows. This information, which has subsequently been reprinted in numerous heat transfer textbooks, was presented in the form of convection regime maps for vertical and horizontal tubes. A portion of the original diagram for vertical tubes, which was based mainly on experimental data, is redrawn in Figure 7.6.
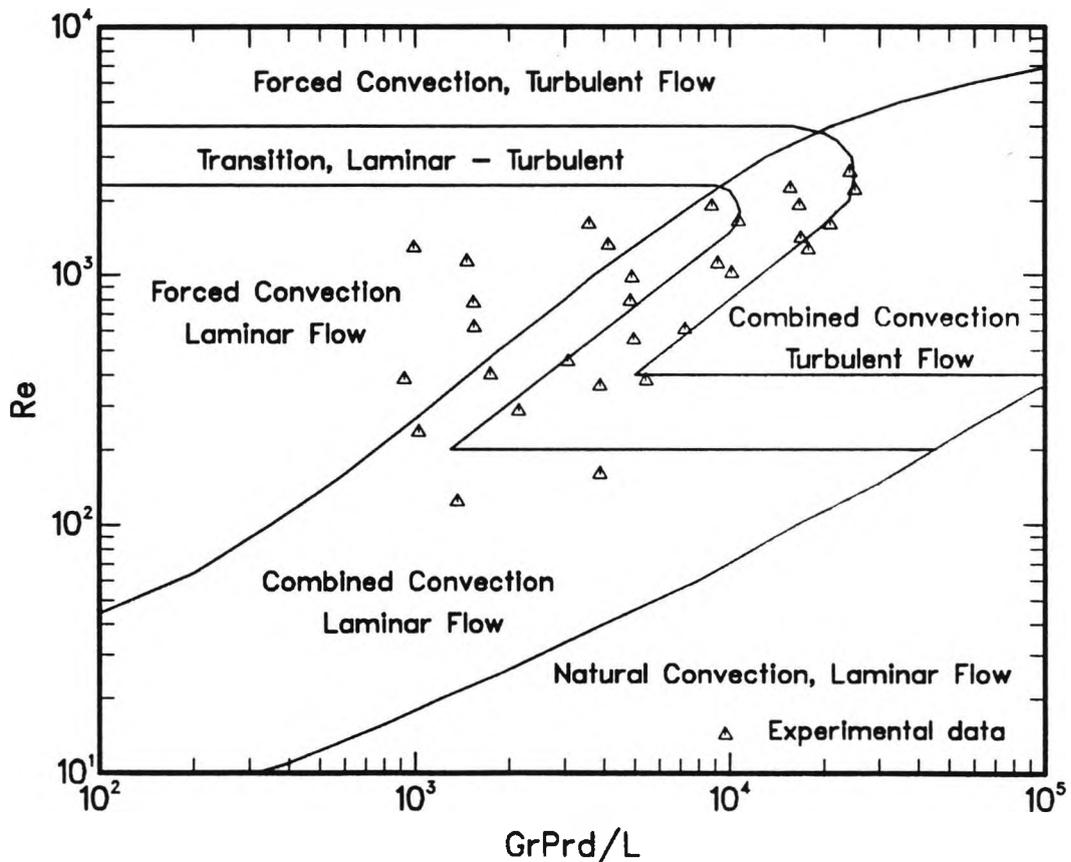
Figure 7.6   Comparison of experimental data with Metais and Eckert (1964) convection regime diagram for vertical tubes.
(mean film properties)

The combined convection regime is defined such that the heat transfer deviates by 10% or more from that for pure forced convection or pure natural convection. The coordinates used in Figure 7.6, Re versus GrPrd/L, were claimed by Metais and Eckert (1964) to give the best correlation of the available information which embraced both assisting and opposing combined convection situations and UHF as well as UWT boundary conditions. To the present author's knowledge the limits shown on the Metais and Eckert (1964) diagram have not been reviewed in the light of more more recently obtained data. Barozzi et al (1984) found the diagram to be unreliable in estimating the effect of natural convection on laminar forced convection for water flowing upward in a uniformly heated vertical tube.

The points plotted on Figure 7.6 show the experimental data set (Tests 6A − 35A) obtained in the present work. The Grashof number used in the product plotted on the abscissa is defined as $Gr = g\beta\rho^2 d^3(T_{w_m} - T_{b_m})/\mu^2$, where T_{w_m} is the average tube wall temperature (approximated by trapezoidal integration of the measured values) and T_{b_m} is the arithmetic mean of the inlet and exit bulk temperatures. It should be noted that the positions of the plotted points are very sensitive to the choice of reference temperature used for the fluid properties. No guidance is given in the primary reference, although Aung (1987) states that the mean film temperature should be used. In Figure 7.6 all fluid properties have been evaluated at the average film temperature T_{f_m}, defined as the arithmetic mean of T_{w_m} and T_{b_m}[1]. The limits of applicability of Figure 7.6, given as $10^{-2} < Prd/L < 1$, are comfortably satisfied by the present data.

By closely examining Figure 7.6 it can be seen that the experimental data points lie along one of seven roughly parallel curves of small positive slope. These curves

---

[1]The use of a lower reference temperature causes a reduction in both Re and GrPrd/L for a viscous liquid. When the inlet bulk temperature was tried with the data for water collected in the present study the majority of the points lay in the laminar forced convection regime of the Metais and Eckert diagram (1964).

correspond to the seven different flow rates (approximately constant inlet Reynolds numbers) covered by the main test series. In order to assess the reliability of Figure 7.6 for estimating the convection regime, the experimental data and the corresponding numerical predictions have been briefly examined to reveal any evidence which might be used to verify the positions of the regime boundaries established by Metais and Eckert (1964).

The two lowest points plotted on Figure 7.6 are for the low Reynolds number tests (Tests 10A and 15A) and fall within the range of parameters for which laminar combined convection is expected to occur. This is in agreement with the evidence provided by the numerical predictions and the experimental data which indicate a strong influence of buoyancy for both tests. Infact, as shown in Table 6.1, the value of the buoyancy parameter Gr_q/Re for Test 15A was the highest for all tests. Furthermore, as shown in Figure 7.1, both tests exhibited a minimum Nu_x with flow reversal being subsequently predicted. Finally, the small wall temperature fluctuations observed in Tests 10A and 15A substantially confirm an absence of transition as predicted in Figure 7.6.

The predicted convection regime for the higher Reynolds number test conditions depends on the value of GrPrd/L. For the five highest flow rates, one and sometimes two of the points with the lowest values of GrPrd/L lie in the forced convection regime in Figure 7.6. Examination of the corresponding experimental Nu_x versus $x*$ variations, shown in full in Figures 6.7 − 6.13, suggests that such conditions occur where no clear minimum value of Nu_x is exhibited. For tests where the Nusselt number falls to a well defined minimum and then recovers at higher $x*$, indicating a stronger buoyancy effect and hence a larger value of GrPrd/L, the predicted convection regime is always combined convection. As GrPrd/L increases for a constant flow rate, transition is predicted to occur. Remarkably, the points falling within the transition region in Figure 7.6, correspond well with the tests for which a sharp increase in the magnitude of the

wall temperature fluctuations was observed along the upper half of the tube.

Despite the paucity of the data and the cursory nature of the methods employed in the above partial validation it is concluded that the Metais and Eckert (1964) diagram remains a useful tool for preliminary estimation of the likely convection regime. Specifically, the positions of the boundaries between forced and combined laminar convection and at the onset of transition are found to be in reasonable agreement with observed behaviour.

7.2.2 Churchill (1983) Nusselt Number Correlation

Churchill (1983) recommended the following correlating equation for predicting fully—developed Nusselt numbers, denoted simply by Nu below, for laminar assisting convection in a uniformly heated vertical tube:

$$Nu^6 = Nu_N^6 + Nu_F^6 \qquad (7.1)$$

In equation (7.1), Nu_N and Nu_F are the contributions for pure natural convection and pure forced convection respectively. Churchill (1983) proposed that Nu_N should be found using

$$Nu_N = A\left[\frac{Gr_q}{Re}\right]^B \qquad (7.2)$$

with $A = 1.2$ and $B = 0.25$. At the forced convection limit the following familiar constant property result was taken for Nu_F:

$$Nu_F = 4.364 \qquad (7.3)$$

Equation (7.1) and its components, equations (7.2) and (7.3), are shown in Figure 7.7.
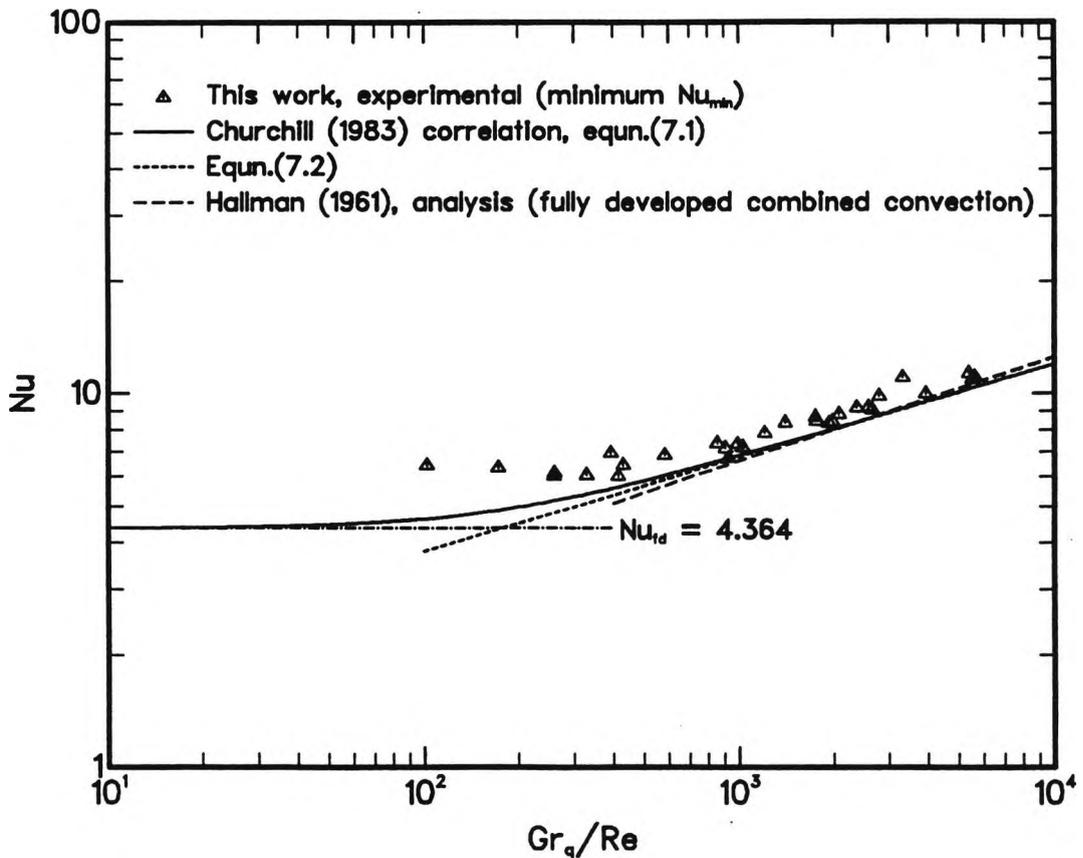
Figure 7.7 Comparison of experimental Nusselt numbers with Churchill (1983) correlation. (local film properties)

Equation (7.1) gives predictions in good agreement with the experimental data obtained for upflow of water by Hallman (1961). Hallman's (1956) analysis of combined laminar convection in a uniformly heated vertical tube, made for fully-developed conditions and constant properties, gives a line of slightly greater slope than equation (7.1). For $400 \leq Gr_q/Re \leq 40000$, Hallman (1961) gave an approximation for his earlier analysis, also plotted in Figure 7.7, which is of the same form as equation (7.2), but with A = 0.95 and B = 0.28. [Slightly different values were given in the earlier analytical paper.] Hallman (1961) found that beyond the thermal entrance region his experimental Nusselt numbers approached the fully-developed analytical predictions (Hallman, 1956) if all properties were evaluated at the local film temperature. This agreement was interpreted as establishing the validity of a "locally fully-developed" concept. Data obtained under conditions where fluctuations were observed were not considered. Hallman (1961) presented some typical experimental Nu_x versus x^* results (his Runs U14

and U24) in his report which indicate that "locally fully–developed" conditions were achieved downstream of the minimum Nu_x position. His experimental data also show an initial decrease in the length of the thermal entrance region L_{th}^* as Gr_q/Re increased, followed by a rise in L_{th}^* at higher values of Gr_q/Re.

Experimental data from the present study are compared with equation (7.1) in Figure 7.7. Each data point in Figure 7.7 corresponds to a different test condition and all tests (Tests 6A − 35A) are represented. The coordinates for each point are taken as the values of Nu_x and Gr_q/Re at the measurement position where the lowest experimental Nu_x was evaluated, irrespective of whether the variation of Nu_x with x^* exhibited a well–defined minimum followed by a rise downstream. In other words, the values of Nu_x and Gr_q/Re for any data point correspond either to an intermediate measurement position along the tube where a minimum Nu_x was found or, in the case of a test where Nu_x decreased throughout, the values at a measurement position near the exit. Consequently, the x/d values corresponding to the data shown in Figure 7.7 range from 5.65 to 159.3. It must be admitted that the method of data selection just described was used in the absence of proof that fully–developed conditions existed at the points chosen. Initially, experimental data from this study were compared to equation (7.1) using values of Nu and Gr_q/Re taken at the same axial position (x/d = 134.5) for all tests. This resulted in a large scatter, mainly due to the inclusion of the high Nu_x values found at positions where strong wall temperature fluctuations were evident.

The data points in Figure 7.7 all lie above the line of equation (7.1) with deviations ranging from + 2.5% to + 42%. Exactly half the data set are within 10% of this line. For $Gr_q/Re > 400$, the experimentally determined Nusselt numbers fall within a band 2.5% to 20% above the values predicted by equation (7.1) but follow broadly the same trend. For $Gr_q/Re < 400$ the comparison deteriorates markedly with the data deviating from equation (7.1) by between 16.8% and 42%. The six data points lying in the latter range are for the tests with

the lowest heat flux (or the two lowest heat fluxes in the case of Re $\approx$ 1100) at the five highest flow rates. Under these conditions the influence of buoyancy was relatively weak, the thermal and hydrodynamic development becoming more characteristic of forced convection with increase in Reynolds number. This can be confirmed by scrutinising the relevant experimental Nu_x versus x^* variations in Figures 6.9 − 6.13 which show that Nu_x declines throughout (assuming that the final point at $x/d = 159.3$ is considered suspect and ignored). These figures also show that the value of x^* at the end of the heated section was less than 0.04, in all cases except for Figure 6.9. This is less than the length required for thermal development of a constant−property, fully−developed flow in a uniformly heated tube, given as $L_{th}^* = 0.043$ by Shah and London (1978). Bearing in mind that a longer development length is needed under simultaneously developing conditions, as used in the experiments, and that any reduction due to heating would be small at low Grashof number, it would appear that the heated test section was too short for a "locally fully−developed" condition to be reached in these tests. This would account for the very large discrepancies seen in Figure 7.7 for $Gr_q/Re < 400$.

Following Hallman (1961), all fluid properties used to evaluate Nu and Gr_q/Re in Figure 7.7 were taken at the local film temperature T_{f_x}. In fact, the choice of reference temperature has only a marginal effect on Nu for water, because the thermal conductivity variation is only slight (see Figure B.2). On the other hand, Gr_q/Re depends on $1/\mu$ and thus the use of a lower reference temperature (e.g. T_{b_x}) would cause the deviations between the experimental data and equation (7.1) to increase.

CHAPTER 8

CONCLUSIONS

8.1 Analysis and Computational Work

The theoretical aspects of this work were aimed at devising a unified predictive method for thermally and hydrodynamically developing combined natural and forced laminar convection in vertical ducts of circular, concentric annular and parallel plate cross–section. This has been successfully achieved. The computational scheme is based on a fully–implicit finite–difference representation of the parabolic flow equations written in generalised axisymmetric form. Numerical solution is effected by a marching procedure in the main flow direction, thus prohibiting consideration of situations with flow reversal.

The numerical procedure developed has been embodied in a flexible computer program which is capable of handling both buoyancy–aided and buoyancy–opposed flows. Either a uniform wall temperature or a uniform heat flux boundary condition can be specified at any duct wall and any inlet flow condition can be catered for, ranging from a uniform to a fully–developed flow. The effects of fluid property variations with temperature and viscous dissipation can be taken into account if required.

Two ideas proposed by Ogunba (1972) are utilised in the solution of the velocity–pressure problem in which pressure is treated as an unknown dependent variable. Firstly, a piecewise treatment is employed for the mass continuity integral and, secondly, the requirement of a zero transverse pressure gradient is made explicit by equating pressures at all grid points on the same transverse grid line. In this work, the first of these techniques has been extended to the treatment of the integral energy equation which is optionally used in the solution of the temperature problem and, as suggested by Collins (1975), enforces global energy conservation. The above techniques permit the systems of algebraic equations

arising from the finite–difference treatment of the governing equations to be assembled in band matrix form. By this means, an advantage in computational economy, both in terms of storage and execution time, is achieved over comparable methods developed earlier which use conventional Gaussian elimination to solve sparsely–populated square matrix systems.

The accuracy of the predictive method has been demonstrated for the following two constant–property, pure forced convection problems: (i) hydrodynamic development in a circular tube and (ii) thermal development under uniform wall temperature conditions in a circular tube (Graetz problem).

In addition, heat transfer predictions have been made for laminar, buoyancy–aided combined convection of water in upward flow through a vertical circular tube with a uniform heat flux imposed at the wall. These predictions take account of thermophysical property variations with temperature and compare favourably with the experimental data collected in this research.

8.2 Experimental Work

The original objective of the experimental study was to provide data on laminar combined convection for validation of the computational method. A test rig, incorporating a uniformly heated vertical tube, has been constructed and instrumentation is provided for heat transfer measurements. A limited amount of experimental data has been obtained for heating of water in upflow.

For a fixed Reynolds number, the data indicate progressively higher local Nusselt numbers with increase in the heat flux based Grashof number. Such improvement in heat transfer is more evident at larger axial distances due to the cumulative effect of buoyancy. For a sufficiently strong buoyancy effect the Nu_x versus x^* distribution exhibits a minimum. The axial position of this Nu_x minimum moves closer to the start of heating as Grashof number is increased for a

constant Reynolds number.

Comparison between experimentally determined local Nusselt numbers and numerical predictions generally demonstrates convincing agreement, although assumptions involved in the latter necessarily restrict comparison to the unidirectional flow region (i.e. no flow reversals). Such deviations as do occur are consistent with axial wall conduction effects near the tube entrance and further downstream with transition from laminar flow resulting from instability of the buoyancy–distorted axial velocity profile.

Transitional flow is detected by wall temperature fluctuations and results in a local improvement in Nusselt number. A technique has been established for recording local wall temperature fluctuations and some preliminary measurements have been made. The transient data, of which only samples are presented, contain evidence of asymmetry in the heated flow. It is concluded that the data are worthy of more detailed examination; possibly using time series analysis techniques, in order to reveal the possible occurrence of periodic structures. This approach could be complemented by predictive studies involving the use of computer codes for time–dependent, three–dimensional flows with heat transfer.

The experimental data have been compared with the Metais and Eckert (1964) flow regime map for combined convection in vertical tubes and the Nusselt number correlation proposed by Churchill (1983). Although the comparisons were made using the limited data available from the experimental study, they indicate that these correlations remain valid for obtaining initial estimates.

8.3 Proposals for Future Work

It is intended to continue with both computational and experimental aspects of this research. Some areas under consideration for future investigation are given below:

i) Predictive work using existing program

The new computer program developed is very versatile, although its potential has, so far, only been exploited for circular tube flows. The studies reported in this thesis are for forced convection with constant fluid properties and aiding combined convection with variable fluid properties under UHF conditions. Further numerical studies could consider:

- forced, combined and natural convection in concentric annuli or between parallel plates;

- combined convection situations with opposing natural and forced convection contributions;

- mixed (UHF/UWT) thermal boundary conditions;

- effect on heat transfer of partial hydrodynamic development upstream of the start of heating or cooling.

ii) Further development of computer program

It is considered that the following changes, which could be made relatively easily, would enhance accuracy and flexibility respectively:

- to incorporate the necessary changes which would permit the use of a variable finite—difference grid spacing in the transverse coordinate direction;

- to incorporate options for specifying thermal boundary conditions where either the wall temperature or the wall—fluid heat flux varies with axial distance;

iii) Modification of experimental apparatus

In view of the experimental results already obtained the following modifications are considered desirable before further measurements are made:

- attachment of additional thermocouples in order to improve the resolution of the axial and circumferential wall temperature variations;

- reduction in the size of the upstream power connection flange to minimise, as far as possible, the axial heat conduction effect;

- modifications to the flow circuit to permit recirculation of the fluid and to allow experiments to be conducted for both downward as well as upward flow.

iv) Further experimental studies

At present the experimental data base for combined convection in a uniformly heated vertical tube is somewhat limited. Further tests covering a wider range of parameters would be extremely helpful in establishing better design correlations. Additional data for high Prandtl number fluids with strongly temperature dependent properties would also provide a better test for the predictive model.

The appearance of wall temperature fluctuations is associated with the transition from laminar flow caused by the growth of instabilities in the buoyancy distorted axial velocity profile. As seen in the present work, the onset of strong wall temperature fluctuations has a marked effect in increasing the heat transfer for an upward heated flow and also limits the usefulness of predictions based on the assumption of steady laminar flow. Additional experimental work in conjunction with predictive studies, is required to define the transition boundaries, with regard to flow rate, heat flux and axial position. The transient recording technique described in this thesis shows promise in this respect.

REFERENCES

AGGARWALA, B.D. and IQBAL, M. (1969). On Limiting Nusselt Numbers from Membrane Analogy for Combined Free and Forced Convection Through Vertical Ducts, International Journal of Heat and Mass Transfer, vol. 12, pp. 737–748.

AIHARA, T. (1973). Effects of Inlet Boundary–Conditions on Numerical Solutions of Free Convection Between Vertical Parallel Plates, Reports of the Institute of High Speed Mechanics, Tohoku University, Sendai, Japan, vol. 28, pp. 1–27.

ALLEN, P.H.G. and FINN, A.H. (1970). Profile Development With Mixed Convection in a High Prandtl Number Fluid, ASME Journal of Heat Transfer, vol. 92, pp. 299–304.

ANDERSON, D.A., TANNEHILL, J.C. and PLETCHER, R.H. (1984). Computational Fluid Mechanics and Heat Transfer, Hemisphere.

AUNG, W. (1987). Mixed Convection in Internal Flow, in Handbook of Single–Phase Convective Heat Transfer, (eds. S.Kakac, R.K.Shah and W.Aung), Chapter 15, John Wiley.

AUNG, W., FLETCHER, L.S. and SERNAS, V. (1972). Developing Laminar Free Convection Between Vertical Flat Plates with Asymmetric Heating, International Journal of Heat and Mass Transfer, vol. 15, pp. 2293–2308.

AUNG, W. MOGHADAM, H.E. and TSOU, F.K. (1991). Simultaneous Hydrodynamic and Thermal Development in Mixed Convection in a Vertical Annulus With Fluid Property Variations, ASME Journal of Heat Transfer, vol. 113, pp. 926–931.

AUNG, W. and WORKU, G. (1986a). Developing Flow and Flow Reversal in a Vertical Channel With Asymmetric Wall Temperatures, <u>ASME Journal of Heat Transfer</u>, vol. 108, pp. 299–304.

AUNG, W. and WORKU, G. (1986b). Theory of Fully Developed, Combined Convection, Including Flow Reversal, <u>ASME Journal of Heat Transfer</u>, vol. 108, pp. 485–488.

AUNG, W. and WORKU, G. (1987). Mixed Convection in Ducts With Asymmetric Wall Heat Fluxes, <u>ASME Journal of Heat Transfer</u>, vol. 109, pp. 947–951.

BAEK, B.J., PALASKI, D.A., ARMALY, B.F. and CHEN, T.S. (1990). Mixed Convection in an Asymmetrically Heated Vertical Parallel–Plate Duct Flow, <u>9th International Heat Transfer Conference</u>, Jerusalem, vol. 2, paper 4–MC–04, pp. 369–374.

BAROZZI, G.S., DUMAS, A. and COLLINS, M.W. (1984). Sharp Entry and Transition Effects for Laminar Combined Convection of Water in Vertical Tubes, <u>International Journal of Heat and Fluid Flow</u>, vol. 5, no. 4, pp. 235–241.

BAROZZI, G.S., DUMAS, A. and POMPOLI, R. (1982). The Influence of an Abrupt Convergence on Heat Transfer in Circular Ducts, <u>International Journal of Heat and Fluid Flow</u>, vol. 3, no. 1, pp. 45–54.

BARROW, H., PRASAD, A. and SHERWIN, K. (1974). Heat Transfer by Free Convection in Open Ended Vertical Ducts, <u>5th International Heat Transfer Conference</u>, Tokyo, vol. 3, paper NC 2.5, pp. 59–63.

BODOIA, J.R. (1959). The Finite Difference Analysis of Confined Viscous Flows, Ph.D. thesis, Carnegie Institute of Technology.

BODOIA, J.R. and OSTERLE, J.F. (1962). The Development of Free Convection Between Heated Vertical Plates, <u>ASME Journal of Heat Transfer</u>, vol. 84, pp. 40–44.

BRADLEY, D. and ENTWISTLE, A.G. (1965). Developed Laminar Flow Heat Transfer from Air for Variable Physical Properties, <u>International Journal of Heat and Mass Transfer</u>, vol. 8, pp. 621–638.

BRAUER, H., DYLAG, M. and KASZ, J. (1988). Heat Transfer by Combined Free and Forced Convection in Vertical Tubes, <u>Wärme– und Stoffübertragung</u>, vol. 23, pp. 61–68.

BROWN, C.K. and GAUVIN, W.H. (1965a). Combined Free and Forced Convection – I. Heat Transfer in Aiding Flow, <u>The Canadian Journal of Chemical Engineering</u>, vol. 43, pp. 306–312.

BROWN, C.K. and GAUVIN, W.H. (1965b). Combined Free and Forced Convection – II. Heat Transfer in Opposing Flow, <u>The Canadian Journal of Chemical Engineering</u>, vol. 43, pp. 313–318.

BROWN, W.G. (1960). Die Überlagerung von erzwungener und natürlicher Konvektion bei niedrigen Durchsätzen in einem lotrechten Rohr, <u>Forschung auf dem Gebiete des Ingenieurwesens</u>, vol. 26, VDI–Forschungsheft 480.

CEBICI, T. and BRADSHAW, P. (1984). <u>Physical and Computational Aspects of Convective Heat Transfer</u>, Springer–Verlag.

CEBICI, T., KHATTAB, A.A. and LAMONT, R. (1982). Combined Natural and Forced Convection in Vertical Ducts, 7th International Heat Transfer Conference, Munich, vol. 3, paper MC 1, pp. 419–424.

CHATO, J.C. (1969). Combined Free and Forced Convection Flows in Channels, in Advanced Heat Transfer, (ed. B.T.Chao), pp.439–459, University of Illinois Press.

CHENG, C.-H., KOU, H.-S. and HUANG, W.-H. (1990). Flow Reversal and Heat Transfer of Fully Developed Mixed Convection in Vertical Channels, AIAA Journal of Thermophysics and Heat Transfer, vol. 4, no. 3, pp. 375–383.

CHOW, L.C., HUSAIN, S.R. and CAMPO, A. (1984). Effects of Free Convection and Axial Conduction on Forced Convection Heat Transfer Inside a Vertical Channel at Low Peclet Number, ASME Journal of Heat Transfer, vol. 106, pp. 297–303.

CHURCHILL, S.W. (1983). Combined Free and Forced Convection in Channels, in Heat Exchanger Design Handbook, (eds. E.U.Schlünder et al), Section 2.5.10, Hemisphere.

COLLINS, M.W. (1972). Combined Convection in Vertical Tubes, Symposium on Heat and Mass Transfer by Combined Forced and Natural Convection, September 1971, paper C115/71, pp. 17–25, Institution of Mechanical Engineers.

COLLINS, M.W. (1975). An Analysis of Combined Natural and Forced Convection and Other Problems in Internal Laminar Flow, Ph.D. thesis, The City University, London.

COLLINS, M.W. (1978). Heat Transfer by Laminar Combined Convection in a Vertical Tube — Predictions for Water, <u>6th International Heat Transfer Conference</u>, Toronto, paper MC–5, pp. 25–30.

COLLINS, M.W. (1980). Finite–Difference Analysis for Developing Laminar Flow in Circular Tubes Applied to Forced and Combined Convection, <u>International Journal for Numerical Methods in Engineering</u>, vol. 15, pp. 381–404.

COLLINS, M.W., ALLEN, P.H.G. and SZPIRO, O. (1977). Computational Methods for Entry Length Heat Transfer by Combined Laminar Convection in Vertical Tubes, <u>Proceedings of the Institution of Mechanical Engineers</u>, vol. 191, part 2, pp.19–29.

COLLINS, M.W. and KEYNEJAD, M. (1983). Effects of Temperature–Dependence of Viscosity and Viscous Dissipation on Laminar Flow Heat Transfer in Circular Tubes, <u>International Journal of Heat and Fluid Flow</u>, vol. 4, No.1, pp.33–42.

CONLEY, N., LAWAL, A. and MUJUMDAR, A.S. (1985). An Assessment of the Accuracy of Numerical Solutions to the Graetz Problem, <u>International Communications in Heat and Mass Transfer</u>, vol. 12, pp. 209–218.

COTTON, M.A. and JACKSON, J.D. (1985). The Effect of Heat Conduction in a Tube Wall upon Forced Convection Heat Transfer in the Thermal Entry Region, <u>4th International Conference on Numerical Methods in Thermal Problems</u>, Swansea.

DALBERT, A.–M. (1982). Natural, Mixed and Forced Convection in a Vertical Channel With Asymmetric Uniform Heating, <u>7th International Heat Transfer Conference</u>, Munich, vol. 3, paper MC 4.

DALBERT, A.–M., PENOT, F. and PEUBE, J.–L. (1981). Convection Naturelle Laminaire dans un Canal Vertical Chauffe a Flux Constant, <u>International Journal of Heat and Mass Transfer</u>, vol. 24, pp. 1463–1473.

DEL GUIDICE, S., COMINI, G. and MIKHAILOV, M.D. (1978). Finite Element Analysis of Combined Free and Forced Convection, <u>International Journal of Heat and Mass Transfer</u>, vol. 21, pp. 1619–1621.

ECKERT, E.R.G. AND DIAGUILA, A.J. (1954). Convective Heat Transfer for Mixed, Free, and Forced Flow Through Tubes, <u>Transactions of the ASME</u>, vol. 76, pp. 497–504.

EFTHIMIADIS, A., and TODREAS, N.E. (1985). Generalized Formulation of the Fully–Developed Mixed Convection Flow Problem in Vertical Ducts, in <u>Fundamentals of Forced and Mixed Convection</u>, (eds. F.A.Kulacki and R.D.Boyd), ASME HTD–vol. 42, pp. 83–89.

EL–GENK, M.S., ZAKI, G.M., WILLIAMS, T.E. and PHILBIN, J.S. (1986). Experimental Heat Transfer Studies of Laminar and Transition Flows of Water in a Vertical Annulus, <u>International Communications in Heat and Mass Transfer</u>, vol.13, pp. 67–75.

EL–GENK, M.S. and RAO, D.V. (1989). Heat Transfer Experiments and Correlations for Low Reynolds Number Flows of Water in Vertical Annuli, <u>Heat Transfer Engineering</u>, vol. 10, no. 2, pp. 44–57.

EL–GENK, M.S. and RAO, D.V. (1990). Buoyancy Induced Instability of Laminar Flows in Vertical Annuli – I. Flow Visualization and Heat Transfer Experiments, International Journal of Heat and Mass Transfer, vol. 33, pp. 2145–2159.

EL–SHAARAWI, M.A.I. and SARHAN, A. (1980). Free Convection Effects on the Developing Laminar Flow in Vertical Concentric Annuli, ASME Journal of Heat Transfer, vol. 102, pp. 617–622.

FAGHRI, M. and SPARROW, E.M. (1980). Simultaneous Wall and Fluid Axial Conduction in Laminar Pipe–Flow Heat Transfer, ASME Journal of Heat Transfer, vol. 102, pp. 58–63.

FUKUI, K., NAKAJIMA, M., UEDA, H. and MIZUSHINA, T. (1982). Flow Instability and Transport Phenomena in Combined Free and Forced Convection Between Vertical Parallel Plates, Journal of Chemical Engineering of Japan, vol.15, no. 3, pp. 172–180.

GREENE, H.L. and SCHEELE, G.F. (1970). Effect of Fluid Viscosity on Combined Free Forced Convection Flow Phenomena in Vertical Pipes, AIChE Journal, vol. 16, no. 6, pp. 1039–1047.

HABCHI, S. and ACHARYA, S. (1986). Laminar Mixed Convection in a Symmetrically or Asymmetrically Heated Vertical Channel, Numerical Heat Transfer, vol. 9, pp. 605–618.

HALLMAN, T.M. (1956). Combined Forced and Free Laminar Heat Transfer in Vertical Tubes With Uniform Internal Heat Generation, Transactions of the ASME, vol.78, pp. 1831–1841.

HALLMAN, T.M. (1961). Experimental Study of Combined Forced and Free Laminar Convection in a Vertical Tube, NASA TN D – 1104.

HAMADAH, T.T. and WIRTZ, R.A. (1991). Analysis of Laminar Fully Developed Mixed Convection in a Vertical Channel With Opposing Buoyancy, <u>ASME Journal of Heat Transfer</u>, vol. 113, pp. 507–510.

HANRATTY, T.J., ROSEN, E.M. and KABEL, R.L. (1958), Effect of Heat Transfer on Flow Field at Low Reynolds Numbers in Vertical Tubes, <u>Industrial and Engineering Chemistry</u>, vol. 50, no.5, pp. 815–820.

HASHIMOTO, K., AKINO, N. and KAWAMURA, H. (1986), Combined Forced–Free Laminar Heat Transfer to a Highly Heated Gas in a Vertical Annulus, <u>International Journal of Heat and Mass Transfer</u>, vol. 29, no. 1, pp. 145–151.

HEGGS, P.J., INGHAM, D.B. and KEEN, D.J. (1988). Laminar Flow Combined Convection in Vertical Annuli, <u>2nd UK National Conference on Heat Transfer</u>, Glasgow, vol. 1, paper C142/88, pp. 371–383.

HEGGS, P.J., INGHAM, D.B. and KEEN, D.J. (1990). The Effects of Heat Conduction in the Wall on the Development of Recirculating Combined Convection Flows in Vertical Tubes, <u>International Journal of Heat and Mass Transfer</u>, vol. 33, pp. 517–528.

HORNBECK, R.W. (1973). Numerical Marching Techniques for Fluid Flows With Heat Transfer, NASA SP–297.

IANNELLO, V., SUH, K.Y. and TODREAS, N.E. (1988). Mixed Convection Friction Factors and Nusselt Numbers in Vertical Annular and Subchannel Geometries, International Journal of Heat and Mass Transfer, vol. 31, no. 10, pp. 2175–2189.

INGHAM, D.B., KEEN, D.J. and HEGGS, P.J. (1988a). Two Dimensional Combined Convection in Vertical Parallel Plate Ducts, Including Situations of Flow Reversal, International Journal for Numerical Methods in Engineering, vol. 26, pp. 1645–1664.

INGHAM, D.B., KEEN, D.J. and HEGGS, P.J. (1988b). Flows in Vertical Channels With Asymmetric Wall Temperatures and Including Situations where Reverse Flows Occur, ASME Journal of Heat Transfer, vol. 110, pp. 910–917.

IQBAL, M., AGGARWALA, B.D. and FOWLER, A.G. (1969). Laminar Combined Free and Forced Convection in Vertical Non–Circular Ducts Under Uniform Heat Flux, International Journal of Heat and Mass Transfer, vol. 12, pp. 1123–1139.

JACKSON, J.D., COTTON, M.A. and AXCELL, B.P. (1989). Studies of Mixed Convection in Vertical Tubes, International Journal of Heat and Fluid Flow, vol. 10, no. 1, pp. 2–15.

JACKSON, T.W., HARRISON, W.B. and BOTELER, W.C. (1958). Combined Free and Forced Convection in a Constant Temperature Vertical Tube, Transactions of the ASME, vol. 80, pp. 739–745.

JEGLIC, F.A., SWITZER, K.A. and LIENHARD, J.H. (1980). Surface Temperature Oscillations of Electrical Resistance Heaters Supplied With Alternating Current, ASME Journal of Heat Transfer, vol. 102, pp. 392–393.

JENNINGS, A. (1977). <u>Matrix Computation for Engineers and Scientists,</u> John Wiley & Sons.

JENSON, M.K. (1989). Simultaneously Developing Laminar Flow in an Isothermal Circular Tube , <u>International Communications in Heat and Mass Transfer,</u> vol. 16, pp. 811–820.

JOSHI, S.D. and BERGLES, A.E. (1978). Heat Transfer in Cooling Channels of Power Transformers, Iowa State University Engineering Research Institute, Annual Report ISU–ERI–AMES–78287, pp.7.1–7.15.

KASZ, J. (1990). Elliptic and Parabolic Approach to Flow Reversal in Thermogravitational Tube Flows, Unpublished paper, Technical University of Cracow, Poland.

KEMENY, G.A. and SOMERS, E.V. (1962). Combined Free and Forced Convective Flow in Vertical Circular Tubes – Experiments With Water and Oil, <u>ASME Journal of Heat Transfer,</u> vol. 84, pp. 339–346.

KIM, J.H. (1985). Analysis of Laminar Mixed Convection in Vertical Tube Annulus With Upward Flow, in <u>Fundamentals of Forced and Mixed Convection,</u> (eds. F.A.Kulacki and R.D.Boyd), ASME HTD–vol. 42, pp. 91–98.

LAWRENCE, W.T. and CHATO, J.C. (1966). Heat Transfer Effects on the Developing Laminar Flow Inside Vertical Tubes, <u>ASME Journal of Heat Transfer,</u> vol. 88, pp. 214–222.

LEWIS, J.S., COLLINS, M.W. and ALLEN, P.H.G. (1990). Flow Rate Predictions for a Thermosyphon Loop, 9th International Heat Transfer Conference, Jerusalem, vol. 2, paper 5—NC—12, pp. 549—554.

LILLEY, P.E. (1987). Thermophysical Properties, in Handbook of Single—Phase Convective Heat Transfer, (eds. S.Kakac, R.K.Shah and W.Aung), Chapter 22, John Wiley.

LU, P.C. (1960). Combined Free and Forced—Convection Heat—Generating Laminar Flow Inside Vertical Pipes With Circular Sector Cross Sections, ASME Journal of Heat Transfer, vol. 82, pp. 227—232.

MALIK, M.R. and PLETCHER, R.H. (1980). Calculation of Variable Property Heat Transfer in Ducts of Annular Cross Section, Numerical Heat Transfer, vol. 3, pp. 241—257.

MAITRA, D. and SUBBA—RAJU, K. (1975). Combined Free and Forced Convection Laminar Heat Transfer in a Vertical Annulus, ASME Journal of Heat Transfer, vol. 97, pp.135—137.

MARNER, W.J. and McMILLAN, H.K. (1970). Combined Free and Forced Laminar Convection in a Vertical Tube With Constant Wall Temperature, ASME Journal of Heat Transfer, vol. 92, pp. 559—562.

MARTINELLI, R.C. and BOELTER, L.M.K. (1942). The Analytical Prediction of Superposed Free and Forced Convection in a Vertical Pipe, University of California Publications in Engineering, vol. 5, no. 2, pp. 23—58.

MARTINELLI, R.C., SOUTHWELL, C.J., ALVES, G., CRAIG, H.L., WEINBERG, E.B., LANSING, N.F. and BOELTER, L.M.K. (1942). Heat Transfer and Pressure Drop for a Fluid Flowing in the Viscous Region Through a Vertical Pipe, Transactions of the American Institute of Chemical Engineers, vol. 38, pp. 493–530.

METAIS, B. and ECKERT, E.R.G. (1964). Forced, Mixed and Free Convection Regimes, ASME Journal of Heat Transfer, vol. 86, pp. 295–296.

MIYATAKE, O. and FUJII, T. (1972). Free Convective Heat Transfer Between Vertical Parallel Plates — One Plate Isothermally Heated and the Other Thermally Insulated, Heat Transfer — Japanese Research, vol. 1, part 3, pp. 30–38.

MOGHADAM, H. and AUNG, W. (1990). Numerical Method for Laminar Convection in Concentric Vertical Annular Duct With Variable Properties, Numerical Heat Transfer, Part A, vol. 18, pp. 3357–370.

MOGHADAM, H.E., AUNG, W., REISS, R., KIM, J.H. and AUNG, R.L. (1990). Buoyancy and Variable Property Effects in Laminar Aided Convection in a Vertical Annulus, 9th International Heat Transfer Conference, Jerusalem, vol. 2, paper 4–MC–07, pp. 387–391.

MORTON, B.R. (1960). Laminar Convection in Uniformly Heated Vertical Pipes, Journal of Fluid Mechanics, vol. 8, pp. 227–240.

MORTON, B.R., INGHAM, D.B., KEEN, D.J. and HEGGS, P.J. (1989). Recirculating Combined Convection in Vertical Pipe Flow, ASME Journal of Heat Transfer, vol. 111, pp. 106–113.

OGUNBA, V.O. (1972). Mixed Convection in the Entry Region of an Internally Heated Annulus in Upward Flow, Ph.D. thesis, University of Liverpool.

OGUNBA, V. and BARROW, H. (1979). A Visual Flow Study of Mixed Convection in the Entry Region of a Vertical Internally Heated Annulus, International Journal of Heat and Fluid Flow, vol. 1, no. 3, pp. 115–121.

OKUNO, M. and SUGITA, J. (1973). Heat Transfer in the Thermal Entrance Section for Fully Developed Upward Laminar Flow in a Vertical Annulus, Chemical Engineering (Japan), vol. 37, pp. 81–86.

OSTRACH, S. (1954). Combined Natural and Forced Convection in Fluids With and Without Heat Sources in a Channel With Linearly Varying Wall Temperatures, NACA TN 3141.

OSTROUMOV, G.A. (1952). Svobodnaia Konvectziia v Usloviiakh Vnutrennei Zadachi, State Publishing House, Moscow. (English translation: Free Convection Under Conditions of the Internal Problem, NACA TM 1407, 1958.)

PATANKAR, S.V. (1988). Parabolic Systems: Finite–Difference Method I, in Handbook of Numerical Heat Transfer, (eds. W.J.Minkowycz, E.M.Sparrow, G.E.Schneider and R.H.Pletcher), John Wiley.

PETUKHOV, B.S., POLYAKOV, A.F. and MARTYNENKO, O.G. (1982). Buoyancy Effect on Heat Transfer in Forced Channel Flows, 7th International Heat Transfer Conference, Munich, paper RK 5, pp. 343–362.

PETUKHOV, B.S., POLYAKOV, A.F. and STRIGIN, B.K. (1969). Heat Transfer in Tubes With Viscous–Gravity Flow, Heat Transfer – Soviet Research, vol. 1, no. 1, pp. 24–31.

PIGFORD, R.L. (1955). Nonisothermal Flow and Heat Transfer Inside Vertical Tubes, <u>Chemical Engineering Progress Symposium Series</u>, vol. 51, no. 17, pp. 79–92.

POIRIER, N.A. and MUJUMDAR, A.S. (1989). Numerical Solution to the Graetz Problem: Achieving Accuracy in the Entrance Region, <u>International Communications in Heat and Mass Transfer</u>, vol. 16, pp. 205–214.

QUINTIERE, J. and MUELLER, W.K. (1973). An Analysis of Laminar Free and Forced Convection Between Finite Vertical Parallel Plates, <u>ASME Journal of Heat Transfer</u>, vol. 95, pp. 53–59.

RAO, D.V. and EL–GENK, M.S. (1990). Buoyancy Induced Instability of Laminar Flows in Vertical Annuli – II. Model Development and Analysis, <u>International Journal of Heat and Mass Transfer</u>, vol. 33, pp. 2161–2172.

RAO, T.L.S. and BARROW, H. (1972). Experimental Study of Combined Free and Forced Laminar Convection in an Asymmetrically Heated Two–Dimensional Aiding Flow, <u>Wärme– und Stoffübertragung</u>, vol. 5, pp. 127–133.

RAO, T.L.S. and MORRIS, W.D. (1968). Superimposed Laminar Forced and Free Convection Between Vertical Parallel Plates when One Plate is Uniformly Heated and the Other is Thermally Insulated, Thermodynamics and Fluid Mechanics Convention, Bristol, paper 40, <u>Proceedings of the Institution of Mechanical Engineers</u>, vol. 182, part 3H, pp. 374–381.

ROGERS, B.B. and YAO, L.S. (1990). The Effect of Mixed Convection Instability on Heat Transfer in a Vertical Annulus, <u>International Journal of Heat and Mass Transfer</u>, vol. 33, pp. 79–90.

ROKERYA, M.S. and IQBAL, M. (1971). Effects of Viscous Dissipation on Combined Free and Forced Convection Through Vertical Concentric Annuli, International Journal of Heat and Mass Transfer, vol. 14, pp. 491–495.

ROSEN, E.M. and HANRATTY, T.J. (1961). Use of Boundary Layer Theory to Predict the Effect of Heat Transfer on the Laminar Flow Field in a Vertical Tube With a Constant Temperature Wall, AIChE Journal, vol. 7, no. 1, pp. 112–123.

SAVKAR, S.D. (1970). Developing Forced and Free Convective Flows Between Two Semi–Infinite Parallel Plates, 4th International Heat Transfer Conference, Paris, vol. IV, paper NC 3.8.

SCHEELE, G.F. and HANRATTY, T.J. (1962). Effect of Natural Convection on Stability of Flow in a Vertical Pipe, Journal of Fluid Mechanics, vol. 14, part 2, pp. 244–256.

SCHEELE, G.F., ROSEN, E.M. and HANRATTY, T.J. (1960). Effect of Natural Convection on Transition to Turbulence in Vertical Pipes, The Canadian Journal of Chemical Engineering, vol 38, pp. 67–73.

SCHLICHTING, H. (1968). Boundary Layer Theory, 6th Edition, McGraw–Hill.

SHADDAY, M.A., Jr. (1986). Combined Forced/Free Convection Through Vertical Tubes at High Grashof Numbers, 8th International Heat Transfer Conference, San Francisco, vol. 3, pp. 1433–1437.

SHAH, R.K. and LONDON, A.L. (1978). Advances in Heat Transfer, Supplement 1, Laminar Flow Forced Convection in Ducts, (eds. T.F.Irvine, Jr. and J.P.Hartnett), Academic Press.

SHERWIN, K. (1968). Laminar Convection in Uniformly Heated Vertical Annuli, British Chemical Engineering, vol. 13, no. 11, pp. 569–574.

SHERWIN, K. and WALLIS, J.D. (1968). A Study of Laminar Convection for Flow Down Vertical Annuli, Thermodynamics and Fluid Mechanics Convention, Bristol, paper 34, Proceedings of the Institution of Mechanical Engineers, vol. 182, part 3H, pp. 330–335.

SHERWIN, K. and WALLIS, J.D. (1970). A Theoretical Study of Combined Natural and Forced Laminar Convection for Developing Flow Down Vertical Annuli, 4th International Heat Transfer Conference, Paris, vol. IV, paper NC 3.9.

SHERWIN, K. and WALLIS, J.D. (1972). Combined Natural and Forced Laminar Convection for Upflow Through Heated Vertical Annuli, Symposium on Heat and Mass Transfer by Combined Forced and Natural Convection, September 1971, paper C112/71, pp. 1–5, Institution of Mechanical Engineers.

SHUMWAY, R.W. and McELIGOT, D.M. (1971). Heated Laminar Gas Flow in Annuli With Temperature–Dependent Transport Properties, Nuclear Science and Engineering, vol. 46, pp. 394–407.

SITHARAMARAO, T.L. and BARROW, H. (1972). Combined Free and Forced Convection in the Entrance Region of Ducts of Constant Cross–Section, Symposium on Heat and Mass Transfer by Combined Forced and Natural Convection, September 1971, paper C116/71, pp. 26–30, Institution of Mechanical Engineers.

SZPIRO, O., ALLEN, P.H.G. and COLLINS, M.W. (1978). The Influence of Temperature Dependence of Thermophysical Properties on the Prediction Accuracy in Laminar Mixed Convection Heat Transfer in Vertical Tubes, 6th International Heat Transfer Conference, Toronto, paper MC–6, pp. 31–36.

SZPIRO, O., LEWIS, J.S. and COLLINS, M.W. (1984). Numerical Solutions for Developing Combined Convection Between Uniformly Heated Parallel Plates, 1st UK National Conference on Heat Transfer, Leeds, vol. 2, pp. 829–838.

TAO, L.N. (1960a). On Combined Free and Forced Convection in Channels, ASME Journal of Heat Transfer, vol. 82, pp. 233–238.

TAO, L.N. (1960b). Heat Transfer of Combined Free and Forced Convection in Circular and Sector Tubes, Applied Scientific Research, Section A, vol. 9, pp. 357–368.

TJELFLAAT, P.O. and YTREHUS, T. (1981). Combined Free and Forced Laminar Convection in a Vertical Channel, 2nd International Conference on Numerical Methods in Thermal Problems, Venice, pp. 990–1001.

WATZINGER, A. and JOHNSON, D.G. (1939). Wärmeübertragung von Wasser an Rohrwand bei senkrechter Strömung im Übergangsgebiet zwischen laminarer und turbulenter Strömung, Forschung auf dem Gebiete des Ingenieurwesens, vol. 10, pp. 182–196.

WIRTZ, R.A. and McKINLEY, P. (1985). Buoyancy Effects on Downward Laminar Convection Between Parallel Plates, in Fundamentals of Forced and Mixed Convection, (eds. F.A.Kulacki and R.D.Boyd), ASME HTD–vol. 42, pp. 105–112.

YAO, L.S. (1983). Free and Forced Convection in the Entry Region of a Heated Vertical Channel, International Journal of Heat and Mass Transfer, vol. 26, no.1, pp. 65–72.

YAO, L.S. (1987a). Is a Fully–Developed and Non–Isothermal Flow Possible in a Vertical Pipe?, International Journal of Heat and Mass Transfer, vol. 30, no. 4, pp. 707–716.

YAO, L.S. (1987b). Linear Stability Analysis for Opposing Mixed Convection in a Vertical Pipe, International Journal of Heat and Mass Transfer, vol. 30, no. 4, pp. 810–811.

YAO, L.S. and ROGERS, B.B. (1989). Mixed Convection in an Annulus of Large Aspect Ratio, ASME Journal of Heat Transfer, vol. 111, pp. 683–689.

ZAKI, G.M., EL–GENK, M.S., WILLIAMS, T.E. and PHILBIN, J.S. (1985). Experimental Heat Transfer Studies for Water in an Annulus at Low Reynolds Number, in Fundamentals of Forced and Mixed Convection, (eds. F.A.Kulacki and R.D.Boyd), ASME HTD–vol. 42, pp. 113–120.

ZELDIN, B. and SCHMIDT, F.W. (1972). Developing Flow and Combined Forced–Free Convection in an Isothermal Vertical Tube, ASME Journal of Heat Transfer, vol. 94, pp. 211–223.

ZENEN, S.R., COLLINS, M.W. and SIMONSON, J.R. (1985), Combined Convection in an Annulus Applied to a Thermal Storage Problem, International Journal for Numerical Methods in Engineering, vol. 21, pp. 691–711.

APPENDICES

APPENDIX A

POLYNOMIAL REPRESENTATION OF TEMPERATURE–DEPENDENT FLUID PROPERTIES

It is convenient to represent fluid property variations over a temperature range of interest by analytical functions that are simple to evaluate. One such form often fitted to experimental or tabular property data is the nth–degree polynomial equation

$$\psi = a_0 + a_1 T + a_2 T^2 + \cdots + a_n T^n \qquad (A.1)$$

where ψ is used to denote any temperature–dependent fluid property and T is the temperature measured on some practical scale of (e.g. $^\circ$C), so that $\psi = a_0$ at $T = 0^\circ$C. The polynomials (B.2), (B.4), (B.5) and (B.6) given in Appendix B, describing the property variations of liquid water at atmospheric pressure, are examples of equation (A.1).

In the analysis presented in Chapter 3, fluid property ratios ψ^* $[=\psi/\psi_0]$ relate the local values of the properties to their corresponding values at temperature T_0, the duct inlet temperature. The essential mathematical details connecting the polynomial equation (A.1) with a nondimensional form representing ψ^* as a function of the dimensionless temperature θ are given below.

Since all of its derivatives higher than the nth–order are equal to zero, equation (A.1) can be represented exactly by the following Taylor series:

$$\psi = \psi_0 + (T - T_0)\left[\frac{\partial \psi}{\partial T}\right]_{T_0} + \frac{(T - T_0)^2}{2!}\left[\frac{\partial^2 \psi}{\partial T^2}\right]_{T_0} + \cdots + \frac{(T - T_0)^n}{n!}\left[\frac{\partial^n \psi}{\partial T^n}\right]_{T_0}$$

$$(A.2)$$

Both T and T_0 must be in the interval over which equation (A.1) applies.

After substituting the derivatives obtained from equation (A.1), equation (A.2) can be arranged as a series having ascending powers of $(T - T_0)$, up to the term of degree n. That is

$$\psi = \psi_0[1 + a_{\psi 1}(T - T_0) + a_{\psi 2}(T - T_0)^2 + \cdots + a_{\psi n}(T - T_0)^n] \qquad (A.3)$$

where the coefficients $a_{\psi 1}$, $a_{\psi 2}$ $\cdots$ $a_{\psi n}$ are related to those in equation (A.1). For a 5th–degree polynomial the following expressions are obtained:

$$
\begin{aligned}
a_{\psi 1} &= \frac{1}{\psi_0}\left(a_1 + 2a_2T_0 + 3a_3T_0{}^2 + 4a_4T_0{}^3 + 5a_5T_0{}^4\right) \\
a_{\psi 2} &= \frac{1}{\psi_0}\left(a_2 + 3a_3T_0 + 6a_4T_0{}^2 + 10a_5T_0{}^3\right) \\
a_{\psi 3} &= \frac{1}{\psi_0}\left(a_3 + 4a_4T_0 + 10a_5T_0{}^2\right) \qquad (A.4) \\
a_{\psi 4} &= \frac{1}{\psi_0}\left(a_4 + 5a_5T_0\right) \\
a_{\psi 5} &= \frac{1}{\psi_0}\left(a_5\right)
\end{aligned}
$$

For lower degree polynomials the redundant terms in equations (A.4) become zero.

In terms of the dimensionless temperature, defined by $\theta = (T - T_0)/\Delta T_r$, equation (A.3) becomes

$$\psi^* = \frac{\psi}{\psi_0} = [1 + A_{\psi 1}\theta + A_{\psi 2}\theta^2 + \cdots + A_{\psi n}\theta^n] \qquad (A.5)$$

where $A_{\psi i} = a_{\psi i}/\Delta T_r{}^i$ with $a_{\psi i}$ given by the expressions (A.4) above.

Two useful quantities, closely related to ψ^*, are the derivative $d\psi^*/d\theta$ and ψ_m^*, the integrated mean value over the dimensionless temperature range from 0 to θ. In the analysis, $d\psi^*/d\theta$ is used for representing the rates at which the viscosity and thermal conductivity change with θ and ψ_m^* is utilised in connection with the specific heat capacity; for the ratio of the mean value (over the temperature range from T_0 to T) to the value at T_0.

The general expressions for $d\psi^*/d\theta$ and ψ_m^* follow directly from equation (A.5) and are given by

$$\frac{d\psi^*}{d\theta} = A_{\psi 1} + 2A_{\psi 2}\theta + \cdots + nA_{\psi n}\theta^{n-1} \qquad (A.6)$$

and

$$\psi_m^* = \frac{1}{\theta}\int_0^\theta \psi^* d\theta = 1 + \frac{1}{2}A_{\psi 1}\theta + \frac{1}{3}A_{\psi 2}\theta^2 + \cdots + \frac{1}{n+1}A_{\psi n}\theta^n \qquad (A.7)$$

APPENDIX B

EQUATIONS FOR THE PROPERTIES OF LIQUID WATER

B.1 Scope

This appendix describes the methods used to evaluate the properties of water required for the reduction of experimental data and in the numerical predictions. The properties concerned are dynamic viscosity μ, thermal conductivity k, specific heat capacity c, density ρ and thermal expansion coefficient β. For computer implementation, it is convenient to represent data giving the variation of each property with temperature in equation form, as this obviates the need for interpolation associated with the use of tabular data.

The authoritative and comprehensive information on the properties of water given in the data items issued by ESDU (Engineering Sciences Data Unit) forms the basis of the equations presented here. Unless otherwise stated, the data for liquid water extracted from this source apply strictly for a pressure of either 1 bar (k, c and ρ) or 1 atmosphere (μ only). However, since the properties of liquid water vary only slightly with pressure, negligible error can be attributed to using the equations for the pressures encountered in the experiments, which are estimated to have been in the approximate range 1 to 1.2 bar.

Equation (B.1) for μ and equation (B.3) for k are taken from the ESDU (1968b) and ESDU (1967) data items respectively. They were used directly in a spreadsheet program developed for experimental data reduction but were judged to be too time consuming for the marching numerical predictions where repetitive property evaluations were required. Instead, these computations were based on simpler polynomials, equations (B.2) and (B.4), obtained using a curve fitting program (Techni–Curve, Scientific Software Systems).

Polynomial regression was also used to obtain equations (B.5) and (B.6), for c_p and ρ respectively, based on the data tabulated by ESDU (1968a, 1968c). Equation (B.7), which predicts values of β for water in excellent agreement with published data, was derived directly from the density equation (B.6).

Details of all the equations and the uncertainties associated with the data upon which they are based are given below. It should be emphasised that each equation provides an empirical representation of a property over a limited range of temperature and therefore must not be used for extrapolation beyond the stated limits. Furthermore, it is not claimed that the derived polynomial equations presented here are necessarily the most accurate or the most appropriate forms possible. Nevertheless, they are considered to be adequate for their intended purposes, since they are relatively inexpensive to evaluate and predict values which are in excellent agreement with the data sources. The dimensionless form of the polynomial functional relationship is considered in Appendix A.

B.2 Dynamic Viscosity

According to ESDU (1968b), the following equation, due to Gibson and Bruges (1969), correlates measured values of μ for water at 1 atmosphere pressure and $0°C \leq T \leq 100°C$ with an uncertainty of $\pm 1\%$ (based on the spread of the experimental data):

$$\mu = \sum_{i=0}^{8} a_i \mathfrak{T}_i(\xi) \qquad \text{kg/m s} \qquad (B.1)$$

where the temperature T (in °C) is represented in the normalised variable ξ, defined by $\xi = [2(T + 273.15)/273.15 - 2.36609921]/0.36609921$, and $\mathfrak{T}_i(\xi)$ is a Chebyshev polynomial of degree i in ξ. The polynomials are defined by $\mathfrak{T}_0(\xi) = 1$, $\mathfrak{T}_1(\xi) = \xi$ and for $i \geq 2$ the recurrence formula $\mathfrak{T}_i(\xi) = 2\xi\mathfrak{T}_{i-1}(\xi) - \mathfrak{T}_{i-2}(\xi)$ is used.

The coefficients to be used in equation (B.1) are

$$a_0 = \quad 7.65449735 \times 10^{-4} \qquad a_5 = -\ 8.05966931 \times 10^{-6}$$
$$a_1 = -\ 6.62858516 \times 10^{-4} \qquad a_6 = \quad 2.58990320 \times 10^{-6}$$
$$a_2 = \quad 2.40802347 \times 10^{-4} \qquad a_7 = -\ 8.32983433 \times 10^{-7}$$
$$a_3 = -\ 7.97360135 \times 10^{-5} \qquad a_8 = \quad 2.75179488 \times 10^{-7}$$
$$a_5 = \quad 2.54196282 \times 10^{-5}$$

Values of μ calculated from equation (B.1), using a spreadsheet, agreed with the data tabulated by ESDU (1968b) to 3 or 4 significant digits. A data set calculated by this means at 10° C intervals in the range 0° C to 100° C was used to obtain a polynomial fit representing μ.
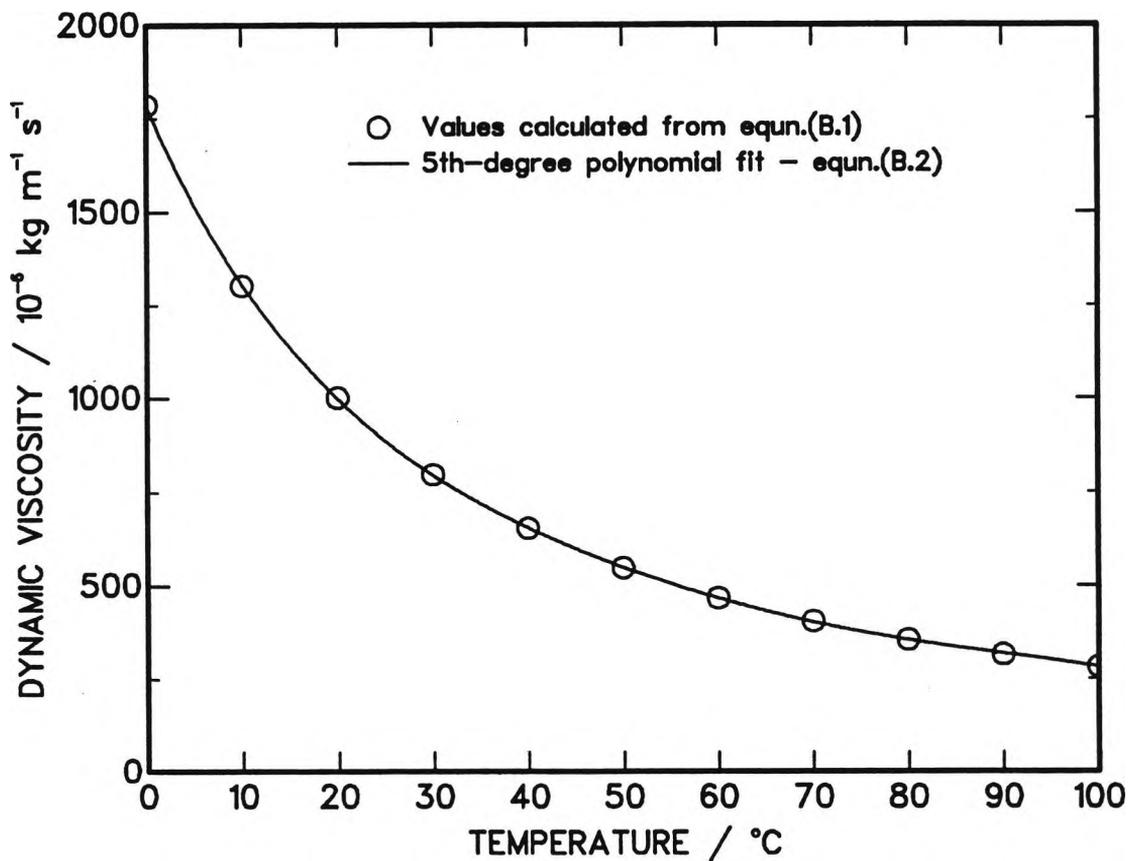
Figure B.1   Dynamic viscosity of water at 1 atmosphere, 0° C − 100° C. Polynomial equation (B.2) fitted to values calculated from equation (B.1).

Polynomial regression gave the following 5th–degree equation:

$$\mu = a_0 + a_1T + a_2T^2 + a_3T^3 + a_4T^4 + a_5T^5 \quad \text{kg/m s} \qquad (B.2)$$

where T is in °C and the coefficient values are

$$a_0 = 1.784145 \times 10^{-3} \qquad\qquad a_3 = -1.827073 \times 10^{-8}$$
$$a_1 = -5.923697 \times 10^{-5} \qquad\quad a_4 = 1.376148 \times 10^{-10}$$
$$a_2 = 1.313016 \times 10^{-6} \qquad\qquad a_5 = -4.200253 \times 10^{-13}$$

The maximum difference between the values calculated using equation (B.1) and the 5th–degree polynomial equation (B.2) is less than 0.8%. Figure B.1 compares the calculated data and the polynomial curve fit obtained.

B.3 Thermal Conductivity

ESDU (1967) recommended the following International Skeleton Tables formula (see supplement to NEL Steam Tables, 1964) for the thermal conductivity of liquid water from the saturation pressure p_s to 500 bar in the temperature range $0°C \leq T \leq (0.15p + 210)°C$, where p is in bar:

$$k = \sum_{i=0}^{4} a_i\zeta^i + (p - p_s)\sum_{i=0}^{3} b_i\zeta^i + (p - p_s)^2\sum_{i=0}^{3} c_i\zeta^i \quad \text{W/m K} \qquad (B.3)$$

In equation (B.3), $\zeta = (T + 273.15)/273.15$ with T in °C and the coefficients are

$$a_0 = -0.92247 \qquad b_0 = -9.4730 \times 10^{-9} \qquad c_0 = 1.6563 \times 10^{-16}$$
$$a_1 = 2.8395 \qquad\quad b_1 = 25.186 \times 10^{-9} \qquad\quad c_1 = -3.8929 \times 10^{-16}$$
$$a_2 = -1.8007 \qquad b_2 = -20.012 \times 10^{-9} \qquad c_2 = 2.9323 \times 10^{-16}$$
$$a_3 = 0.52577 \qquad b_3 = 5.1536 \times 10^{-9} \qquad\quad c_3 = -0.71693 \times 10^{-16}$$
$$a_4 = -0.07344$$

According to ESDU (1967), a tolerance of ± 2% should be applied to values calculated from equation (B.3) to reflect the spread of the experimental results on which it is based. Equation (B.3) was found to be satisfactory for spreadsheet calculations. Values of k calculated for 1 bar pressure deviated by less than 0.2% from the corresponding values calculated and tabulated by ESDU (1967). The following equation, given in the NEL Steam Tables (1964), was used to determine the saturation pressure p_s: $\log_{10}(p_s) = A + B\log_{10}(z) + Cz + D/z$, where $z = T + 273.16$, $A = 28.59051$, $B = -8.2$, $C = 2.4804 \times 10^{-3}$ and $D = 3142.31$.

For use in the numerical predictions, a much simpler 2nd–degree polynomial equation has been fitted to a set of values for k calculated from equation (B.3).
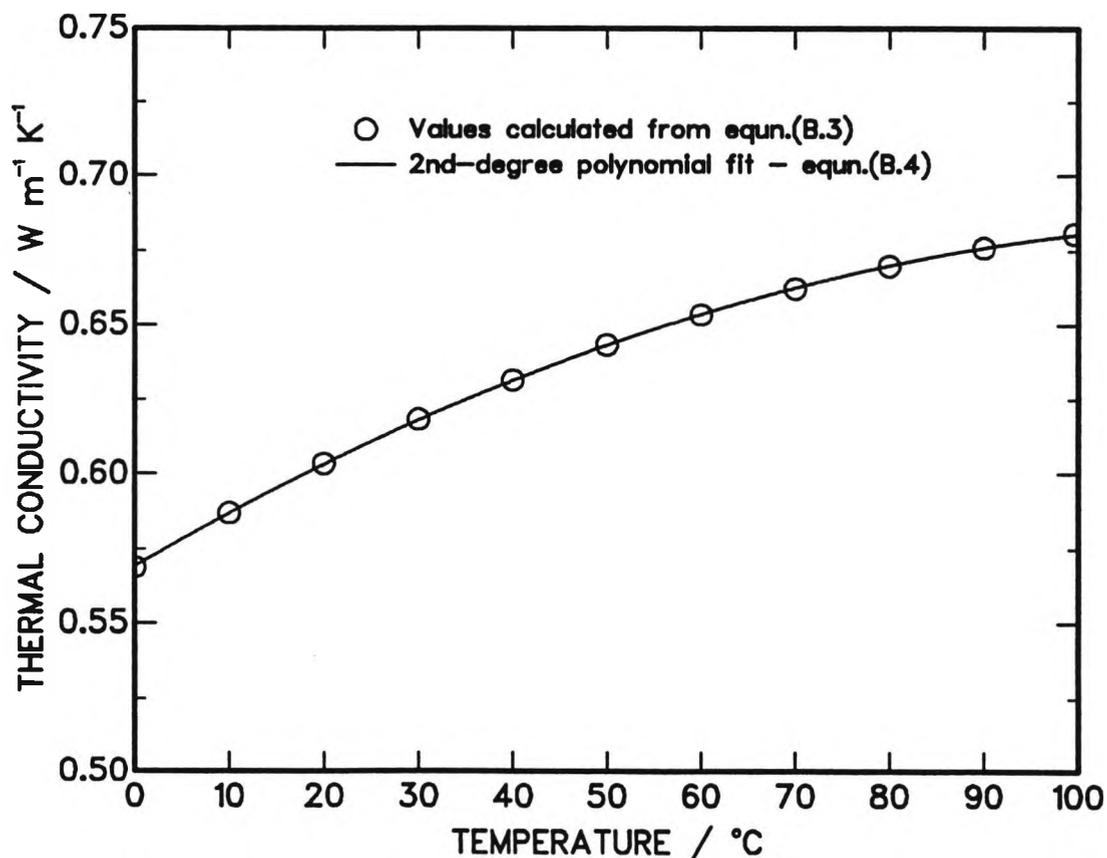
Figure B.2   Thermal conductivity of water at 1 bar, $0°\,C - 99.6°\,C$. Polynomial equation (B.4) fitted to values calculated from equation (B.3).

The values were found at 10°C intervals in the range 0°C to 90°C and at the saturation temperature (i.e. 99.6°C). A pressure of 1 bar was assumed. The equation derived using this data set is

$$k = a_0 + a_1T + a_2T^2 \qquad\qquad W/m\ K \qquad (B.4)$$

where the temperature T is in °C and the coefficient values are $a_0 = 0.5690103$, $a_1 = 1.857021 \times 10^{-3}$ and $a_2 = -7.434436 \times 10^{-6}$. The differences between the values of k calculated using equation (B.3) and the corresponding estimates given by equation (B.4) are all within ± 0.06%. The polynomial fit and the calculated values upon which it is based are compared in Figure B.2.

B.4 Specific Heat Capacity

Values of c_p for 1 bar pressure are tabulated (to 4 significant figures) at 10°C intervals from 0°C to 90°C by ESDU (1968a). Based on the spread of the original experimental results, it is stated that an uncertainty of ± 0.2% should be allowed for in these values. Since $c_p \approx c_v$ for liquid water, and in accordance with the present quasi–incompressible treatment, the specific heat capacity is here simply denoted by c.

The following equation has been fitted to the ESDU (1968a) data set by polynomial regression:

$$c = a_0 + a_1T + a_2T^2 + a_3T^3 + a_4T^4 + a_5T^5 \qquad J/kg\ K \qquad (B.5)$$

where T is in °C and the coefficient values are

$$
\begin{array}{ll}
a_0 = \quad 4217.938 & a_3 = -2.154948 \times 10^{-3} \\
a_1 = -3.638315 & a_4 = \quad 1.84914 \ \times 10^{-5} \\
a_2 = \quad 0.1270167 & a_5 = -6.038683 \times 10^{-8}
\end{array}
$$
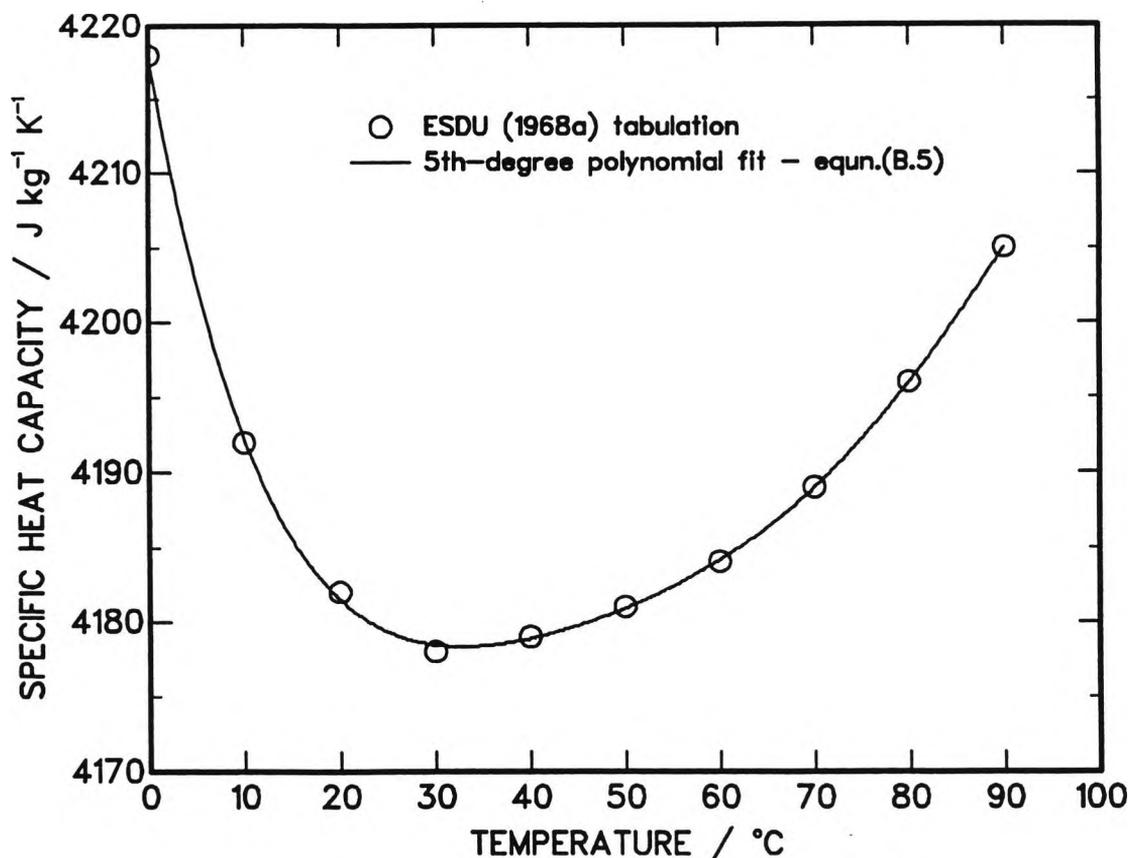
Figure B.3   Specific heat capacity of water at 1 bar, $0°C - 90°C$.
Polynomial equation (B.5) fitted to data tabulated by ESDU (1968a).

Values calculated from equation (B.5), as a check on the fit obtained, are identical with the ESDU (1968a) tabulation if the same number of significant figures are retained. A further comparison of the given data values and the derived polynomial equation is made in Figure B.3.

B.5 Density

Values for the density of water at 1 bar pressure and temperatures in the range $0°C$ to $90°C$ are given to 6 significant figures by ESDU (1968c). The data are tabulated at $1°C$ intervals from $0°C$ to $10°C$, $2°C$ intervals from $10°C$ to $20°C$, $5°C$ intervals from $20°C$ to $50°C$ and $10°C$ intervals from $50°C$ to $90°C$. The stated uncertainty is $\pm 0.0005\%$.

A 5th–degree polynomial fit obtained for these 26 data points is given by

$$\rho = a_0 + a_1 T + a_2 T^2 + a_3 T^3 + a_4 T^4 + a_5 T^5 \quad kg/m^3 \qquad (B.6)$$

where T is in °C and the coefficient values are

$a_0 =$	999.8429	$a_3 =$	7.463283×10^{-5}
$a_1 =$	6.522775×10^{-2}	$a_4 = -$	5.311156×10^{-7}
$a_2 = -$	8.642677×10^{-3}	$a_5 =$	1.702156×10^{-9}

As shown in Figure B.4, equation (B.6) provides an extremely close fit to the ESDU (1968c) tabulation and even predicts the density extremum exhibited by water at 4° C. The maximum deviation is about 0.001%.
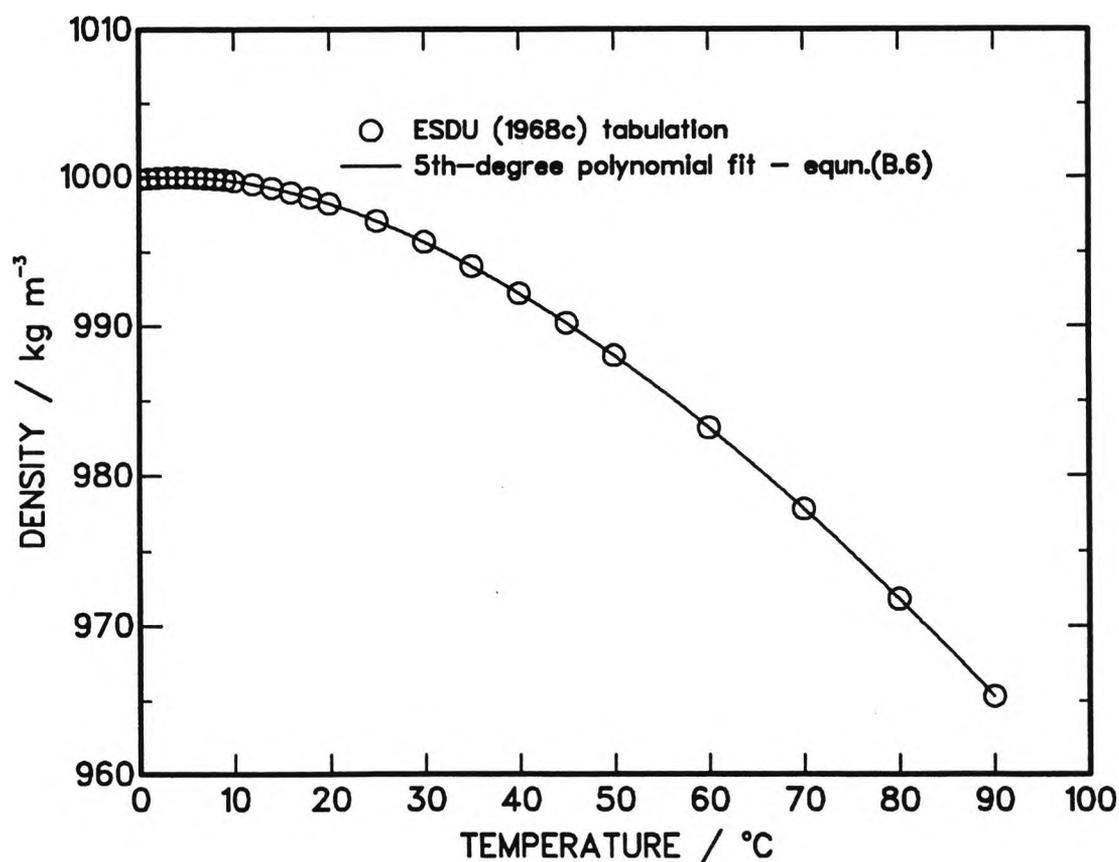
Figure B.4   Density of water at 1 bar, 0° C − 90° C.
Polynomial equation (B.6) fitted to data tabulated by ESDU (1968c).

B.6 Thermal Expansion Coefficient

Using the definition of β, the following equation can be derived from the density equation (B.6):

$$\beta = -\frac{1}{\rho}\left[\frac{\partial \rho}{\partial T}\right]_p = -\frac{a_1 + 2a_2 T + 3a_3 T^2 + 4a_4 T^3 + 5a_5 T^4}{a_0 + a_1 T + a_2 T^2 + a_3 T^3 + a_4 T^4 + a_5 T^5} \quad (B.7)$$

where β is in K^{-1}. The coefficients a_1, $a_2 \cdots a_5$ and the range of applicability for equation (B.7) are the same as for equation (B.6).

As an independent check, equation (B.7) has been compared with the data for β (at 1 atmosphere) tabulated by Bayley et al (1972). Figure B.5 illustrates the
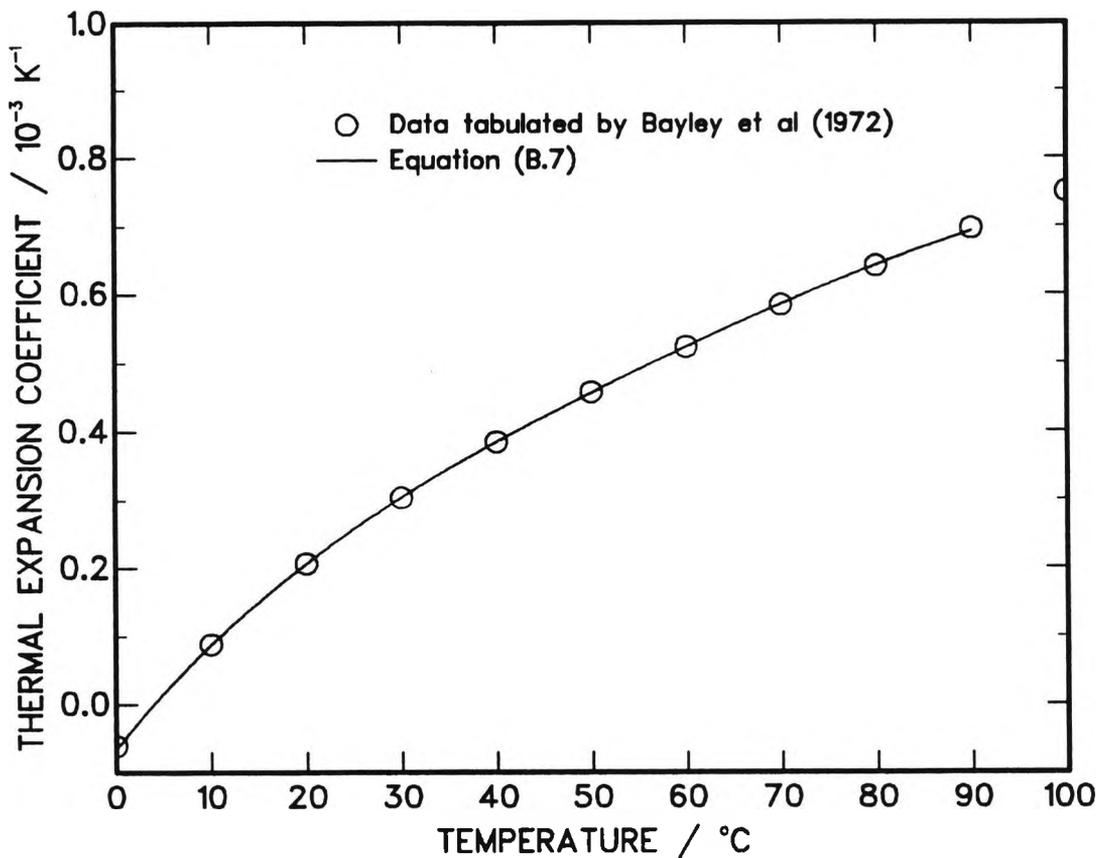
Figure B.5   Thermal expansion coefficient of water. Comparison of equation (B.7) for 1 bar, $0°C - 90°C$ with data tabulated by Bayley et al (1972) for 1 atmosphere.

comparison. Apart from 0°C, where the tabulated value is only given to 1 significant figure, the differences are within ± 0.8%. This level of agreement provides further evidence of the reliability of the density equation (B.6) upon which equation (B.7) is based.

B.7 References

BAYLEY, F.J., OWEN, J.M. and TURNER, A.B. (1972). Heat Transfer, Nelson, London.

ESDU. (1967). Thermal Conductivity of Water Substance, Item No. 67031, Engineering Sciences Data Unit, London.

ESDU. (1968a). Specific Heat at Constant Pressure of Water Substance, Item No. 68008, Engineering Sciences Data Unit, London.

ESDU. (1968b). Dynamic Viscosity of Water Substance, Item No. 68009, Engineering Sciences Data Unit, London.

ESDU. (1968c). Density of Water Substance, Item No. 68010, Engineering Sciences Data Unit, London.

GIBSON, M.R. and BRUGES, E.A. (1969). Dynamic Viscosity of Compressed Water to 10 kilobar and Steam to 1500°C, Journal of Mechanical Engineering Science, Vol. 11, pp. 189–205.

NATIONAL ENGINEERING LABORATORY (1964). NEL Steam Tables 1964, (Prepared by R.W.Bain), (also supplement: International Skeleton Tables of the Transport Properties of Water Substance, 1964), HMSO, Edinburgh.

APPENDIX C

LUMPED–SYSTEM ANALYSIS OF WALL TEMPERATURE OSCILLATIONS DUE TO ALTERNATING CURRENT HEATING

C.1 Object and Assumptions

In the experimental apparatus used in this work, alternating current (AC) power was employed to generate ohmic heating in the test section wall. The purpose of this appendix is to set down the details of a lumped–system analysis made by the author to estimate the magnitude of the wall temperature oscillations resulting from the AC heating.

A lumped–system analysis is considered appropriate because the Biot number Bi $[= h\delta_w/k_w]$ was less than 0.1 under all experimental conditions. This approach is equivalent to considering the temperature of the tube wall to be spatially uniform and hence a function of time only. Furthermore, as the wall thickness was only about 5% of the tube radius, tube wall curvature is ignored. Accordingly, the object of the analysis is to determine the transient temperature response of a flat slab, insulated on one side and convectively cooled at the other, when heat is generated internally by a sinusoidally varying electric current. In particular, the maximum amplitude of the temperature oscillations is of interest.
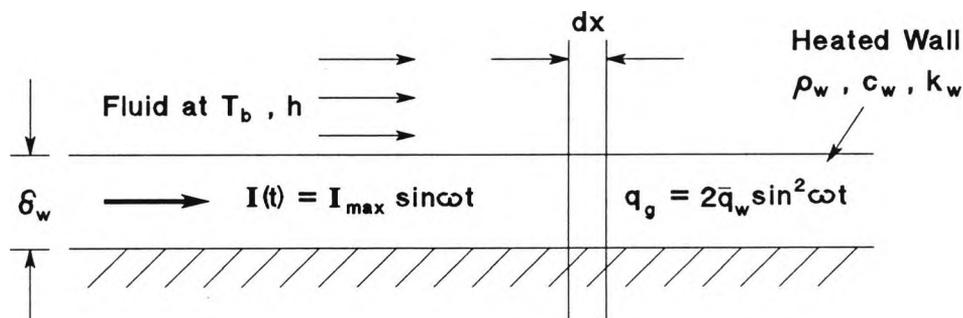
Figure C.1   Nomenclature for lumped–system analysis of the transient response of a flat wall heated by alternating current.

The situation considered is depicted in Figure C.1, where δ_w, ρ_w, c_w and k_w denote the thickness, density, specific heat capacity and thermal conductivity of the wall respectively. Energy generation in the wall is considered to be spatially uniform but the rate of generation varies with time because of the sinusoidally alternating current. The instantaneous rate of generation per unit surface area, denoted by q_g, depends on the square of the current and it can easily be shown that

$$q_g = 2\bar{q}_w \sin^2\omega t \qquad (C.1)$$

where ω is the AC angular frequency, t is time and $\bar{q}_w$ is the time–averaged surface heat flux which can be written as

$$\bar{q}_w = h(\bar{T} - T_b) \qquad (C.2)$$

In equation (C.2), h is the surface heat transfer coefficient, $\bar{T}$ is the time–averaged wall temperature and T_b is the fluid bulk temperature. Both h and T_b are assumed to remain constant.

An energy balance for a small element of length dx equates the sum of the rate of increase in internal energy and the rate of convective cooling to the rate of energy generation within the element. That is

$$\rho_w c_w \delta_w \, dx \, \frac{dT}{dt} + h \, dx \, (T - T_b) = q_g \, dx \qquad (C.3)$$

Following division by $\rho_w c_w \delta_w$ dx and substitution for q_g, using equations (C.1) and (C.2), equation (C.3) becomes

$$\frac{dT}{dt} + \frac{h}{\rho_w c_w \delta_w} (T - T_b) = \frac{2h}{\rho_w c_w \delta_w} (\bar{T} - T_b) \sin^2\omega t \qquad (C.4)$$

For convenience the following definitions are introduced:

$$\theta = (T - \bar{T})/(\bar{T} - T_b) \qquad\qquad \tau = \omega t$$

$$\mathrm{Fo} = \frac{(k/\rho c)_w}{\omega\, \delta_w{}^2} \qquad\qquad \mathrm{Bi} = \frac{h\,\delta_w}{k_w}$$

(C.5)

where the constant parameter Fo is a modified Fourier number based on the reciprocal of the angular frequency. These substitutions give the following dimensionless form of equation (C.4):

$$\frac{d\theta}{d\tau} + \mathrm{BiFo}\,\theta = \mathrm{BiFo}(2\sin^2\tau - 1)$$

(C.6)

Equation (C.6) governs the wall temperature variation, with θ expressing the variation about the average value as a fraction of the average wall–to–bulk temperature difference. An initial condition must be specified to complete the formulation. As we are concerned only with the steady periodic behaviour established after the initial transient, the condition $\theta = 0$ at $\tau = 0$ is used here.

To solve equation (C.6) it is first multiplied through by the integrating factor $e^{\mathrm{BiFo}\tau}$ to make the left–hand side the exact differential of $e^{\mathrm{BiFo}\tau}\theta$. Integrating both sides with respect to τ then yields

$$e^{\mathrm{BiFo}\tau}\theta = \mathrm{BiFo}\int_0^\tau e^{\mathrm{BiFo}\tau}(2\sin^2\tau - 1)d\tau$$

(C.7)

The right–hand side of equation (C.7) can be handled by replacing $2\sin^2\tau$ by $(1 - \cos 2\tau)$ and integrating by parts twice. This leads to the following equation describing the steady periodic wall temperature oscillations:

$$\theta = -\frac{1}{4 + (\mathrm{BiFo})^2}\left[2\mathrm{BiFo}\,\sin 2\tau + (\mathrm{BiFo})^2\cos 2\tau\right]$$

(C.8)

It follows directly from equation (C.8) that the maximum amplitude of the oscillations is given by

$$|\theta_{max}| = \frac{\sqrt{(2BiFo)^2 + (BiFo)^4}}{4 + (BiFo)^2} = \frac{BiFo}{\sqrt{4 + (BiFo)^2}} \qquad (C.9)$$

It can be seen from equation (C.9) that the above lumped–system analysis determines $|\theta_{max}|$ to be function of the product BiFo only. This is in contrast to the one–dimensional distributed analysis made by Jeglic et al (1980) for the same problem, where $|\theta_{max}|$ is given as a function of the two parameters Bi and Fo^{-1} separately. Jeglic et al (1980) presented their results in the form of graphs which unfortunately cannot be read accurately for values of $|\theta_{max}|$ close to either 0 or 1. At intermediate values of $|\theta_{max}|$, however, the predictions of the above lumped–system analysis appear to be in excellent agreement with their results for Bi < 0.1.

Values of $|\theta_{max}|$, calculated from equation (C.9), are given in Table C.1 below for a range of BiFo.

Table C.1   Maximum amplitude of temperature oscillations (as a fraction of the wall–to–bulk temperature difference) for various values of the dimensionless product BiFo.

BiFo	$|\theta_{max}|$
0.001	5.0×10^{-4}
0.01	5.0×10^{-3}
0.1	0.0499
1.0	0.4472
10	0.9806
100	0.9998

C.3 Application to Experimental Conditions

In order to use equation (C.9) for determining the magnitude of the largest wall temperature oscillations under the experimental conditions of this work, the maximum value of BiFo must be estimated. For this purpose it is considered adequate to take the following approximate values for the stainless steel tubular test section:

$$\delta_w = 0.3 \text{ mm}$$
$$\rho_w = 8000 \text{ kg/m}^3$$
$$c_w = 500 \text{ J/kg K}$$
$$k_w = 16 \text{ W/m K}$$

For alternating current at a mains frequency of 50 Hz, the angular frequency ω is equal to 100π rad/s. A roughly six–fold variation in local heat transfer coefficient ($\approx 300 - 1800 \text{ W/m}^2 \text{ K}$) was encountered in the main test series, with the higher values occuring at the start of heating.

Using the above data the maximum value of BiFo and hence the largest possible value of $|\theta_{max}|$ can be estimated as follows:

$$\text{Fo} = \frac{(k/\rho c)_w}{\omega \; \delta_w{}^2} = \frac{16}{8000 \; \text{x} \; 500 \; \text{x} \; 100\pi \; \text{x} \; (0.3 \; \text{x} \; 10^{-3})^2} = 0.14$$

$$\text{Bi}_{max} = \frac{h \delta_w}{k_w} = \frac{1800 \; \text{x} \; 0.3 \; \text{x} \; 10^{-3}}{16} = 0.034$$

$$\text{BiFo}_{max} = 0.14 \text{ x } 0.034 = 4.8 \text{ x } 10^{-3}$$

$$|\theta_{max}|_{max} = 2.4 \text{ x } 10^{-3}$$

It is concluded that the wall temperatures oscillations caused by alternating current heating were indeed negligible under all experimental conditions.

APPENDIX D

EXPERIMENTAL DATA REDUCTION METHOD

D.1 Specimen Calculation

A specimen calculation is presented below to illustrate the main procedures used for the reduction of the experimental data. For each test, the measurement data set comprised 20 items. In the following calculations the data from Test 35A are used as an example. The number of digits shown in the result of each calculation should not be taken as an indication of the associated accuracy.

After making the thermocouple calibration corrections to the test section surface temperature measurements the following data were obtained for Tests 35A:

Volume flow rate: $\dot{V} = 0.7679$ litre/minute

Test section voltage, $\tilde{V} = 11.19$ V

Test section current, $\tilde{I} = 81.44$ A

Inlet bulk temperature, $T_{b_0} = 13.06° C$

Exit bulk temperature, $T_{b_e} = 29.32° C$

Ambient temperature, $T_{amb} = 21.63° C$

Test section surface temperatures:

Lower terminal temperature,	$T_{w_0} = 15.95° C;$	$x_0 = 0$ mm
Tube wall temperature,	$T_{w_1} = 20.69° C;$	$x_1 = 3.7$ mm
Tube wall temperature,	$T_{w_2} = 20.99° C;$	$x_2 = 10.1$ mm
Tube wall temperature,	$T_{w_3} = 24.89° C;$	$x_3 = 29.1$ mm
Tube wall temperature,	$T_{w_4} = 27.09° C;$	$x_4 = 67.2$ mm
Tube wall temperature,	$T_{w_5} = 31.28° C;$	$x_5 = 118$ mm
Tube wall temperature,	$T_{w_6} = 33.16° C;$	$x_6 = 194$ mm
Tube wall temperature,	$T_{w_7} = 40.42° C;$	$x_7 = 397$ mm
Tube wall temperature,	$T_{w_8} = 45.74° C;$	$x_8 = 601$ mm
Tube wall temperature,	$T_{w_9} = 47.56° C;$	$x_9 = 804$ mm
Tube wall temperature,	$T_{w_{10}} = 54.29° C;$	$x_{10} = 1210$ mm
Tube wall temperature,	$T_{w_{11}} = 59.55° C;$	$x_{11} = 1617$ mm
Tube wall temperature,	$T_{w_{12}} = 59.02° C;$	$x_{12} = 1896$ mm
Upper terminal temperature,	$T_{w_{13}} = 53.59° C;$	$x_{13} = 1900$ mm

i) Average wall temperature, T_{w_m}

This is approximated by trapezoidal integration as follows:

$$T_{w_m} = \frac{1}{2L}\Big[(T_{w_0} + T_{w_1})\Delta x_1 + (T_{w_1} + T_{w_2})\Delta x_2 + \cdots + (T_{w_{12}} + T_{w_{13}})\Delta x_{13}\Big]$$

where L is the heated tube length ($= 1900$ mm) and $\Delta x_j = (x_j - x_{j-1})$. Substituting the values tabulated above gives $T_{w_m} = 48.39°$C.

ii) Rate of energy generation in tube wall, $\dot{Q}_g$

The rate of heat generation in found from the electrical power dissipation, given by

$$\dot{Q}_g = \tilde{I}\tilde{V} = 81.44 \times 11.19 = 911.3 \text{ W}$$

where $\tilde{I}$ and $\tilde{V}$ are the rms values of the test section current and voltage drop respectively.

iii) Rate of heat loss from test section, $\dot{Q}_{loss}$

The heat loss is estimated from the empirically determined heat loss equation, equation (5.3)

$$\dot{Q}_{loss} = 0.436 + 0.192(T_{w_m} - T_{amb}) = 0.436 + 0.192(48.39 - 21.63) = 5.57 \text{ W}$$

iv) Corrected rate of energy input to fluid, $\dot{Q}_{corr}$

The energy input to the fluid is taken equal to the test section electrical power input less the heat loss. That is

$$\dot{Q}_{corr} = \dot{Q}_g - \dot{Q}_{loss} = 911.3 - 5.57 = 905.7 \text{ W}$$

<u>v) Average heat flux at wall–fluid interface, q_w</u>

The heat flux is based on the corrected energy input to the fluid and is averaged over the inside surface area of the heated tube. It is found from

$$q_w = \frac{\dot{Q}_{corr}}{\pi dL} = \frac{905.7}{\pi \times 0.0119 \times 1.9} = 12.75 \times 10^3 \text{ W/m}^2 = 12.75 \text{ kW/m}^2$$

where d is the heated tube bore ($= 11.9$ mm).

<u>vi) Calculated exit bulk temperature, $(T_{b_e})_{calc}$</u>

The exit bulk temperature based on the corrected rate of energy input to the fluid is given by

$$(T_{b_e})_{calc} = T_{b_0} + \frac{\dot{Q}_{corr}}{c_{b_m} \rho_0 \dot{V}}$$
$$= 13.06 + \frac{905.7}{4180.7 \times 999.4 \times (0.7679 \times 10^{-3}/60)} = 30.00°\text{C}$$

The specific heat capacity c_{b_m} used in this calculation is evaluated at the average bulk temperature T_{b_m}, given in vii) below. Consequently, $(T_{b_e})_{calc}$, T_{b_m} and c_{b_m} must be found iteratively. The measured exit bulk temperature is used as an initial estimate of $(T_{b_e})_{calc}$.

<u>vii) Average bulk temperature, T_{b_m}</u>

In accordance with the assumed UHF boundary condition the local bulk temperature is assumed to vary linearly along the tube. Its average value is taken equal to the arithmetic mean of the inlet bulk temperature and the calculated exit bulk temperature. That is

$$T_{b_m} = \frac{1}{2}(T_{b_0} + T_{b_e}) = \frac{1}{2}(13.06 + 30.00) = 21.53°\text{C}$$

viii) <u>Average film temperature, T_{f_m}</u>

The average film temperature is taken as the arithmetic mean of T_{b_m} and T_{w_m}, given by

$$T_{f_m} = \frac{1}{2}(T_{b_m} + T_{w_m}) = \frac{1}{2}(21.53 + 48.39) = 34.96^{\circ}C$$

ix) <u>Fluid properties</u>

Values of μ, k, c, ρ and β are evaluated at the reference temperatures T_{b_o}, T_{b_m} and T_{f_m} using equations (B.1), (B.3), (B.5), (B.6) and (B.7) respectively.

Reference Temperature	$^{\circ}C$	$\dfrac{\mu}{kg/m\ s}$	$\dfrac{k}{W/m\ K}$	$\dfrac{c}{J/kg\ K}$	$\dfrac{\rho}{kg/m^3}$	$\dfrac{\beta}{10^{-4}K^{-1}}$
T_{b_o}	13.06	0.001197	0.5922	4187.8	999.337	1.269
T_{b_m}	21.53	0.000966	0.6058	4180.7	997.88	2.230
T_{f_m}	34.96	0.000721	0.6250	4178.4	994.05	3.455

Note that ρ (at T_{b_o}) and c (at T_{b_m}) are used in calculation vi) above.

x) <u>Dimensionless parameters</u>

The Reynolds number Re, Prandtl number Pr and the heat flux based Grashof number Gr_q are respectively given by

$$Re = \frac{4\rho_o \dot{V}}{\pi d\mu}$$

$$Pr = \frac{c\mu}{k}$$

$$Gr_q = \frac{g\beta\rho^2 d^4 q_w}{\mu^2 k}$$

The Grashof number based on the temperature difference $(T_{w_m} - T_{b_m})$, denoted simply by Gr here, is defined by

$$Gr = \frac{g\beta\rho^2 d^3(T_{w_m} - T_{b_m})}{\mu^2}$$

Values of Re, Pr, Gr_q and Gr evaluated from the above equations with the properties (except for ρ_0 in Re) taken at the reference temperatures T_{b_0}, T_{b_m} and T_{f_m} are tabulated below.

Reference Temperature	Re	Pr	Gr_q	Gr
T_{b_0}	1143	8.46	3.75×10^5	3.93×10^4
T_{b_m}	1417	6.67	9.85×10^5	1.06×10^5
T_{f_m}	1898	4.83	2.64×10^6	2.92×10^5

D.2 Sample Spreadsheet

A spreadsheet program was developed to perform all the data reduction calculations for each test. Extracts from the spreadsheet for Test 35A are shown on the following pages.

==
TEST NO: 35A   DATE: 18-04-91   TIME: 16:26:04
==

RAW DATA:
========

VOLUME FLOWRATE =	0.7679 L/min	LOWER TERMINAL TEMP = 15.67 degC
		WALL TEMP(4 mm) = 20.39 degC
		WALL TEMP(10 mm) = 20.68 degC
HEATING VOLTAGE =	11.189 V	WALL TEMP(29 mm) = 24.58 degC
HEATING CURRENT =	81.44 A	WALL TEMP(67 mm) = 26.78 degC
		WALL TEMP(118 mm) = 30.96 degC
INLET BULK TEMP =	13.06 degC	WALL TEMP(194 mm) = 32.84 degC
EXIT BULK TEMP =	29.32 degC	WALL TEMP(397 mm) = 40.10 degC
		WALL TEMP(601 mm) = 45.42 degC
AMBIENT TEMP =	21.63 degC	WALL TEMP(804 mm) = 47.24 degC
		WALL TEMP(1210 mm) = 53.97 degC
		WALL TEMP(1617 mm) = 59.22 degC
		WALL TEMP(1896 mm) = 58.70 degC
		UPPER TERMINAL TEMP = 53.27 degC

==
TEST NO: 35A   DATE: 18-04-91   TIME: 16:26:04
==

CORRECTED DATA:
==============

VOLUME FLOWRATE =	0.7679 L/min	LOWER TERMINAL TEMP = 15.95 degC
		WALL TEMP(4 mm) = 20.69 degC
		WALL TEMP(10 mm) = 20.99 degC
HEATING VOLTAGE =	11.189 V	WALL TEMP(29 mm) = 24.89 degC
HEATING CURRENT =	81.44 A	WALL TEMP(67 mm) = 27.09 degC
		WALL TEMP(118 mm) = 31.28 degC
INLET BULK TEMP =	13.06 degC	WALL TEMP(194 mm) = 33.16 degC
EXIT BULK TEMP =	29.32 degC	WALL TEMP(397 mm) = 40.42 degC
		WALL TEMP(601 mm) = 45.74 degC
AMBIENT TEMP =	21.63 degC	WALL TEMP(804 mm) = 47.56 degC
		WALL TEMP(1210 mm) = 54.29 degC
		WALL TEMP(1617 mm) = 59.55 degC
		WALL TEMP(1896 mm) = 59.02 degC
		UPPER TERMINAL TEMP = 53.59 degC

==
TEST NO: 35A   DATE: 18-04-91   TIME: 16:26:04
==

PHYSICAL PROPERTIES:
===================

	INLET BULK	*MEAN BULK*
TEMPERATURE	13.06 degC	21.53 degC
DYN.VISCOSITY	0.001197 kg/m s	0.000966 kg/m s
CONDUCTIVITY	0.5922 W/m K	0.6058 W/m K
SPECIFIC HEAT	4187.8 J/kg K	4180.7 J/kg K
DENSITY	999.37 kg/m^3	997.88 kg/m^3
EXPANSION COEFF.	1.27E-04 1/K	2.23E-04 1/K
	MEAN WALL	*EXIT BULK*
TEMPERATURE	48.36 degC	30.00 degC
DYN.VISCOSITY	0.000563 kg/m s	0.000798 kg/m s
CONDUCTIVITY	0.6414 W/m K	0.6183 W/m K
SPECIFIC HEAT	4180.5 J/kg K	4178.4 J/kg K
DENSITY	988.77 kg/m^3	995.65 kg/m^3
EXPANSION COEFF.	4.46E-04 1/K	3.04E-04 1/K

```
=================================================================
TEST NO:  35A    DATE:     18-04-91   TIME:  16:26:04
=================================================================
DERIVED RESULTS:
===============
                                       *BASED ON INLET BULK PROPS*
POWER INPUT            911.20 W        REYNOLDS NUMBER         1143.4
                                       PRANDTL NUMBER             8.46
MEAN WALL TEMP         48.36 degC      GRASHOF NUMBER –
                                          (Twm–Tbm) based       39244
HEAT LOSS               5.58 W            heat flux based      374663
                                       MEAN NUSSELT NUMBER       9.55
WALL HEAT FLUX       12749.6 W/m^2      *BASED ON MEAN BULK PROPS*
                                       REYNOLDS NUMBER         1417.1
EXIT BULK TEMPcal      30.00 degC      PRANDTL NUMBER             6.66
                                       GRASHOF NUMBER –
ENERGY BAL.ERROR       -3.96 %            (Twm–Tbm) based      105624
                                          heat flux based      985678
                                       MEAN NUSSELT NUMBER       9.33
=================================================================
TEST NO:  35A    DATE:     18-04-91   TIME:  16:26:04
=================================================================
         ** LOCAL VARIATIONS (based on inlet bulk properties) **
```

x/d	(Tw–Tb)x K	h(x) W/m^2 K	(x/d)/RePr	Nu(x)
0.31	7.60	1678.0	3.2126E-05	33.72
0.85	7.84	1626.9	8.7694E-05	32.69
2.45	11.57	1102.0	2.5266E-04	22.15
5.65	13.43	949.1	5.8347E-04	19.07
9.92	17.17	742.5	1.0245E-03	14.92
16.32	18.37	694.1	1.6862E-03	13.95
33.39	23.82	535.3	3.4505E-03	10.76
50.47	27.33	466.5	5.2148E-03	9.38
67.55	27.33	466.4	6.9791E-03	9.37
101.69	30.45	418.7	1.0507E-02	8.41
135.84	32.08	397.4	1.4035E-02	7.99
159.33	29.06	438.7	1.6462E-02	8.82

```
=================================================================
TEST NO:  35A    DATE:     18-04-91   TIME:  16:26:04
=================================================================
         ** LOCAL VARIATIONS (based on mean bulk properties) **
```

x/d	(Tw–Tb)x K	h(x) W/m^2 K	(x/d)/RePr	Nu(x)
0.31	7.60	1678.0	3.2922E-05	32.96
0.85	7.84	1626.9	8.9868E-05	31.96
2.45	11.57	1102.0	2.5893E-04	21.65
5.65	13.43	949.1	5.9794E-04	18.64
9.92	17.17	742.5	1.0499E-03	14.58
16.32	18.37	694.1	1.7280E-03	13.63
33.39	23.82	535.3	3.5360E-03	10.51
50.47	27.33	466.5	5.3440E-03	9.16
67.55	27.33	466.4	7.1521E-03	9.16
101.69	30.45	418.7	1.0767E-02	8.23
135.84	32.08	397.4	1.4383E-02	7.81
159.33	29.06	438.7	1.6870E-02	8.62

```
==================================================================
TEST NO:  35A     DATE:     18-04-91    TIME:  16:26:04
==================================================================
RESULTS BASED ON PROPERTIES AT MEAN FILM TEMPERATURE:
=================================================
TEMPERATURE           34.95 degC      REYNOLDS NUMBER          1898.0
DYN.VISCOSITY      0.000721 kg/m s     PRANDTL NUMBER             4.82
CONDUCTIVITY         0.6250 W/m K      GRASHOF NUMBER -
SPECIFIC HEAT        4178.4 J/kg K       (Twm-Tbm) based         291288
DENSITY             994.05 kg/m^3       heat flux based        2634652
EXPANSION COEFF.   3.45E-04 1/K        MEAN NUSSELT NUMBER        9.04


==================================================================
TEST NO:  35A     DATE:     18-04-91    TIME:  16:26:04
==================================================================
          ** LOCAL VARIATIONS (based on mean film properties) **
```

x/d	(Tw-Tb)x K	h(x) W/m^2 K	(x/d)/RePr	Nu(x)
0.31	7.60	1678.0	3.3986E-05	31.95
0.85	7.84	1626.9	9.2772E-05	30.97
2.45	11.57	1102.0	2.6729E-04	20.98
5.65	13.43	949.1	6.1725E-04	18.07
9.92	17.17	742.5	1.0839E-03	14.14
16.32	18.37	694.1	1.7838E-03	13.22
33.39	23.82	535.3	3.6502E-03	10.19
50.47	27.33	466.5	5.5167E-03	8.88
67.55	27.33	466.4	7.3832E-03	8.88
101.69	30.45	418.7	1.1115E-02	7.97
135.84	32.08	397.4	1.4848E-02	7.57
159.33	29.06	438.7	1.7415E-02	8.35

```
==================================================================
TEST NO:  35A     DATE:     18-04-91    TIME:  16:26:04
==================================================================
(RePr)i                                    9.67838E+03
(RePrd/L)i                                 6.06172E+01
(GrPrd/L)i                                 2.08060E+03
(Gr/Re)i                                   3.43236E+01
(Gr/Re^2)i                                 3.00200E-02
(GrqPrd/L)i                                1.98634E+04
(Grq/Re)i                                  3.27686E+02
(Grq/Re^2)i                                2.86600E-01
(RePr)b                                    9.44426E+03
(RePrd/L)b                                 5.91509E+01
(GrPrd/L)b                                 4.40871E+03
(Gr/Re)b                                   7.45332E+01
(Gr/Re^2)b                                 5.25939E-02
(GrqPrd/L)b                                4.11417E+04
(Grq/Re)b                                  6.95538E+02
(Grq/Re^2)b                                4.90802E-01
(RePr)f                                    9.14869E+03
(RePrd/L)f                                 5.72997E+01
(GrPrd/L)f                                 8.79383E+03
(Gr/Re)f                                   1.53471E+02
(Gr/Re^2)f                                 8.08591E-02
(GrqPrd/L)f                                7.95388E+04
(Grq/Re)f                                  1.38812E+03
(Grq/Re^2)f                                7.31357E-01
```

Table E.1 Summary of experimental results. (Tests 6A − 35A).

Test No.	$\dot{V}$ L/min	T_{b_o} °C	$(T_{b_e})_{meas}$ °C	$(T_{b_e})_{calc}$ °C	T_{b_m} °C	T_{w_m} °C	T_{f_m} °C	$\dot{Q}_g$ W	$\dot{Q}_{loss}$ W	q_w W/m²	% Energy Bal.Error
10A	0.0493	16.95	51.91	50.84	33.89	37.90	35.90	119.87	3.68	1635.7	3.16
15A	0.0452	17.20	88.07	87.15	52.18	58.29	55.23	227.43	7.55	3095.6	1.31
19A	0.1169	14.91	30.62	30.34	22.63	27.65	25.14	127.37	1.87	1766.8	1.80
8A	0.1232	15.26	41.36	40.75	28.01	35.49	31.75	221.83	3.34	3075.9	2.41
24A	0.1271	17.58	58.23	57.35	37.46	46.56	42.01	356.10	4.66	4947.7	2.22
14A	0.1191	14.42	73.60	72.43	43.43	53.76	48.59	487.74	6.76	6771.4	2.02
21A	0.2028	15.40	23.50	24.29	19.85	25.14	22.49	126.46	0.95	1767.0	−8.87
17A	0.1986	13.09	27.76	28.92	21.00	29.44	25.22	221.58	2.53	3083.8	−7.35
7A	0.1918	14.42	39.58	40.09	27.25	37.64	32.45	346.41	3.73	4824.4	−1.98
23A	0.2022	16.88	50.21	50.92	33.90	46.33	40.12	483.64	4.90	6740.0	−2.10
12A	0.2000	14.45	61.74	62.39	38.42	53.35	45.88	673.72	6.49	9393.5	−1.36
34A	0.3240	14.03	22.81	23.48	18.76	27.28	23.02	214.89	1.81	2999.9	−7.03
33A	0.3296	15.16	34.63	35.67	25.41	41.19	33.30	474.94	4.49	6623.0	−5.04
31A	0.3351	16.30	54.78	55.03	35.67	56.53	46.10	909.13	6.18	12712.0	−0.66
32A	0.3357	16.84	76.07	76.45	46.64	71.94	59.29	1401.63	8.97	19606.3	−0.63
18A	0.4145	13.51	20.55	21.55	17.53	26.57	22.05	233.91	1.72	3268.8	−12.52
22A	0.4196	15.14	30.85	32.11	23.62	40.50	32.06	499.29	3.72	6976.8	−7.40
6A	0.4070	13.25	44.08	44.56	28.91	51.75	40.33	893.61	6.67	12486.6	−1.53
11A	0.4157	14.53	62.40	62.11	38.32	66.89	52.61	1384.98	8.99	19371.5	0.62
25A	0.4254	16.14	71.90	72.02	44.08	74.01	59.05	1663.71	9.74	23285.1	−0.21

Test No.	$\dot{V}$ L/min	T_{b_0} °C	$(T_{b_e})_{meas}$ °C	$(T_{b_e})_{calc}$ °C	T_{b_m} °C	T_{w_m} °C	T_{f_m} °C	$\dot{Q}_g$ W	$\dot{Q}_{loss}$ W	q_w W/m²	% Energy Bal.Error
26A	0.5988	15.89	20.81	21.30	18.59	26.84	22.72	226.40	1.02	3172.9	−8.92
27A	0.5979	15.84	26.43	27.17	21.51	37.49	29.50	474.34	2.89	6637.1	−6.56
28A	0.6009	16.08	37.66	38.44	27.26	53.70	40.48	940.59	5.80	13160.1	−3.47
29A	0.6015	16.35	49.03	49.09	32.72	64.46	48.59	1377.61	7.77	19285.0	−0.18
30A	0.5983	15.68	63.06	63.04	39.36	76.29	57.82	1981.70	10.15	27756.0	0.04
16A	0.7612	11.91	15.76	16.15	14.03	21.90	17.97	226.76	1.45	3172.0	−9.32
20A	0.7792	13.73	22.11	22.77	18.25	34.51	26.38	493.55	3.01	6905.9	−7.27
35A	0.7679	13.06	29.32	30.00	21.53	48.36	34.95	911.20	5.58	12749.6	−3.96
9A	0.7723	13.15	37.13	38.67	25.91	60.86	43.39	1380.17	8.22	19314.7	−6.05
13A	0.7702	12.77	50.69	50.74	31.76	73.01	52.38	2046.30	10.58	28659.4	−0.14

Table E.2 Values of dimensionless groups with properties evaluated at inlet bulk temperature T_{b_0}. (Tests 6A − 35A).

Test Number	Re	Pr	RePr = Pe	RePrd/L = Gz	Gr	Gr/Re	GrPr = Ra	GrPrd/L	Gr(q)	Gr(q)/Re	Gr(q)Pr = Ra(q)	Gr(q)Prd/L
10A	81.2	7.55	6.137e+02	3.844e+00	9.809e+03	1.207e+02	7.409e+04	4.641e+02	7.958e+04	9.795e+02	6.011e+05	3.765e+03
15A	74.9	7.50	5.617e+02	3.518e+00	1.539e+04	2.055e+02	1.154e+05	7.230e+02	1.548e+05	2.068e+03	1.161e+06	7.275e+03
19A	182.8	8.01	1.464e+03	9.170e+00	9.546e+03	5.223e+01	7.647e+04	4.789e+02	6.716e+04	3.674e+02	5.380e+05	3.370e+03
8A	194.5	7.93	1.542e+03	9.658e+00	1.490e+04	7.662e+01	1.181e+05	7.399e+02	1.223e+05	6.287e+02	9.694e+05	6.071e+03
24A	212.7	7.42	1.579e+03	9.887e+00	2.392e+04	1.124e+02	1.775e+05	1.112e+03	2.581e+05	1.213e+03	1.916e+06	1.200e+04
14A	183.9	8.13	1.495e+03	9.363e+00	1.839e+04	9.998e+01	1.495e+05	9.361e+02	2.413e+05	1.312e+03	1.961e+06	1.228e+04
21A	321.3	7.90	2.537e+03	1.589e+01	1.073e+04	3.340e+01	8.476e+04	5.309e+02	7.147e+04	2.224e+02	5.644e+05	3.535e+03
17A	296.0	8.46	2.503e+03	1.568e+01	1.239e+04	4.188e+01	1.048e+05	6.565e+02	9.099e+04	3.074e+02	7.696e+05	4.820e+03
7A	296.1	8.13	2.407e+03	1.508e+01	1.848e+04	6.240e+01	1.502e+05	9.408e+02	1.718e+05	5.800e+02	1.396e+06	8.744e+03
23A	332.5	7.57	2.517e+03	1.577e+01	3.016e+04	9.069e+01	2.283e+05	1.430e+03	3.251e+05	9.777e+02	2.461e+06	1.541e+04
12A	309.1	8.12	2.510e+03	1.572e+01	2.667e+04	8.631e+01	2.166e+05	1.357e+03	3.361e+05	1.087e+03	2.729e+06	1.709e+04
34A	495.2	8.22	4.071e+03	2.550e+01	1.439e+04	2.905e+01	1.183e+05	7.407e+02	1.014e+05	2.048e+02	8.337e+05	5.221e+03
33A	518.8	7.95	4.126e+03	2.584e+01	3.097e+04	5.969e+01	2.463e+05	1.543e+03	2.597e+05	5.006e+02	2.066e+06	1.294e+04
31A	543.3	7.69	4.180e+03	2.618e+01	4.727e+04	8.701e+01	3.637e+05	2.278e+03	5.736e+05	1.056e+03	4.414e+06	2.764e+04
32A	551.8	7.58	4.181e+03	2.619e+01	6.110e+04	1.107e+02	4.630e+05	2.900e+03	9.416e+05	1.707e+03	7.135e+06	4.469e+04
18A	624.7	8.35	5.216e+03	3.267e+01	1.413e+04	2.263e+01	1.180e+05	7.392e+02	1.027e+05	1.643e+02	8.572e+05	5.369e+03
22A	660.0	7.96	5.253e+03	3.290e+01	3.305e+04	5.007e+01	2.630e+05	1.647e+03	2.730e+05	4.136e+02	2.172e+06	1.360e+04
6A	609.2	8.42	5.127e+03	3.211e+01	3.439e+04	5.645e+01	2.894e+05	1.813e+03	3.775e+05	6.198e+02	3.177e+06	1.990e+04
11A	643.6	8.10	5.214e+03	3.265e+01	5.163e+04	8.022e+01	4.183e+05	2.620e+03	7.005e+05	1.088e+03	5.675e+06	3.554e+04
25A	686.7	7.73	5.309e+03	3.325e+01	6.650e+04	9.684e+01	5.141e+05	3.220e+03	1.031e+06	1.501e+03	7.968e+06	4.990e+04
26A	960.6	7.79	7.479e+03	4.684e+01	1.777e+04	1.850e+01	1.384e+05	8.667e+02	1.363e+05	1.419e+02	1.061e+06	6.647e+03
27A	958.0	7.80	7.469e+03	4.678e+01	3.423e+04	3.573e+01	2.669e+05	1.671e+03	2.835e+05	2.959e+02	2.210e+06	1.384e+04
28A	968.6	7.74	7.501e+03	4.698e+01	5.832e+04	6.021e+01	4.516e+05	2.828e+03	5.784e+05	5.971e+02	4.479e+06	2.805e+04
29A	976.3	7.68	7.502e+03	4.698e+01	7.234e+04	7.410e+01	5.559e+05	3.481e+03	8.753e+05	8.965e+02	6.725e+06	4.212e+04
30A	954.7	7.83	7.478e+03	4.684e+01	7.752e+04	8.120e+01	6.072e+05	3.803e+03	1.162e+06	1.218e+03	9.105e+06	5.703e+04
16A	1098.4	8.77	9.630e+03	6.032e+01	9.574e+03	8.716e+00	8.394e+04	5.257e+02	7.776e+04	7.079e+01	6.818e+05	4.270e+03
20A	1181.4	8.30	9.800e+03	6.138e+01	2.627e+04	2.224e+01	2.179e+05	1.365e+03	2.238e+05	1.894e+02	1.856e+06	1.163e+04
35A	1143.4	8.46	9.678e+03	6.062e+01	3.924e+04	3.432e+01	3.322e+05	2.081e+03	3.747e+05	3.277e+02	3.171e+06	1.986e+04
9A	1152.8	8.44	9.731e+03	6.094e+01	5.184e+04	4.497e+01	4.376e+05	2.741e+03	5.756e+05	4.993e+02	4.859e+06	3.043e+04
13A	1137.7	8.54	9.716e+03	6.086e+01	5.766e+04	5.068e+01	4.925e+05	3.084e+03	8.057e+05	7.082e+02	6.881e+06	4.310e+04

Table E.3 Values of dimensionless groups with properties evaluated at average bulk temperature T_{b_m}. (Tests 6A − 35A).

Test Number	Re	Pr	RePr = Pe	RePrd/L = Gz	Gr	Gr/Re	GrPr = Ra	GrPrd/L	Gr(q)	Gr(q)/Re	Gr(q)Pr = Ra(q)	Gr(q)Prd/L
10A	119.2	4.93	5.883e+02	3.685e+00	4.070e+04	3.413e+02	2.008e+05	1.258e+03	3.169e+05	2.658e+03	1.564e+06	9.793e+03
15A	152.2	3.42	5.209e+02	3.263e+00	1.664e+05	1.093e+03	5.695e+05	3.567e+03	1.553e+06	1.021e+04	5.316e+06	3.330e+04
19A	221.3	6.47	1.433e+03	8.974e+00	2.185e+04	9.874e+01	1.415e+05	8.861e+02	1.506e+05	6.807e+02	9.753e+05	6.109e+03
8A	263.4	5.66	1.490e+03	9.335e+00	5.055e+04	1.919e+02	2.860e+05	1.791e+03	4.016e+05	1.524e+03	2.272e+06	1.423e+04
24A	329.7	4.56	1.505e+03	9.425e+00	1.152e+05	3.493e+02	5.256e+05	3.292e+03	1.186e+06	3.597e+03	5.413e+06	3.390e+04
14A	345.7	4.04	1.396e+03	8.741e+00	1.827e+05	5.284e+02	7.375e+05	4.619e+03	2.241e+06	6.482e+03	9.046e+06	5.666e+04
21A	359.4	6.97	2.505e+03	1.569e+01	1.772e+04	4.930e+01	1.235e+05	7.735e+02	1.166e+05	3.244e+02	8.127e+05	5.090e+03
17A	362.0	6.76	2.446e+03	1.532e+01	3.162e+04	8.734e+01	2.137e+05	1.338e+03	2.272e+05	6.277e+02	1.535e+06	9.617e+03
7A	403.5	5.76	2.325e+03	1.456e+01	6.626e+04	1.642e+02	3.818e+05	2.392e+03	5.959e+05	1.477e+03	3.434e+06	2.151e+04
23A	489.0	4.93	2.412e+03	1.511e+01	1.263e+05	2.582e+02	6.229e+05	3.902e+03	1.306e+06	2.671e+03	6.444e+06	4.036e+04
12A	529.0	4.47	2.366e+03	1.482e+01	1.999e+05	3.778e+02	8.937e+05	5.598e+03	2.378e+06	4.495e+03	1.063e+07	6.660e+04
34A	559.0	7.18	4.015e+03	2.514e+01	2.549e+04	4.560e+01	1.831e+05	1.147e+03	1.774e+05	3.174e+02	1.274e+06	7.980e+03
33A	665.3	6.03	4.012e+03	2.513e+01	8.703e+04	1.308e+02	5.248e+05	3.287e+03	7.108e+05	1.068e+03	4.286e+06	2.685e+04
31A	839.9	4.74	3.985e+03	2.496e+01	2.369e+05	2.820e+02	1.124e+06	7.038e+03	2.743e+06	3.266e+03	1.302e+07	8.152e+04
32A	1031.0	3.79	3.909e+03	2.448e+01	5.280e+05	5.121e+02	2.002e+06	1.254e+04	7.615e+06	7.386e+03	2.887e+07	1.808e+05
18A	693.6	7.43	5.154e+03	3.228e+01	2.362e+04	3.406e+01	1.755e+05	1.099e+03	1.697e+05	2.447e+02	1.261e+06	7.898e+03
22A	813.0	6.31	5.130e+03	3.213e+01	8.018e+04	9.862e+01	5.059e+05	3.169e+03	6.476e+05	7.966e+02	4.087e+06	2.559e+04
6A	887.6	5.54	4.914e+03	3.078e+01	1.649e+05	1.858e+02	9.129e+05	5.718e+03	1.739e+06	1.959e+03	9.627e+06	6.030e+04
11A	1097.1	4.48	4.917e+03	3.079e+01	3.804e+05	3.467e+02	1.705e+06	1.068e+04	4.876e+06	4.444e+03	2.185e+07	1.368e+05
25A	1248.7	3.98	4.976e+03	3.116e+01	5.478e+05	4.387e+02	2.183e+06	1.367e+04	7.967e+06	6.380e+03	3.175e+07	1.988e+05
26A	1028.6	7.21	7.421e+03	4.648e+01	2.423e+04	2.356e+01	1.748e+05	1.095e+03	1.845e+05	1.794e+02	1.331e+06	8.337e+03
27A	1102.5	6.67	7.351e+03	4.604e+01	6.277e+04	5.694e+01	4.186e+05	2.621e+03	5.122e+05	4.646e+02	3.415e+06	2.139e+04
28A	1263.8	5.76	7.281e+03	4.560e+01	1.687e+05	1.335e+02	9.722e+05	6.089e+03	1.627e+06	1.287e+03	9.372e+06	5.870e+04
29A	1420.5	5.07	7.197e+03	4.507e+01	2.985e+05	2.101e+02	1.512e+06	9.472e+03	3.470e+06	2.443e+03	1.758e+07	1.101e+05
30A	1610.7	4.38	7.062e+03	4.423e+01	5.221e+05	3.241e+02	2.289e+06	1.434e+04	7.404e+06	4.596e+03	3.246e+07	2.033e+05
16A	1163.5	8.22	9.566e+03	5.991e+01	1.327e+04	1.141e+01	1.091e+05	6.834e+02	1.071e+05	9.209e+01	8.810e+05	5.518e+03
20A	1327.6	7.28	9.669e+03	6.056e+01	4.604e+04	3.468e+01	3.353e+05	2.100e+03	3.874e+05	2.918e+02	2.821e+06	1.767e+04
35A	1417.1	6.66	9.444e+03	5.915e+01	1.056e+05	7.453e+01	7.039e+05	4.409e+03	9.857e+05	6.955e+02	6.569e+06	4.114e+04
9A	1577.1	5.96	9.392e+03	5.882e+01	2.007e+05	1.273e+02	1.196e+06	7.488e+03	2.156e+06	1.367e+03	1.284e+07	8.041e+04
13A	1784.0	5.18	9.240e+03	5.787e+01	3.637e+05	2.039e+02	1.884e+06	1.180e+04	4.844e+06	2.715e+03	2.509e+07	1.571e+05

Table E.4 Values of dimensionless groups with properties evaluated at average film temperature T_{f_m}. (Tests 6A − 35A).

Test Number	Re	Pr	RePr = Pe	RePrd/L = Gz	Gr	Gr/Re	GrPr = Ra	GrPrd/L	Gr(q)	Gr(q)/Re	Gr(q)Pr = Ra(q)	Gr(q)Prd/L
10A	124.1	4.72	5.858e+02	3.669e+00	4.616e+04	3.720e+02	2.179e+05	1.365e+03	3.579e+05	2.884e+03	1.689e+06	1.058e+04
15A	159.9	3.24	5.185e+02	3.247e+00	1.909e+05	1.194e+03	6.192e+05	3.878e+03	1.774e+06	1.109e+04	5.752e+06	3.603e+04
19A	234.5	6.07	1.424e+03	8.916e+00	2.708e+04	1.155e+02	1.645e+05	1.030e+03	1.856e+05	7.915e+02	1.127e+06	7.057e+03
8A	285.3	5.18	1.478e+03	9.255e+00	6.598e+04	2.313e+02	3.418e+05	2.141e+03	5.197e+05	1.822e+03	2.692e+06	1.686e+04
24A	359.2	4.15	1.492e+03	9.342e+00	1.491e+05	4.152e+02	6.192e+05	3.878e+03	1.522e+06	4.237e+03	6.320e+06	3.958e+04
14A	378.4	3.65	1.383e+03	8.662e+00	2.374e+05	6.274e+02	8.677e+05	5.434e+03	2.886e+06	7.625e+03	1.054e+07	6.604e+04
21A	382.9	6.50	2.487e+03	1.558e+01	2.278e+04	5.951e+01	1.480e+05	9.271e+02	1.489e+05	3.889e+02	9.675e+05	6.059e+03
17A	399.4	6.06	2.420e+03	1.515e+01	4.586e+04	1.148e+02	2.779e+05	1.740e+03	3.261e+05	8.166e+02	1.976e+06	1.238e+04
7A	450.6	5.10	2.297e+03	1.439e+01	9.596e+04	2.129e+02	4.892e+05	3.064e+03	8.529e+05	1.893e+03	4.348e+06	2.723e+04
23A	551.9	4.32	2.382e+03	1.492e+01	1.835e+05	3.325e+02	7.919e+05	4.960e+03	1.874e+06	3.395e+03	8.088e+06	5.065e+04
12A	606.4	3.85	2.333e+03	1.461e+01	2.998e+05	4.944e+02	1.153e+06	7.223e+03	3.516e+06	5.798e+03	1.353e+07	8.471e+04
34A	619.3	6.41	3.969e+03	2.486e+01	3.844e+04	6.207e+01	2.463e+05	1.543e+03	2.646e+05	4.273e+02	1.696e+06	1.062e+04
33A	787.8	5.00	3.940e+03	2.467e+01	1.541e+05	1.956e+02	7.707e+05	4.827e+03	1.236e+06	1.569e+03	6.181e+06	3.872e+04
31A	1019.6	3.83	3.906e+03	2.446e+01	4.237e+05	4.156e+02	1.623e+06	1.017e+04	4.808e+06	4.716e+03	1.842e+07	1.154e+05
32A	1266.0	3.03	3.833e+03	2.400e+01	9.406e+05	7.430e+02	2.847e+06	1.783e+04	1.329e+07	1.050e+04	4.023e+07	2.519e+05
18A	774.4	6.57	5.090e+03	3.188e+01	3.731e+04	4.818e+01	2.452e+05	1.536e+03	2.649e+05	3.420e+02	1.741e+06	1.090e+04
22A	977.7	5.14	5.028e+03	3.149e+01	1.519e+05	1.554e+02	7.813e+05	4.894e+03	1.203e+06	1.231e+03	6.188e+06	3.875e+04
6A	1116.2	4.30	4.797e+03	3.004e+01	3.412e+05	3.057e+02	1.466e+06	9.183e+03	3.512e+06	3.146e+03	1.509e+07	9.452e+04
11A	1411.5	3.40	4.793e+03	3.002e+01	7.934e+05	5.621e+02	2.695e+06	1.688e+04	9.907e+06	7.019e+03	3.365e+07	2.107e+05
25A	1598.2	3.04	4.858e+03	3.043e+01	1.102e+06	6.892e+02	3.348e+06	2.097e+04	1.563e+07	9.777e+03	4.749e+07	2.975e+05
26A	1136.1	6.46	7.338e+03	4.596e+01	3.619e+04	3.186e+01	2.338e+05	1.464e+03	2.727e+05	2.400e+02	1.761e+06	1.103e+04
27A	1320.1	5.46	7.207e+03	4.514e+01	1.204e+05	9.118e+01	6.571e+05	4.116e+03	9.633e+05	7.297e+02	5.259e+06	3.294e+04
28A	1651.9	4.28	7.076e+03	4.432e+01	3.983e+05	2.411e+02	1.706e+06	1.069e+04	3.732e+06	2.259e+03	1.599e+07	1.001e+05
29A	1910.1	3.65	6.980e+03	4.372e+01	7.293e+05	3.818e+02	2.665e+06	1.669e+04	8.218e+06	4.302e+03	3.003e+07	1.881e+05
30A	2206.5	3.10	6.846e+03	4.287e+01	1.291e+06	5.849e+02	4.004e+06	2.508e+04	1.772e+07	8.032e+03	5.498e+07	3.443e+05
16A	1288.0	7.34	9.455e+03	5.922e+01	2.161e+04	1.678e+01	1.587e+05	9.937e+02	1.726e+05	1.340e+02	1.267e+06	7.937e+03
20A	1607.8	5.89	9.465e+03	5.928e+01	9.692e+04	6.028e+01	5.706e+05	3.573e+03	7.990e+05	4.969e+02	4.703e+06	2.946e+04
35A	1898.0	4.82	9.149e+03	5.730e+01	2.913e+05	1.535e+02	1.404e+06	8.794e+03	2.635e+06	1.388e+03	1.270e+07	7.954e+04
9A	2240.2	4.04	9.049e+03	5.668e+01	6.167e+05	2.753e+02	2.491e+06	1.560e+04	6.381e+06	2.848e+03	2.577e+07	1.614e+05
13A	2606.4	3.41	8.887e+03	5.566e+01	1.134e+06	4.349e+02	3.866e+06	2.421e+04	1.451e+07	5.568e+03	4.948e+07	3.099e+05

COMPUTER PROGRAM LISTING

A full listing of the computer program embodying the numerical procedures described in Chapter 3 is given below. The program is coded in FORTRAN 77 and has been run on IBM and DEC–VAX mainframes. NAG Library routines for the solution of unsymmetric band matrix systems are called in Subroutine SOLVE.

```
C*******************************************************************************
C                                                                             *
C                        *** L A C O N I C ***                                *
C                                                                             *
C         A PROGRAM FOR TWO-DIMENSIONAL LAMINAR FORCED                        *
C             OR COMBINED (VERTICAL DUCTS ONLY) CONVECTION                    *
C     IN PARALLEL PLATE, CIRCULAR AND CONCENTRIC ANNULAR CHANNELS             *
C                                                                             *
C      MAIN FEATURES OF CALCULATION PROCEDURE:                               *
C          * QUASI-INCOMPRESSIBLE (BOUSSINESQ), VARIABLE PROPERTY            *
C            FLUID                                                            *
C          * SIMULTANEOUS SOLUTION OF INTEGRAL CONTINUITY EQUATION           *
C            AND MOMENTUM EQUATIONS FOR VELOCITIES AND PRESSURE              *
C          * CALCULATION OF TRANSVERSE VELOCITIES FROM CONTINUITY           *
C            DIFFERENTIAL EQUATION                                            *
C          * SIMULTANEOUS SOLUTION OF ENERGY DIFFERENTIAL EQUATION           *
C            AND STEPWISE ENERGY BALANCE (OPTIONAL) FOR TEMPERATURE          *
C          * FULLY IMPLICIT FINITE DIFFERENCE SCHEME                         *
C          * DIRECT SOLUTION OF EQUNS BY BAND MATRIX METHOD                  *
C          * ITERATION AT EACH AXIAL STEP TO HANDLE TEMPERATURE             *
C            COUPLING OF EQUNS                                                *
C                                                                             *
C*******************************************************************************


          BLOCK DATA INOUT
C*******************************************************************************
C         INITIALIZES INPUT/OUTPUT UNIT REFERENCE NUMBERS                     *
C                 NI - INPUT DATA FILE                                         *
C                 NO - LINEPRINTER OUTPUT                                      *
C                 NSC- STORAGE FILE (CONTINUITY CHECK SUMMARY      )          *
C                 NSS- STORAGE FILE (ITERATIVE REFINEMENT SUMMARY )          *
C                 NSF- STORAGE FILE (FLUID FLOW RESULTS SUMMARY    )          *
C                 NSH- STORAGE FILE (HEAT TRANSFER RESULTS SUMMARY)          *
C                 NS1- STORAGE FILE (NUSSELT NO. VS. XSTAR - INNER)          *
C                 NS2- STORAGE FILE (NUSSELT NO. VS. XSTAR - OUTER)          *
C                 NS3- STORAGE FILE (U PROFILES AT SPECIFIED STEPS)          *
C                 NS4- STORAGE FILE (T PROFILES AT SPECIFIED STEPS)          *
C                 NS5- STORAGE FILE (FRICT.MOD. VS. XCROSS - INNER)          *
C                 NS6- STORAGE FILE (FRICT.MOD. VS. XCROSS - OUTER)          *
C                 NS7- STORAGE FILE (U VS. XCROSS AT Y=0.0(0.1)1.0)          *
C*******************************************************************************
C
          COMMON /IO/NI,NO,NSC,NSS,NSF,NSH,NS1,NS2,NS3,NS4,NS5,NS6,NS7
          DATA NI,NO,NSC,NSS,NSF,NSH,NS1,NS2,NS3,NS4,NS5,NS6,NS7/
     1    20,6,7,8,9,10,11,12,13,14,15,16,17/
          END
```

```
          PROGRAM MAIN
C*********************************************************************
C         MAIN SEGMENT READS INPUT DATA, ORGANISES MARCHING PROCEDURE,   *
C         CALCULATES STATION VARIABLES AND OUTPUTS RESULTS.              *
C                                                                        *
C         INPUT DATA:                                                    *
C         KCOORD: COORDINATE SYSTEM (1=2-D PLANE, 2=AXISYMMETRIC)        *
C         KASE  : DOMAIN TYPE (1=C/L-WALL, 2=WALL-WALL)                  *
C         KUIN  : INLET VELOCITY PROFILE (1=UNIFORM, 2=PARABOLIC)        *
C         NDIR  : FORCED FLOW DIRECTION (-1=DOWN, 0=FORCED ONLY, 1=UP)   *
C         KSOLN : FLOW AND/OR TEMP SOLUTIONS (1=BOTH, 2=FLOW, 3=TEMP)    *
C         KEBAL : INTEGRAL ENERGY BALANCE OPTION (0=NO, 1=YES)           *
C         KVIDI : VISCOUS DISSIPATION INCLUDED (0=NO, 1=YES)             *
C         RADRAT: RADIUS RATIO, R1/R2 (E.G. 0=TUBE, 1=PARALLEL PLATES)   *
C         KTBCI : THERMAL BOUNDARY CONDITION AT INNER WALL (1=UHF, 2=UWT)*
C         TBCI  : HEAT FLUX RATIO (FOR KTBCI=1) OR DIMENSIONLESS TEMP    *
C                 (FOR KTBCI=2) AT INNER WALL                            *
C         LTBCI : AXIAL STEP NUMBER FOR START OF TBCI AT INNER WALL      *
C                 (KTBCI, TBCI AND LTBCI ONLY READ IF KASE=2)            *
C         KTBCO : AS FOR KTBCI BUT AT OUTER WALL                         *
C         TBCO  : AS FOR TBCI BUT AT OUTER WALL                          *
C         LTBCO : AS FOR LTBCO BUT AT OUTER WALL                         *
C         GNUM  : GRAVITATIONAL PARAMETER                                *
C         RENUM : REYNOLDS NUMBER BASED ON DOMAIN WIDTH - INLET PROPS    *
C         PRNUM : PRANDTL NUMBER - INLET PROPS                           *
C         BRNUM : BRINKMANN NUMBER - INLET PROPS (ONLY READ IF KVIDI=1)  *
C         RHORAT: AVERAGE/INLET DENSITY RATIO                            *
C         KPROP(1:4) : TEMPERATURE DEPENDENCE OF RHO, MU, K AND CP       *
C                      (0=NONE, 1=POLYNOMIAL, 2=POWER LAW)               *
C         PCON(1,1:6): DIMENSIONLESS CONSTANTS FOR RHO-VS-T EQUN         *
C         PCON(2,1:6): DIMENSIONLESS CONSTANTS FOR MU-VS-T EQUN          *
C         PCON(3,1:6): DIMENSIONLESS CONSTANTS FOR K-VS-T EQUN           *
C         PCON(4,1:6): DIMENSIONLESS CONSTANTS FOR CP-VS-T EQUN          *
C                      (PCON(N,1:6) ONLY READ IF KPROP(N) = 1 OR 2)      *
C         NDIV  : NUMBER OF TRANSVERSE GRID DIVISIONS (NDIV MUST BE EVEN)*
C         NSTEP : NUMBER OF AXIAL STEPS                                  *
C         NDX   : NUMBER OF DIFFERENT AXIAL STEP SIZES (21 MAX)          *
C         DX(1), LDX(1) ... DX(NDX), LDX(NDX): AXIAL STEP SIZE ,STARTING *
C                                              STEP NUMBER   (LDX(1)=1)  *
C         ISTAT : AXIAL STEP INCREMENT FOR STATION RESULTS PRINTOUT      *
C         IPROF : AXIAL STEP INCREMENT FOR PROFILE RESULTS PRINTOUT      *
C         IPLOT : AXIAL STEP INCREMENT FOR U-VS-Y AND T-VS-Y PRINTOUT    *
C         KSNUI : STORE NUSSELT NO.-VS-XSTAR - INNER (0=NO, 1=YES)       *
C         KSNUO : AS FOR KSNUI BUT AT OUTER WALL                         *
C         KSFRI : STORE FRICTION MOD.-VS-XCROSS - INNER (0=NO, 1=YES)    *
C         KSFRO : AS FOR KSFRI BUT AT OUTER WALL                         *
C         NSU   : NUMBER OF U PROFILES TO STORE (SPECIFIED AXIAL STEPS)  *
C         INCRU : TRANSVERSE DIVISIONS INCREMENT FOR U PROFILE STORAGE   *
C         LSU(1) ... LSU(NSU): AXIAL STEP NUMBERS FOR U PROFILE STORAGE  *
C         NST   : AS FOR NSU BUT FOR T PROFILES                          *
C         INCRT : AS FOR INCRU BUT FOR T PROFILES                        *
C         LST(1) ... LST(NST): AS FOR LSU(1) ... BUT FOR T PROFILES      *
C*********************************************************************
C
          PARAMETER (MAX1=101,MAX2=51,MAX3=103,MAX4=21,MAX5=24,MAX33=297)
C
          DIMENSION DX(MAX4),LDX(MAX4),IU(MAX2),IT(MAX2),
     1    LSU(MAX5),LST(MAX5),US(MAX5+2,MAX1),TS(MAX5+2,MAX1)
C
```

```
      REAL NUI3,NUI4,NUI5,NUO3,NUO4,NUO5,NUMEAN,
     1 NUI3X,NUI4X,NUI5X,NUO3X,NUO4X,NUO5X
C

      COMMON /IO/NI,NO,NSC,NSS,NSF,NSH,NS1,NS2,NS3,NS4,NS5,NS6,NS7
      COMMON /C1/FRHO(MAX3),FMU(MAX3),DFMU(MAX3),FK(MAX3),DFK(MAX3),
     1 FCP(MAX3),FCPM(MAX3),PCON(4,6),KPROP(4),CUP,RHORAT
      COMMON /C2/U(2,MAX1),V(2,MAX1),P(2,MAX1),W(MAX1),
     1 T(2,MAX3),E(MAX1)
      COMMON /C3/KKTBCI,KKTBCO,HFLUXI,HFLUXO,TBAL,TBAL1
      COMMON /C4/X,DELTX,DELTY,RADRAT,RADFN1,RAD(MAX1),Y(MAX1)
      COMMON /C5/R1,R2,R3,R4,R5,R6,R7,R8,R9,NM2,NM1,NDIV,NP1,NP2,N2M3,
     1 N3M3,RX1,RX2,RDYDX2
      COMMON /C6/KASE,KVIDI,KEBAL,NDIR
      COMMON /C8/KITER
C

      CHARACTER TY0(3)*19
      CHARACTER TY1(2)*12,TY2(2)*10,TY3(3)*11,TY4(3)*5,TY5(4)*7,
     1 TY6(2)*3,TY7(3)*4,TY8(2)*5,TY9(2)*6,SYMB(41)*1,DIGIT(10)*1
      CHARACTER DOT,CROSS,BLANK,VEL,TEMP
C

      DATA TY0/' PARALLEL PLATE    ','      CIRCULAR      ',
     1 ' CONCENTRIC ANNULAR'/
      DATA TY1/' C/L - WALL ',' WALL - WALL'/
      DATA TY2/' UNIFORM  ',' PARABOLIC'/
      DATA TY3/' DOWNWARD  ',' HORIZONTAL',' UPWARD    '/
      DATA TY4/'CONST','POLYN','POWER'/
      DATA TY5/'DENSITY','VISCOS.','CONDUC.','SP.HEAT'/
      DATA TY6/' NO','YES'/
      DATA TY7/'BOTH','FLOW','TEMP'/
      DATA TY8/'HFLUX','TWALL'/
      DATA TY9/'BANDUP','BANDET'/
      DATA DIGIT/'1','2','3','4','5','6','7','8','9','0'/
      DATA DOT,CROSS,BLANK,VEL,TEMP/'.','+',' ','U','T'/
C-----------------------------------------------------------------
C     READ, ECHO AND INTERPRET  INPUT DATA FOR EACH PROBLEM
C-----------------------------------------------------------------
      WRITE(NO,1)
    1 FORMAT('1','PROBLEM INPUT DATA:',/,1X,128('*'),/)
C
C     **** PROBLEM DEFINITION
C
      READ(NI,*)KCOORD,KASE,KUIN,NDIR
      WRITE(NO,*)'KCOORD=',KCOORD,'KASE=',KASE,'KUIN=',KUIN,
     1 'NDIR=',NDIR
      READ(NI,*)KSOLN,KEBAL,KVIDI
      WRITE(NO,*)'KSOLN=',KSOLN,'KEBAL=',KEBAL,'KVIDI=',KVIDI
      IF(KCOORD.EQ.1.AND.KASE.EQ.1)THEN
      KGEOM=1
      RADRAT=1.0
      DHFACT=4.0
      UFACT=1.5
      ELSE IF(KCOORD.EQ.1.AND.KASE.EQ.2)THEN
      KGEOM=1
      RADRAT=1.0
      DHFACT=2.0
      UFACT=1.5
      ELSE IF(KCOORD.EQ.2.AND.KASE.EQ.1)THEN
      KGEOM=2
      RADRAT=0.0
      DHFACT=2.0
```

```fortran
                UFACT=2.0
                ELSE IF(KCOORD.EQ.2.AND.KASE.EQ.2)THEN
                KGEOM=3
                READ(NI,*)RADRAT
                WRITE(NO,*)'RADRAT=',RADRAT
                DHFACT=2.0
                UFACT=2.0
                END IF
                IF(KASE.EQ.1)THEN
                KTBCI=1
                TBCI=0.0
                LTBCI=1
                ELSE
                READ(NI,*)KTBCI,TBCI,LTBCI
                WRITE(NO,*)'KTBCI=',KTBCI,'TBCI=',TBCI,'LTBCI=',LTBCI
                END IF
                READ(NI,*)KTBCO,TBCO,LTBCO
                WRITE(NO,*)'KTBCO=',KTBCO,'TBCO=',TBCO,'LTBCO=',LTBCO
                READ(NI,*)GNUM,RENUM,PRNUM
                WRITE(NO,*)'GNUM=',GNUM,'RENUM=',RENUM,'PRNUM=',PRNUM
                IF(KVIDI.EQ.1)THEN
                READ(NI,*)BRNUM
                WRITE(NO,*)'BRNUM=',BRNUM
                ELSE
                BRNUM=0.0
                END IF
C
C               **** FLUID PROPERTY VARIATIONS
C
                DO 5 I=1,4
                DO 5 J=1,6
                PCON(I,J)=0.0
5               CONTINUE
                READ(NI,*)RHORAT
                WRITE(NO,*)'RHORAT=',RHORAT
                NCONP=0
                READ(NI,*)(KPROP(J),J=1,4)
                WRITE(NO,*)'KPROP(J),J=1,4:',(KPROP(J),J=1,4)
                DO 8 I=1,4
                IF(KPROP(I).EQ.0)THEN
                NCONP=NCONP+1
                ELSE
                READ(NI,*)(PCON(I,J),J=1,6)
                WRITE(NO,*)'PCON(I,J),J=1,6:',(PCON(I,J),J=1,6)
                END IF
8               CONTINUE
                KVP=2
                IF(NCONP.EQ.4)KVP=1
                KBE=2
                IF(NDIR.EQ.0.OR.KPROP(1).EQ.0)KBE=1
C
C               ****ITERATIONS PER AXIAL STEP
C
                IF(NCONP.EQ.4)THEN
                NITMAX=1
                ELSE
                NITMAX=2
                END IF
```

```
C
C      **** GRID GEOMETRY
C
       READ(NI,*)NDIV,NSTEP,NDX
       WRITE(NO,*)'NDIV=',NDIV,'NSTEP=',NSTEP,'NDX=',NDX
       DO 9 J=1,NDX
       READ(NI,*)DX(J),LDX(J)
       WRITE(NO,*)'J=',J,'DX=',DX(J),'LDX=',LDX(J)
9      CONTINUE
C
C      ****PRINTING INSTRUCTIONS
C
       READ(NI,*)ISTAT,IPROF,IPLOT
       WRITE(NO,*)'ISTAT=',ISTAT,'IPROF=',IPROF,'IPLOT=',IPLOT
C
C      **** RESULTS STORAGE INSTRUCTIONS
C
       READ(NI,*)KSNUI,KSNUO,KSFRI,KSFRO
       WRITE(NO,*)'KSNUI=',KSNUI,'KSNUO=',KSNUO,
     1 'KSFRI=',KSFRI,'KSFRO=',KSFRO
       READ(NI,*)NSU,INCRU
       WRITE(NO,*)'NSU=',NSU,'INCRU=',INCRU
       IF(NSU.GT.0)THEN
       READ(NI,*)(LSU(J),J=1,NSU)
       WRITE(NO,*)'LSU(J),J=1,NSU:',(LSU(J),J=1,NSU)
       ELSE
       LSU(1)=0
       END IF
       READ(NI,*)NST,INCRT
       WRITE(NO,*)'NST=',NST,'INCRT=',INCRT
       IF(NST.GT.0)THEN
       READ(NI,*)(LST(J),J=1,NST)
       WRITE(NO,*)'LST(J),J=1,NST:',(LST(J),J=1,NST)
       ELSE
       LST(1)=0
       END IF
C--------------------------------------------------------------------
C      PRINT HEADING AND INPUT SPECIFICATIONS
C--------------------------------------------------------------------
       WRITE(NO,10)
10     FORMAT('1','PROBLEM, GRID & OUTPUT SPECIFICATIONS:',
     1 /,1X,128('*'),/)
       WRITE(NO,16)TY0(KGEOM)
16     FORMAT(7X,'PROBLEM TYPE AND SOLUTION OPTIONS:',//
     1 9X,'CHANNEL GEOMETRY:',1A19)
       IF(KGEOM.EQ.3)WRITE(NO,18)RADRAT
18     FORMAT(25X,'(RI/RO = ',F5.3,')')
       WRITE(NO,20)TY1(KASE),DHFACT,TY2(KUIN),TY3(NDIR+2),
     1 TY6(KVP),TY6(KBE),TY6(KVIDI+1),TY6(KEBAL+1),
     2 TY7(KSOLN)
20     FORMAT(9X,'DOMAIN WIDTH:',1A12,2X,
     1 'HYDRAULIC DIAM. = ',F3.1,' x WIDTH',/,
     2 9X,'INLET VELOCITY:',1A10,5X,'FLOW DIRECTION:',1A11,/
     3 9X,'VARIABLE PROPERTIES?',3X,1A3,/
     4 9X,'BUOYANCY EFFECT INCLUDED?',3X,1A3,/
     5 9X,'VISCOUS DISSIPATION INCLUDED?',3X,1A3,/
     6 9X,'STEPWISE ENERGY BALANCE USED?',3X,1A3,/
     7 9X,'FLOW AND TEMP.FIELD SOLUTIONS REQUIRED?',3X,1A4,//)
       WRITE(NO,30)
```

```
30         FORMAT(7X,'DIMENSIONLESS PARAMETERS: (BASED ON WIDTH',1X,
     1     'AND INLET PROPS.)',/)
           IF(KASE.EQ.2)THEN
           WRITE(NO,32)TY8(KTBCI),TBCI,LTBCI
32         FORMAT(9X,1A5,' (INNER) = ',E12.5,4X,'FROM AXIAL STEP NO.',I4)
           END IF
           WRITE(NO,34)TY8(KTBCO),TBCO,LTBCO,GNUM,RENUM,PRNUM,QDISS
34         FORMAT(9X,1A5,' (OUTER) = ',E12.5,4X,'FROM AXIAL STEP NO.',I4,/
     1     9X,'G = ',E13.5,2X,'RE = ',F13.2,2X,'PR = ',F12.2,/
     2     9X,'BR = ',E12.5,//)
           WRITE(NO,40)RHORAT,(TY5(I),I=1,4),(TY4(KPROP(I)+1),I=1,4)
40         FORMAT(7X,'FLUID PROPERTY VARIATIONS:',//
     1     9X,'DENSITY RATIO(MEAN/DATUM) = ',F8.4,//
     2     14X,4(7X,1A7),/,9X,'TYPE',4(9X,1A5),/)
           DO 46 J=1,6
           WRITE(NO,42)J,(PCON(I,J),I=1,4)
42         FORMAT(9X,'CONST ',I1,4(2X,E12.5))
46         CONTINUE
           WRITE(NO,50)NDIV,NSTEP,DX(1),LDX(1)
50         FORMAT(//,7X,'GRID AND MARCHING DETAILS:',//
     1     9X,'NO.TRANSVERSE DIVISIONS = ',I5,/
     2     9X,'TOTAL NO.AXIAL STEPS = ',I5,/
     3     9X,'AXIAL STEP CHANGES:',4X,'DX',4X,'FROM STEP',//
     4     28X,E11.4,2X,I4)
           IF(NDX.GT.1)WRITE(NO,53)(DX(J),LDX(J),J=2,NDX)
53         FORMAT(28X,E11.4,2X,I4)
           WRITE(NO,55)NITMAX
55         FORMAT(/,9X,'NO.ITERATIONS PER AXIAL STEP = ',I2,//)
           WRITE(NO,57)ISTAT,IPROF,IPLOT
57         FORMAT(7X,'PRINTING INSTRUCTIONS:',//
     1     9X,'INCREMENT FOR PRINTING STATION VARIABLES =',I4,' STEP(S)',/
     2     9X,'INCREMENT FOR PRINTING PROFILE VARIABLES =',I4,' STEP(S)',/
     3     9X,'INCREMENT FOR PRINTING PROFILE PLOTS =',I4,' STEP(S)',//)
           WRITE(NO,60)TY6(KSNUI+1),TY6(KSNUO+1),TY6(KSFRI+1),
     1     TY6(KSFRO+1),NSU
60         FORMAT(7X,'VARIABLES STORED:',//
     1     9X,'NUSSELT NO. VS. XSTAR (INNER)?',3X,1A3,/
     2     9X,'NUSSELT NO. VS. XSTAR (OUTER)?',3X,1A3,/
     3     9X,'FRICT.MOD. VS. XCROSS (INNER)?',3X,1A3,/
     4     9X,'FRICT.MOD. VS. XCROSS (OUTER)?',3X,1A3,/
     5     9X,'NO. U PROFILES STORED = ',I3)
           IF(NSU.GT.0)WRITE(NO,61)INCRU,(LSU(J),J=1,NSU)
61         FORMAT(9X,'U PROFILES STORED: TRANSVERSE INCREMENTS = ',I2,/,
     1     27X,' AT AXIAL STEPS        =',6I5,/,(51X,6I5))
           WRITE(NO,62)NST
62         FORMAT(9X,'NO. T PROFILES STORED = ',I3)
           IF(NST.GT.0)WRITE(NO,63)(LST(J),J=1,NST)
63         FORMAT(9X,'T PROFILES STORED: TRANSVERSE INCREMENTS = ',I2,/,
     1     27X,' AT AXIAL STEPS        =',6I5,(/51X,6I5))
C-------------------------------------------------------------------------
C      INITIALISE
C-------------------------------------------------------------------------
C
C
C      ****GRID SPACING, AXIAL POSITION, STEP LENGTH AND PRINT CONTROL
C
       DELTY=1.0/NDIV
       DELTX=DX(1)
       X=0.0
       NDX=2
       NSTAT=ISTAT+1
```

```
      MPROF=IPROF+1
      MPLOT=IPLOT+1
      MSU=1
      MST=1
C
C     ****INTEGER CONSTANTS BASED ON NO.TRANSVERSE DIVISIONS
C
      ND2=NDIV/2
      NM3=NDIV-3
      NM2=NDIV-2
      NM1=NDIV-1
      NP1=NDIV+1
      NP2=NDIV+2
      NP3=NDIV+3
      N2M3=NDIV*2-3
      N3M3=NDIV*3-3
C
C     ****COMPUTE TRANSVERSE & RADIAL POSITIONS
C
      DO 64 M=1,NP1
      Y(M)=(M-1)*DELTY
      RAD(M)=RADRAT+(1.0-RADRAT)*Y(M)
   64 CONTINUE
C
C     ****REAL CONSTANTS
C
      R1=1.0/DELTY
      R2=1.0/(2*DELTY)
      R3=1.0/(RENUM*PRNUM*DELTY**2)
      R4=R3*BRNUM/4.0
      R5=1.0/(RENUM*DELTY**2)
      R6=NDIR*(GNUM*RHORAT/(RENUM**2))
      R7=1.0/(RENUM*PRNUM)
      R8=1.0/(RENUM*DELTY)
      R9=1.0/RENUM
      RX1=1.0/DELTX
      RX2=1.0/(2*DELTX)
      RDYDX2=0.5*DELTY/DELTX
      RADFN1=0.5*DELTY*(1.0-RADRAT)
      RADFN4=2.0*DELTY/(3.0*(1.0+RADRAT))
C
C     ****UNIFORM OR PARABOLIC INLET PROFILE
C
      IF(KUIN.EQ.1.AND.KASE.EQ.1)THEN
      DO 65 M=1,NP1
   65 U(1,M)=1.0
      ELSE IF(KUIN.EQ.1.AND.KASE.EQ.2)THEN
      DO 70 M=1,NP1
   70 U(1,M)=1.0
      ELSE IF(KUIN.EQ.2.AND.KASE.EQ.1)THEN
      DO 80 M=1,NDIV
   80 U(1,M)=UFACT*(1-Y(M)**2)
      U(1,NP1)=0.0
      ELSE IF(KUIN.EQ.2.AND.KASE.EQ.2)THEN
      IF(KGEOM.EQ.1)THEN
      DO 90 M=1,NDIV
   90 U(1,M)=UFACT*(1-(ABS(2*Y(M)-1)**2))
      ELSE IF(KGEOM.EQ.3)THEN
      RADFN2=(RADRAT**2-1.0)/ALOG(RADRAT)
      RADFN3=1.0/(1.0+RADRAT**2-RADFN2)
```

```fortran
      DO 95 M=1,NDIV
95    U(1,M)=UFACT*RADFN3*(1.0-RAD(M)**2+RADFN2*ALOG(RAD(M)))
      END IF
      U(1,NP1)=0.0
      END IF
C
C     ****INLET MOMENTUM
C
      IF(KUIN.EQ.1)THEN
      PMOM=1.0
      ELSE
      PMOM=0.0
      DO 96 M=2,NDIV,2
      PMOM=PMOM+RADFN4*(RAD(M-1)*U(1,M-1)**2+4*RAD(M)*U(1,M)**2+
     1 RAD(M+1)*U(1,M+1)**2)
96    CONTINUE
      END IF
C
C     ****STATION VARIABLES
C
      TBAL1=0.0
      TBAL=0.0
      T(1,NP2)=0.0
      T(2,NP2)=0.0
      T(1,NP3)=0.0
      T(2,NP3)=0.0
      NUI3=0.0
      NUI4=0.0
      NUI5=0.0
      NUO3=0.0
      NUO4=0.0
      NUO5=0.0
      FMODI3=0.0
      FMODI4=0.0
      FMODI5=0.0
      FMODO3=0.0
      FMODO4=0.0
      FMODO5=0.0
      FMOD3=0.0
      FMOD4=0.0
      FMOD5=0.0
      DPMOM=0.0
      DPBUOY=0.0
C
C     ****PROFILE VARIABLES
C
      DO 100 M=1,NP1
      V(M)=0.0
      E(M)=0.0
      P(1,M)=0.0
      P(2,M)=0.0
      V(1,M)=0.0
      V(2,M)=0.0
      T(2,M)=0.0
      T(1,M)=0.0
      U(2,M)=U(1,M)
100   CONTINUE
```

```
C
C       ****STORE INLET VELOCITY AND TEMPERATURE PROFILES
C

        IF(NSU.GT.0.AND.LSU(MSU).EQ.0)THEN
        IROWU=0
        DO 105 M=1,NP1,INCRU
        IROWU=IROWU+1
        US(1,IROWU)=0.0
        US(2,IROWU)=Y(M)
        US(3,IROWU)=U(1,M)
105     CONTINUE
        US(1,1)=X
        MSU=MSU+1
        END IF
C
        IF(NST.GT.0.AND.LST(MST).EQ.0)THEN
        IROWT=0
        DO 110 M=1,NP1,8
        IROWT=IROWT+1
        TS(1,IROWT)=0.0
        TS(2,IROWT)=Y(M)
        TS(3,IROWT)=T(1,M)
110     CONTINUE
        TS(1,1)=X
        MST=MST+1
        END IF
C
C       ****ADIABATIC BOUNDARIES IN ENTRANCE REGION
C
        IF(KASE.EQ.2.AND.LTBCI.GT.1)THEN
        KKTBCI=1
        HFLUXI=0.0
        END IF
        IF(LTBCO.GT.1)THEN
        KKTBCO=1
        HFLUXO=0.0
        END IF
C
C       ****NON-ZERO INLET WALL TEMPERATURES
C
        IF(KTBCI.EQ.2.AND.LTBCI.EQ.1)THEN
        KKTBCI=2
        T(1,1)=TBCI
        T(2,1)=TBCI
        END IF
        IF(KTBCO.EQ.2.AND.LTBCO.EQ.1)THEN
        KKTBCO=2
        T(1,NP1)=TBCO
        T(2,NP1)=TBCO
        END IF
C
C       ****INLET FLUID PROPERTIES
C
        CALL PROPS(1,NP3,1)
        CUP=FCPM(NP2)
        FRHOA=FRHO(NP2)
        FRHOA1=FRHO(NP2)
```

```
C————————————————————————————————————————————————————————
C         MARCHING PROCEDURE STARTS HERE
C————————————————————————————————————————————————————————
C
C
C         ****COMPUTE NEW AXIAL STEP, RELATED CONSTANTS AND POSITION
C
          DO 900 MSTEP=1,NSTEP
          IF(MSTEP.EQ.LDX(MDX))THEN
          DELTX=DX(MDX)
          MDX=MDX+1
          RX1=1.0/DELTX
          RX2=1.0/(2*DELTX)
          RDYDX2=0.5*DELTY/DELTX
          END IF
          X=X+DELTX
C
C         ****THERMAL BOUNDARY CONDITIONS
C
          IF(MSTEP.EQ.LTBCI)THEN
          KKTBCI=KTBCI
          IF(KTBCI.EQ.1)THEN
          HFLUXI=TBCI
          ELSE IF(KTBCI.EQ.2.AND.LTBCI.GT.1)THEN
          T(1,1)=TBCI
          T(2,1)=TBCI
          END IF
          END IF
          IF(MSTEP.EQ.LTBCO)THEN
          KKTBCO=KTBCO
          IF(KTBCO.EQ.1)THEN
          HFLUXO=TBCO
          ELSE IF(KTBCO.EQ.2.AND.LTBCO.GT.1)THEN
          T(1,NP1)=TBCO
          T(2,NP1)=TBCO
          END IF
          END IF
C————————————————————————————————————————————————————————
C         ITERATIVE SEQUENCE STARTS HERE
C————————————————————————————————————————————————————————
          DO 775 NITER=1,NITMAX
C
C         ****COMPUTE VELOCITIES, PRESSURE AND STREAMFUNCTION IF REQUIRED
C
          IF(KSOLN.EQ.1.OR.KSOLN.EQ.2)THEN
          CALL BANDUP
          KROUT=1
          WRITE(NSS,*)MSTEP,KROUT,KITER
          END IF
C
C         ***CONTINUITY CHECK
C
          CHECK=0.0
          DO 115 M=2,NDIV
          CHECK=CHECK+(RAD(M-1)*U(2,M-1)+RAD(M)*U(2,M))*(DELTY/2)
115       CONTINUE
          CHECK=2*(CHECK+RAD(NDIV)*U(2,NDIV)*DELTY/2)/(1+RADRAT)
          WRITE(NSC,*)'CONTINUITY CHECK: = ',CHECK
```

```
C
C      ****COMPUTE TEMPERATURE AND HEATFUNCTION (OPTIONAL) IF REQUIRED
C
       IF(KSOLN.EQ.1.OR.KSOLN.EQ.3)THEN
       CALL BANDET
       KROUT=2
       WRITE(NSS,*)MSTEP,KROUT,KITER
       END IF
C————————————————————————————————————————————————————————————————
C      COMPUTE STATION VARIABLES
C————————————————————————————————————————————————————————————————
C
C      ****LOCAL DIMENSIONLESS NUMBERS AND AXIAL DISTANCES
C
       REI=RENUM*DHFACT
       REX=REI/FMU(NP2)
       PRI=PRNUM
       PRX=PRI*FCP(NP2)*FMU(NP2)/FK(NP2)
       PEI=REI*PRI
       PEX=REX*PRX
       XCROSS=X/(DHFACT*REI)
       XCROSX=X/(DHFACT*REX)
       XSTAR=XCROSS/PRI
       XSTARX=XCROSX/PRX
C
C      ****LOCAL WALL FRICTION MODULI
C
       IF(KSOLN.EQ.1.OR.KSOLN.EQ.2.OR.KSOLN.EQ.3.AND.MSTEP.EQ.1)THEN
C      ————OUTER BOUNDARY————
       FMODO3=(DHFACT*R1*FMU(NP1))*(-3*U(2,NP1)+4*U(2,NDIV)-U(2,NM1))
       FMODO4=(DHFACT*R1*FMU(NP1)/3)*(-11*U(2,NP1)+18*U(2,NDIV)-
     1 9*U(2,NM1)+2*U(2,NM2))
       FMODO5=(DHFACT*R1*FMU(NP1)/6)*(-25*U(2,NP1)+48*U(2,NDIV)-
     1 36*U(2,NM1)+16*U(2,NM2)-3*U(2,NM3))
C      ————INNER BOUNDARY————
       IF(KASE.EQ.2)THEN
       FMODI3=(DHFACT*R1*FMU(1))*(-3*U(2,1)+4*U(2,2)-U(2,3))
       FMODI4=(DHFACT*R1*FMU(1)/3)*(-11*U(2,1)+18*U(2,2)-9*U(2,3)+
     1 2*U(2,4))
       FMODI5=(DHFACT*R1*FMU(1)/6)*(-25*U(2,1)+48*U(2,2)-36*U(2,3)+
     1 16*U(2,4)-3*U(2,5))
       END IF
C      ————PERIPHERAL AVERAGE————
       IF(KASE.EQ.1)THEN
       FMOD3=FMODO3
       FMOD4=FMODO4
       FMOD5=FMODO5
       ELSE IF(KASE.EQ.2)THEN
       FMOD3=(FMODI3*RADRAT+FMODO3)/(1.0+RADRAT)
       FMOD4=(FMODI4*RADRAT+FMODO4)/(1.0+RADRAT)
       FMOD5=(FMODI5*RADRAT+FMODO5)/(1.0+RADRAT)
       END IF
       END IF
C
C      ****INTEGRATED MEAN WALL FRICTION MODULUS (SIMPSON'S RULE)
C
       IF(NITER.EQ.NITMAX)THEN
       IF(MSTEP.EQ.1)THEN
       FMODM=2*FMOD3
       FMOD1=FMOD3
```

```
                ICOUNT=1
                ELSE IF(MSTEP.GT.1)THEN
                ICOUNT=ICOUNT+1
                IF(ICOUNT.EQ.2)THEN
                FMOD2=FMOD3
                ELSE IF(ICOUNT.EQ.3)THEN
                FMODM=(FMODM*(X-2*DELTX)+(FMOD3+4*FMOD2+FMOD1)*(DELTX/3))/X
                FMOD1=FMOD3
                ICOUNT=1
                END IF
                END IF
                END IF
C
C       ****COMPUTE DEFECT PRESSURE AND CONTRIBUTIONS IF REQUIRED
C
                IF(KSOLN.EQ.3)THEN
                DPFRIC=-2*FMOD3*X/(RENUM*DHFACT**2)
                DPAV=DPFRIC
                ELSE IF(KSOLN.EQ.1.OR.KSOLN.EQ.2)THEN
C       ————X-SECTION AVERAGED DEFECT PRESSURE————
                DPAV=0.0
                DO 140 M=2,NDIV,2
                DPAV=DPAV+RADFN4*(RAD(M-1)*P(2,M-1)+4*RAD(M)*P(2,M)+
          1     RAD(M+1)*P(2,M+1))
140             CONTINUE
C       ————MOMENTUM CONTRIBUTION————
                PMOM1=0.0
                DO 150 M=2,NDIV,2
                PMOM1=PMOM1+RADFN4*(RAD(M-1)*U(2,M-1)**2+4*RAD(M)*U(2,M)**2+
          1     RAD(M+1)*U(2,M+1)**2)
150             CONTINUE
                DPMOM=-(PMOM1-PMOM)
C       ————X-SECTION AVERAGED DENSITY AND BUOYANCY CONTRIBUTION————
                FRHOA1=0.0
                DO 160 M=2,NDIV,2
                FRHOA1=FRHOA1+RADFN4*(RAD(M-1)*FRHO(M-1)+4*RAD(M)*FRHO(M)+
          1     RAD(M+1)*FRHO(M+1))
160             CONTINUE
                DPBUOY=DPBUOY-R6*(FRHOA+FRHOA1-2.0)*DELTX/2.0
C       ————WALL FRICTION CONTRIBUTION————
                DPFRIC=DPAV-DPBUOY-DPMOM
                END IF
C
C       ****LENGTH AVERAGED FRICTION MODULI BASED ON PRESSURE
C
                IF(KSOLN.EQ.1.OR.KSOLN.EQ.2)THEN
                FMODAP=-(DPAV*RENUM*DHFACT**2)/(2*X)
                FMODAV=-(DPFRIC*RENUM*DHFACT**2)/(2*X)
                ELSE IF(KSOLN.EQ.3)THEN
                FMODAV=FMOD3
                FMODAP=FMOD3
                END IF
C
C       ****LOCAL WALL HEAT FLUXES
C
                HFI3=HFLUXI
                IF(KKTBCI.EQ.1)THEN
                HFI4=HFLUXI
                HFI5=HFLUXI
                ELSE
```

```
      HFI4=(11*T(2,1)-18*T(2,2)+9*T(2,3)-2*T(2,4))*(FK(1)/(6*DELTY))
      HFI5=(25*T(2,1)-48*T(2,2)+36*T(2,3)-16*T(2,4)+3*T(2,5))*
     1 (FK(1)/(12*DELTY))
      END IF
      HFO3=HFLUXO
      IF(KKTBCO.EQ.1)THEN
      HFO4=HFLUXO
      HFO5=HFLUXO
      ELSE
      HFO4=(11*T(2,NP1)-18*T(2,NDIV)+9*T(2,NM1)-2*T(2,NM2))*
     1 (FK(NP1)/(6*DELTY))
      HFO5=(25*T(2,NP1)-48*T(2,NDIV)+36*T(2,NM1)-16*T(2,NM2)+
     1 3*T(2,NM3))*(FK(NP1)/(12*DELTY))
      END IF
C
C     ****LOCAL BOUNDARY TEMPERATURES
C
      TI3=T(2,1)
      IF(KKTBCI.EQ.2)THEN
      TI4=T(2,1)
      TI5=T(2,1)
      ELSE
      TI4=(HFLUXI*(6*DELTY/FK(1))+18*T(2,2)-9*T(2,3)+2*T(2,4))/11
      TI5=(HFLUXI*(12*DELTY/FK(1))+48*T(2,2)-36*T(2,3)+16*T(2,4)
     1 -3*T(2,5))/25
      END IF
      TO3=T(2,NP1)
      IF(KKTBCO.EQ.2)THEN
      TO4=T(2,NP1)
      TO5=T(2,NP1)
      ELSE
      TO4=(HFLUXO*(6*DELTY/FK(NP1))+18*T(2,NDIV)-9*T(2,NM1)+
     1 2*T(2,NM2))/11
      TO5=(HFLUXO*(12*DELTY/FK(NP1))+48*T(2,NDIV)-36*T(2,NM1)+
     1 16*T(2,NM2)-3*T(2,NM3))/25
      END IF
C
C     ****LOCAL BULK TEMPERATURE
C
      SUMUCT=0.0
      DO 500 M=2,NDIV,2
      UC1=U(2,M-1)*FCPM(M-1)*RAD(M-1)
      UC2=4*U(2,M)*FCPM(M)*RAD(M)
      UC3=U(2,M+1)*FCPM(M+1)*RAD(M+1)
      SUMUCT=SUMUCT+(UC1*T(2,M-1)+UC2*T(2,M)+UC3*T(2,M+1))*DELTY/3.0
500   CONTINUE
      TBULK=2.0*SUMUCT/(FCPM(NP2)*(1.0+RADRAT))
C
C     ****LOCAL X-SECTION AVERAGED TEMPERATURE
C
      TAV=0.0
      DO 550 M=2,NDIV,2
      TAV=TAV+RADFN4*(RAD(M-1)*T(2,M-1)+4*RAD(M)*T(2,M)+
     1 RAD(M+1)*T(2,M+1))
550   CONTINUE
C
C     ****FLUID PROPERTIES
C
      T(2,NP2)=TBULK
      T(2,NP3)=TAV
```

```
      CALL PROPS(1,NP3,2)
C
C     ****LOCAL NUSSELT NUMBERS
C
      IF(KASE.EQ.2.AND.HFI3.NE.0.0)THEN
      NUI3=HFI3*DHFACT/(TI3-TBULK)
      NUI3X=NUI3/FK(NP2)
      NUI4=HFI4*DHFACT/(TI4-TBULK)
      NUI4X=NUI4/FK(NP2)
      NUI5=HFI5*DHFACT/(TI5-TBULK)
      NUI5X=NUI5/FK(NP2)
      END IF
      IF(HFO3.NE.0.0)THEN
      NUO3=HFO3*DHFACT/(TO3-TBULK)
      NUO3X=NUO3/FK(NP2)
      NUO4=HFO4*DHFACT/(TO4-TBULK)
      NUO4X=NUO4/FK(NP2)
      NUO5=HFO5*DHFACT/(TO5-TBULK)
      NUO5X=NUO5/FK(NP2)
      END IF
C--------------------------------------------------------------------
C     PRINT AND STORE STATION RESULTS
C--------------------------------------------------------------------
C
C     ****PRINT STATION RESULTS AT SPECIFIED STEPS
C
      IF(MSTEP.EQ.MSTAT.OR.MSTEP.EQ.1)THEN
      WRITE(NO,650)NITER,MSTEP,X,DELTX
650   FORMAT('1','STATION VARIABLES:',3X,
     1 'ITERATION NO.=',I2,7X,'STEP NO.=',I4,7X,'X=',F10.5,7X,
     2 'DX=',F8.5,7X,'(BASED ON DOMAIN WIDTH)',/,1X,128('*'))
      WRITE(NO,660)REI,REX,PRI,PRX,PEI,PEX,XCROSS,XCROSX,XSTAR,XSTARX
660   FORMAT(/,40X,'**HYDRAULIC DIAMETER BASED DIMENSIONLESS GROUPS**'
     1 ,//,30X,'INLET BULK PROPS',10X,'LOCAL BULK PROPS',/,
     2 15X,'REYNOLDS NO. = ',F14.2,13X,F14.2,/,
     3 15X,'PRANDTL NO.  = ',F14.2,13X,F14.2,/,
     4 15X,'PECLET NO.   = ',E14.5,13X,E14.5,/,
     5 15X,'(X/DH)/RE    = ',E14.5,13X,E14.5,/,
     6 15X,'(X/DH)/PE    = ',E14.5,13X,E14.5,//)
      IF(KSOLN.EQ.1.OR.KSOLN.EQ.2)THEN
      WRITE(NO,661)DPAV,DPMOM,DPBUOY,DPFRIC
661   FORMAT(15X,'PRESSURE DIFFERENCES:',
     1 20X,'TOTAL ',11X,'MOMENTUM',10X,'BUOYANCY',10X,'FRICTION',/
     2 56X,'DEFECT',11X,'CONTRIB.',10X,'CONTRIB.',10X,'CONTRIB.',/
     3 47X,4(6X,E12.5),//)
      END IF
      WRITE(NO,662)FMODAV,FMODAP,FMOD03,FMOD04,FMOD05
662   FORMAT(15X,'WALL FRICTION MODULI (F.RE):',
     1 /,47X,'(F.RE)AVE = ',F10.4,' (FLOW LENGTH AVERAGE)',
     2 /,47X,'(F.RE)APP = ',F10.4,' (APPARENT FLOW LENGTH AVERAGE)',
     3 //,56X,'3-POINT',11X,'4-POINT',11X,'5-POINT',
     4 /,37X,'(OUTER) ',3(8X,F10.4))
      IF(KASE.EQ.2)THEN
      WRITE(NO,664)FMODI3,FMODI4,FMODI5
664   FORMAT(37X,'(INNER) ',3(8X,F10.4))
      END IF
      WRITE(NO,666)FMOD3,FMOD4,FMOD5
666   FORMAT(24X,'(PERIPHERAL AVERAGE) ',3(8X,F10.4)//)
      WRITE(NO,670)NUO3,NUO4,NUO5,NUO3X,NUO4X,NUO5X
```

```fortran
  670       FORMAT(15X,'NUSSELT NUMBERS:',
     1   25X,'3-POINT',11X,'4-POINT',11X,'5-POINT',/,
     2   18X,'(OUTER - INLET BULK PROPS) ',3(8X,F10.4),/,
     3   18X,'(OUTER - LOCAL BULK PROPS) ',3(8X,F10.4))
            IF(KASE.EQ.2)THEN
            WRITE(NO,675)NUI3,NUI4,NUI5,NUI3X,NUI4X,NUI5X
  675       FORMAT(18X,'(INNER - INLET BULK PROPS) ',3(8X,F10.4),/,
     1   18X,'(INNER - LOCAL BULK PROPS) ',3(8X,F10.4))
            END IF
            WRITE(NO,680)T03,T04,T05,TI3,TI4,TI5
  680       FORMAT(//,15X,'BOUNDARY TEMPERATURES:',
     1   19X,'3-POINT',11X,'4-POINT',11X,'5-POINT',/
     3   37X,'(OUTER) ',3(6X,E12.5),/,37X,'(INNER) ',3(6X,E12.5)//)
            WRITE(NO,685)TBULK,TBAL1,TAV
  685       FORMAT(15X,'MEAN TEMPERATURES:',
     1   /,47X,'(T)BULK = ',E12.5,' (FROM U & T PROFILES)',
     2   /,47X,'(T)BAL  = ',E12.5,' (FROM ENERGY BALANCE)',
     3   /,47X,'(T)AVE  = ',E12.5,' (X-SECTIONAL AVERAGE)',//)
            WRITE(NO,690)(TY5(I),I=1,4),FRHO(NP2),FMU(NP2),FK(NP2),FCP(NP2),
     1   FRHO(NP3),FMU(NP3),FK(NP3),FCP(NP3),
     2   FRHO(NP1),FMU(NP1),FK(NP1),FCP(NP1),FRHO(1),FMU(1),FK(1),FCP(1)
  690       FORMAT(15X,'PROPERTY RATIOS:',14X,
     1   4(11X,1A7)
     2   /,32X,'(BULK/DATUM) ',4(9X,F9.5),
     3   /,29X,'(AVERAGE/DATUM) ',4(9X,F9.5),
     4   /,22X,'(OUTER BOUNDARY/DATUM) ',4(9X,F9.5),
     5   /,22X,'(INNER BOUNDARY/DATUM) ',4(9X,F9.5),//)
            IF(NITER.EQ.NITMAX.AND.MSTEP.EQ.MSTAT)MSTAT=MSTAT+ISTAT
            END IF
C
C     ****STORE FLUID FLOW RESULTS
C
            IF(NITER.EQ.NITMAX)THEN
            WRITE(NSF,692)MSTEP,XCROSS,FMODI3,FMOD03,FMOD3,FMODM,
     1   FMODAV,FMODAP,DPAV,DPMOM,DPBUOY,DPFRIC
  692       FORMAT(1X,I4,2X,E12.5,6(1X,F9.3),4(2X,E11.4))
            END IF
C
C     ****STORE HEAT TRANSFER RESULTS
C
            IF(NITER.EQ.NITMAX)THEN
            WRITE(NSH,694)MSTEP,XSTAR,TBULK,TBAL1,TAV,TI3,T03,NUI3,NU03
  694       FORMAT(1X,I4,6(2X,E12.5),2(2X,F10.4))
            END IF
C
C     ****STORE NUSSELT NO. & FRICTION MODULUS FOR EACH BOUNDARY
C
            IF(KSNUI.EQ.1.AND.NITER.EQ.NITMAX)WRITE(NS1,*)XSTAR,NUI3
            IF(KSNUO.EQ.1.AND.NITER.EQ.NITMAX)WRITE(NS2,*)XSTAR,NU03
            IF(KSFRI.EQ.1.AND.NITER.EQ.NITMAX)WRITE(NS5,*)XCROSS,FMODI3
            IF(KSFRO.EQ.1.AND.NITER.EQ.NITMAX)WRITE(NS6,*)XCROSS,FMOD03
C-----------------------------------------------------------------
C     PRINT AND STORE PROFILE RESULTS
C-----------------------------------------------------------------
C
C     ****PRINT PROFILE VARIABLES AT SPECIFIED STEPS
C
            IF(MSTEP.EQ.MPROF.OR.MSTEP.EQ.1)THEN
            WRITE(NO,695)NITER,MSTEP,X,DELTX
```

```
  695        FORMAT('1','PROFILE VARIABLES:',3X,
      1        'ITERATION NO.=',I2,7X,'STEP NO.=',I4,7X,'X=',F10.5,7X,
      2        'DX=',F8.5,7X,'(BASED ON DOMAIN WIDTH)',/,1X,128('*'))
             WRITE(NO,700)(M,U(2,M),V(2,M),P(2,M),W(M),T(2,M),E(M),
      1        M+ND2,U(2,M+ND2),V(2,M+ND2),P(2,M+ND2),W(M+ND2),
      2        T(2,M+ND2),E(M+ND2),M=1,ND2)
  700        FORMAT(/,
      1        2(3X,'M        U          V          P        W          T              E',
      2        9X),//,2(1X,I3,F9.5,F11.6,F10.4,F8.5,2E12.5))
             WRITE(NO,705)NP1,U(2,NP1),V(2,NP1),P(2,NP1),
      1        W(NP1),T(2,NP1),E(NP1)
  705        FORMAT(67X,I3,F9.5,F11.6,F10.4,F8.5,2E12.5)
             IF(NITER.EQ.NITMAX.AND.MSTEP.EQ.MPROF)MPROF=MPROF+IPROF
             END IF
C
C            ****STORE AXIAL VELOCITY PROFILE AT SPECIFIED STEPS
C
             IF(MSTEP.EQ.LSU(MSU).AND.NITER.EQ.NITMAX)THEN
             IROWU=0
             DO 706 M=1,NP1,INCRU
             IROWU=IROWU+1
             US(MSU+2,IROWU)=U(2,M)
  706        CONTINUE
             US(1,MSU)=XCROSS
             MSU=MSU+1
             END IF
C
C            ****STORE AXIAL VELOCITY AT EQUALLY-SPACED TRANSVERSE POSITIONS
C
             IF(NITER.EQ.NITMAX)THEN
             INCRU1=NDIV/10
             WRITE(NS7,708)MSTEP,XCROSS,(U(2,M),M=1,NP1,INCRU1)
  708        FORMAT(1X,I4,1X,E12.5,11(1X,F9.5))
             END IF
C
C            ****STORE TEMPERATURE PROFILE AT SPECIFIED STEPS
C
             IF(MSTEP.EQ.LST(MST).AND.NITER.EQ.NITMAX)THEN
             IROWT=0
             DO 710 M=1,NP1,INCRT
             IROWT=IROWT+1
             TS(MST+2,IROWT)=T(2,M)
  710        CONTINUE
             TS(1,MST)=XSTAR
             MST=MST+1
             END IF
C―――――――――――――――――――――――――――――――――――――――――――――――――
C            PRINT TRANSVERSE PROFILES ON LINEPRINTER
C―――――――――――――――――――――――――――――――――――――――――――――――――
             IF((MSTEP.EQ.MPLOT.OR.MSTEP.EQ.1).AND.NITER.EQ.NITMAX)THEN
             WRITE(NO,712)NITER,MSTEP,X,DELTX
  712        FORMAT('1','PROFILE PLOTS:',7X,
      1        'ITERATION NO.=',I2,7X,'STEP NO.=',I4,7X,'X=',F10.5,7X,
      2        'DX=',F8.5,7X,'(BASED ON DOMAIN WIDTH)',/,1X,128('*'))
C
C            ****FIND MAX.AND MIN.VALUES OF DEPENDENT VARIABLES
C
             UMIN=1.0E30
             UMAX=-1.0E30
             TMIN=1.0E30
```

```fortran
      TMAX=-1.0E30
      DO 715 M=1,NP1
      UMIN=AMIN1(UMIN,U(2,M))
      UMAX=AMAX1(UMAX,U(2,M))
      TMIN=AMIN1(TMIN,T(2,M))
715   TMAX=AMAX1(TMAX,T(2,M))
C
C     ****PRINT MIN.AND MAX.VALUES
C
      WRITE(NO,720)UMIN,TMIN,UMAX,TMAX
720   FORMAT(1X,'ORDINATE',7X,'U',11X,'T',/
     1 2X,'MIN.VAL.',2E12.3,/,2X,'MAX.VAL.',2E12.3,/)
C
C     ****SCALE ALTERNATE VALUES OF VARIABLES TO RANGE 0 TO 50
C
      DO 725 M=1,NP1,2
      IA=(M+1)/2
      IU(IA)=NINT(1.0+50*(U(2,M)-UMIN)*(1.0/(UMAX-UMIN+1.0E-30)))
725   IT(IA)=NINT(1.0+50*(T(2,M)-TMIN)*(1.0/(TMAX-TMIN+1.0E-30)))
C
C     ****LOOP TO PRODUCE CONSTANT ORDINATE LINES
C
      IODIV=51
      DO 745  LINE =1,51
      IO=52-LINE
C
C     ****MARK AXES
C
      IF(IO.EQ.1.OR.IO.EQ.51)THEN
      DO 730 IA=1,ND2+1
730   SYMB(IA)=DOT
      DO 735 IA=6,ND2+1,5
735   SYMB(IA)=CROSS
      ELSE IF(IO.EQ.IODIV)THEN
      SYMB(1)=CROSS
      SYMB(ND2+1)=CROSS
      ELSE
      SYMB(1)=DOT
      SYMB(ND2+1)=DOT
      END IF
C
C     ****SEARCH FOR VALUES AND ASSIGN SYMBOLS
C
      DO 738 IA=1,ND2+1
      IF(IU(IA).EQ.IO)SYMB(IA)=VEL
      IF(IT(IA).EQ.IO)SYMB(IA)=TEMP
738   CONTINUE
C
C     ****PRINT LINE AND ORDINATE VALUE
C
      IF(IO.EQ.IODIV)THEN
      IODIV=IODIV-5
      ORD=0.02*(IO-1)
      WRITE(NO,740)ORD,(SYMB(IA),IA=1,ND2+1)
740   FORMAT(2X,F3.1,1X,51A1)
      ELSE
      WRITE(NO,742)(SYMB(IA),IA=1,ND2+1)
742   FORMAT(6X,51A1)
      END IF
```

```
C
C       ****REFILL ARRAY SYMB WITH BLANKS
        DO 744 IA=1,ND2+1
744     SYMB(IA)=BLANK
745     CONTINUE
C
C       ****PRINT ABSCISSA VALUES AND ANNOTATE AXES
C
        IADIV=INT(NP1/10)
        DO 748 IY=1,IADIV
        SYMB(5*IY)=DIGIT(IY)
748     SYMB(5*IY+1)=DIGIT(1)
        SYMB(1)=DIGIT(1)
        WRITE(NO,749)(SYMB(IA),IA=1,ND2+1)
749     FORMAT(6X,51A1)
        WRITE(NO,750)TY1(KASE)
750     FORMAT('0','ABSCISSA IS TRANSVERSE GRID POSITION FROM',1A12)
        IF(NITER.EQ.NITMAX.AND.MSTEP.EQ.MPLOT)MPLOT=MPLOT+IPLOT
        END IF
775     CONTINUE
C───────────────────────────────────────────────────────────────────
C       END OF STEP - UPDATE VARIABLES
C───────────────────────────────────────────────────────────────────
C
C       ****PROFILE VARIABLES
C
        DO 800 M=1,NP1
        P(1,M)=P(2,M)
        U(1,M)=U(2,M)
        V(1,M)=V(2,M)
800     T(1,M)=T(2,M)
C
C       ****STATION VARIABLES
C
        TBAL=TBAL1
        CUP=FCPM(NP2)
        FRHOA=FRHOA1
900     CONTINUE
C───────────────────────────────────────────────────────────────────
C       END OF PROBLEM - PRINT SUMMARY TABLES & STORAGE FILES
C───────────────────────────────────────────────────────────────────
        WRITE(NO,920)
920     FORMAT('1','SUMMARY - FLUID FLOW RESULTS: (INLET BULK PROPS)',/,
     1  1X,128('*'),//,1X,'STEP',3X,'(X/DH)/RE',2X,'(F.RE)IN ',1X,
     2  '(F.RE)OUT',1X,'(F.RE)LOC',1X,'(F.RE)MEAN',1X,'(F.RE)AVE',
     3  1X,'(F.RE)APP',5X,'(DP)',7X,'(DP)MOM',6X,'(DP)BUOY',
     4  5X,'(DP)FRIC',/)
        REWIND NSF
        DO 940 M=1,NSTEP
        READ(NSF,*)MSTEP,XCROSS,FMODI3,FMODO3,FMOD3,FMODM,
     1  FMODAV,FMODAP,DPAV,DPMOM,DPBUOY,DPFRIC
        WRITE(NO,930)MSTEP,XCROSS,FMODI3,FMODO3,FMOD3,FMODM,
     1  FMODAV,FMODAP,DPAV,DPMOM,DPBUOY,DPFRIC
930     FORMAT(1X,I4,2X,E12.5,6(1X,F9.3),4(2X,E11.4))
940     CONTINUE
C
        IF(KSOLN.EQ.1.OR.KSOLN.EQ.3)THEN
        WRITE(NO,950)
950     FORMAT('1','SUMMARY - HEAT TRANSFER RESULTS: (INLET BULK PROPS)'
     1  ,/,1X,128('*'),//,1X,'STEP',3X,'(X/DH)/PE',5X,'(T)BULK',8X,
```

```
      2    '(T)BAL ',8X,'(T)AVE ',6X,'(T)INNER',6X,'(T)OUTER',5X,
      3    '(NU)INNER',3X,'(NU)OUTER',/)
           REWIND NSH
           DO 975 M=1,NSTEP
           READ(NSH,*)MSTEP,XSTAR,TBULK,TBAL1,TAV,TI3,TO3,NUI3,NUO3
           WRITE(NO,960)MSTEP,XSTAR,TBULK,TBAL1,TAV,TI3,TO3,NUI3,NUO3
960        FORMAT(1X,I4,6(2X,E12.5),2(2X,F10.4))
975        CONTINUE
           END IF
C
           IF(NSU.GT.0)THEN
           WRITE(NO,986)
986        FORMAT('1','SUMMARY - VELOCITY PROFILE DEVELOPMENT:',
      1    /,1X,128('*'),//,1X,'STEP',5X,'(X/D)/RE',2X,'U(Y=0.0)',2X,
      2    'U(Y=0.1)',2X,'U(Y=0.2)',2X,'U(Y=0.3)',2X,'U(Y=0.4)',2X,
      3    'U(Y=0.5)',2X,'U(Y=0.6)',2X,'U(Y=0.7)',2X,'U(Y=0.8)',2X,
      4    'U(Y=0.9)',2X,'U(Y=1.0)',/)
           REWIND NS7
           MSU=1
           IF(LSU(MSU).EQ.0)MSU=2
           DO 990 I=1,NSTEP
           READ(NS7,*)MSTEP,XCROSS,(U(2,M),M=1,NP1,INCRU1)
           IF(MSTEP.EQ.LSU(MSU))THEN
           MSU=MSU+1
           WRITE(NO,987)MSTEP,XCROSS,(U(2,M),M=1,NP1,INCRU1)
987        FORMAT(1X,I4,1X,E12.5,11(1X,F9.5))
           END IF
990        CONTINUE
C
           DO 992 M=1,IROWU
           WRITE(NS3,991)(US(I,M),I=1,NSU+2)
991        FORMAT(26(1X,E12.5))
992        CONTINUE
           END IF
C
           IF(NST.GT.0)THEN
           DO 995 M=1,IROWT
           WRITE(NS4,994)(TS(I,M),I=1,NST+2)
994        FORMAT(26(1X,E12.5))
995        CONTINUE
           END IF
C-----------------------------------------------------------------
C     END OF RUN
C-----------------------------------------------------------------
           WRITE(NO,2000)
2000       FORMAT('0',56X,'E N D   O F   R U N')
           STOP
           END
```

```fortran
C*******************************************************************
C       SUBROUTINE TO COMPUTE PROPERTY RATIOS(RHO,MU,K,CP)AND PROPERTY *
C       TEMPERATURE DERIVATIVES(MU AND K ONLY)AT SPECIFIED TEMPERATURES*
C*******************************************************************
C
        PARAMETER (MAX1=101,MAX2=51,MAX3=103,MAX4=21,MAX5=24,MAX33=297)
        COMMON /C1/FRHO(MAX3),FMU(MAX3),DFMU(MAX3),FK(MAX3),DFK(MAX3),
     1  FCP(MAX3),FCPM(MAX3),PCON(4,6),KPROP(4),CUP,RHORAT
        COMMON /C2/U(2,MAX1),V(2,MAX1),P(2,MAX1),W(MAX1),
     1  T(2,MAX3),E(MAX1)
        COMMON /C4/X,DELTX,DELTY,RADRAT,RADFN1,RAD(MAX1),Y(MAX1)
C
C       ****DENSITY
C
        IF(KPROP(1).EQ.0.AND.X.EQ.0.0)THEN
        DO 5 M=M1,M2
5       FRHO(M)=1.0
        ELSE IF(KPROP(1).EQ.1)THEN
        DO 10 M=M1,M2
10      FRHO(M)=PCON(1,1)+T(M3,M)*(PCON(1,2)+T(M3,M)*(PCON(1,3)+
     1  T(M3,M)*(PCON(1,4)+T(M3,M)*(PCON(1,5)+T(M3,M)*PCON(1,6)))))
        END IF
C
C       ****VISCOSITY
C
        IF(KPROP(2).EQ.0.AND.X.EQ.0.0)THEN
        DO 15 M=M1,M2
        FMU(M)=1.0
15      DFMU(M)=0.0
        ELSE IF(KPROP(2).EQ.1)THEN
        DO 20 M=M1,M2
        FMU(M)=PCON(2,1)+T(M3,M)*(PCON(2,2)+T(M3,M)*(PCON(2,3)+
     1  T(M3,M)*(PCON(2,4)+T(M3,M)*(PCON(2,5)+T(M3,M)*PCON(2,6)))))
        DFMU(M)=PCON(2,2)+T(M3,M)*(2*PCON(2,3)*T(M3,M)*(3*PCON(2,4)+
     1  T(M3,M)*(4*PCON(2,5)+T(M3,M)*5*PCON(2,6))))
20      CONTINUE
        ELSE IF(KPROP(2).EQ.2)THEN
        DO 30 M=M1,M2
        COMMN=PCON(2,1)*T(M3,M)+PCON(2,2)
        FMU(M)=COMMN**(-PCON(2,3))
30      DFMU(M)=-PCON(2,1)*PCON(2,3)*COMMN**(-PCON(2,3)+1)
        END IF
C
C       ****THERMAL CONDUCTIVITY
C
        IF(KPROP(3).EQ.0.AND.X.EQ.0.0)THEN
        DO 35 M=M1,M2
        FK(M)=1.0
35      DFK(M)=0.0
        ELSE IF(KPROP(3).EQ.1)THEN
        DO 40 M=M1,M2
        FK(M)=PCON(3,1)+T(M3,M)*(PCON(3,2)+T(M3,M)*(PCON(3,3)+
     1  T(M3,M)*(PCON(3,4)+T(M3,M)*(PCON(3,5)+T(M3,M)*PCON(3,6)))))
        DFK(M)=PCON(3,2)+T(M3,M)*(2*PCON(3,3)*T(M3,M)*(3*PCON(3,4)+
     1  T(M3,M)*(4*PCON(3,5)+T(M3,M)*5*PCON(3,6))))
40      CONTINUE
        END IF
```

```fortran
C
C     ****SPECIFIC HEAT
C
      IF(KPROP(4).EQ.0.AND.X.EQ.0.0)THEN
      DO 45 M=M1,M2
      FCP(M)=1.0
45    FCPM(M)=1.0
      ELSE IF(KPROP(4).EQ.1)THEN
      DO 50 M=M1,M2
      FCP(M)=PCON(4,1)+T(M3,M)*(PCON(4,2)+T(M3,M)*(PCON(4,3)+
     1 T(M3,M)*(PCON(4,4)+T(M3,M)*(PCON(4,5)+T(M3,M)*PCON(4,6)))))
      FCPM(M)=PCON(4,1)+T(M3,M)*(PCON(4,2)/2+T(M3,M)*(PCON(4,3)/3+
     1 T(M3,M)*(PCON(4,4)/4+T(M3,M)*(PCON(4,5)/5+
     2 T(M3,M)*PCON(4,6)/6))))
50    CONTINUE
      END IF
      RETURN
      END
```

```
      SUBROUTINE BANDUP
C*********************************************************************
C        SUBROUTINE TO COMPUTE VELOCITIES, PRESSURE AND STREAMFUNCTION. *
C        COEFFICIENTS AND RIGHT-HAND SIDES OF INTEGRAL CONTINUITY       *
C        EQUATION AND CONTINUITY AND MOMENTUM DIFFERENTIAL EQUATIONS    *
C        ARE BANDED IN A FORM SUITABLE FOR SOLUTION BY SUBROUTINE SOLVE.*
C        TRANSVERSE VELOCITIES ARE SUBSEQUENTLY CALCULATED USING        *
C        CONTINUITY DIFFERENTIAL EQUATION.                              *
C*********************************************************************
C
      DOUBLE PRECISION A,B,Z
C
      PARAMETER (MAX1=101,MAX2=51,MAX3=103,MAX4=21,MAX5=24,MAX33=297)
      COMMON /C1/FRHO(MAX3),FMU(MAX3),DFMU(MAX3),FK(MAX3),DFK(MAX3),
     1 FCP(MAX3),FCPM(MAX3),PCON(4,6),KPROP(4),CUP,RHORAT
      COMMON /C2/U(2,MAX1),V(2,MAX1),P(2,MAX1),W(MAX1),
     1 T(2,MAX3),E(MAX1)
      COMMON /C4/X,DELTX,DELTY,RADRAT,RADFN1,RAD(MAX1),Y(MAX1)
      COMMON /C5/R1,R2,R3,R4,R5,R6,R7,R8,R9,NM2,NM1,NDIV,NP1,NP2,N2M3,
     1 N3M3,RX1,RX2,RDYDX2
      COMMON /C6/KASE,KVIDI,KEBAL,NDIR
      COMMON /C7/A(8,MAX33),B(MAX33),Z(MAX33)
C
C--------------------------------------------------------------------
C     COMPUTE BAND PARAMETERS
C--------------------------------------------------------------------
      MSUB=4
      MSUP=3
      MBAND=MSUB+MSUP+1
      NBAND=N3M3
      JMID=MSUB+1
C--------------------------------------------------------------------
C     CLEAR ARRAYS
C--------------------------------------------------------------------
      DO 10 I=1,NBAND
      B(I)=0.0
      DO 10 J=1,MBAND
10    A(J,I)=0.0
C--------------------------------------------------------------------
C     MOMENTUM EQUATIONS
C--------------------------------------------------------------------
C
C
C     ****ASSEMBLE COEFFICIENTS AND RIGHT-HAND SIDES
C
      DO 30 M=2,NDIV
      A1=RX1*U(2,M)
      A2=R2*V(2,M)
      A3=R5*FMU(M)
      A4=DFMU(M)*(R5/4)*(T(2,M+1)-T(2,M-1))
      RADFN=RADFN1/RAD(M)
C        ------AXIAL------
      I=2+(M-2)*3
      A(JMID-3,I)=-A2-A3*(1.0-RADFN)+A4
      A(JMID,I)=A1+2*A3
      A(JMID-1,I)=RX1
      A(JMID+3,I)=A2-A3*(1.0+RADFN)-A4
      B(I)=A1*U(1,M)+RX1*P(1,M)-R6*(FRHO(M)-1.0)
```

```fortran
C             ———TRANSVERSE———
              I=I-1
              A(JMID,I)=1.0
              A(JMID+3,I)=-1.0
30            CONTINUE
C
C         ****INNER BOUNDARY MODIFICATIONS
C
C             ———AXIAL———
              IF(KASE.EQ.1)THEN
              A(JMID,2)=A(JMID,2)+(4.0/3)*A(JMID-3,2)
              A(JMID+3,2)=A(JMID+3,2)-(1.0/3)*A(JMID-3,2)
              END IF
              A(JMID-3,2)=0.0
C
C         ****OUTER BOUNDARY MODIFICATIONS
C
C             ———AXIAL———
              A(JMID+3,N3M3-1)=0.0
C             ———TRANSVERSE———
              A(JMID+2,N3M3-2)=A(JMID+3,N3M3-2)
              A(JMID+3,N3M3-2)=0.0
C————————————————————————————————————————————————————————
C         INTEGRAL CONTINUITY EQUATION
C————————————————————————————————————————————————————————
C
C         ****ASSEMBLE COEFFICIENTS AND RIGHT-HAND SIDES
C
              A1=DELTY/2
              DO 50 M=2,NDIV
              I=3*(M-1)
              A(JMID,I)=-1.0
              A(JMID-3,I)=1.0
              A(JMID-4,I)=A1*RAD(M-1)
              A(JMID-1,I)=A1*RAD(M)
50            CONTINUE
C
C         ****INNER BOUNDARY MODIFICATIONS
C
              IF(KASE.EQ.1)THEN
              A(JMID-1,3)=A(JMID-1,3)+(4.0/3)*A(JMID-4,3)
              A(JMID+2,3)=A(JMID+2,3)-(1.0/3)*A(JMID-4,3)
              END IF
              A(JMID-4,3)=0.0
              A(JMID-3,3)=0.0
C
C         ****OUTER BOUNDARY MODIFICATIONS
C
              A(JMID-1,N3M3)=2.0*A(JMID-1,N3M3)
              A(JMID,N3M3)=0.0
              B(N3M3)=(1.0+RADRAT)/2.0
C————————————————————————————————————————————————————————
C         SOLVE EQUATIONS AND RETURN RESULTS
C————————————————————————————————————————————————————————
              CALL SOLVE(MBAND,NBAND,MSUB,MSUP)
```

```fortran
C
C     ****STORE NEW AXIAL VELOCITY PROFILE
C
      DO 60 M=2,NDIV
      I=2+(M-2)*3
      U(2,M)=Z(I)
60    CONTINUE
      U(2,NP1)=0.0
      IF(KASE.EQ.1)THEN
      U(2,1)=(4.0/3)*U(2,2)-(1.0/3)*U(2,3)
      ELSE
      U(2,1)=0.0
      END IF
C
C     ****STORE NEW PRESSURE PROFILE
C
      DO 70 M=2,NDIV
      I=1+(M-2)*3
70    P(2,M)=Z(I)
      P(2,NP1)=Z(NBAND)
      P(2,1)=P(2,2)
C
C     ****STORE NEW STREAMFUNCTION PROFILE
C
      DO 80 M=2,NM1
      I=3*(M-1)
80    W(M)=Z(I)
      W(1)=0.0
      W(NP1)=(1.0+RADRAT)/2.0
      W(NDIV)=W(NP1)-A1*RAD(NDIV)*U(2,NDIV)
C
C     ****COMPUTE NEW TRANSVERSE VELOCITIES
C
      V(2,1)=0.0
      V(2,NP1)=0.0
      DO 90 M=2,NDIV
      V(2,M)=(RAD(M-1)*V(2,M-1)-RDYDX2*(RAD(M)*(U(2,M)-U(1,M))+
     1 RAD(M-1)*(U(2,M-1)-U(1,M-1))))/RAD(M)
90    CONTINUE
      VRLAST=0.0
      DO 100 M=NDIV,2,-1
      VR=(RAD(M+1)*VRLAST+RDYDX2*(RAD(M)*(U(2,M)-U(1,M))+
     1 RAD(M+1)*(U(2,M+1)-U(1,M+1))))/RAD(M)
      V(2,M)=(1.0-Y(M))*V(2,M)+Y(M)*VR
      VRLAST=VR
100   CONTINUE
      RETURN
      END
```

```fortran
      SUBROUTINE BANDET
C**********************************************************************
C     SUBROUTINE TO COMPUTE TEMPERATURE AND HEATFUNCTION (OPTIONAL). *
C     COEFFICIENTS AND RIGHT-HAND SIDES OF ENERGY DIFFERENTIAL       *
C     EQUATION AND STEPWISE ENERGY BALANCE (OPTIONAL) ARE BANDED     *
C     IN A FORM SUITABLE FOR SUBROUTINE SOLVE.                       *
C**********************************************************************
C
      DOUBLE PRECISION A,B,Z
C
      PARAMETER (MAX1=101,MAX2=51,MAX3=103,MAX4=21,MAX5=24,MAX33=297)
      COMMON /C1/FRHO(MAX3),FMU(MAX3),DFMU(MAX3),FK(MAX3),DFK(MAX3),
     1 FCP(MAX3),FCPM(MAX3),PCON(4,6),KPROP(4),CUP,RHORAT
      COMMON /C2/U(2,MAX1),V(2,MAX1),P(2,MAX1),W(MAX1),
     1 T(2,MAX3),E(MAX1)
      COMMON /C3/KKTBCI,KKTBCO,HFLUXI,HFLUXO,TBAL,TBAL1
      COMMON /C4/X,DELTX,DELTY,RADRAT,RADFN1,RAD(MAX1),Y(MAX1)
      COMMON /C5/R1,R2,R3,R4,R5,R6,R7,R8,R9,NM2,NM1,NDIV,NP1,NP2,N2M3,
     1 N3M3,RX1,RX2,RDYDX2
      COMMON /C6/KASE,KVIDI,KEBAL,NDIR
      COMMON /C7/A(8,MAX33),B(MAX33),Z(MAX33)
C
C--------------------------------------------------------------------
C     COMPUTE BAND PARAMETERS
C--------------------------------------------------------------------
      IF(KEBAL.EQ.0)THEN
      MSUB=1
      MSUP=1
      NBAND=NM1
      INCR=1
      ELSE IF(KEBAL.EQ.1)THEN
      MSUB=3
      MSUP=2
      NBAND=N2M3
      INCR=2
      END IF
      MBAND=MSUB+MSUP+1
      JMID=MSUB+1
      JM=JMID-INCR
      JP=JMID+INCR
C--------------------------------------------------------------------
C     CLEAR ARRAYS
C--------------------------------------------------------------------
      DO 10 I=1,NBAND
      B(I)=0.0
      DO 10 J=1,MBAND
      A(J,I)=0.0
10    CONTINUE
C--------------------------------------------------------------------
C     ENERGY DIFFERENTIAL EQUATION
C--------------------------------------------------------------------
C
C     ****ASSEMBLE COEFFICIENTS AND RIGHT-HAND SIDES
C
      DO 20 M=2,NDIV
      I=1+(M-2)*INCR
      A1=RX1*U(2,M)
      A2=R2*V(2,M)
      A3=R3*FK(M)/FCP(M)
      A4=DFK(M)*(R3/(4*FCP(M)))*(T(2,M+1)-T(2,M-1))
```

- 299 -

```
            RADFN=RADFN1/RAD(M)
            A(JM,I)=-A2-A3*(1.0-RADFN)+A4
            A(JMID,I)=A1+2*A3
            A(JP,I)=A2-A3*(1.0+RADFN)-A4
            B(I)=A1*T(1,M)
   20       CONTINUE
C
C           ****INNER BOUNDARY MODIFICATIONS
C
            IF(KKTBCI.EQ.1)THEN
            A(JMID,1)=A(JMID,1)+(4.0/3)*A(JM,1)
            A(JP,1)=A(JP,1)-(1.0/3)*A(JM,1)
            B(1)=B(1)-HFLUXI*(2*DELTY/(3*FK(1)))*A(JM,1)
            ELSE IF(KKTBCI.EQ.2)THEN
            B(1)=B(1)-A(JM,1)*T(2,1)
            END IF
            A(JM,1)=0.0
C
C           ****OUTER BOUNDARY MODIFICATIONS
C
            IF(KKTBCO.EQ.1)THEN
            A(JMID,NBAND)=A(JMID,NBAND)+(4.0/3)*A(JP,NBAND)
            A(JM,NBAND)=A(JM,NBAND)-(1.0/3)*A(JP,NBAND)
            B(NBAND)=B(NBAND)-HFLUXO*(2*DELTY/(3*FK(NP1)))*A(JP,NBAND)
            ELSE IF(KKTBCO.EQ.2)THEN
            B(NBAND)=B(NBAND)-A(JP,NBAND)*T(2,NP1)
            END IF
            A(JP,NBAND)=0.0
C───────────────────────────────────────────────────────────────
C           STEPWISE ENERGY BALANCE (OPTIONAL)
C───────────────────────────────────────────────────────────────
            CEBAL=DELTX*R7
            IF(KEBAL.EQ.1)THEN
C
C           ****ASSEMBLE COEFFICIENTS AND RIGHT-HAND SIDES
C
            DO 30 M=2,NM1
            I=2*(M-1)
            A(JMID,I)=-1.0
   30       A(JM,I)=1.0
            DO 35 M=2,NM2,2
            I=2*(M-1)
            A(1,I)=U(2,M-1)*FCPM(M-1)*RAD(M-1)*DELTY/3.0
            A(3,I)=4*U(2,M)*FCPM(M)*RAD(M)*DELTY/3.0
            A(5,I)=U(2,M+1)*FCPM(M+1)*RAD(M+1)*DELTY/3.0
   35       CONTINUE
C
C           ****INNER BOUNDARY MODIFICATIONS
C
            A(JM,2)=0.0
            IF(KKTBCI.EQ.1)THEN
            A(3,2)=A(3,2)+(4.0/3)*A(1,2)
            A(5,2)=A(5,2)-(1.0/3)*A(1,2)
            B(2)=B(2)+HFLUXI*(CEBAL*RADRAT-A(1,2)*2*DELTY/(3*FK(1)))
            ELSE IF(KKTBCI.EQ.2)THEN
            A(3,2)=A(3,2)+CEBAL*RADRAT*2*FK(1)/DELTY
            A(5,2)=A(5,2)-CEBAL*RADRAT*0.5*FK(1)/DELTY
            B(2)=B(2)+T(2,1)*CEBAL*RADRAT*3*FK(1)/(2.0*DELTY)
            END IF
            A(1,2)=0.0
```

```
C
C          ****OUTER BOUNDARY MODIFICATIONS
C
           A(3,NBAND)=1.0
           A(JM,NBAND)=U(2,NM1)*FCPM(NM1)*RAD(NM1)*DELTY/3.0
           A(JMID,NBAND)=4*U(2,NDIV)*FCPM(NDIV)*RAD(NDIV)*DELTY/3.0
           B(NBAND)=0.5*CUP*(1.0+RADRAT)*TBAL
           IF(KKTBCO.EQ.1)THEN
           B(NBAND)=B(NBAND)+HFLUXO*CEBAL
           ELSE IF(KKTBCO.EQ.2)THEN
           A(JM,NBAND)=A(JM,NBAND)-CEBAL*0.5*FK(NP1)/DELTY
           A(JMID,NBAND)=A(JMID,NBAND)+CEBAL*2.0*FK(NP1)/DELTY
           B(NBAND)=B(NBAND)+T(2,NP1)*CEBAL*3*FK(NP1)/(2*DELTY)
           END IF
           END IF
C————————————————————————————————————————————————————————————
C          VISCOUS DISSIPATION EFFECT (OPTIONAL)
C————————————————————————————————————————————————————————————
           IF(KVIDI.EQ.1)THEN
           VDSUM=0.0
           DO 45 M=2,NDIV
           I=1+(M-2)*INCR
           VD=FMU(M)*R4*RAD(M)*(U(2,M+1)-U(2,M-1))**2
           B(I)=B(I)+VD/FCP(M)
           IF(KEBAL.EQ.1)VDSUM=VDSUM+VD
45         CONTINUE
           IF(KEBAL.EQ.1)THEN
           VDI=FMU(1)*R4*RAD(1)*(-3*U(2,1)+4*U(2,2)-U(2,3))**2
           VDO=FMU(NP1)*R4*RAD(NP1)*(3*U(2,NP1)-4*U(2,NDIV)+U(2,NM1))**2
           VDSUM=(VDSUM+(VDI+VDO)/2)*DELTY
           B(NBAND)=B(NBAND)+VDSUM*DELTX
           END IF
           END IF
C————————————————————————————————————————————————————————————
C          SOLVE EQUATIONS AND RETURN RESULTS
C————————————————————————————————————————————————————————————
           IF(MBAND.EQ.3)THEN
           CALL TRID(NBAND)
           ELSE
           CALL SOLVE(MBAND,NBAND,MSUB,MSUP)
           END IF
C
C          ****STORE NEW TEMPERATURE PROFILE
C
           DO 80 M=2,NDIV
           I=1+(M-2)*INCR
80         T(2,M)=Z(I)
           IF(KKTBCI.EQ.1)THEN
           T(2,1)=HFLUXI*(2*DELTY/(3*FK(1)))+(4.0/3)*T(2,2)-
     1     (1.0/3)*T(2,3)
           END IF
           IF(KKTBCO.EQ.1)THEN
           T(2,NP1)=HFLUXO*(2*DELTY/(3*FK(NP1)))+(4.0/3)*T(2,NDIV)-
     1     (1.0/3)*T(2,NM1)
           END IF
```

```
C------------------------------------------------------------------
C       COMPUTE BULK TEMPERATURE FROM ENERGY BALANCE
C------------------------------------------------------------------
        IF(KKTBCI.EQ.2)HFLUXI=(3*T(2,1)-4*T(2,2)+T(2,3))*FK(1)/(2*DELTY)
        IF(KKTBCO.EQ.2)HFLUXO=(3*T(2,NP1)-4*T(2,NDIV)+T(2,NM1))*FK(NP1)/
     1  (2*DELTY)
        TBAL1=TBAL*CUP/FCPM(NP2)+2.0*(HFLUXI*RADRAT+HFLUXO)*CEBAL/
     1  (FCPM(NP2)*(1.0+RADRAT))
C
C       ****STORE NEW HEATFUNCTION PROFILE (OPTIONAL)
C
        IF(KEBAL.EQ.1)THEN
        DO 90 M=2,NM1
        I=2*(M-1)
        E(M)=Z(I)
90      CONTINUE
        E(1)=HFLUXI*CEBAL*RADRAT
        E(NDIV)=0.5*CUP*(1.0+RADRAT)*TBAL+HFLUXO*CEBAL+VDSUM*DELTX
        E(NP1)=E(NDIV)
        END IF
        RETURN
        END
```

```
      SUBROUTINE SOLVE(MBAND,NBAND,MSUB,MSUP)
C**********************************************************************
C        SOLUTION OF UNSYMMETRIC BAND MATRIX WITH ITERATIVE REFINEMENT. *
C           NAG ROUTINES CALLED DIRECTLY:F01LBF,F04LDF,X02AAF        *
C                                                                   *
C     Z IS THE CURRENT SOLUTION. COEFFICIENT MATRIX A IS FIRST COPIED*
C     INTO AA. ON EXIT FROM F01LBF AA CONTAINS THE ELEMENTS OF UPPER *
C     TRIANGULAR MATRIX. BB STORES THE RHS B INITIALLY AND ON LATER  *
C     ITERATIONS THE RESIDUAL VECTOR R=B-AZ. ON EXIT FROM F04LDF BB  *
C     CONTAINS THE SOLUTION OF THE RESIDUAL VECTOR EQUATION WHICH     *
C     OVERWRITES THE RESIDUAL. KITER IS THE ITERATION COUNTER.       *
C     CONVERGENCE CRITERION IS (MAX.CORRECTION).LE.2.0*EPS*ZMAX.     *
C     EPS IS THE SMALLEST NUMBER FOR WHICH 1.0+EPS.GT.1.0 AND        *
C     REPRESENTS WORD LENGTH AND ATTAINABLE ACCURACY GIVEN BY X02AAF.*
C**********************************************************************
C
      PARAMETER (MAX1=101,MAX2=51,MAX3=103,MAX4=21,MAX5=24,MAX33=297)
      DIMENSION IN(MAX33)
      DOUBLE PRECISION A,B,Z,EPS,DUMMY
      DOUBLE PRECISION AL(4,MAX33),AA(8,MAX33),BB(MAX33)
      REAL*16 ADP,RDP,ZDP
C
      COMMON /IO/NI,NO,NSC,NSS,NSF,NSH,NS1,NS2,NS3,NS4,NS5,NS6,NS7
      COMMON /C7/A(8,MAX33),B(MAX33),Z(MAX33)
      COMMON /C8/KITER
C
C-------------------------------------------------------------------
C     SMALLEST REAL NUMBER
C-------------------------------------------------------------------
      EPS=X02AAF(DUMMY)
C-------------------------------------------------------------------
C     TOP JUSTIFY BAND
C-------------------------------------------------------------------
      DO 30 J=1,MSUB
      JJ=MSUB-J+1
      DO 10 I=1,MBAND-JJ
10    A(I,J)=A(I+JJ,J)
      DO 20 I=MBAND-JJ+1,MBAND
20    A(I,J)=0.0
30    CONTINUE
C-------------------------------------------------------------------
C     COPY A INTO AA, B INTO BB AND INITIALIZE SOLUTION VECTOR
C-------------------------------------------------------------------
      DO 1 I=1,NBAND
      Z(I)=0.0
      BB(I)=B(I)
      DO 1 J=1,MSUB+MSUP+1
1     AA(J,I)=A(J,I)
C-------------------------------------------------------------------
C     DECOMPOSE AA
C-------------------------------------------------------------------
      IFAIL=0
      IV=0
      CALL F01LBF(NBAND,MSUB,MSUP,AA,8,AL,4,IN,IV,IFAIL)
      IF(IFAIL.EQ.0)GO TO 101
      WRITE(NO,100)IFAIL,IV
100   FORMAT(1X,' ERROR IN F01LBF: IFAIL = ',I2,2X,', IV = ',I6,/
     1 1X,' (SEE NAG DOCUMENTATION FOR FOR POSSIBLE EXPLANATIONS)')
      STOP
```

```
C————————————————————————————————————————————————————————————
C       INITIALIZE ITERATION COUNTER AND MAX.RELATIVE CORRECTION.
C————————————————————————————————————————————————————————————
101     KITER=0
        DO=0.0
C————————————————————————————————————————————————————————————
C       START OF ITERATION
C————————————————————————————————————————————————————————————
2       KITER=KITER+1
C
C       ****SOLUTION OF RESIDUAL VECTOR EQUATION
C
        CALL F04LDF(NBAND,MSUB,MSUP,1,AA,8,AL,4,IN,BB,316,IFAIL)
        IF(IFAIL.EQ.0)GO TO 103
        WRITE(NO,102)KITER,IFAIL
102     FORMAT(1X,' ERROR IN F04LDF ON ITERATION',I2,', IFAIL = ',I2,/
       1 1X,' (SEE NAG DOCUMENTATION FOR POSSIBLE EXPLANATIONS)')
        STOP
C
C       ****CORRECT SOLN.AND FIND MAX.VALUES IN SOLN.AND CORRN.VECTORS
C
103     BBMAX=0.0
        ZMAX=0.0
        DO 3 I=1,NBAND
        Z(I)=Z(I)+BB(I)
        IF(ABS(Z(I)).GT.ZMAX) ZMAX=ABS(Z(I))
        IF(ABS(BB(I)).GT.BBMAX) BBMAX=ABS(BB(I))
3       CONTINUE
C
C       ****CALCULATE RESIDUAL ELEMENT IN I-TH ROW IN DOUBLE PRECISION
C
        DO 6 I=1,NBAND
        RDP=B(I)
        MFIRST=1
        MLAST=MSUB+MSUP+1
        IF(I.LE.MSUB) MLAST=MSUP+I
        IF(I.GT.NBAND-MSUP) MLAST=MSUB+1+NBAND-I
        DO 4 J=MFIRST,MLAST
        ADP=A(J,I)
        ZDP=Z(J)
        IF(I.GT.MSUB) ZDP=Z(I+J-MSUB-1)
4       RDP=RDP-ADP*ZDP
6       BB(I)=RDP
C
C       ****CONVERGENCE TEST
C
        ID2=0
        D1=0.0
        IF(BBMAX.GT.0.0) D1=BBMAX/ZMAX
        IF(BBMAX.GT.2.0*EPS*ZMAX) ID2=1
        IF(D1.GT.D0/2.AND.KITER.NE.1) GO TO 7
        DO=D1
        IF(ID2.EQ.1) GO TO 2
        RETURN
7       WRITE(NO,1000) KITER
1000    FORMAT(1X,'MAX.CORRN.IN ITERATIVE REFINEMENT IS GREATER THAN',
       1 ' HALF OF THE PREVIOUS STEP.',/1X,'ILL CONDITION INDICATED.'/1X,
       2 'PROGRAM TERMINATED IN SUBROUTINE SOLVE ON ITERATION',I3)
        STOP
        END
```

```
          SUBROUTINE TRID(NBAND)
C*********************************************************************
C       SOLVES AX=B FOR VECTOR X WHERE A IS TRIDIAGONAL             *
C       (FROM S.D.CONTE-'ELEMENTARY NUMERICAL                       *
C       ANALYSIS',MCGRAW-HILL,1965.)                                *
C                                                                   *
C       NBAND=ORDER OF SYSTEM                                       *
C       SUB=SUBDIAGONAL OF A                                        *
C       DIAG=MAIN DIAGONAL OF A                                     *
C       SUP=SUPERDIAGONAL OF A                                      *
C       B=CONSTANT VECTOR                                           *
C                                                                   *
C       SUP AND DIAG ARE DESTROYED                                  *
C       SOLUTION VECTOR IS RETURNED IN Z                           *
C*********************************************************************
C
          PARAMETER (MAX1=101,MAX2=51,MAX3=103,MAX4=21,MAX5=24,MAX33=297)
          IMPLICIT DOUBLE PRECISION (A-H,O-Z)
          DIMENSION SUB(MAX1),DIAG(MAX1),SUP(MAX1)
          COMMON /C7/A(8,MAX33),B(MAX33),Z(MAX33)
C
C       ****COPY A INTO SUB, DIAG AND SUP
C
          DO 1 J=1,NBAND
          SUB(J)=A(1,J)
          DIAG(J)=A(2,J)
1         SUP(J)=A(3,J)
C
          N=NBAND
          NN=N-1
          SUP(1)=SUP(1)/DIAG(1)
          B(1)=B(1)/DIAG(1)
C
          DO 10 I=2,N
          II=I-1
C
C       ****DECOMPOSE A TO FORM A=LU
C
          DIAG(I)=DIAG(I)-SUP(II)*SUB(I)
          IF(I.EQ.N)GO TO 10
          SUP(I)=SUP(I)/DIAG(I)
C
C       ****COMPUTE Z WHERE LZ=B
C
10        B(I)=(B(I)-SUB(I)*B(II))/DIAG(I)
C
C       ****COMPUTE X BY BACK SUBSTITUTION WHERE UX=Z
C
          DO 20 K=1,NN
          I=N-K
20        B(I)=B(I)-SUP(I)*B(I+1)
C
C       ****RETURN SOLUTION IN Z
C
          DO 30 J=1,NBAND
30        Z(J)=B(J)
C
          RETURN
          END
```

APPENDIX G

AUTHOR'S RELEVANT PUBLISHED WORK

The following refereed papers published during the course of this research are referred to in Chapter 4 of this thesis:

(i)   SZPIRO, O., LEWIS, J.S. and COLLINS, M.W. (1984). Numerical Solutions for Developing Combined Convection Between Uniformly Heated Parallel Plates, <u>1st UK National Conference on Heat Transfer,</u> Leeds, vol. 2, pp. 829–838.

(ii)   LEWIS, J.S., COLLINS, M.W. and ALLEN, P.H.G. (1990). Flow Rate Predictions for a Thermosyphon Loop, <u>9th International Heat Transfer Conference,</u> Jerusalem, vol. 2, paper 5–NC–12, pp. 549–554.

To avoid unnecessary duplication the full texts of both papers are reproduced in this appendix.

NUMERICAL SOLUTIONS FOR DEVELOPING COMBINED CONVECTION

BETWEEN UNIFORMLY HEATED VERTICAL PARALLEL PLATES

O.Szpiro [*], J.S.Lewis [**] and M.W.Collins [***]

The calculation of heat transfer rates for low Reynolds number duct flows when the effects of property variations, including buoyancy forces, are important, is a topic of practical interest. Two different numerical calculation procedures are applied to the problem of aiding combined natural and forced convection between uniformly heated vertical parallel plates. Temperature dependence of the fluid properties is fully represented by both methods. Results are presented for upward flow showing increased local Nusselt numbers for ethylene glycol when both plates are equally heated and for transformer oil when only one plate is heated. A flow reversal at the unheated wall is predicted in the latter case.

INTRODUCTION

The influences of temperature dependent properties and a gravitational body force in modifying the coupled velocity and temperature fields in duct heat transfer problems with viscous fluids at low Reynolds numbers are well recognised [1]. Under these conditions the Nusselt number deviates markedly from constant property solutions for forced convection. This is due, in part, to buoyancy forces generated by the interaction of density gradients with the gravitational field. This paper focuses on the steady two-dimensional laminar flow of a fluid with temperature dependent properties between vertical parallel plates. Uniform heating is imposed at one or both of the plates and the flow is upward resulting in aiding combined natural and forced convection.

The geometrical and thermal boundary conditions described approximate those encountered in the modelling of flow and heat transfer in transformer layer windings, solar collectors and some nuclear reactor cooling problems. Liquid coolants of moderate or high Prandtl number are employed in these applications but a literature search revealed few relevant heat transfer measururements for combined convection in parallel plate ducts. Preiningerova and Allen [2] and Taylor et al [18] quote data for asymmetric heating of transformer oil and Joshi and Bergles [3] have made measurements with ethylene glycol in both symmetrically and asymmetrically heated ducts. Clearly the data presently available for viscous liquids are insufficient to establish dimensionless correlating equations applicable to a wide range of conditions. In the absence of such design data the use of a numerical method incorporating buoyancy force and specified property variations should be considered.

[*] Department of Electrical Engineering, Imperial College of Science and Technology, London SW7 2BT.
[**] School of Mechanical and Production Engineering, Middlesex Polytechnic, London N11 2NQ.
[***] Department of Mechanical Engineering, The City University, London EC1V 4PB.

829

In contrast to the lack of experiments, previous analytical and numerical studies of the flow and heat transfer between parallel plates abound for a variety of conditions, this geometry often serving as a test case for new techniques. A useful review of constant property forced convection solutions upto the end of 1975 is provided by Shah and London [4].

Theoretical treatments of aiding combined convection with the uniform wall heat flux boundary condition include the analysis by Rao and Morris [5] for a postulated established flow, and that by Savkar [6] which considers a parabolic entry velocity profile and a linearized form of the energy equation. Yao [7] considered the effect of natural convection near entry as a small perturbation on the developing flow in an unheated channel, and also suggested the possibility of periodic recirculating cells moving downstream for the region where natural convection dominates. Dalbert [8] solved the boundary layer equations for a simultaneously developing flow in finite difference form. Apart from the density difference in the buoyancy generation term constant property values were assumed in these studies. Moreover the heat transfer results presented are either in inconvenient form or are inappropriate to high Prandtl number fluids. The numerical studies of Allen and coworkers (see [14] for example) and Nikitenko [15] are exceptions in which all property variations are considered for the conditions of present interest.

Similar restrictions apply to analytical [9,10] and numerical [11-13] treatments of the corresponding natural convection problem.

In the following sections two finite difference calculation procedures are presented; namely, an implicit, marching integration scheme and a technique in which the developing temperature profiles are approximated by a series of 'truncated' versions of a fully developed profile. Common features of the two methods include primitive variable formulation, use of the integral energy balance equation and iteration to handle the coupling of governing equations caused by the temperature dependent properties.

GOVERNING EQUATIONS

Flow Geometry

Vertically upward laminar flow of a fluid with temperature dependent properties in a heated parallel plate duct is considered. Fluid is supplied to the bottom of the duct at a uniform temperature t_o with a specified velocity profile $u_o(y)$. Two problems with different thermal boundary conditions are treated: (i) uniform and equal wall heat fluxes (symmetric problem), and (ii) uniform wall heat flux at one plate, the other plate being thermally insulated (asymmetric problem). The symmetry of boundary conditions in the former case determines that solutions need only be obtained for the duct half-width, whereas the full duct width must be considered in the asymmetric problem.

The origin of the x-y coordinate system is located at the leading edge of the left-hand side plate with the x-coordinate aligned in the direction of flow i.e. opposite to the gravitational body force vector generating buoyancy effects in the duct (see Fig.1). To unify the treatment of the two problems the transverse width of the calculation domain is denoted by the symbol a in both cases.

Differential Equations

The following partial differential equations govern the conservation of mass, axial momentum, transverse momentum and energy respectively for the steady two-dimensional laminar flow:

830

$$\frac{\partial u}{\partial x} + \frac{\partial v}{\partial y} = 0 \tag{1}$$

$$\rho\left(u\frac{\partial u}{\partial x} + v\frac{\partial u}{\partial y}\right) = -\rho g - \frac{\partial p}{\partial x} + \frac{\partial}{\partial y}\left(\mu\frac{\partial u}{\partial y}\right) \tag{2}$$

$$\rho\left(u\frac{\partial v}{\partial x} + v\frac{\partial v}{\partial y}\right) = -\frac{\partial p}{\partial y} + \frac{\partial}{\partial y}\left(\mu\frac{\partial v}{\partial y}\right) + \frac{\partial\mu}{\partial y}\cdot\frac{\partial v}{\partial y} + \frac{\partial\mu}{\partial x}\cdot\frac{\partial u}{\partial y} \tag{3}$$

$$\rho c\left(u\frac{\partial t}{\partial x} + v\frac{\partial t}{\partial y}\right) = \frac{\partial}{\partial y}\left(k\frac{\partial t}{\partial y}\right) \tag{4}$$

Viscous dissipation, axial diffusion and some small terms are ignored. Eqations(1)-(4) are coupled through the fluid properties which are assumed to be functions of temperature alone, so that the property space derivatives required in Equations(2)-(4) can be replaced by:

$$\frac{\partial\mu}{\partial y} = \frac{d\mu}{dt}\cdot\frac{\partial t}{\partial y} \quad , \quad \frac{\partial\mu}{\partial x} = \frac{d\mu}{dt}\cdot\frac{\partial t}{\partial x} \quad , \quad \frac{\partial k}{\partial y} = \frac{dk}{dt}\cdot\frac{\partial t}{\partial y}$$

Density variation is admitted in the x-direction body force term, but otherwise the fluid is treated as incompressible.

Integral Balance Equations

Further constraints are expressed by the integral continuity and step-wise energy balance equations; viz,

$$u_m = \frac{1}{a}\int_0^a u\,dy \tag{5}$$

and

$$\Delta t_b = \frac{q}{\rho\,u_m\,a\,c_m}\,\Delta x \tag{6}$$

where for variable specific heat the bulk temperature is defined by

$$t_b = \int_0^a u\,c_m\,t\,dy \Big/ \int_0^a u\,c_m\,dy \tag{7}$$

In Equations(6) and (7) c_m denotes the mean specific heat appropriate to the temperature interval or local temperature respectively.

Boundary and Initial Conditions

The following boundary conditions apply generally :

$$v(x,0) = 0 \quad , \quad v(x,a) = 0 \quad , \quad u(x,0) = 0 \quad , \quad \frac{\partial t}{\partial y}(x,0) = -\frac{q}{k_w} \quad , \quad \frac{\partial t}{\partial y}(x,a) = 0$$

whereas $\frac{\partial u}{\partial y}(x,a) = 0$ for the symmetric problem only and $u(x,a) = 0$ for the asymmetric problem only. Initial conditions are specified as follows:

$$u(0,y) = u_0(y) \quad , \quad v(0,y) = 0 \quad , \quad p(0,y) = p_0 \quad , \quad t(0,y) = t_0$$

where $u_0(y)$ allows either a uniform or a parabolic axial velocity profile to be specified at entry.

831

NUMERICAL METHODS

Marching Integration Scheme

This method follows closely the procedure applied by Collins[16] and others to a variety of axisymmetric cylindrical coordinate problems. The method is now presented for the two-dimensional cartesian coordinate problem described.

A rectangular finite difference grid (see Fig.2) with M transverse divisions is employed. The axial spacing is also uniform about the grid point (n,m) but may be doubled at arbitrarily chosen locations in the marching procedure. Equations(1)-(4) are first rendered dimensionless using the substitutions given in the Nomenclature and then replaced according to the following implicit scheme:

$$\frac{U(n+1,m)-U(n,m)+U(n+1,m-1)-U(n,m-1)}{2 \ \Delta X} + \frac{V(n+1,m)-V(n+1,m-1)}{\Delta Y} = 0 \tag{8}$$

$$U(n,m)\left[\frac{U(n+1,m)-U(n,m)}{\Delta X}\right] + V(n,m)\left[\frac{U(n+1,m+1)-U(n+1,m-1)}{2 \ \Delta Y}\right] = F_\rho \ \frac{G}{(Re_a)_o^2}$$

$$-\left[\frac{P(n+1,m)-P(n,m)}{\Delta X}\right] + \frac{1}{(Re_a)_o}\left(F_\mu\left[\frac{U(n+1,m+1)-2U(n+1,m)+U(n+1,m-1)}{\Delta Y^2}\right]\right.$$

$$\left.+F'_\mu\left[\frac{T(n+1,m+1)-T(n+1,m-1)}{2 \ \Delta Y} \cdot \frac{U(n+1,m+1)-U(n+1,m-1)}{2 \ \Delta Y}\right]\right) \tag{9}$$

$$U(n,m)\left[\frac{V(n+1,m)-V(n,m)}{\Delta X}\right] + V(n,m)\left[\frac{V(n+1,m+1)-V(n+1,m-1)}{2 \ \Delta Y}\right]$$

$$= -\left[\frac{8P(n+1,m+1)-8P(n+1,m-1)-P(n+1,m+2)-P(n+1,m-2)}{12 \ \Delta Y}\right]$$

$$+\frac{1}{(Re_a)_o}\left(F_\mu\left[\frac{V(n+1,m+1)-2V(n+1,m)+V(n+1,m-1)}{\Delta X^2}\right] + F'_\mu\left[\frac{T(n+1,m+1)-T(n+1,m-1)}{2 \ \Delta Y}\right.\right.$$

$$\left.\left.\cdot \frac{V(n+1,m+1)-V(n+1,m-1)}{\Delta Y} + \frac{T(n+1,m)-T(n,m)}{\Delta X} \cdot \frac{U(n,m+1)-U(n,m-1)}{2 \ \Delta Y}\right]\right) \tag{10}$$

$$U(n,m)\left[\frac{T(n+1,m)-T(n,m)}{\Delta X}\right] + V(n,m)\left[\frac{T(n+1,m+1)-T(n+1,m-1)}{2 \ \Delta Y}\right]$$

$$= \frac{1}{F_c(Re_a Pr)_o}\left(F_k\left[\frac{T(n+1,m+1)-2T(n+1,m)+T(n+1,m-1)}{\Delta Y^2}\right]\right.$$

$$\left.+F'_k\left[\frac{T(n,m)-T(n,m-1)}{\Delta Y} \cdot \frac{T(n+1,m+1)-T(n+1,m-1)}{2 \ \Delta Y}\right]\right) \tag{11}$$

It is assumed that the elliptic nature of the pressure field is sufficiently weak to permit a marching solution with the transverse momentum equation retained. This was confirmed by the predictions which demonstrated negligible transverse pressure variations.

For the solutions presented in this paper 80 transverse grid divisions were employed and the initial marching step ΔX was 1.0. A full description, including details of the treatment of boundary conditions and a stability analysis, are given by Collins[16].

832

The dimensionless forms of Equations(5)-(7) are

$$1 = \int_0^1 U \, dY \tag{12}$$

$$\Delta T_b = \frac{Gr_a}{(F_c)_m (Re_a Pr)_0} \Delta X \tag{13}$$

and

$$T_b = \int_0^1 U \, (F_c)_m T \, dY \Big/ \int_0^1 U \, (F_c)_m \, dY \tag{14}$$

Equations(12) and (14) are evaluated numerically in terms of ordinates.

The calculation procedure for each marching step may be summarised as follows: Equations(8)-(10) written for each interior point are solved simultaneously with Equation(12) for the 3M-2 unknown values of U,V and P at the n+1 level. The velocities thus obtained are next used in the solution of the energy equations for the unknown temperatures. A total of M-1 equations are involved, Equation(13) replacing Equation(11) for the transverse grid position nearest to the heated wall (m = 2). This technique at once guarantees the energy balance and satisfies the wall thermal boundary condition. A refinement of the solutions is achieved by repeating the calculations allowing the temperatures at the n+1 level to be used in evaluating the property ratios F_μ, F_k, (and their derivatives with respect to T : F'_μ and F'_k) F_c and F_ρ, and other temperature dependent expressions.

Truncation Technique

This method was developed specifically for high Prandtl number fluids, has been applied to both cylindrical and plane duct flows and is described in detail elsewhere [14,17]. Only the essentials will be explained here.

It is assumed that the axial velocity profile develops rapidly in comparison with the temperature profile, adopting a new 'fully developed' form coupled to the temperature profile at each axial position. Initially, the axial momentum equation is solved for the fully developed, constant property velocity profile which is subsequently used in the solution of the energy equation for the fully developed temperature profile.

The main approximation, from which derives the adjective 'truncation', relates to the treatment of the developing temperature profile. It is assumed that the fluid temperature increases from the uniform duct entry value to attain a profile appropriate to a fully developed, forced convection condition far downstream which neglects transverse convection. At intermediate positions, truncated versions of this fully developed profile are employed in the vicinity of the heated wall with the remainder of the cross-section uniformly at the duct entry temperature. Then at any (initially unknown) axial distance that truncated temperature profile is used for evaluating all temperature dependent quantities, including buoyancy, in a further solution of the axial momentum equation to find the distorted 'fully developed' velocity profile. The assumed similarity of temperature profiles at the heated wall follows from the uniform wall heat flux boundary condition, whereas, the truncation distance is viewed as the depth of penetration of the thermal boundary layer which increases with axial distance.

Finally, both profiles are used to calculate the bulk temperature and the axial distance is found from Equation(6).

The finite difference equivalents of the governing equations are solved by successive over-relaxation, typically, using 100 transverse divisions.

833

RESULTS

The conditions and heat transfer predictions for two sample cases are shown in Fig.3 and Fig.4 respectively. For the symmetric heating of ethylene glycol no direct comparison could be made with [3] since the original test data were not available[19]. The asymmetric heating conditions correspond to an experiment on natural convection of transformer oil through a narrow vertical annular duct[18]. Fully developed flow at the start of heating was assumed in all calculations other than the marching integration treatment of the asymmetric problem, where the more appropriate uniform entry profile was used. The parabolic initial condition is implicit in the truncation method.

The accuracy of the marching integration scheme can be judged from the constant property solutions (Gr=0), which agree closely with analytical forced convection solutions in [4] except near entry. In Fig.4 the difference is partly attributable to the different entry velocity profiles assumed. The corresponding variable property predictions exhibit large increases in Nusselt number for the aiding combined convection conditions investigated. In Fig.3 a minimum in Nu_0 around $(x/d_h)/(RePr)_b = 0.007$ is noted. This arrestment of the usual Nusselt number decline is in qualitative agreement with experimental data[3,19]. Consistently lower values are predicted by the truncation method, since for the same bulk temperature a higher wall temperature (and hence a lower Nu) is required compared with a full solution. This discrepancy reduces with axial distance as the velocity and temperature profiles align. The disappointing comparison with the experimental data of Taylor et al[18] is not unexpected, since a large uncertainty must attach to the mean oil velocity used in the predictions, which was estimated from pressure defect considerations. All physical property variations were taken into account for both fluids. Apart from dynamic viscosity, these were adequately represented by linear functions of temperature. The need to treat all property variations (and especially viscosity) for viscous liquids was established in separate calculations, where buoyancy and other effects were assessed individually.

Axial velocity and temperature profile predictions are compared in Fig.5 and Fig.6 at two axial locations for each case treated. The accumulative effect of buoyancy and variable viscosity on the velocity profile is evident. In view of the approximate nature of the temperature profile prescribed by truncation the agreement of velocity profiles is excellent. In the asymmetric case, the strong heating eventually causes a flow reversal at the unheated wall. Predictions of the axial position of onset differ slightly as indicated in Fig.4.

CONCLUDING REMARKS

Two effective numerical methods are available for the calculation of laminar combined convection duct flows which consider all property variations.

Calculations made for the flow of viscous liquids between vertical parallel plates under aiding conditions show a consistent increase in heat transfer over constant property forced convection solutions. For accurate predictions with these fluids all property variations must be accounted for.

The methods are able to predict phenomena associated with a strong buoyancy contribution such as the arrestment of decreasing Nusselt number and the onset of flow reversal.

ACKNOWLEDGEMENTS

NOMENCLATURE

a	width of calculation domain, $[= d_h/4$, symmetric case] $[= d_h/2$, asymmetric case]	Re_a	Reynolds number based on a, $[= \rho u_m a / \mu]$
c	specific heat	t	temperature
d_h	duct hydraulic diameter, $[= 2 \times$ plate spacing]	T	dimensionless temperature, $[= G\beta(t-t_o)]$
F_μ, F_ρ	fluid property ratios,	u	axial velocity
F_c, F_k	$[= c/c_o, k/k_o, \mu/\mu_o, \rho/\rho_o]$	U	dimensionless axial velocity, $[= u/u_m]$
g	gravitational acceleration	v	transverse velocity
G	dimensionless parameter, $[= ga^3/\nu_o^2]$	V	dimensionless transverse velocity, $[= v/u_m]$
Gr	uniform wall heat flux Grashof number based on d_h, $[= g \beta d_h^4 q/k_o \nu_o^2]$	x	axial coordinate
		X	dimensionless axial coordinate, $[= x/a]$
Gr_a	uniform wall heat flux Grashof number based on a, $[= G\beta aq/k_o]$	ΔX	X-grid spacing, [see Fig.2]
		y	transverse coordinate
h	local heat transfer coefficient, $[= q/(t_w-t_b)]$	Y	dimensionless transverse coordinate, $[= y/a]$
		ΔY	Y-grid spacing, [see Fig.2]
k	thermal conductivity	β	average volumetric expansion
m	Y-grid location, [see Fig.2]		coefficient, $[= (-1/\rho)(\rho-\rho_o)/(t-t_o)]$
M	number of transverse divisions	μ	dynamic viscosity
n	X-grid location, [see Fig.2]	ν	kinematic viscosity
Nu	local Nusselt number, $[= hd_h/k]$	ρ	density
p	pressure		
P	dimensionless pressure, $[= p-p_o/\rho_m u^2]$		Subscripts
Pr	Prandtl number, $[= c\mu/k]$	b	bulk condition
q	wall heat flux	f	film condition
Re	Reynolds number based on d_h, $[= \rho u_m d_h/\mu]$	m	mean value
		o	duct entrance condition
		w	heated wall condition

REFERENCES

1. PORTER,J.E.-Heat transfer at low Reynolds number (Highly viscous liquids in laminar flow): Industrial Research Fellow Report,Trans.I.Chem.E. Vol.49, Part 1,pp.1-29, 1971.

2. PREININGEROVA,V. and ALLEN,P.H.G.-Laminar flow entry length heat transfer with varying physical properties in simple and complex duct goemetries, Proc.5th Int.Heat Transfer Conf. Tokyo, Vol.III,Paper NC 5.4, pp.188-192, 1974.

3. JOSHI,S.D. and BERGLES,A.E.-Heat transfer in cooling channels of power transformers, Iowa State Univ.Engng.Research Institute, Annual Report ISU-ERI-AMES-78287, pp.7.1-7.15, 1978.

4. SHAH,R.K. and LONDON,A.L.-Laminar Flow Forced Convection In Ducts, Supplement 1 - Advances in Heat Transfer,Edited by T.F.Irvine,Jr. and J.P.Hartnett, Academic Press, 1978.

835

5. RAO,T.L.S. and MORRIS,W.D.-Superimposed laminar forced and free convection between vertical parallel plates when one plate is uniformly heated and the other is thermally insulated, Proc.I.Mech.E. Vol.182, Part 3H, 1967-68.

6. SAVKAR,S.D.-Developing forced and free convective flows between two semi-infinite parallel plates, Proc.4th Int.Heat Transfer Conf. Paris, Vol.IV, Paper NC 3.8, 1970.

7. YAO,L.S.-Free and forced convection in the entry region of a heated vertical channel, Int.J.Heat Mass Transfer, Vol.26, Part 1, pp.65-72, 1983.

8. DALBERT,A.-M.-Natural, mixed and forced convection in a vertical channel with asymmetric uniform heating, Proc.7th Int.Heat Transfer Conf. Munich, Vol.3, Paper MC 4, 1982.

9. WORDSWORTH,D.V.-Laminar free convection between heat producing vertical plates in a liquid, AERE E/R 1270, 1953.

10. ENGEL,R.K. and MUELLER,W.K.-An analytical investigation of natural convection in vertical channels, A.S.M.E. Paper 67-HT-16, 1967.

11. AUNG,W.,FLETCHER,L.S. and SERNAS,V.-Developing laminar free convection between vertical flat plates with asymmetric heating, Int.J.Heat Mass Transfer, Vol.15, pp.2293-2308, 1972.

12. MIYATAKE,O.,FUJII,T.,FUJII,M. and TANAKA,H.-Natural convective heat transfer between vertical parallel plates - One plate with a uniform heat flux and the other thermally insulated, Heat Transfer-Japanese Research, Vol.2, Part 1, pp.25-33, 1973.

13. KIM,H.D.-A study of natural convection flow between vertical plates with constant heat flux, Yongnam Taehakkyo Kongop Kisul Yonguso Yongu Pogo, Vol.6, Part 1, pp.33-39,1978.

14. ALLEN,P.H.G. and FINN,A.H.-Profile development with mixed convection in a high Prandtl number fluid, J.Heat Transfer, Trans.A.S.M.E. Vol.92, Part 2,pp.299-304, 1970.

15. NIKITENKO,N.I. et al.-Study of flow and heat exchange in liquid cooled transformer channels, (In Russian), Promyshlennaya Teplotekhnika, Vol.1, Part 1, pp.33-38, 1979.

16. COLLINS,M.W.-Finite difference analysis for developing laminar flow in circular tubes applied to forced and combined convection, Int.J.Num.Meth.Engng. Vol.15, pp.381-404, 1980.

17. COLLINS,M.W., ALLEN,P.H.G. and SZPIRO,O.-Computational methods for entry length heat transfer by combined laminar convection in vertical tubes, Proc. I.Mech.E. Vol.191, Part 2, pp.19-29, 1977.

18. TAYLOR,E.D.,BERGER,B. and WESTON,B.E.-An experimental approach to the cooling of transformer coils by natural convection, Proc.I.E.E. Vol.105A, pp.141-152, 1958.

19. JOSHI,S.D.-Private communications,1982-83.

836
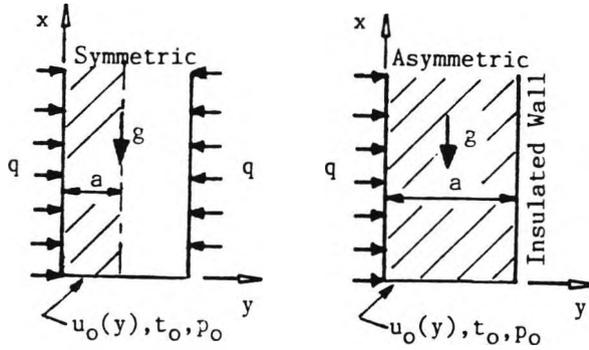
Fig.1 Models and coordinate systems.

Fig.2 Finite difference grid

d_h = 25.4 mm, q =4064 W/m^2
u_m = 14.9 mm/s, Re$_o$ = 20
t_o = 20°C, Pr$_o$ = 172.2

variable properties, combined convection
Gr = 102400

constant properties,
forced convection, Gr = 0

Marching solution
Truncation solution
Analytical solution [4]

$(x/d_h)/(RePr)_b$
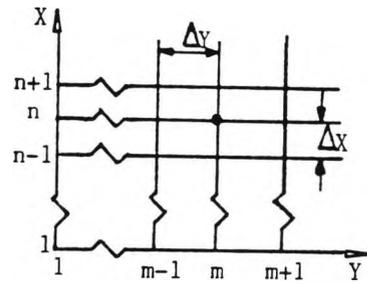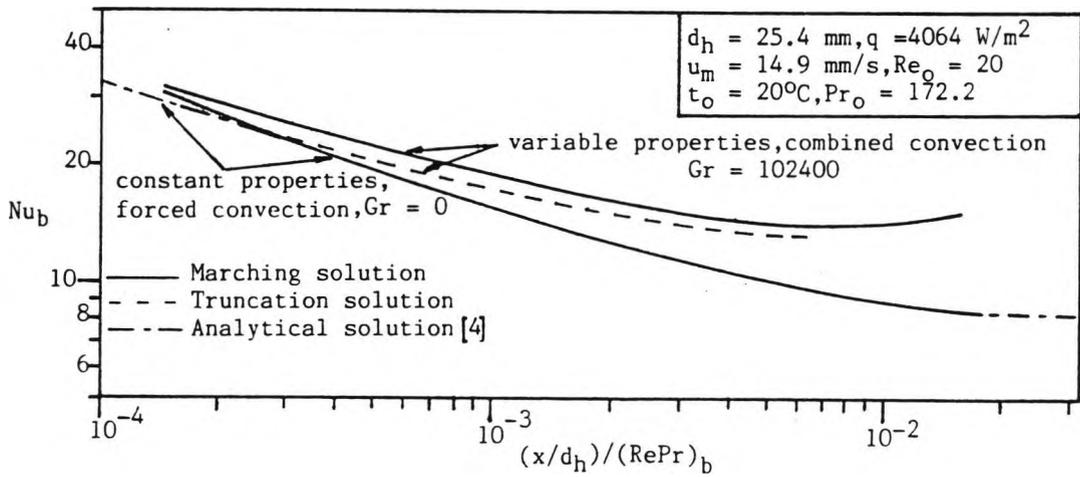
Fig.3 Local Nusselt number variation. Symmetric heating of ethylene glycol.

flow reversal predicted

d_h = 12.7 mm, q = 7830 W/m^2
u_m = 7.1 mm/s, Re$_o$ = 3.39
t_o = 22°C, Pr$_o$ = 406.4

variable properties, combined convection
Gr = 19950

constant properties,
forced convection, Gr = 0

Marching solution
Truncation solution
Analytical solution [4]
o Exptl. data of Taylor et al [18]

$(x/d_h)/(RePr)_b$
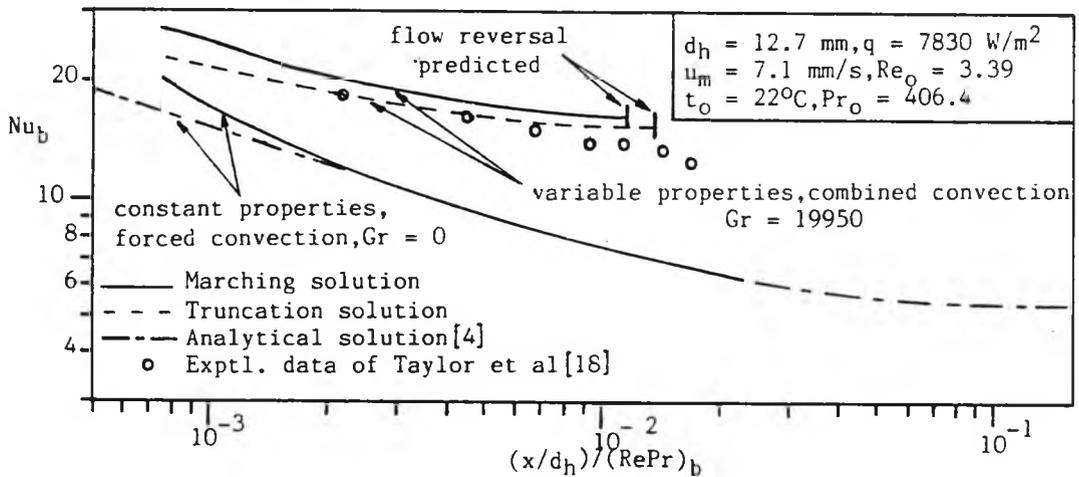
Fig.4 Local Nusselt number variation. Asymmetric heating of transformer oil.
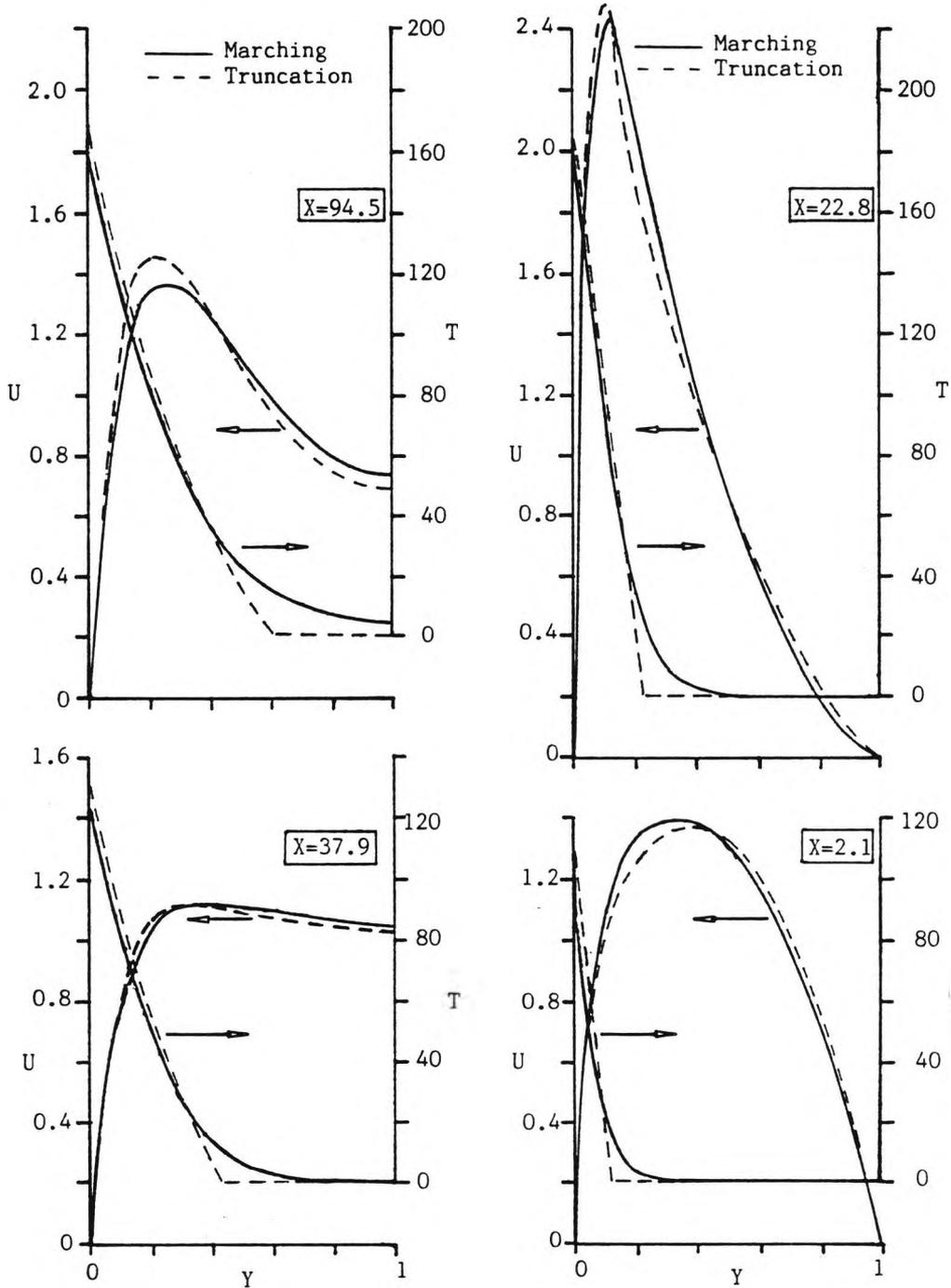
Fig.5 Comparison of velocity and temperature profiles. Symmetric heating of ethylene glycol.

Fig.6 Comparison of velocity and temperature profiles. Asymmetric heating of transformer oil.

FLOW RATE PREDICTIONS FOR A THERMOSYPHON LOOP

J.S. Lewis[1], M.W. Collins[2] and P.H.G. Allen[2]

[1] Energy Technology Centre, Middlesex Polytechnic, London N11 2NQ
[2] Thermo-Fluids Engineering Research Centre, The City University, London EC1V 0HB, UK

A theoretical investigation of steady-state thermosyphoning in a closed-loop comprising two vertical tubes joined by upper and lower plenums has been undertaken. The equations governing two-dimensional developing laminar combined natural and forced convection in the heated and cooled sections were solved, by a finite-difference method, to provide pressure differences required for the thermosyphon problem. Numerical results obtained for water (Pr = 4.9) flows in loops with different source-to-sink elevation differences, at various Grashof numbers, confirm that buoyancy strongly influences the shape of the developing axial velocity profile, and hence the wall friction. The axial variation of the average cross-section temperature causing the buoyant driving force is explained. A comparison of the results, including flow rate predictions, is made with conventional one-dimensional analysis.

1. INTRODUCTION

Closed-loop thermosyphoning is a reliable method of thermal energy transfer from a heat source to a heat sink at a higher level. Examples of practical equipment designed to exploit natural circulation include, oil and gas insulated transformers, fuel-fired and solar water heaters, and nuclear reactor and engine cooling systems. The recent increased interest in all aspects (steady-state, transients and stability characteristics) of natural circulation loops is evident from the reviews given by Japiske (1973), Zvirin (1981), Mertol and Grief (1985) and Grief (1988). This paper contrasts two methods for calculating the steady flow rate in a simple (single flow path) thermosyphon loop.

Although of central importance in determining the surface temperatures obtaining for a given rate of heat transfer, thermosyphon flow rate cannot be specified a priori and is difficult to determine experimentally. In general, the fluid circulation rate depends on the loop geometry, the fluid properties and the thermal boundary conditions at the source and sink. Circulation occurs naturally due to a buoyant driving force caused by the density variation around the loop. At steady-state, this force balances the flow resistances of the circulation path. The distributed nature of both sides of this equality necessitates integration over the whole system.

Most previous analyses of thermosyphon loops have used one-dimensional models which consider all properties of the flow to be uniform over any cross-section and to vary only along the circulation path. An implicit weakness of this approach is that the spatially averaged cross-section temperature is taken equal to the local bulk temperature. These two measures generally exhibit different values under heat transfer, and whereas the longitudinal gradient of the latter is related to heat flux, it is the variation of the former that is responsible for generating buoyancy. Furthermore, as one-dimensional analyses contain no information on transverse temperature and velocity gradients, friction and heat transfer coefficients must be supplied. Fully-developed forced convection values are often used although the experimental studies of Addlesee (1980), Creveling et al. (1975) and Huang (1987), which cover various loop geometries, indicate that such values are inappropriate for natural circulation. In reality, thermosyphon loop flows are characterised by simultaneously developing velocity and temperature profiles, and by combined natural and forced convection, prompting the alternative classification 'mixed convection thermosyphon' adopted by Japiske (1973). Moreover, these flows are not always unidirectional as observed by Creveling et al. (1975) and Stern et al (1988) who both reported regions of longitudinal flow reversal.

Morrison and Ranatunga (1980) compared laser doppler anemometry measurements of the water flow rate in an electrically heated thermosyphon loop with a one-dimensional analysis. The theoretical predictions underestimated the flow rate for Reynolds numbers below 300 and overestimated it for higher Reynolds numbers. Attempts to include estimates of the developing flow friction factors and the average cross-section temperature in the analysis, based on forced convection correlations, met with mixed success.

Multidimensional analyses have emphasised a toroidal loop mounted in a vertical plane with uniform heating over the lower half and constant wall temperature cooling over the upper half. The two-dimensional, axisymmetric, finite-difference analysis of Mertol et al. (1982) ignored pipe curvature effects and cross-stream velocities, so that axial velocity was independent of the axial coordinate. Their friction factor and local Nusselt number results approached forced flow values at low Graetz number, but were significantly higher at high Graetz number. The flow rate predictions were in good agreement with the experimental data of Creveling et al. (1975). Ronen and Zvirin (1985) extended the results to higher Graetz numbers and compared the two-dimensional model and a one-dimensional model utilising friction and heat transfer coefficients from the two-dimensional results. The maximum difference in the predicted flow rates occured at low Graetz number and was less than 7%. Lavine et al. (1986,1987) solved the conservation equations in their complete elliptic form, including curvature effects, using a hybrid (upwind and central) finite-differencing scheme. The calculated velocity and temperature fields

revealed strong three—dimensional effects, such as regions of longitudinal flow reversal, nonzero cross—stream velocities and nonaxisymmetric temperature profiles.

The present study deals with steady—state circulation in a thermosyphon loop with heating and cooling isolated in two vertical circular tubes which are joined by upper and lower plenums. This arrangement is of interest in transformer cooling, although the fluid considered in this preliminary investigation is water. Following a review of simple one—dimensional thermosyphon analysis, details are presented of an improved analysis which assumes two—dimensional, axisymmetric, developing combined convection in the heated and cooled tubes. Although it is recognised that buoyancy can cause flow reversals in vertical tubes, only unidirectional flows are treated. Tube flow computations have been performed for fixed tube lengths over limited ranges of the flow and heat transfer rates. The results were used to generate solutions for thermosyphons with different elevations, by matching pressure differences between the top and bottom of the loop for the heated and cooled paths. In this paper, results from the two—dimensional analysis are compared with the values predicted, or assumed, by the one—dimensional analysis.

2. MATHEMATICAL MODELS

2.1 Basic Assumptions

The one— and two—dimensional analyses which follow consider steady flow and heat transfer in a closed—loop thermosyphon (Figure 1) comprising two vertical parallel tubular sections joined by large upper and lower plenums. Relevant dimensions which define this geometry are the lengths L_h and L_c, the diameters D_h and D_c and the vertical distance Δz between the centres of the heated (lower) and cooled (higher) tubular sections respectively.

The loop is filled with a single—phase, incompressible, Newtonian fluid which circulates in the direction of the axial coordinate z. Laminar flow is assumed and axial diffusion and viscous heating are both neglected. All fluid properties are considered constant except in the body force term of the axial momentum equation where the density ρ is assumed to vary linearly with temperature T according to $\rho = \rho_0[1 - \beta(T - T_0)]$. In this (Boussinesq) approximation the volumetric expansion coefficient β is constant and ρ_0 is the density at reference

Figure 1   Loop geometry and bulk temperature variation.

temperature T_0, taken to be the temperature in the bottom plenum. To simplify comparison of the two models, uniform wall heat fluxes q_h and q_c are imposed at the heated and cooled sections respectively. The plenums are assumed to be adiabatic and to contain well mixed fluid, so that each attains a uniform temperature equal to the bulk temperature of the entering fluid. Fluid velocities in the plenums are considered small enough to ignore friction and to assume the pressure varies hydrostatically.

2.2 One—Dimensional Model

The one—dimensional governing equations for thermosyphon loops with cross sectional area $A(z)$ a function of z are now presented, following closely the work of Zvirin and coworkers (1981a,1981b) and Ramos et al. (1985). Under the assumptions stated in the previous section conservation of mass, momentum and energy can be expressed by equations (1)–(3) respectively:

$$\frac{d(uA)}{dz} = 0 \tag{1}$$

$$\rho_0 u \frac{du}{dz} = -\frac{dp}{dz} - \rho_0[1 - \beta(T - T_0)]g\cos\alpha - F_f \tag{2}$$

$$\rho_0 c u \frac{dT}{dz} = \begin{cases} 4q_h/D_h & \text{heated section} \\ 4q_c/D_c & \text{cooled section} \\ 0 & \text{plenums} \end{cases} \tag{3}$$

where $u(z)$, $p(z)$ and $T(z)$ are the axial velocity, pressure and temperature of the fluid, which can all vary with z. In equation (2), F_f represents the friction force per unit volume and $g\cos\alpha$ is the component of the gravitational acceleration in the negative z direction. The specific heat capacity is denoted by c.

The velocity and temperature distributions around the loop are obtained by solving the coupled set of equations (1)–(3) recognising that both pressure and temperature are continuous. Applying the latter condition to the integral of the energy equation (3) around the closed loop shows that the uniform heat fluxes are related by $q_h D_h L_h = -q_c D_c L_c$. Separate solutions of equation (3) for the heated and cooled tubes yield linear temperature variations as depicted in Figure 1.

Integration of equation (2) around the loop, using $dz = \cos\alpha\ dz$, where z is the vertically upward coordinate, eliminates the pressure and inertia terms. The momentum equation for the steady—state motion reduces to a balance between buoyancy and friction

$$g\rho_0\beta \oint T\ dz = \frac{1}{2}\rho_0 V^2 \left[\sum_{\text{tubes}} 4f_i\frac{L_i}{D_i A_i^2} + \sum_{\text{for}} \frac{K_j}{A_j^2}\right] \tag{4}$$

where V is the volume flow rate, f_i are the Fanning friction factors for the tubes and K_j are the form loss coefficients associated with the changes of cross section. In this work, the fully—developed laminar forced flow friction factor $f = 8/\text{Re}$ (radius based Reynolds number) is used and K_j is taken as 0.5 for each inlet and exit. The integral on the LHS of equation (4) is the area enclosed by the $T \sim z$ diagram (Figure 1) and is algebraically equal to $\Delta T\Delta z$, where ΔT is the fluid temperature rise.

The flow rate and temperature rise are given by

$$V = \left[\frac{2g\beta\Delta z\ Q}{\rho_0 c R}\right]^{1/3} \tag{5}$$

550
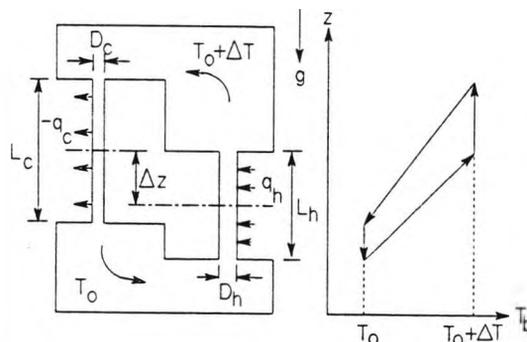
and
$$\Delta T = \left[\frac{Q}{\rho_0 c}\right]^{2/3} \left[\frac{R}{2g\beta\Delta z}\right]^{1/3} \qquad (6)$$

where Q is the heat transfer rate and R is the total flow resistance parameter in square brackets in equation (4).

2.3 Two—Dimensional Model

For the loop geometry considered, some limitations of the one—dimensional analysis can be overcome by two—dimensional modelling of the heated and cooled tubes. Thus both radial and axial variations of velocity and temperature are allowed for in the partial differential equations expressing conservation of mass, momentum and energy for each tubular section, viz.

$$\frac{\partial U}{\partial X} + \frac{V}{R} + \frac{\partial V}{\partial R} = 0 \qquad (7)$$

$$U\frac{\partial U}{\partial X} + V\frac{\partial U}{\partial R} = -\frac{\partial P}{\partial X} * \frac{Gr}{Re^2}\theta + \frac{1}{Re}\left(\frac{\partial^2 U}{\partial R^2} + \frac{1}{R}\frac{\partial U}{\partial R}\right) \quad (8)$$

$$U\frac{\partial V}{\partial X} + V\frac{\partial V}{\partial R} = -\frac{\partial P}{\partial R} + \frac{1}{Re}\left(\frac{\partial^2 V}{\partial R^2} + \frac{1}{R}\frac{\partial V}{\partial R} - \frac{V}{R^2}\right) \quad (9)$$

$$U\frac{\partial \theta}{\partial X} + V\frac{\partial \theta}{\partial R} = \frac{1}{RePr}\left(\frac{\partial^2 \theta}{\partial R^2} + \frac{1}{R}\frac{\partial \theta}{\partial R}\right) \qquad (10)$$

where the $*$ in equation (8) refers to upward flow and downward flow respectively. Equations (7)—(10) are made dimensionless using the following definitions:

$$X = \frac{x}{a}, R = \frac{r}{a}, U = \frac{u}{u_\mathrm{m}}, V = \frac{v}{u_\mathrm{m}}, P = \frac{p - p_0}{\rho_0 u_\mathrm{m}^2} \qquad (11)$$

$$\theta = \frac{T - T_0}{\Delta T}, Re = \frac{\rho_0 u_\mathrm{m} a}{\mu}, Pr = \frac{c\mu}{k}, Gr = \frac{g\beta\rho_0^2 a^3 \Delta T}{\mu^2}$$

where r is the radial coordinate and a is the tube radius. Both the axial and radial velocity components, u and v respectively, are normalised by the mean axial velocity u_m. The pressure variable is based on the difference between the local static pressure and the hydrostatic pressure at the same elevation in a fluid of density ρ_0.

The integral continuity equation and the energy balance equation are also used, namely

$$\frac{1}{2} = \int_0^1 UR \, dR \qquad (12)$$

and
$$\frac{d\theta_b}{dX} = \begin{cases} XL_h^{-1} & \text{heated} \\ -XL_c^{-1} & \text{cooled} \end{cases} \qquad (13)$$

where subscript b refers to bulk temperature and XL is the dimensionless tube length. The subscripts h and c refer to the heated tube and the cooled tube respectively.

For each computation the origin of the (X,R) coordinate system is relocated to the tube entrance, where the following uniform conditions are specified:

$$U(0,R) = 1, \ V(0,R) = 0$$
$$P(0,R) = 0, \ \theta(0,R) = \begin{cases} 0 & \text{heated} \\ 1 & \text{cooled} \end{cases} \qquad (14)$$

Note that for convenience the pressure is set to zero at both entrances since only differences are of concern.

The axis and tube wall boundary conditions are

$$\partial U/\partial R(X,0) = 0, \ V(X,0) = 0$$
$$\partial P/\partial R(X,0) = 0, \ \partial\theta/\partial R(X,0) = 0$$
$$U(X,1) = 0, \ V(X,1) = 0 \qquad (15)$$
$$\partial\theta/\partial R(X,1) = \begin{cases} Re_h Pr/2XL_h & \text{heated} \\ -Re_c Pr/2XL_c & \text{cooled} \end{cases}$$

The wall temperature gradient condition in equation (15) is not used directly in solving the energy equation (10) since conservation is enforced through equation (13) (see below). It is used, however, to recover tube wall temperature, for subsequent use in evaluating average cross—section temperature and local Nusselt number.

Computational details. The governing equations were solved in finite—difference form using the marching procedure for laminar combined convection tube flows described by Collins (1980). Computations were performed on a rectangular grid with 80 uniform divisions in the radial direction. The axial step size ΔX was 0.625 at each tube entrance and was doubled at arbitrarily chosen locations in the marching direction. For the solutions presented below, the numbers of axial steps used for the heated and cooled tubes were 82 and 92 respectively.

Implicit finite—difference equivalents of equations (8)—(10) were written for each radial grid position using backward differences in the axial direction and central differences in the radial direction. For equation (7), $\partial V/\partial Y$ was centred about a position mid—way between radial grid points and $\partial U/\partial X$ was approximated by averaging backward differences for the two adjacent radial positions. The integral in equation (12) and the bulk temperature in equation (13) were replaced using Simpson's rule and the trapezoidal rule respectively. Derivative boundary conditions were expressed as one—sided differences.

At each marching step, unknown U, V and P values were found by solving the finite—difference equivalents of equations (7)—(9) and (12) using an elimination method. The velocities thus obtained were then used to solve the energy equations for the unknown θ profile in a similar way. To guarantee that the overall energy balance was
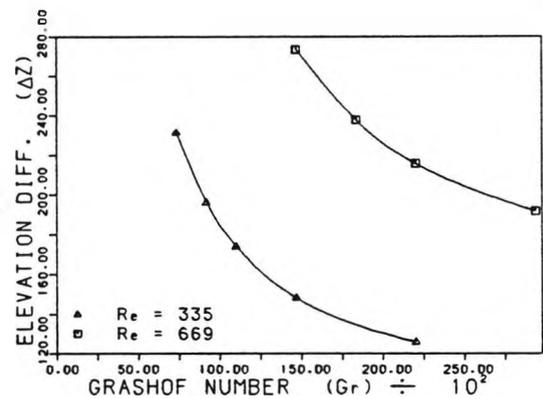
Figure 2 Heat source—to—heat sink elevation difference versus Grashof number for two Reynolds numbers.

551

satisfied, equation (13) replaced equation (10) for the radial grid position nearest the tube wall. Refinement of the solutions was made by repeating the above procedure at each step, using the latest temperature information to evaluate the body force term in equation (8).

    <u>Thermosyphon pressure balance</u>. Since pressure is path independent it follows that the pressure differences between the bottom and top of the loop for separate paths passing through the heated leg and the cooled leg are equal. This balance is expressed non—dimensionally by

$$\left[\Delta P_{\tilde{h}} - \tfrac{1}{2}K_{e,h} + \frac{Gr_h}{Re_h{}^2}(\Delta Z - \tfrac{1}{2}X_{L_h})\right]$$

$$= -\left[\Delta P_{\tilde{c}} - \tfrac{1}{2}K_{e,c} + \frac{Gr_c}{Re_c{}^2}(\tfrac{1}{2}X_{L_c})\right]\left(\frac{Re_c}{Re_h}\right)^4 \qquad (16)$$

where the dimensionless distance ΔZ is based (arbitrarily) on the radius of the heated tube. For each tube, K_e is a combined loss coefficient for entry and exit (assumed equal to 1) and ΔP^* represents the change of defect pressure due to buoyancy and wall friction. The integral of the axial momentum equation (8) over the complete tube volume shows that the overall pressure difference, as determined by the finite—difference method, is

$$\Delta P_{0-XL} = \left(1 - 2\int_0^1 U(X_L,R)^2 R\, dR\right)$$

$$\pm \frac{Gr}{Re^2}\int_0^{X_L}\theta_a\, dX + \frac{2}{Re}\int_0^{X_L}\frac{\partial U}{\partial R}(X,1)\, dX$$

$$= \Delta P_{mom} + \Delta P_{buoy} + \Delta P_{fric} \qquad (17)$$

where θ_a is the average cross—section temperature. The first term in equation (17) corresponds to the momentum difference between the tube inlet and exit sections, and can be evaluated from the exit velocity profile solution. As the momentum change around the entire loop is zero, values of ΔP^* for use in equation (16) are found by subtracting this term from ΔP.

    For the two—dimensional calculation procedure, the Reynolds numbers (same flow rate) in the heated and cooled sections must be specified. As this would involve trial—and—error to find the steady circulation rate for a fixed loop geometry and a given heat flux, a related problem is considered. Instead of fixing all of the geometry factors, ΔZ is now treated as the unknown which is to be found from equation (16). In this formulation all the remaining parameters, including the Reynolds numbers, must be specified. Since the computations for the two tubular sections are performed separately, without reference to their relative vertical displacement, then each set of parameters will generate a solution for ΔZ.

3. RESULTS AND DISCUSSION

    The results presented are for a loop (Figure 1) with heated and cooled tubes of equal diameter, so that $Re_h = Re_c$ and $Gr_h = Gr_c$. The non—dimensional lengths of these two sections, X_{L_h} and X_{L_c}, are taken as 200 and 300 respectively. Consequently, the heat flux ratio $-q_c/q_h$ is always 2/3. Two—dimensional flow and temperature field solutions were computed for a total of 9 cases, covering two Reynolds numbers (Re = 335 and Re = 669) and Grashof numbers from 7336 to 29345. The Prandtl number is taken as that for water at approximately 40°C, Pr = 4.3.

3.1 Thermosyphon Height

    Since fixed values of X_{L_h} and X_{L_c} are assumed, non—dimensional thermosyphon height is determined solely by ΔZ, the difference in elevation (dimensionless) between the centres of the heated and cooled sections. Values of ΔZ, calculated from equation (16) using ΔP results from the two—dimensional tube flow calculations, are plotted in Figure 2. Each plotted point corresponds to a thermosyphon of a different height. For a loop of known ΔZ, the Re ~ Gr characteristic is described by the intersection points of the appropriate horizontal line and the constant Re curves.

    As Figure 2 can be viewed as a dimensionless presentation of Δz versus ΔT with flow rate as a parameter, it follows from equation (4) that one—dimensional theory would predict each curve to be hyperbolic. The actual curves, based on two—dimensional calculations, are in fact somewhat flatter.

3.2 Axial Velocity Profiles

    Figure 3 shows upward flow velocity profiles at four positions along the heated tube for the case of the furthest right point in Figure 2. The profile shapes can be explained in terms of the combined forced and natural convection effects. Close to the tube entrance the development appears to be qualitatively as for pure forced convection, with the maximum axial velocity occuring at or near to the tube centreline and increasing with X. At the same time, the fluid near the heated wall is being subjected to a buoyancy force, which eventually causes it to accelerate, drawing more fluid towards the wall. To satisfy mass continuity, axial velocities in the centre of the tube then decrease, leading to the development of a concavity in the velocity profile and a consequent shift in the position of the maximum velocity towards the wall.

    The governing equations given in Section 2.3 show that for fixed Pr and X_L values, the profile shape at a
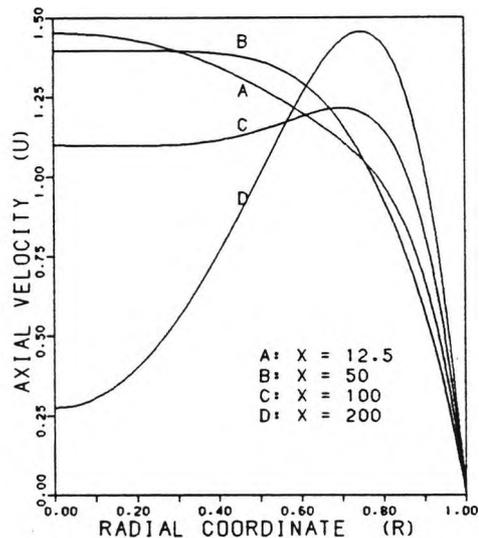
Figure 3   Development of axial velocity profile in heated tube (Gr = 29345, Re = 669).

552

given axial distance X depends on Re and Gr. The effect of increasing Grashof number, at constant Re, is produce more axial velocity profile distortion. Increasing Reynolds number has an opposite effect. For example, at a constant $Gr = 22009$, the magnitudes and radial positions of the minimum and maximum U values in the heated tube exit profiles (not shown) are 0.21 (at $R = 0$) and 1.46 (at $R \approx 0.73$) for Re =335, and 0.60 (at $R = 0$) and 1.36 (at $R \approx 0.71$) for Re = 669.

For some combinations of parameters investigated, it was predicted that onset of flow reversal would occur in the centre of the heated tube before the exit was reached. These cases could not be further pursued using the marching procedure described in this paper.

Axial velocity profiles for the cooled downward flows follow broadly the same pattern of development as in the heated tube. However, due to the reduced heat flux, the centreline axial velocity at tube exit is greater in all cases.

Local Nusselt numbers calculated for the tube exit positions are significantly higher than for simultaneously developing forced convection at the same value of $X/RePr$. The highest Nu_x values determined, corresponding to the case shown in Figures 3 and 4, are 8.42 and 7.55 for the heated tube and the cooled tube respectively.

Finally, it should be noted that the steep wall velocity gradients, illustrated in Figure 3, indicate that $f\!Re$ is much higher than the fully–developed isothermal laminar flow value used in the one–dimensional analysis.

3.3 Bulk and Average Cross–Section Temperatures

Figure 4 compares the θ_b and θ_a variations around a loop with $\Delta Z = 192$ for $Gr = 29345$. In the uniformly heated and uniformly cooled sections, dimensionless bulk temperature varies linearly between 0 and 1, the uniform temperatures in the lower and upper plenums respectively. In contrast, the average cross–section temperature varies non–linearly, only agreeing with the bulk temperature at the tube entrances and in the plenums.

The temperature difference $(\theta_a - \theta_b)$ changes along each tubular section in a manner explained by the interaction between the $\theta(R)$ and $U(R)$ distributions. Near the entrance to the heated tube, θ_a ($= 2 \int_{0-1} \theta R \, dR$) increases more rapidly than θ_b ($= 2 \int_{0-1} U\theta R \, dR$).
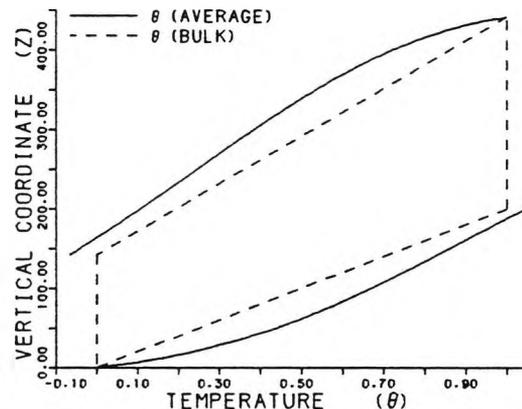
Figure 4   Bulk temperature and average cross–section temperature variations (Gr = 29345, Re = 669, $\Delta Z = 192$).
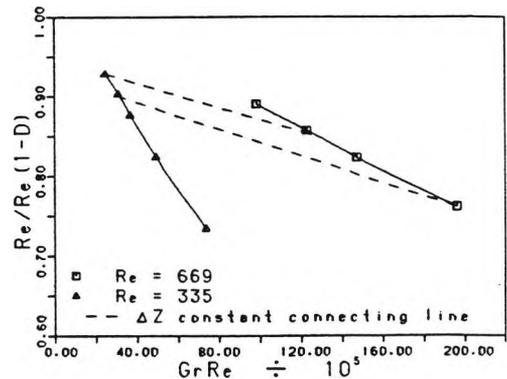
Figure 5   Comparison of Reynolds numbers based on 2–D and 1–D analyses.

This increase is associated with the growth of the thermal boundary layer on the heated wall, which has a greater effect on θ_a than on θ_b, since at this stage the flow is mainly concentrated in the centre of the tube. At greater X, where maximum axial velocity and the maximum fluid temperature tend to coincide, $(\theta_a - \theta_b)$ decreases.

The $(\theta_b - \theta_a)$ variation in the cooled section is qualitatively similar to that just described, although despite the lower heat flux its magnitude is slightly greater throughout. This is consistent with a less distorted axial velocity profile and the consequent lower Nusselt number.

3.4 Comparison of 1–D and 2–D Models

Figure 5 compares the flow rates found from the one–dimensional and two–dimensional analyses, for all 9 cases shown in Figure 2. For each case, corresponding to a thermosyphon of a different height, the same heat transfer rate is assumed for both analyses. Since ΔT is inversely proportional to u_m, it follows that the product GrRe is also the same for both. The dashed lines in Figure 5 are not intended to show exact Re/Re(1–D) variations for fixed height thermosyphons, but simply connect points on the constant Re curves with the same ΔZ. They correspond to the region in Figure 2 where ΔZ values overlap for the separate curves. The parameter Re is the Reynolds number from the two–dimensional analysis.

Table 1 shows the pressure difference contributions due to wall friction (–ve), buoyancy (+ve for heated tube and upper plenum, –ve for cooled tube) and form loss (–ve) in various loop components, for a loop with $\Delta Z = 192$. In the case considered, $Gr = 22360$ and Re = 878 for the one–dimensional analysis. The corresponding values for the two–dimensional analysis are $Gr = 29345$ and Re = 669 (≈ 0.76 x 1–D value). The sum of all entries for each analysis is equal to zero. Note that the buoyancy contribution of the lower plenum is zero, since it is uniformly at the reference temperature.

In non–dimensional terms, average friction factor is equal to $-\Delta P_{fric}/\Delta X$. All pressure differences in Table 1 are divided by ΣXL ($= XL_h + XL_c$), the total length of tubing, and by the laminar forced convection value ($f = 8/Re$), so that the sum of the wall friction entries is equal to -1 for the one–dimensional analysis. The relative sizes of corresponding pressure differences can be compared by multiplying by the appropriate Reynolds number.

553

Table 1   Wall friction, buoyancy and form loss for
1—D and 2—D analyses (GrRe $\approx 1.96 \times 10^7$,
$\Delta Z = 192$)

	$\dfrac{Re\ \Delta P_{fric}}{8\ \Sigma XL}$	$\dfrac{Re\ \Delta P_{buoy}}{8\ \Sigma XL}$	$\dfrac{Re\ \Delta P_{form}}{8\ \Sigma XL}$
Heated Tube			
1—D	−0.400	0.636	−0.110
2—D	−1.134	1.390	−0.084
Cooled Tube			
1—D	−0.600	−0.954	−0.110
2—D	−1.515	−1.258	−0.084
Upper Plenum			
1—D		1.538	
2—D		2.656	

As suggested in Section 3.2, the one—dimensional analysis severely underpredicts wall friction. In Table 1 the average value of $f\!Re$ for the two—dimensional analysis is around 2.65 times (7% higher in the heated tube and 5% lower in the cooled tube) that assumed in the one—dimensional analysis. From the discussion in Section 3.3, it is clear that the one—dimensional analysis also underpredicts the buoyant driving force, by assuming that θ_a is equal to θ_b. In comparison, the magnitude of $\int \theta_a\, dX$ in the two—dimensional analysis, is greater for the heated tube and less for the cooled tube. Indeed, in Table 1, the buoyancy force assisting the flow in the heated tube completely offsets that opposing the flow in the cooled tube. As Figure 5 shows, the friction ~ buoyancy balance established by the two—dimensional analysis gives a lower flow rate (Reynolds number) than estimated by the one—dimensional analysis, the discrepancy increasing with Grashof number. The accompanying increase in ΔT is partly responsible for generating the additional buoyancy necessary to overcome the higher wall friction.

Table 1 also illustrates the importance of taking account of form losses associated with abrupt changes of section. Although only nominal loss coefficients (i.e. all $K_j = 0.5$) were used in this study, they contributed approximately 6% of the total pressure loss due to wall friction and form drag in the two—dimensional analysis. For the one—dimensional analysis this figure is approximately 18%, because of the much lower friction factor and the higher Reynolds number.

5. CONCLUDING REMARKS

An analysis has been performed of the steady flow in a simple closed—loop thermosyphon, incorporating two—dimensional modelling for the developing laminar combined convection in the vertical heated and cooled tubes. Buoyancy distortion of the axial velocity profile becomes more severe, producing steeper wall gradients, for increasing values of the Grashof number. Calculated values of the associated wall friction parameter, $f\!Re$, are correspondingly higher than for fully—developed forced flow. Total buoyancy is underpredicted by one—dimensional analyses, due partly to their failure to distinguish between bulk temperature and average cross—section temperature. The difference between these temperatures varies axially around the loop, both in sign and in magnitude. Flow rates predicted for water (Pr = 4.3) filled loops, covering several values of driving head and Grashof number, are up to 27% below those estimated by a simple one—dimensional analysis for the same rates of heat transfer.

It was also found that form losses associated with changes of cross—section can be a significant proportion of the total flow resistance.

5. REFERENCES

Addlesee, A.J. 1980, Frictional Resistance of Low Reynolds Number Flows Destabilised by Heat Transfer, Letters in Heat and Mass Transfer. vol. 7, pp. 249—255.

Collins, M.W. 1980, Finite—Difference Analysis for Developing Laminar Flow in Circular Tubes Applied to Forced and Combined Convection, International Journal of Numerical Methods in Engineering. vol. 15, pp. 381—404.

Creveling, H.F., de Paz, J.F., Baladi, J.Y. & Schoenhals, R.J. 1975, Stability Characteristics of a Single—Phase Free Convection Loop, Journal of Fluid Mechanics. vol. 67, pp. 65—84.

Grief, R. 1988, Natural Circulation Loops, ASME Journal of Heat Transfer. vol. 110, pp. 1243—1258.

Huang, B.J. 1987, A Combined Convection Correlation for Vertical Downward Cooling Flow in a Natural Convection Loop, International Journal of Heat and Mass Transfer. vol. 30, pp. 1544—1546.

Japiske, D. 1973, Advances in Thermosyphon Technology, in Advances in Heat Transfer. eds. T.F.Irvine & J.P.Hartnett , vol.9, pp. 1—111, Academic Press.

Lavine, A.S., Grief, R. & Humphrey, J.A.C. 1986, Three—Dimensional Analysis of Natural Convection in a Toroidal Loop: Effect of Tilt Angle, ASME Journal of Heat Transfer. vol. 108, pp. 796—805.

Lavine, A.S., Grief, R. & Humphrey, J.A.C. 1987, A Three—Dimensional Analysis of Natural Convection in a Toroidal Loop — The Effect of Grashof Number, International Journal of Heat and Mass Transfer. vol. 30, pp. 251—262.

Mertol, A. & Grief, R. 1985, A Review of Natural Circulation Loops, in Natural Convection: Fundamentals and Applications. eds. S.Kakac, W.Aung & R.Viskanta, p. 1033, Hemisphere.

Mertol, A., Grief, R. & Zvirin, Y. 1982, Two—Dimensional Study of Heat Transfer and Fluid Flow in a Natural Circulation Loop, ASME Journal of Heat Transfer. vol. 104, pp. 508—514.

Morrison,G.L. & Ranatunga, D.B.J. 1980, Thermosyphon Circulation in Solar Collectors, Solar Energy. vol. 24, pp. 191—198.

Ramos, E., Sen,M. & Trevino, C. 1985, A Steady—State Analysis for Variable Area One— and Two—Phase Thermosyphon Loops, International Journal of Heat and Mass Transfer. vol. 28, pp. 1711—1719.

Ronen, A. & Zvirin, Y. 1985, The Behaviour of a Toroidal Thermosyphon at High Graetz (and Grashof) Numbers, ASME Journal of Heat Transfer. vol. 107, pp. 254—258.

Stern, C.H., Grief, R. & Humphrey.J.A.C. 1988, An Experimental Study of Natural Convection In a Toroidal Loop, ASME Journal of Heat Transfer, vol. 110, pp. 877—884.

Zvirin, Y. 1981a, A Review of Natural Circulation Loops in Pressurized Water Reactors and Other Systems, Nuclear Engineering and Design. vol. 67, pp. 203—225.

Zvirin,Y., Jeuck, P.R.,III, Sullivan, C.W. & Duffey, R.B. 1981b, Experimental and Analytical Investigation of a Natural Circulation System with Parallel Loops, ASME Journal of Heat Transfer, vol. 103, pp. 645—652.

554